DEVELOPMENT OF A SPRAY PROCESS FOR MANUFACTURING CARBON NANOTUBE FILMS

MADHURI DUTTA

WOLFSON COLLEGE



Submitted for the Degree of
Doctor of Philosophy in Materials
Hilary Term, 2015

Dedicated to my grandfather Mr. Dutta Radhakrishna,

who taught me the importance of education.

"Education is the most powerful weapon which you can use to change the world."

- Nelson Mandela

Acknowledgments

This wonderful doctoral journey would not have been possible without the support and guidance of many people, whom I would like to thank with all my heart. The most important person whose support and motivation has been a major driving force during my PhD – my mentor Prof. Nicole Grobert. I will forever be indebted to her for her constant guidance, help, encouragement, and for being a true inspiration.

I would like to express my gratitude to Prof. Valeria Nicolosi and Dr Peter Rockett for sharing their valuable knowledge with me and to whom I owe everything I know about dispersions and spraying. A special thanks to Dr Antal Koós and Dr Frank Dillon whose help, suggestions, and contributions have been extremely important in the completion of this PhD. I would also like to thank Dr Laura Miranda and Dr Lavina Snoek for accepting the painstaking task of reviewing my dissertation and for the most useful advices. Dr Jonathan Moghal deserves special thanks for the being a problem solver at various times of my PhD and for all the interesting conversations. I would also like to take this opportunity to thank Dr Rebecca Nicholls for her help with the EELS studies.

My sincere thanks to Adrian, Fatma, Jude, Natalia, Johnny, Shayan, Juan, Michelle, and Serena for their support and help, particularly during my sick leave. Thanks also go out to all the current and past members of the Grobert group for the amazing scientific conversations and for making my arduous lab time enjoyable.

I would like to extend my gratitude to Prof. Patrick Grant for allowing me to use his lab equipment and for his helpful suggestions with the spraying experiments. My sincere thanks to the Oxford Materials Electron Microscopy support group for training me to use the microscopes and for all the additional help, especially Dr Neil Young, Mrs Gabriella Chapman, and Mr Greg Cook. I would also like to thank Dr Henry Snaith for letting me use his lab equipment and Dr Michael Saliba for the gold coating experiments. Thanks to Dr Stefanie Eiden for arranging the secondment at Bayer Technology Services, which has been a good learning experience. Wolfson College's support in the completion of this PhD will always be appreciated, especially Prof. Andrew Neil, Prof. Dame Hermione Lee, and Ms Gillan Hamnett for their kind words and for help in obtaining hardship funding. Thanks to the Oxford DAS for loaning me

a wide screen monitor for my dissertation writing. I would also like to thank Mr. Richard Franzese – a summer student, whose work was important in the completion of dispersion studies.

My heartfelt thanks to all the funding bodies without whose financial support this PhD would not have been possible. I would like to thank the European Commission's Seventh Framework Programme for sponsoring this PhD project (under grant agreement no. 238363), which was a part of the CONTACT Marie Curie Initial Training Network. I am thankful to all the Marie Curie researchers and the coordinators – Dr Christof Hübner and Ms Carolyn Fisher for the good times and knowledge sharing. I would also like to extend my thanks to Oxford University, Wolfson College, and Churches Together Foundation for providing financial assistance in the form of hardship funding and loan. I would like to specially thank Ms Ratana Brooker for the motivational conversations and for providing me a part time job when I was in desperate need.

Special people who have been pillars of support during my PhD definitely need to be acknowledged. Thanks to mamma, daddy, Lalithakka, and Bajju for putting up with me through the ups and downs, and most importantly for the financial help. Thanks to Shashank and Radha aunty for their support. Friends who have instilled strength in me during the dark times of PhD and who stood by my side no matter what – Akshat, Poulomee, Nina, Raghu, Suresh, Laura, Moghal, Shwetha, Muneera – your support and friendship will always be cherished. Thanks to the wonderful friends at Oxford for sharing the pain and wine – Julia, Adela, Rob, Zanna, David, Maxine, Tom, Lena, Auré, and Nuria. My housemates Raluca, Azly, and Thilina deserve my deepest thanks for being immensely supportive all this while and for sharing the last minute stress. I would also like to specially thank Raghu, Akshat, Polumee, Meena aunty, and Jamie for proof reading the thesis.

The list cannot be complete without acknowledging the most beautiful – Dheer and Lily, whose mere presence has brought joy to me during the difficult times of PhD.

Declaration

The work described in this thesis is entirely my own with the exemption of the referenced citations and a part of the dispersion work conducted by a summer student - Mr. Richard Franzese. Any characterisation assistance provided by others has been indicated in the acknowledgements and in the text. This work has not been submitted at any other university, in part or in its entirety, for the award of any degree. Parts of this work have been published and reported as follows:

Publications

1. Meysami, S. S., Koós, A. A., Dillon, F., Dutta, M., and Grobert, N., "Aerosol-assisted chemical vapour deposition synthesis of multi-wall carbon nanotubes: III. Towards upscaling," Carbon, 2015, **88**, pp. 148–156.

2. Dutta, M., Nicolosi, V., Obratzsova, E., Koós, A. A., Crossley, A., and Grobert, N., "Stable dispersions of nitrogen containing multi-walled carbon nanotubes," Materials Express, 2011, **1**(3), pp. 201–209.

Posters

1. Dutta, M., Dillon, F., Koós, A. A., Nicolosi, V., Grobert, N., "Development of a spray process for manufacturing carbon nanotube films," CONTACT meeting 2013; Delft, Netherlands.

2. Dutta, M., Dillon, F., Koós, A. A., Nicolosi, V., Grobert, N., "Ultrasonic probe effects on carbon nanotubes," Advanced Study Institute Nanomaterials and Nanoarchitectures 2013; Cork, Ireland.

3. Dutta, M., Nicolosi, V., Obratzsova, E., Koós, A. A., Crossley, A., Grobert, N., "Stable dispersions of nitrogen containing carbon nanotubes," NanoteC 2011; Nantes, France.

4. Dutta, M., Rockett, P., Nicolosi, V., Grobert, N., "Dispersions of carbon nanotubes," InnoCNT 2011; Karlsruhe, Germany.

© 2015 – Madhuri Dutta
All rights reserved.

Contents

Abstract XVIII

Chapter 1. Introduction 1
1.1. Background 1
1.2. Outline 5
1.3. References 6

Chapter 2. Synthesis of carbon nanotubes 10
2.1. Introduction to carbon nanotubes 12
2.2. Nanotubes containing hetero atoms 14
2.3. Carbon nanotube synthesis techniques 17
2.3.1. Electric arc 18
2.3.2. Laser ablation 19
2.3.3. Chemical vapour deposition (CVD) 19
2.4. Insulating carbon nanotubes 25
2.5. Experimental procedure and characterisation 26
2.5.1. Synthesis of conventional, doped, and silica covered MWCNTs 26
2.5.2. Characterisation of conventional and doped MWCNTs 28
2.5.3. Characterisation of silica covered MWCNTs 29
2.6. Results and discussion 30
2.6.1. Length analysis by SEM 30
2.6.2. Structural and diameter analysis by TEM 32
2.6.3. Defect analysis by Raman spectroscopy 34
2.6.4. Oxidation studies using TGA analysis 36
2.6.5. Characterisation of silica coated MWCNTs 38
a) TEM studies coupled with EDX 38
b) STEM and EELS 40
2.7. Summary 43
2.8. References 45

Chapter 3. Sonication effects on carbon nanotubes 52
3.1. Introduction to sonication theories and literature review 54
3.1.1. Sono-physical and sono-chemical reactions 54
3.1.2. Sonication effects 55
a) Ultrasonic baths (US baths) 57
b) Ultrasonic probes (US probes) 57
3.2. Experimental procedure 59
3.3. Characterisation techniques 61
3.4. Sonication study I: effect of US probes; results and discussion 62
3.4.1. Structural characterisation using SEM and TEM 62
a) Pristine MWCNTs 62
b) MWCNTs-SP 64
3.4.2. Analysis of length and diameter distributions 66
a) Length distributions of pristine and US probe treated MWCNTs 67
b) Diameter distributions of pristine and US probe treated MWCNTs 72
3.4.3. Analysis of the induced defects 78
3.5. Sonication study II: Development of a sonication protocol; results and discussion 85
3.5.1. Structural characterisation using TEM 85
3.5.2. Defect analysis using Raman spectroscopy 86
3.6. Summary 88
3.7. References 90

Chapter 4. Development of stable MWCNT dispersions 94
4.1. Introduction 94
4.2. Dispersion strategies 95
4.2.1. Covalent approach 95
a) Acid functionalisation 95
b) Secondary acid-functionalisation 98
4.2.2. Non-covalent approach 98
a) Surfactant Assisted 99
b) Polymer functionalisation 101
c) Non-aqueous dispersions in organic solvents 103
4.3. Materials and equipment used 106

4.4. Experimental procedure and characterisation 108
4.4.1. Labscale production 108
4.4.2. Upscale production 109
4.5. Results and discussion 109
4.5.1. UV-Vis-NIR spectroscopy of MWCNT dispersions 109
4.5.2. Defect density characterisation using Raman 119
4.5.3. Visual inspection of MWCNT dispersions 123
4.6. Summary 125
4.7. References 126

Chapter 5. MWCNT/polymer dielectrics 134
5.1. Capacitors and current technologies 136
5.1.1. Capacitors 136
5.1.2. Capacitor technologies 138
5.2. Introduction to composite film forming techniques 143
5.2.1. Drop casting and spin coating 144
5.2.2. Electrospraying 145
5.2.3. Aerosol spray deposition technique 147
5.3. Materials used for composite fabrication 149
5.4. Experimental procedure and characterisation 151
5.4.1. Fabrication of MWCNT/polymer composite films 151
a) Spin Coating and Drop Casting 151
b) Electrospraying 152
c) Aerosol Spraying 154
5.4.2. Characterisation of MWCNT/PU and MWCNT/PFA films 157
a) Surface characterisation 157
b) Thickness analysis 158
c) Impedance spectroscopy 158
5.5. Results and discussion 159
5.5.1. Optical characterisation of composite films 159
5.5.2. Surface characterisation using SEM 161
5.5.3. Impedance Spectroscopy of aerosol sprayed films 162
5.6. Summary 173
5.7. References 175

Chapter 6. Summary and future work 181
6.1. Summary 181
6.1.1. MWCNTs 182
6.1.2. MWCNT dispersions 183
6.1.3. MWCNT/polymer dielectric films 184
6.2. Future work 185

List of figures

Figure 1-1. Volvo's prototype of a future electric car comprising of lightweight energy storage supercapacitors made of nanomaterials. 1

Figure 2-1. Comparison of the quality in CVD-produced MWCNTs: a) SEM image of reasonably good quality MWCNTs that are fairly uniform, b) SEM image of bad quality MWCNTs that are a mixture of non-uniform nanotubes with amorphous carbon and fine tubular structures. Also seen in the images are entrapped iron catalyst particles that are characteristic to CVD-produced MWCNTs. 11

Figure 2-2. Schematic of the cross-sections of: a) SWCNT and b) MWCNT. (Image courtesy: Dr. Rebecca Nicholls.) 13

Figure 2-3. Graphical illustration of the density of states as a function of energy (E) of: (a) nitrogen, (b) boron doped nanotubes. The dotted lines denote the Fermi energy position (E_F) (black – initial, green and blue – final) before and after the ionisation of the dopant states. The arrows represent the Fermi level shift and the hatched region relates to the occupied states. 15

Figure 2-4. a,b,c) SEM micrographs, (d,e,f) TEM micrographs, (g,h,i) High-resolution TEM micrographs of conventional, N-, and B- MWCNTs that show the structural effects introduced by nitrogen and boron doping. 17

Figure 2-5. a) Schematic of the electric arc discharge technique, b) TEM image of MWCNTs produced by this technique that shows the highly graphitised walls in the nanotubes. 18

Figure 2-6. a) Schematic of the laser ablation technique, b) TEM image of SWCNTs produced by this technique showing the quality of the nanotubes. 19

Figure 2-7. a) Schematic of the CVD technique, b) TEM image of a well-graphitised MWCNT produced by this technique. 20

Figure 2-8. Illustration of the nanotube growth mechanism: a) tip-growth, b) base-growth; C- Carbon, M- Metal catalyst particle. 21

Figure 2-9. Typical Raman spectrum of AACCVD-produced MWCNTs. 24

Figure 2-10. Schematic of the AACCVD setup used in this work. The area between 10 cm after the start position 'a' and 10 cm before the end position 'b' was considered for collecting the nanotubes. 27

Figure 2-11. Low and high resolution SEM images of pristine MWCNTs produced by AACCVD: (a,b) Conventional MWCNTs, (c,d) N-MWCNTs, (e,f) B-MWCNTs. 32

Figure 2-12. TEM images of pristine MWCNTs produced by AACCVD: (a,b) Conventional MWCNTs, (c,d) N-MWCNTs, (e,f) B-MWCNTs. 33

Figure 2-13. Raman spectra of pristine MWCNTs showing the variation in the defect peaks in different nanotubes. All spectra are normalised with respect to the G band intensity. 35

Figure 2-14. TGA measurements of pristine conventional and doped MWCNTs showing the effects of doping on the oxidation resistance. 38

Figure 2-15. TEM images and their respective EDX area scans of silica covered MWCNTs: (a,b) Conventional MWCNTs, (c,d) N-MWCNTs, and (e,f) B-MWCNTs. 40

Figure 2-16. STEM images of silica coated conventional MWCNTs with their respective EDX line scans. The images belong to different areas of the same sample. (Scans conducted by Dr. Rebecca Nicholls.) 42

Figure 2-17. EELS spectra of the coating on the conventional MWCNTs. (Scan conducted by Dr. Rebecca Nicholls.) 43

Figure 3-1. Agglomeration types of various CVD-produced nanotubes: a) Aligned MWCNT bundles grown via spray pyrolysis3, b) SWCNT bundles grown via CCVD, c) Baytubes® C150P grown via floating catalyst CVD, d) Nanocyl™ NC7000 grown via CCVD, e) An aligned N-MWCNTs bundle grown via AACVD, f) An agglomerate of B-MWCNTs grown via AACVD. 52

Figure 3-2. A schematic showing the forces acting on a nanotube near a collapsing bubble. The compressive forces (red) and the inward torque (green) result in the nanotube buckling. If the torque imbalance is sufficiently large, the nanotube rotates radially *i.e.*, clockwise (yellow). 57

Figure 3-3. Schematic of: a) An US Bath, b) An US Probe. 58

Figure 3-4. SEM and TEM images of pristine: a,b) Conventional MWCNTs, (c,d) N-MWCNTs, (e,f) B-MWCNTs respectively. 64

Figure 3-5. SEM and TEM micrographs of N-MWCNTs treated in HFIP for 2 min in pulsed mode using: (a,b,c) UP 100H, (d,e,f) UP 200S (Note: b,e are magnified SEM images of a,d respectively). 66

Figure 3-6. Lognormal probability density functions of conventional MWCNT lengths: (a) Pristine MWCNTs,
(b) MWCNTs-SP in DMF with varied US probes, sonication times and modes,
(c) MWCNTs-SP treated for 2 minutes with varied US probes, sonication modes and solvents. 68

Figure 3-7. Comparison of conventional MWCNT lengths in the lower 75th percentile with variable sonication parameters: 69
(a) Conventional MWCNTs-SP in DMF treated with varying US probes, sonication modes and times,
(b) Conventional MWCNTs-SP treated for 2 minutes in different solvents with varying US probes, and sonication modes.

Figure 3-8. Lognormal probability density functions of N-MWCNT lengths: 71
(a) Pristine N-MWCNTs,
(b) N-MWCNTs-SP in DMF with varied US probes, sonication times and modes,
(c) N-MWCNTs-SP treated for 2 minutes with varied US probes and sonication modes and solvents.

Figure 3-9. Comparison of N-MWCNT lengths in the lower 75th percentile with variable sonication parameters: 72
(a) N-MWCNTs-SP in DMF treated with varying US probes, sonication modes and times,
(b) N-MWCNTs-SP treated for 2 minutes in different solvents with varying US probes, and sonication modes.

Figure 3-10. Lognormal probability density functions of conventional MWCNT outer diameters (pristine and US probe treated): 74
(a) Treated in DMF with varied US probes, sonication times and modes,
(b) Treated for 2 minutes in different solvents with varying US probes, and sonication modes.

Figure 3-11. Comparison of conventional MWCNT outer diameters (pristine and US probe treated) in the lower 75th percentile with variable sonication parameters: 75
(a) Treated in DMF with varying US probes, sonication modes and times,
(b) Treated for 2 minutes in different solvents with varying US probes, and sonication modes.

Figure 3-12. Lognormal probability density functions N-MWCNT outer diameters (pristine and US probe treated): 76
(a) Treated in DMF with varied US probes, sonication times and modes,
(b) Treated for 2 minutes in different solvents with varying US probes, and sonication modes.

Figure 3-13. Comparison of the N-MWCNT outer diameters (pristine and US probe treated) in the lower 75th percentile with variable sonication parameters: 77
(a) Treated in DMF with varying US probes, sonication modes and times,
(b) Treated for 2 minutes in different solvents with varying US probes, and sonication modes.

Figure 3-14. Raman spectra of pristine conventional and N- MWCNTs used for sonication study I; all spectra are normalised with respect to the G band intensity. 78

Figure 3-15. Raman spectra of the conventional MWCNTs (pristine and US probe treated) in DMF treated for 2 minutes using three different US probes in continuous and pulsed modes; All spectra are normalised with respect to the G band intensity. 81

Figure 3-16. Raman spectra of the conventional MWCNTs (pristine and US probe treated) in DMF treated with UP 200S for various times and modes; All spectra are normalised with respect to the G band intensity. 82

Figure 3-17. Raman spectra of the N-MWCNTs (pristine and US probe treated) in DMF treated for 2 minutes using the three different US probes in continuous and pulsed modes; All spectra are normalised with respect to the G band intensity. 83

Figure 3-18. Raman spectra of the N-MWCNTs (pristine and US probe treated) in DMF treated with UP 200S for various times and modes; All spectra are normalised with respect to the G band intensity. 84

Figure 3-19. TEM images of: a) Pristine conventional MWCNTs, (b) Dispersed conventional MWCNTs in NMP after step 4 of the sonication regime, (c, d) As synthesised and acid treated MWCNTs from the work of Buang *et al*. 86

Figure 3-20. Raman spectra of conventional MWCNTs in NMP after every step of the sonication regime. 87

Figure 4-1. A model showing some typical inherent defects and those arising from functionalisation in a SWCNT: a) A topological anomaly in the regular six-membered carbon ring that results in bending of the tube, b) sp^3-hybridised defects (R=H and OH), c) Damage in the SWCNT structure due to the oxidative acid treatment, which also results in a hole lined with -COOH groups, and d) -COOH terminal groups at the open end of the nanotube caused due to the oxidative treatment. 97

Figure 4-2. Structures of: a) Sodium dodecyl sulfate and b) Sodium dodecylbenzene sulfonate with the additional aromatic ring. 100

Figure 4-3. An illustration of the crowning effect due to the interaction between the SDS, SDBS surfactants and the nanotube. 100

Figure 4-4. A molecular simulation showing the possible wrapping arrangements of PVP polymer around a SWCNT (8,8). 102

Figure 4-5. Graphs showing the % of MWCNTs retained after centrifugation as a function of the surface energy of the dispersing solvent. A Gaussian curve (in red) fitted to the data clearly shows a shift in the dispersing ability of the N-MWCNTs towards the lower surface energy solvents. 110

Figure 4-6. UV-Vis-NIR absorbance spectra of dispersions of MWCNTs in NMP, N-MWCNTs in DMA, B-MWCNTs in GBL (concentration – 0.01 mg/ml). Spectra of the dispersions before and after centrifugation (CF) are shown. 115

Figure 4-7. Extinction coefficients of conventional, N-, and B- MWCNTs at 660 nm. 117

Figure 4-8. Raman spectra of the pristine MWCNTs and their respective labscale dispersions. All spectra are normalised with respect to the G band intensity. 121

Figure 4-9. Raman spectra of the pristine MWCNTs and their respective upscale dispersions. All spectra are normalised with respect to the G band intensity. 122

Figure 4-10. Photographs of the lab scale dispersions: a) Conventional MWCNTs in NMP, b) N-MWCNTs in DMA, c) B-MWCNTs in GBL. The stability of the dispersions over a period of 3 years can be observed. Volume of the dispersions - 10 ml. 124

Figure 4-11. Photographs of the upscale dispersions on the date of manufacture: a) Conventional MWCNTs in NMP, b) N-MWCNTs in Benzyl alcohol, c) B-MWCNTs in GBL. Volume of the dispersions - 150 ml. 124

Figure 5-1. TEM images showing the nanotube agglomerations in various polymer composites: a) MWCNTs/Epoxy, b) MWCNTs/poly(vinyl alcohol), and c) MWCNTs/polycarbonate. 135

Figure 5-2. Schematic of a traditional parallel plate capacitor showing the charge accumulation when a voltage is applied. 136

Figure 5-3. Schematic of a new generation capacitor with a composite dielectric containing aligned MWCNTs showing increased charge accumulation on application of voltage. 138

Figure 5-4. Schematic showing the various stages of: a) Drop casting, b) Spin coating. 145

Figure 5-5. Schematic of the electrospray principle. 146

Figure 5-6. a) Schematic of a basic aerosol spray deposition technique, b) An optical photograph of a high quality SWCNT/polyelectrolyte film. 148

Figure 5-7. Experimental set-up used for: a) Drop casting, and b) Spin coating. 152

Figure 5-8. Photograph of the electrospray system as set-up in the lab: a) Details of the associated electronics and instrumentation, b) Capillary illumination; Photo courtesy: Dr Peter Rockett. 153

Figure 5-9. Photographs of stable electrospray cone jet modes of different types of dispersions along with their respective flow rates, applied voltages and collected currents. 154

Figure 5-10. Photograph of the modified aerosol spray set-up used for forming nanotube/polymer composite films. 155

Figure 5-11. Flow chart showing the steps involved in the aerosol spraying for forming nanotube/PFA films. Also shown are optical photographs of the samples at every step. 157

Figure 5-12. Optical photographs of composite films synthesised through different techniques:
a) Drop casted 0.01 wt.% conventional MWCNT/PU films dried at room temperature,
b) Drop casted 0.01 wt.% conventional MWCNT/PU films dried at 100 °C,
c) Spin coated 0.01 wt.% conventional MWCNT/PU films dried at room temperature,
d) Spin coated 0.01 wt.% conventional MWCNT/PU films dried at 100 °C,
e) Electrosprayed sample of 0.1 wt.% conventional MWCNT/PU film before drying,
f) Electrosprayed film of 0.1 wt.% conventional MWCNT/PU film after drying,
g) Aerosol sprayed plain PFA film after curing, and
h) Aerosol sprayed 0.5 wt.% conventional MWCNT/PFA film after curing. 160

Figure 5-13. SEM images of:
a) 0.1 wt.% MWCNT/PU electrosprayed film that had no evident nanotubes on the surface,
b) 0.5 wt.% MWCNT/PFA aerosol sprayed film that shows the presence of individual nanotubes on the surface of the film. 162

Figure 5-14. Cole-plots depicting the change from lossy to resistive behaviour in the capacitor containing conventional MWCNT/PFA dielectric films containing different nanotube concentrations. 163

Figure 5-15. Dielectric constants of conventional MWCNT/PFA and B-MWCNT/PFA films as a function of nanotube wt.% at 10 kHz that show an improvement in the dielectric constant with increasing nanotube concentration. 164

Figure 5-16. Dielectric constants of: a) Conventional MWCNT/PFA films, and b) B-MWCNT/PFA films with varying nanotube concentrations as a function of increasing frequency that show the stability of the dielectric values over a range of frequencies. 166

Figure 5-17. Real permittivities of: a) Conventional MWCNT/PFA films, and b) B-MWCNT/PFA films with varying concentrations of CNTs as a function of increasing frequency. The change in dielectric behaviour of the B-MWCNT containing films relative to films with conventional MWCNTs can be clearly observed. 168

Figure 5-18. Imaginary permittivities of: a) Conventional MWCNT/PFA films, and b) B-MWCNT/PFA films with varying concentrations of CNTs as a function of increasing frequency. It can be seen that the imaginary permittivity was independent of nanotube concentration and frequency for most of the films. 170

Figure 5-19. Dissipation factors of PFA films containing conventional and B-MWCNTs as a function of nanotube wt.% at 10 kHz. A decrease in the values with the increasing nanotube concentration signifies a strong interfacial interaction of the nanotubes with the PFA matrix. 171

Figure 5-20. Dissipation factors of: a) MWCNT/PFA films, b) B-MWCNT/PFA films with varying nanotube concentration showing the consistency of the values with increasing frequency. 172

List of tables

Table 2-1. List of precursors used for the synthesis of conventional and doped MWCNTs along with the synthesis parameters. 27

Table 2-2. Lengths and diameters of pristine MWCNTs produced by AACCVD. 31

Table 2-3. Raman intensity ratios: I_D/I_G and I_{2D}/I_G of pristine MWCNTs. 36

Table 2-4. Temperatures at which 20% and 80% mass loss occurs in the MWCNTs along with their catalyst content. 37

Table 3-1: Energy concentration in a cavitation bubble (before and after collapse) caused by a 3 MHz sound wave. 55

Table 3-2. Synthesis parameters used for synthesising MWCNTs for the sonication studies. 59

Table 3-3. List of parameters used for sonication study I. 60

Table 3-4. Lengths and diameters of pristine MWCNTs produced by AACCVD used for sonication study I. 64

Table 3-5. Raman I_D/I_G and I_{2D}/I_G intensity ratios of conventional MWCNTs in NMP after every step of the sonication regime. 87

Table 4-1. List of the solvents along with their properties used for study I for dispersing conventional and N-MWCNTs. Also listed is the percentage of retained MWCNT concentration in the supernatant dispersion after CF ($\chi_{retained}$) calculated using UV-Vis-NIR studies. 107

Table 4-2. Hansen and Hildebrand solubility parameters of the 22 solvents used for nanotube dispersibility test. The Hansen parameters were taken from the book - Hansen's handbook on solubility parameters. 111

Table 4-3. Concentrations of the labscale and upscale MWCNT dispersions over a period of 3 years. 118

Table 4-4. List of the Raman intensity ratios of labscale and upscale dispersions and their respective pristine counterparts. 120

Table 5-1. Comparison of some of the commonly available capacitors. 139

Table 5-2. List of typical parameters used for electrospraying. 154

Abbreviations and symbols

AACCVD	Aerosol assisted catalytic chemical vapour deposition
AACVD	Aerosol assisted chemical vapour deposition
After-CF	After centrifugation
B-MWCNT	Boron doped multi-wall carbon nanotube
Before-CF	Before centrifugation
CCTO	Calcium copper titanate
CF	Centrifugation
CNT	Carbon nanotube
CNTs-SP	Ultra sonic probe treated carbon nanotubes
CCVD	Catalytic chemical vapour deposition
CVD	Chemical vapour deposition
DMA	Dimethylacetamide
DMEU	Dimethyl-imidazolidinone
DMF	Dimethylformamide
DMS	Dimethyl sulfoxide
DOS	Density of states
EDX	Energy dispersive X-ray
EELS	Electron energy loss spectroscopy
EtOH	Ethanol
GBL	γ-Butyrolactone
HFIP	Hexafluoroisopropanol
MWCNT	Multi-wall carbon nanotube
MWCNT-SP	Ultra sonic probe treated multi-wall carbon nanotube
N-MWCNT	Nitrogen doped multi-wall carbon nanotube
NMP	N-Methyl pyrrolidone
PFA	Perfluoro alkoxy
PU	Polyurethane
PVP	Polyvinyl pyrrolidone
SDBS	Sodium dodecylbenzene sulfonate
SDS	Sodium dodecyl sulfate
SEM	Scanning electron microscope

STEM	Scanning transmission electron microscope
SWCNT	Single-wall carbon nanotube
TEM	Transmission electron microscope
TGA	Thermogravimetric analyser
US Bath	Ultrasonic bath
US Tip	Ultrasonic tip
δ (in the context of dispersions)	Hildebrand solubility parameter
δ_D	Dispersion forces between the molecules
δ_H	Molecular hydrogen bonding
δ_P	Dipolar intermolecular forces
δ_T	Total Hildebrand value
ΔG_{mix}	Free energy of mixing
ΔH_{mix}	Enthalpy of mixing
ΔS_{mix}	Entropy of mixing
δ (in the context of impedance analysis)	Loss tangent
C	Effective capacitance
ε_o	Permittivity of free space
ε'	Real dielectric permittivity
ε''	Imaginary dielectric permittivity
k	Dielectric constant
DF	Dissipation factor
$\chi_{retained}$	% of final retained nanotube concentration after centrifugation
A	Absorbance of a material
I_D	Intensity of D Peak in a Raman spectrum
I_{2D}	Intensity of 2D Peak in a Raman spectrum
I_G	Intensity of G Peak in a Raman spectrum
l	Nanotube length
t	Sonication time
m	Power law exponent
$T_{20\%}$	Oxidation temperature at 20% mass loss
$T_{80\%}$	Oxidation temperature at 80% mass loss

Abstract

Development of a spray process for manufacturing carbon nanotube films
Madhuri Dutta
Wolfson College
Submitted for the degree of Doctor of Philosophy, Hilary Term 2015

This dissertation describes the development of a processing route for fabricating conventional and doped multi-wall carbon nanotube (MWCNT)/polymer composite films for dielectric applications. Previous research has shown that such composites are promising dielectric materials, but their commercial development has been impeded by the nanotube agglomeration in the polymer matrix and the inefficiency in forming uniform films. Moreover, the harsh fabrication treatments often disrupt the structure of the nanotubes, hence damaging their inherent electrical properties. This work presents safer routes for forming non-aqueous, surfactant free dispersions of conventional and doped MWCNTs, which can be readily mixed with polymers and formed into films through aerosol spraying.

Dispersibility behaviour of in-house synthesised conventional, nitrogen doped (N-MWCNTs), and boron doped (B-MWCNTs) MWCNTs was studied in 22 organic solvents. Based on thermodynamic theories it was suggested that doping, in particular nitrogen doping, significantly reduced the surface energy of the nanotubes. This aspect was crucial to understand the dispersibility of N-MWCNTs in low surface energy solvents and to achieve dispersions with high nanotube concentrations (0.82 mg/ml). Also, a "destruction reduced sonication protocol" involving mild sonication was suggested for forming MWCNT dispersions in organic solvents. Dispersions formed using this protocol were homogeneous and showed high stability of at least 2.5 years. Furthermore, the effect of ultrasonic probes on MWCNT lengths was studied and a decrease of 96–99% for MWCNTs and 85–95% for N-MWCNTs was observed. A numerical value for the nanotube length decrease during sonication has been reported for the first time.

Preliminary studies to generate dielectric films of MWCNT/perfluoro alkoxy polymer were performed using aerosol spraying. An improvement in the dielectric constant (3.56) with a low dissipation factor (0.003) was observed in 0.3 wt.% B-MWCNT/PFA composite films. Consistency in the test results from various parts of the films confirmed the uniformity of the nanotube distribution within the composite. Future work should concentrate on the effects of B-MWCNTs and N-MWCNTs at the percolation threshold due to their inherent electric properties.

Chapter 1. Introduction

1.1. Background

With an increasing energy demand, energy storage materials are the most sought-after research topic in the current day[1,2]. Investigations are incessantly being conducted to improve existing materials and develop new ones for the energy storage market that requires low density materials with high reliability and efficiency at low costs[3,4]. So far, major focus has been on developing novel batteries for meeting these criteria. However, in the past few years, there has been a new interest in using capacitors as energy storage devices[5–7]. Capacitors have mostly been used for storing small amounts of energy in electrical applications such as for camera flashes, as decoupling devices in integrated circuits to maintain stable voltage level, as filters in amplifiers and mobile telephones to remove signals at unwanted frequencies, and components in timing circuits such as light-flashing intervals for introducing time delay or changing the shape of wave form. However, with the right combination of materials, capacitors can be upgraded for storing far greater amounts of energy in miniaturised devices[8–10] (Figure 1-1).

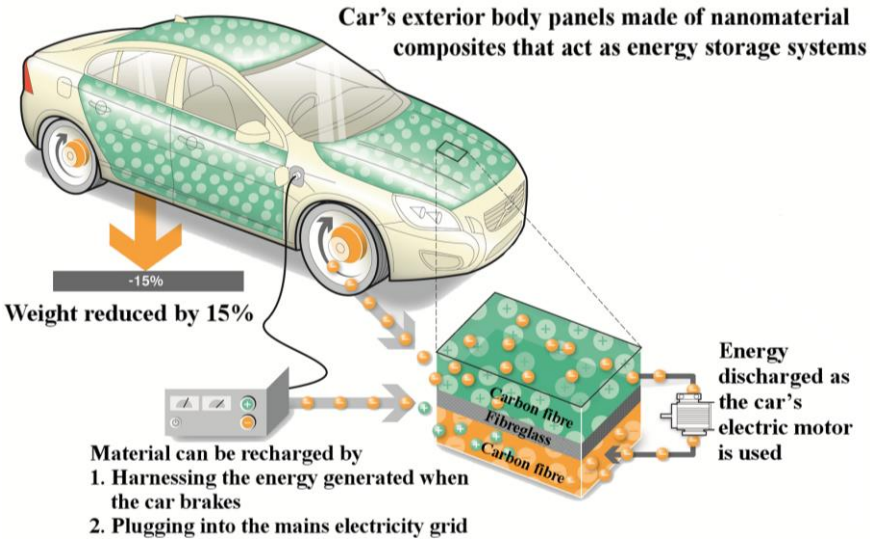


Figure 1-1. Volvo's prototype of a future electric car comprising of lightweight energy storage supercapacitors made of nanomaterials[11].

Such ‘new age’ capacitors can address four main challenges of the energy storage market: faster charging, higher energy storage, long-term discharging, and small device size. Capacitors of this type can potentially find applications in hybrid electric vehicles as well as alternative energy storage devices. Research has shown that one way of fabricating such high efficiency capacitors is by replacing the conventional dielectric materials with advanced nanomaterials[12–15]. Among the various new ‘nano’ materials being developed, carbon nanotubes (CNTs), including single- and multi-wall CNTs (SWCNTs, MWCNTs), are undoubtedly the best candidate fillers mainly due to their exceptionally low densities and high aspect ratios[16–18]. Various studies have confirmed that the dielectric properties of the conventional polymer systems can be significantly improved by reinforcing them with MWCNTs[19–23]. However, not many doped MWCNTs have been investigated for this purpose. Doped MWCNTs, particularly nitrogen “doped” multi-wall carbon nanotubes (N-MWCNTs) and boron doped multi-wall carbon nanotubes (B-MWCNTs), possess inherent electrical properties owing to their electronic density of states[24]. Nitrogen, with an additional electron relative to carbon, can introduce n-type characteristics in the nanotubes. Boron, on the other hand, which has one electron less than carbon, can introduce p-type characteristics in the nanotubes. Furthermore, nitrogen and boron doping also introduce structural changes in the conventional nanotube structure[25]. The effect of nanotube fillers in composites for dielectrics is usually associated with their inherent electrical properties along with nanotube size and structure. Therefore, one can certainly expect promising effects from the doped nanotubes fillers. Although the presence of SWCNTs and MWCNTs can improve the dielectric properties, they are limited by their conducting nature, which means that an exceedingly high number of nanotubes in the dielectric system can come into contact with each other and potentially form a conducting path that can cause capacitor

failure. Hence, forming an insulating coating (such as silica) around the nanotubes is one way to overcome this issue and to allow more nanotube packaging in the system. Hence, it is of great interest to study the effects of such insulated nanotubes on the dielectric properties.

Although research has proposed a variety of suitable energy storage nanomaterials, their applicability in commercial applications has not yet seen the light of day. This is because most of the existing fabrication techniques lack the ability to uniformly form nano-composite thin films on a large area. Additionally, it has been seen time and again that the issues associated with the agglomeration of nanotubes and their inhomogeneous distribution in the polymer matrices, and weak nanotube/polymer interfacial interactions can have detrimental effects on the capacitor devices[26–28]. Furthermore, technologies for efficiently processing conventional and doped nanotubes without the aid of surfactant or surface treatment have not been studied in detail before, which limits their application as fillers in composites in their pristine form. Also, it should be noted that the extraordinary properties of nanotubes are dependent on the structural arrangement of the carbon atoms within its lattice. This arrangement varies with the slightest of changes in the nanotube synthesis parameters; as a consequence a huge structural variation exists within every synthesised batch of nanotubes[29,30]. When such nanotubes are used as composite fillers, the final products will most certainly present non-uniform properties. Unfortunately, a clear definition and description of the nanotube type and quality is lacking in most of the research articles reported in the literature. This creates ambiguity in the right combination of parameters required for the synthesis of such materials, which slows down the overall scientific progress of the nanomaterial research. Hence, despite having a range of potential nanomaterials for energy storage

applications, existing research has not been able to fully move to the commercialisation stage.

Amongst the various routes available for forming the dielectric films, spraying techniques stand out for their low cost, precision control on the spray parameters, and ability to fabricate ultra-thin films, with the possibility of upscaling[12,15,31]. The feedstock for spraying techniques is in the form of solutions or liquid dispersions. This means that in order to form nanotubes/polymer dielectric films via spraying, both nanotubes and polymer need to be suspended homogeneously in a solvent (*i.e.*, formed into dispersions). However, individual nanotubes agglomerate into bundles during their growth[32], which makes it important to separate them in solvents and form dispersions containing individual nanotubes[33]. The dispersions can then be readily mixed with appropriate polymers and can be processed into composite films through spraying. The problem, however, lies in the separation of nanotube bundles and finding the right solvents that can efficiently disperse them and prevent re-agglomeration of the separated nanotubes. Surface treatments or surfactant aids have been widely investigated for this purpose and have been found to be particularly efficient for forming aqueous nanotube dispersions[34–36]. However, these treatments damage the structure of the nanotubes and introduce defects such as wall damage and disruption of the extended π-conjugation[27]. The crucial point is that the extraordinary inherent properties of the nanotubes are a result of their structural arrangement, and damaging the structure would defeat the purpose of using them. Therefore, there is a need for new techniques that can safely separate nanotube bundles and form dispersions of individual nanotubes in solvents, whilst protecting their inherent structure and properties.

The main aim of this dissertation was to develop a nano-composite film forming technique to produce MWCNTs filled polymer dielectric films with the

possibility of upscaling. This involved synthesising MWCNTs (conventional, doped and silica covered MWCNTs) from inception, forming homogeneous dispersions of the MWCNTs in regular organic solvents through mild sonication, and developing an appropriate spraying technique to form the nano-composite dielectric films. It should be noted that the dispersion forming techniques proposed in this dissertation are purely based on sonication routes; any sort of surface treatments or use of surfactants has been avoided to preserve the inherent properties of the nanotubes. However, proof of concept film-forming experiments were conducted using surfactant based aqueous nanotube dispersions to evaluate the aptitude of the spraying technique. It can be confirmed that the protocols required for the development of uniform and homogeneous nanotube dispersions in organic solvents were successfully established, and a spraying technique for forming MWCNT/polymer dielectric films was also established. The methods reported in this dissertation are a good extension to the previous doctoral works of Dr Claire Hinchliffe[37] and Dr Xin Zhao[38], and allow further processing that has been denied to doped MWCNTs so far. In addition, the techniques described here can be readily scaled up, and involve safe and user-friendly solvents. Hence, these studies are crucial for the successful application of a much wider range of nanotube-typologies in future nanotechnological applications at a larger scale.

1.2. Outline

This dissertation constitutes of a selection of nearly independent chapters. Each chapter has its own introduction, literature review, methodology, results, conclusion, and references sections. Every subsequent chapter uses the results of the previous chapter and presents new studies that were conducted. The dissertation is structured as follows:

- Chapter 2 covers the background on carbon nanotubes and the techniques followed to synthesise them, in particular conventional, nitrogen doped and boron doped MWCNTs, and silica-covered MWCNTs. The instrumentation for characterisation and measurements used to understand the structure of the nanotubes and to assess their quality are also discussed in this chapter.
- Chapter 3 details the studies conducted to understand the effects of sonication routes on MWCNTs with respect to lengths, diameters, and defect densities. This chapter also presents a 'destruction reduced sonication protocol' for forming MWCNT dispersions in solvents.
- Chapter 4 discusses the techniques used for forming uniform and homogeneous MWCNT dispersions using the 'destruction reduced sonication protocol' presented in chapter 3. This chapter also discusses the development of labscale and upscale MWCNT dispersions along with stability measurements and the concentration calculations of MWCNTs in the final dispersions.
- Chapter 5 discusses the various composite forming techniques for the production of uniform nanotube/polymer films. This chapter details the steps followed for identifying the most suitable technique for this work and presents the various types of nanotube/polymer films formed and the effects of B-MWCNTs on the dielectric properties.
- Finally, a summary of the findings, and prospects for future work are provided in chapter 6.

1.3. References

[1] Gogotsi, Y., "Materials science: Energy storage wrapped up," Nature, 2014, **509**(7502), pp. 568–70.

[2] Whittingham, M. S., "Materials challenges facing electrical energy storage," MRS Bulletin, 2011, **33**(04), pp. 411–419.

[3] Tummala, R. R., Haley, M. R., and Czornyj, G., "Materials in microelectronics," Ceramics International, 1993, **19**(3), pp. 191–210.

[4] University College London, Case Study - "Enabling SEMATECH and industrial member companies to improve their transistor technology.": *http://impact.ref.ac.uk/casestudiesapi/refservice.svc/GetCaseStudyPDF/34176*

[5] Pandey, R. K., Stapleton, W. A., Tate, J., Bandyopadhyay, A. K., Sutanto, I., Sprissler, S., and Lin, S., "Applications of CCTO supercapacitor in energy storage and electronics," AIP Advances, 2013, **3**(6), p. 062126.

[6] Coughlin, C., "Ultracapacitors: The next big thing in energy storage?," Green Biz, 2012: *http://www.greenbiz.com/blog/2012/06/10/ultracapacitors-next-big-thing-energy-storage*

[7] Hamilton, T., "Next Stop: Ultracapacitor Buses," MIT Technology Review, 2009: *http://www.technologyreview.com/news/415773/next-stop-ultracapacitor-buses/*

[8] "Graphene supercapacitors ready for electric vehicle energy storage," MIT Technology Review, 2013: *http://www.technologyreview.com/view/521651/graphene-supercapacitors-ready-for-electric-vehicle-energy-storage-say-korean-engineers/*

[9] Kannappan, S., Kaliyappan, K., Manian, R. K., Pandian, A. S., Yang, H., Lee, Y. S., Jang, J.-H., and Lu, W., "Graphene based supercapacitors with improved specific capacitance and fast charging time at high current density," 2013.

[10] Miller, N., "A breakthrough in energy storage: graphene micro supercapacitors," Clean Technica, 2013: *http://cleantechnica.com/2013/03/12/a-breakthrough-in-energy-storage-graphene-micro-supercapacitors/*

[11] Ingram, A., "Volvo develops structural, supercapacitor nanobatteries for future electric cars," Green Car Reports, 2013: *http://www.greencarreports.com/news/1087770_volvo-develops-structural-supercapacitor-nanobatteries-for-future-electric-cars*

[12] Hu, L., Hecht, D. S., and Grüner, G., "Carbon nanotube thin films: fabrication, properties, and applications.," Chemical Reviews, 2010, **110**(10), pp. 5790–844.

[13] Ding, Y., Wu, Q., Zhao, D., Ye, W., Hanif, M., and Hou, H., "Flexible PI/$BaTiO_3$ dielectric nanocomposite fabricated by combining electrospinning and electrospraying," European Polymer Journal, 2013, **49**(9), pp. 2567–2571.

[14] Muhammad Abdul Jamal, E., Joy, P. A., Kurian, P., and Anantharaman, M. R., "Synthesis of nickel–rubber nanocomposites and evaluation of their dielectric properties," Materials Science and Engineering: B, 2009, **156**(1-3), pp. 24–31.

[15] Zhao, X., Hinchliffe, C., Johnston, C., Dobson, P., and Grant, P., "Spray deposition of polymer nanocomposite films for dielectric applications," Materials Science and Engineering: B, 2008, **151**(2), pp. 140–145.

[16] Saito, R., Dresselhaus, G., and Dresselhaus, M. S., "Physical properties of carbon nanotubes," 1998, Imperial College Press, London, p.35.

[17] Otieno, G., "Processing and properties of aligned carbon nanotube/glass ceramic composite," 2012, D.Phil dissertation, University of Oxford.

[18] O'Connell, M. J., "Carbon nanotubes: properties and applications," 2006, CRC Press, Florida, p.11.

[19] Liu, H., Shen, Y., Song, Y., Nan, C.-W., Lin, Y., and Yang, X., "Carbon nanotube array/polymer core/shell structured composites with high dielectric permittivity, low dielectric loss, and large energy density.," Advanced Materials, 2011, pp. 1–5.

[20] Dang, Z.-M., Wang, L., Yin, Y., Zhang, Q., and Lei, Q.-Q., "Giant dielectric permittivities in functionalized carbon-nanotube/ electroactive-polymer nanocomposites," Advanced Materials, 2007, **19**(6), pp. 852–857.

[21] Ning, N., Bai, X., Yang, D., Zhang, L., Lu, Y., Nishi, T., and Tian, M., "Dramatically improved dielectric properties of polymer composites by controlling the alignment of carbon nanotubes in matrix," RSC Advances, 2013, **4**(9), pp. 4543–4551.

[22] Ameli, A., Nofar, M., Park, C. B., Pötschke, P., and Rizvi, G., "Polypropylene/carbon nanotube nano/microcellular structures with high dielectric permittivity, low dielectric loss, and low percolation threshold," Carbon, 2014.

[23] Khajehpour, M., Arjmand, M., and Sundararaj, U., "Dielectric properties of multiwalled carbon nanotube/clay/polyvinylidene fluoride nanocomposites: Effect of clay incorporation," Polymer Composites, 2014.

[24] Glerup, M., Ewels, C., Holzinger, M., and Val Lier, G., "Doping of carbon nanotubes" in doped nanomaterials and nanodevices, Volume 3, American Scientific Publishers.

[25] Koós, A. A., Dillon, F., Obraztsova, E. A., Crossley, A., and Grobert, N., "Comparison of structural changes in nitrogen and boron-doped multi-walled carbon nanotubes," Carbon, 2010, **48**(11), pp. 3033–3041.

[26] Zhu, B., Xie, S., Xu, Z., and Xu, Y., "Preparation and properties of the polyimide/multi-walled carbon nanotubes (MWNTs) nanocomposites," Composites Science and Technology, 2006, **66**(3-4), pp. 548–554.

[27] Bose, S., Khare, R. A., and Moldenaers, P., "Assessing the strengths and weaknesses of various types of pre-treatments of carbon nanotubes on the

properties of polymer/carbon nanotubes composites: A critical review," Polymer, 2010, **51**(5), pp. 975–993.

[28] Tiwari, S. K., Choudhary, R. N. P., and Mahapatra, S. P., "Effect of multiwalled carbon nanotube and temperature on dielectric and impedance spectroscopy of chlorobutyl elastomer nanocomposites," Journal of Elastomers and Plastics, 2014, p. 0095244314526742.

[29] Meysami, S. S., "Development of an aerosol-CVD technique for the production of CNTs with integrated online control," 2013, D.Phil dissertation, University of Oxford.

[30] Grobert, N., "Nanotubes – grow or go?," Materials Today, 2006, **9**(10), p. 64.

[31] Grant, P. S., "Spray forming," Progress in Materials Science, 1995, **39**(4-5), pp. 497–545.

[32] Meysami, S. S., Dillon, F., Koós, A. A., Aslam, Z., and Grobert, N., "Aerosol-assisted chemical vapour deposition synthesis of multi-wall carbon nanotubes: I. Mapping the reactor," Carbon, 2013, **58**, pp. 151–158.

[33] Dutta, M., Nicolosi, V., Obratzsova, E., Koós, A. A., Crossley, A., and Grobert, N., "Stable dispersions of nitrogen containing multi-walled carbon nanotubes," Materials Express, 2011, **1**(3), pp. 201–209.

[34] Islam, M. F., Rojas, E., Bergey, D. M., Johnson, A. T., and Yodh, A. G., "High weight fraction surfactant solubilization of single-wall carbon nanotubes in water," Nano Letters, 2003, **3**(2), pp. 269–273.

[35] Hu, C., Xu, Y., Duo, S., Zhang, R., and Li, M., "Non-covalent functionalization of carbon nanotubes with surfactants and polymers," Journal of the Chinese Chemical Society, 2009, **56**(2), pp. 234–239.

[36] Rastogi, R., Kaushal, R., Tripathi, S. K., Sharma, A. L., Kaur, I., and Bharadwaj, L. M., "Comparative study of carbon nanotube dispersion using surfactants.," Journal of Colloid and Interface Science, 2008, **328**(2), pp. 421–428.

[37] Hinchliffe, C., "Processing and properties of nanocomposite dielectric films," 2006, D.Phil dissertation, University of Oxford.

[38] Zhao, X., "Spray deposition of nanostructured materials for energy storage," 2009, D.Phil dissertation, University of Oxford.

Chapter 2. Synthesis of carbon nanotubes

Applications of nanomaterials existed throughout the centuries, for example the Lycurgus cup – a product of classic Roman art, contains nanoparticles that are responsible for the change of colour depending on how light is shone on the cup. Existence of such materials has always been an interest to the scientific community. Particularly research from the late 1980s reported a new category of nanomaterials based on carbon that initiated a new era of carbon science, which one could only imagine in science fiction[1–3].

One such carbon nanomaterial that attracted the most attention was carbon nanotubes (CNTs). These were believed to have the ability to entirely transform the use of science in almost all aspects of life with their extraordinary properties. Much research has been carried out since their discovery to understand everything about them, including the science involved in their formation, their structure, and their suitability for various applications. The predicted applications of nanotubes are limitless[4–6]. However, this demands the nanotube material to be produced uniformly on a large-scale, which to date remains a challenge unsolved. Despite several commercial suppliers claiming to produce well-defined nanotubes, the product quality still remains questionable and in many cases poor[7,8]. Such inferior quality severely affects the nanotube properties and lowers its potential for several applications. Hence, it is extremely important to analyse the structural information of nanotubes before finalising on their application.

The use of tailored good quality nanotubes in composites is one of the fundamental aspects of this doctoral work. The definition of the nanotube quality is usually determined by its application; in this work ‘good quality’ refers to a moderately homogeneous size of crystalline nanotubes with few or no carbonaceous

by-products. An example of this is shown in Figure 2-1. Most of the commercially available nanotubes suffer from inferior quality. Hence, the nanotubes required for this work were synthesised in-house using aerosol assisted catalytic chemical vapour deposition (AACCVD) that has the capability of producing large amount of clean nanotubes. This chapter discusses the synthesis techniques used for the production of conventional MWCNTs along with nitrogen and boron doped MWCNTs (N-MWCNTs, B-MWCNTs). Characterisation studies, such as high-resolution scanning and transmission electron microscopy, thermo-gravimetric analysis, and Raman spectroscopy, which were used to understand the effects of nitrogen and boron doping on the nanotube structure are also discussed in this chapter. Additionally, considering the application of the nanotubes for dielectric films (*i.e.*, for insulating purposes), a range of silica (SiO_2) covered MWCNTs were developed to transform the generally conducting nanotubes to insulating materials. The technique used for synthesising the SiO_2 covered MWCNTs is presented in this chapter. Characterisation tests used for understanding the silica coverage over the nanotubes are discussed further in this chapter.

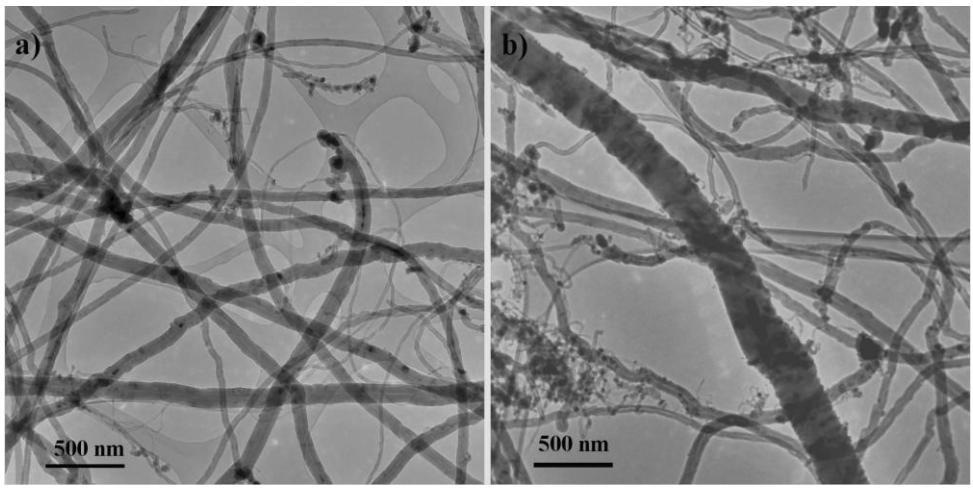


Figure 2-1. Comparison of the quality in CVD-produced MWCNTs: a) SEM image of reasonably good quality MWCNTs that are fairly uniform, b) SEM image of bad quality MWCNTs that are a mixture of non-uniform nanotubes with amorphous carbon and fine tubular structures. Also seen in the images are entrapped iron catalyst particles that are characteristic to CVD-produced MWCNTs.

It should be noted that in this thesis the term 'nanotubes' is used as a general representation for all types of carbon nanotubes, which include SWCNTs, MWCNTs, undoped form (conventional), and doped form. Where specific nanotube type is discussed, it is clearly indicated by its corresponding acronym.

2.1. Introduction to carbon nanotubes

In 1991 Iijima[3] observed filamentous and hollow carbon structures that measured 4–30 nm in diameter and up to 1 μm in length. Owing to their nanometre size, these structures came to be known as carbon nanotubes. Similar nanostructured elements in the form of thin filaments with diameters < 100 nm had been observed previously[9,10]. However, they were considered as undesired by-products in chemical processes and did not receive much attention due to the unavailability of experimental equipment to study them. Nevertheless, since Iijima's observations, considerable research has been invested into the development of nanotubes.

A carbon nanotube can be described as a sheet of graphene rolled up into a hollow tube with a honeycomb lattice capped with hemispherical fullerene molecules. They can be broadly classified into single-walled carbon nanotubes (SWCNTs; Figure 2-2a) and MWCNTs (Figure 2-2b). SWCNTs have a single graphitic wall with diameters typically in the order of 1–3 nm[11] and can be several millimetres long. On the other hand, MWCNTs are essentially concentric tubes of SWCNTs with diameters typically within 20–100 nm and can be several millimetres long.

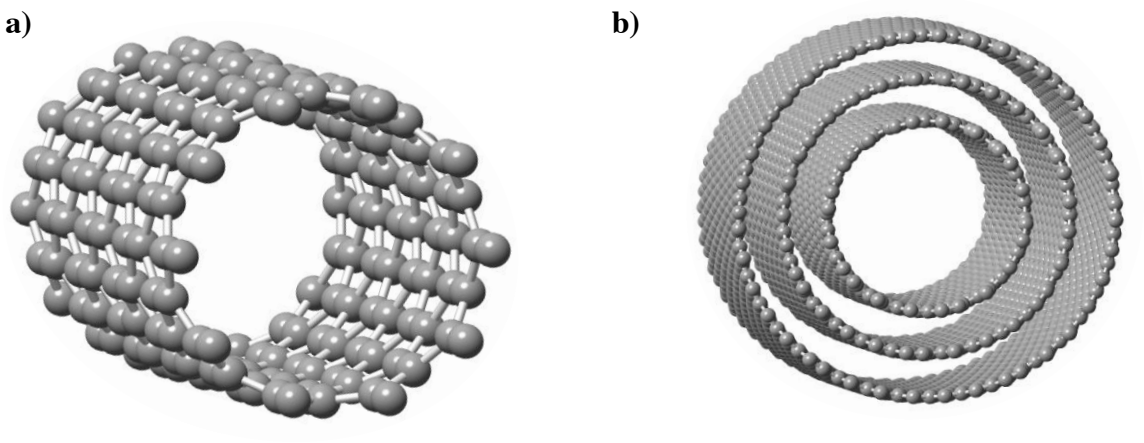


Figure 2-2. Schematic of the cross-sections of: a) SWCNT and b) MWCNT. (Image courtesy: Dr. Rebecca Nicholls.)

Nanotubes are composed of strong in-plane sp^2 hybrid bonds of carbon that gives them excellent properties; the best nanotubes can exhibit elastic modulus of 1.0–3.7 TPa[12], tensile strength of *ca*. 63 GPa[13], electrical conductivity equivalent to that of copper[14], and thermal conductivity of 6600 $Wm^{-1}K^{-1}$ [15]. These properties coupled with their large length-to-diameter ratio (usually referred to as aspect ratio) and low densities (1.3–1.4 $g.cm^{-3}$ [16]) allow them to be used in a multitude of applications, including electronic applications (interconnects, electromechanical actuators and memory devices, super-capacitors, batteries, field-effect transistors, thin film transistors, nanoscale integrated circuits)[17–19], energy applications (energy storage media, electrodes in lithium-ion batteries)[20,21], mechanical applications (molecular reinforcements in composites)[22,23], gas sensors[24], field emission and lightning applications[25,26], biological applications (drug delivery)[6], nanoprobes[27], and supports for catalytic particles[28].

Properties of any material depends on its structure, likewise properties of the nanotubes are also structure dependant. Length, diameter, number of walls, arrangement and symmetry of carbon atoms in the lattice are some of the factors that influence the properties. Therefore, some nanotubes are metallic while others are

semiconducting[29]. This means that some nanotubes present electrical conductivities comparable to that of copper, while some behave like silicon. Therefore, to employ nanotubes for a specific commercial application such as for mechanical or electrical applications, it is essential to make millions of them in a uniform defined pattern. Synthesis parameters such as gaseous feed composition, synthesis temperature, synthesis time, type of catalyst support, and carrier gas can control the nanotube structure to some extent[30]. However, a full control for a tailored nanotube structure has not been achieved so far.

2.2. Nanotubes containing hetero atoms

In addition to the existing properties of nanotubes, inclusion of non-carbon hetero-atoms into its hexagonal lattice *i.e.*, nanotube doping, enhances their already outstanding properties[31,32]. For example, MWCNTs with nitrogen dopants exhibit improved conductance and large current carrying capability[33]. The dopant atoms are usually intercalated in the inter-shell spaces or settle inside/in-between individual tubes[34]. This changes the local bonding arrangement and results in a change of nanotube structure and formation of additional density of states (DOS). Based on the dopant used, the additional DOS can either be electron-donor or electron-acceptor. Some of the doping elements previously studied were nitrogen[35], boron[36], silicon[32], phosphorus[37], lithium[38], potassium[39], and bromine[39]. This thesis is directed towards the improvement of the electronic properties of nanotubes, hence nitrogen and boron dopants that have the ability to tune electronic properties are of main interest in this assessment.

Nitrogen and boron atoms can be easily incorporated into the nanotube graphitic lattice through substitutional doping, *i.e.*, substitution of the carbon atoms with atoms of different number of valence electrons. Nitrogen and boron differ by

only one valence electron compared to carbon, which makes it easier to incorporate them. In N-MWCNTs, nitrogen acts as an electron donor since it has five valence electrons *i.e.*, one electron more than carbon, causing an upward shift in the Fermi level compared to its initial position (Figure 2-3a), therefore making the nanotubes n-type[40]. Boron, on the other hand, plays the inverse effect of nitrogen doping. Boron has one electron less than carbon and acts as an electron acceptor, causing a downward shift of Fermi energy compared to its initial position (Figure 2-3b) creating a p-type nanotube[40]. It should be noted that the Fermi energy shift in both cases also depends on the diameter of the dopant atom and the number of incorporated dopant atoms.

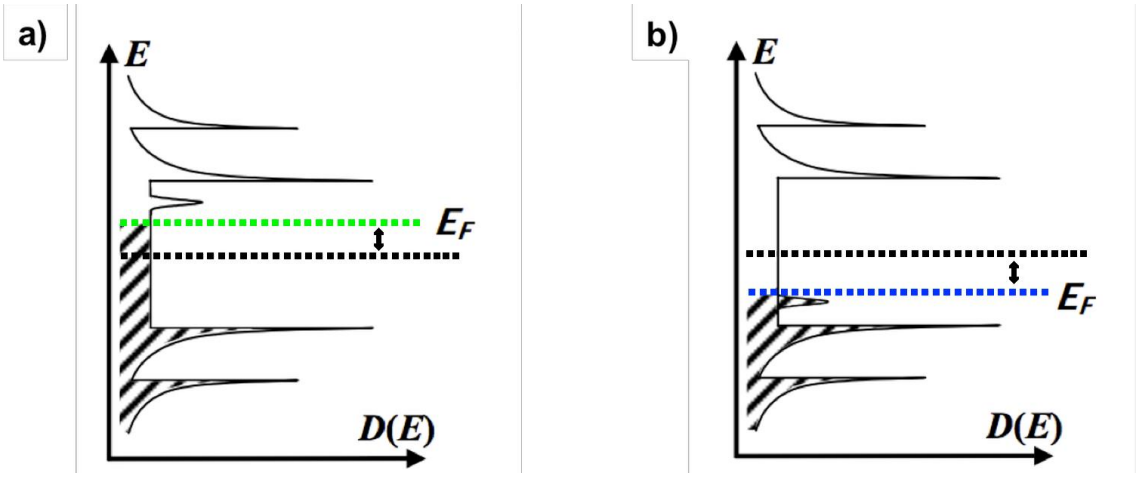


Figure 2-3. Graphical illustration of the density of states as a function of energy (E) of: (a) nitrogen, (b) boron doped nanotubes. The dotted lines denote the Fermi energy position (E_F) (black – initial, green and blue – final) before and after the ionisation of the dopant states. The arrows represent the Fermi level shift and the hatched region relates to the occupied states.[40]

Apart from the electronic properties, nitrogen and boron doping also has an effect on the structure of MWCNTs. The model proposed by Sumpter *et al.*,[41] based on theoretical calculations and experimental evidence offers a good insight into the structural effects induced by nitrogen doping. They propose that nitrogen prefers to be at the tube edges and results in edge saturation that inhibits the tube growth;

resulting in considerably shorter nanotubes. Moreover, nitrogen has a tendency to facilitate inclusion of pentagons into the graphitic lattice that promotes tube closure. As more nitrogen atoms are added, the tube must open again and regrow, which results in the formation of compartments/bamboo-like internal structure. It has been observed that nitrogen is richer in the cores and the inner walls of these compartments and it preferentially sits on tubes with narrow diameters. On the other hand, it has been observed that boron promotes tube growth and forms larger diameter MWCNTs by altering the substrate-catalyst interaction[42]. Blase *et al*.,[43] proposed a theoretical explanation for boron influence on the growth of longer nanotubes. According to their model, boron preferentially substitutes the carbon atoms at the tube end and forms pentagons at the ends similar to nitrogen doping. This bends the nanotube inwards and leads to a partial closure by forming an atomic bridge. However, the boron-boron bonds easily break and reopen the tube structure; pentagons in this open tube structure form hexagons on encountering a carbon atom from the vapour phase, which enable the nanotube to grow further. Also, boron reduces the interlayer spacing and increases the in-plane distance in the carbon lattice, thereby improving the crystallinity and graphitisation in the nanotubes[44]. Boron doped nanotubes exhibit different morphologies due to the non-uniform distribution of boron across different nanotubes[29]. This is caused by the variation in the chemical composition and temperature within the furnace during their synthesis. Some of the commonly observed morphologies in boron doped nanotubes are a well-defined nested cone structure surrounded by a disordered outer layer, a well-defined nested cone structure without the disordered outer layer, and an inner channel surrounded by disordered walls[29]. In the cone-structured nanotubes, the cones are usually rich in boron and the disordered walls are rich in carbon. Some of the morphologies of nitrogen and boron doped MWCNTs are shown in Figure 2-4.

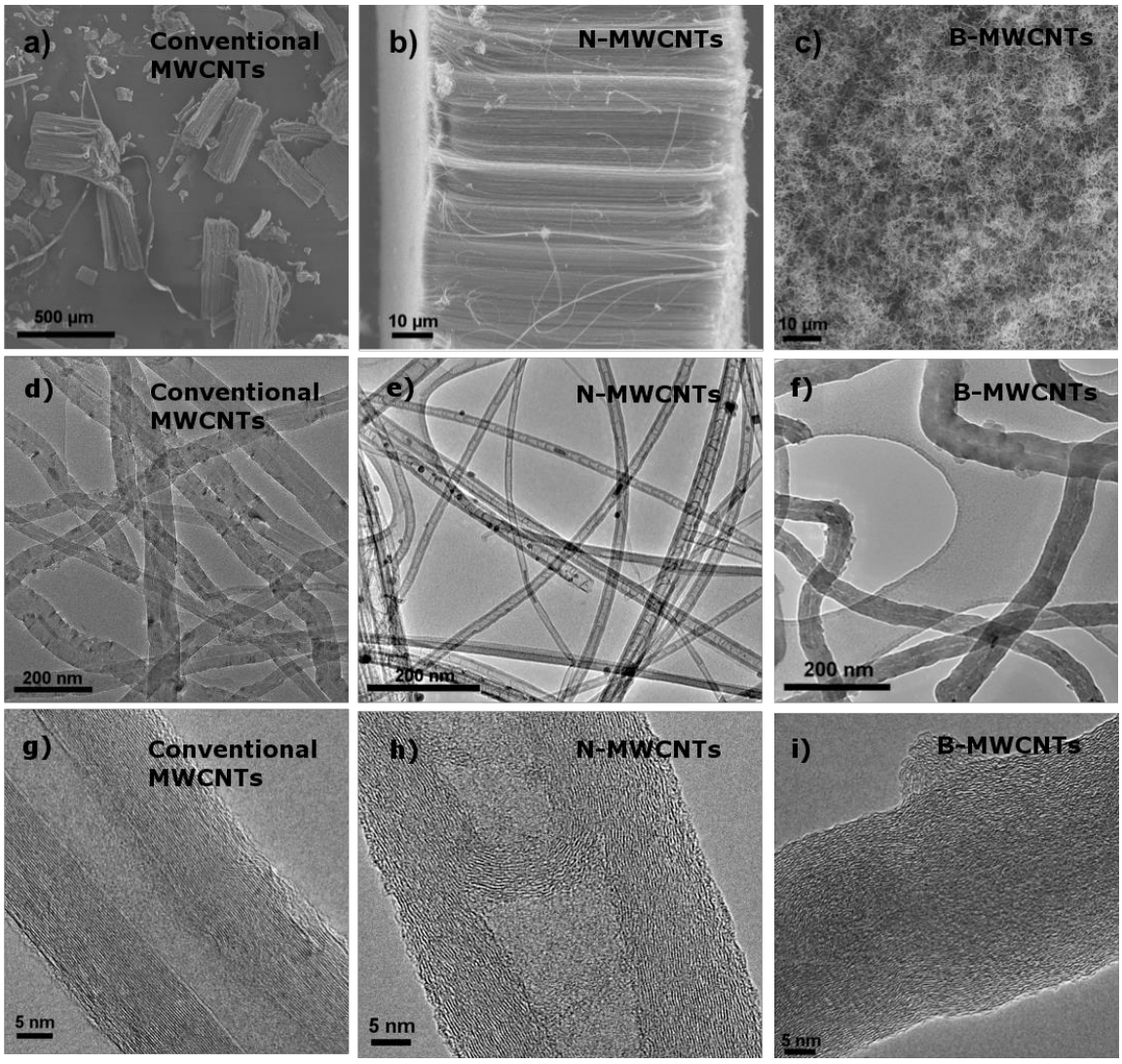


Figure 2-4. a,b,c) SEM micrographs, (d,e,f) TEM micrographs, (g,h,i) High-resolution TEM micrographs of conventional, N-, and B- MWCNTs that show the structural effects introduced by nitrogen and boron doping.[41,42,45–47]

2.3. Carbon nanotube synthesis techniques

Most of the nanotube production techniques require a carbon feedstock, a metal catalyst, and heat. When a carbonaceous feedstock is brought into a gas-phase, the evaporated species self-assembles into tubular structures during thermalisation. Nanotube synthesis can be classified mainly into two categories depending on the synthesis temperature[48]: high-temperature routes (2000–3200 °C) and medium-temperature routes (600–1100 °C). High-temperature routes include electric arc

discharge methods, laser ablation, and vaporisation induced by a solar beam. The medium-temperature routes are based on chemical vapour deposition processes.

2.3.1. Electric arc

The electric arc method is one of the oldest techniques used for synthesising nanotubes and it was this very technique that was used by Iijima when he accidentally identified nanotubes[3]. In this method, direct current is passed through graphite electrodes in an inert atmosphere, resulting in a temperature of 5000–6000°C[49] (Figure 2-5a). At this point the anode is consumed and highly crystalline nanotubes are deposited on the anode, whereas polyhedral particles and amorphous carbon are formed on the cathode. This technique is capable of producing highly graphitised nanotubes[50] as seen in Figure 2-5b. However, the quantity of nanotubes that can be produced using this technique is limited due to the high temperatures of the reactor that consumes the majority of the generated power for cooling, leaving only a fraction of the power for vaporising the graphite. Hence, making it economically not feasible.

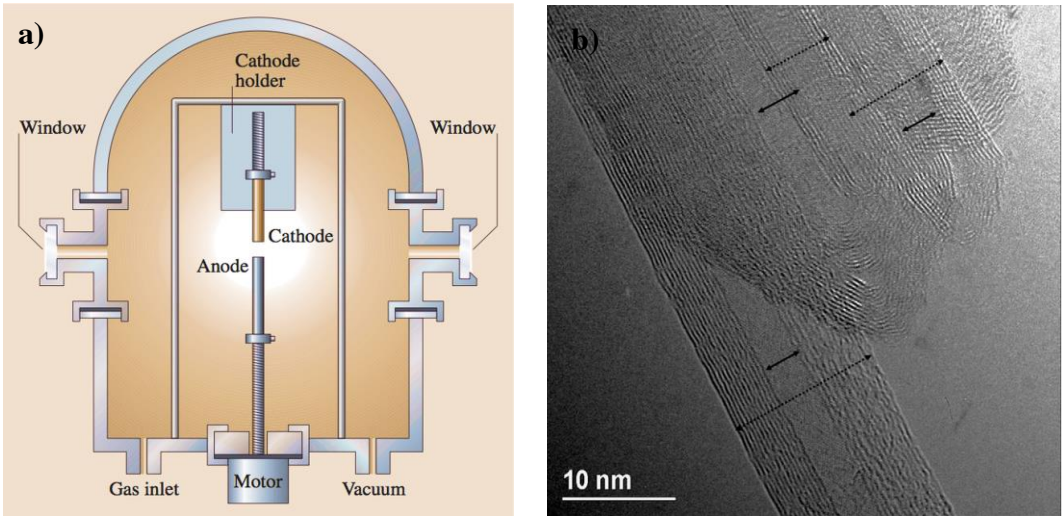


Figure 2-5. a) Schematic of the electric arc discharge technique[49], b) TEM image of MWCNTs produced by this technique that shows the highly graphitised walls in the nanotubes[50].

2.3.2. Laser ablation

Another commonly used technique for nanotube production is laser ablation. This technique uses an incident laser beam to excite carbon atoms by vaporising graphite targets held at high temperatures (> 1000 ºC) in an inert atmosphere (Figure 2-6a). The nanotubes produced by the laser ablation are similar in structure and quality to those produced by electric arc method. Furthermore, this technique mostly favours SWCNT production[51] (Figure 2-6b). However, this technique involves expensive equipment, which makes it economically unviable.

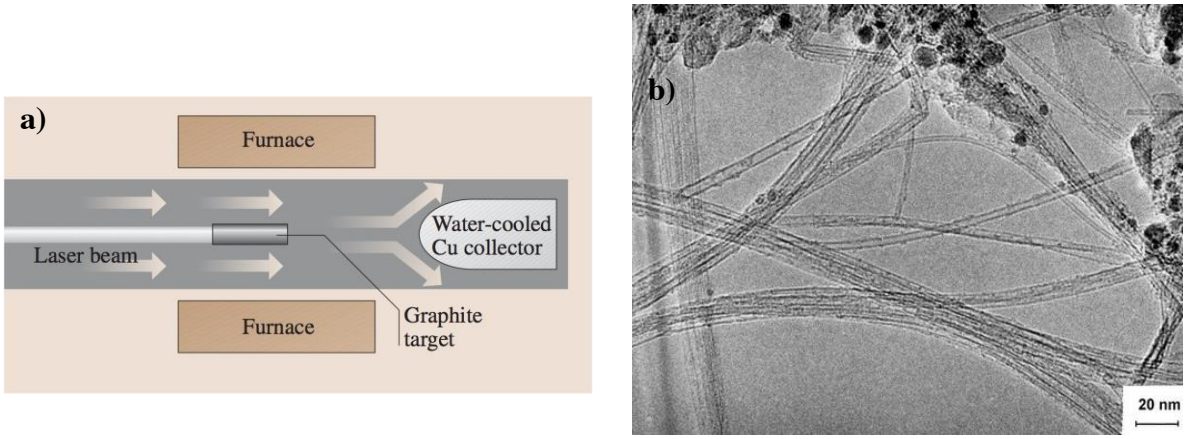


Figure 2-6. a) Schematic of the laser ablation technique[49], b) TEM image of SWCNTs produced by this technique showing the quality of the nanotubes[51].

2.3.3. Chemical vapour deposition (CVD)

For utilising the full potential of nanotubes, producing them economically at a mass scale with high homogeneity and few/no carbonaceous by-products is of prime importance. However, the high temperature techniques discussed above consume a large amount of carbon source and energy. This makes them inefficient and economically unsuitable for laboratory and industrial research. Moreover, the produced nanotubes are inferior in quality and present impurities such as amorphous carbon and metal catalyst particles, hence requiring post-treatments. Some of these drawbacks can be overcome through CVD because of its flexibility and ability to be

scaled up. In CVD, decomposition of a gaseous or volatile carbon source occurs that is catalysed by metallic nanoparticles acting as nucleation sites for the nanotube growth (Figure 2-7a). CVD uses relatively lower temperatures[52] (300–800 °C for MWCNTs, 600–1150 °C for SWCNTs) for synthesising well-graphitised nanotubes; an example of this is shown in Figure 2-7b. However, the CVD-produced nanotubes are usually accompanied with metal catalyst particles trapped inside them. It should be noted that it is difficult for a single synthesis technique to solely overcome all the drawbacks associated with the nanotube production. Hence, a compromise has to be drawn on certain issues, which in the case of CVD is the presence of catalyst particles in the produced nanotubes. CVD for its ability to produce large quantity of nanotubes with reasonable quality has attracted significant attention in the past few years. Moreover, this technique is especially useful for applications that are either benefitted by the presence of the catalyst particles or not severely affected by them.

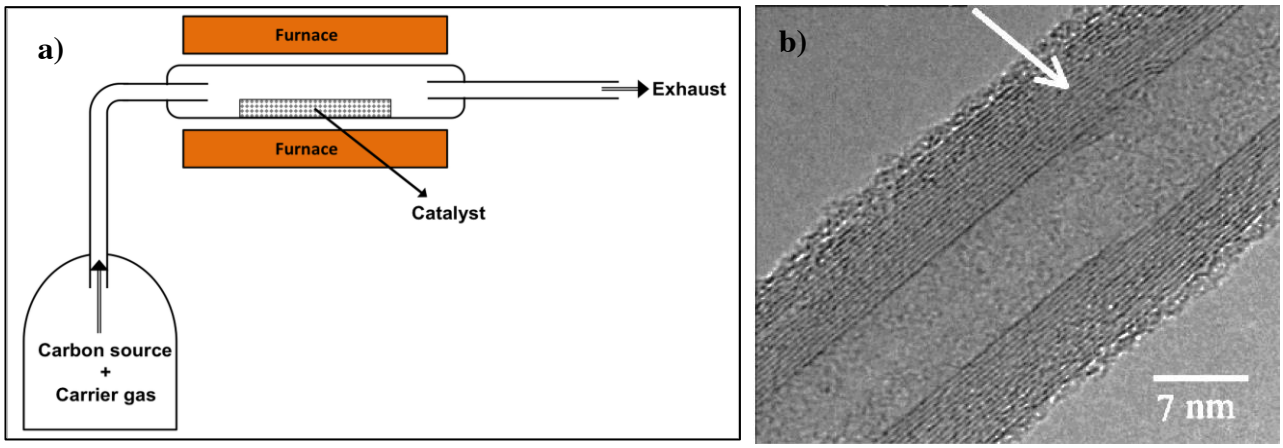


Figure 2-7. a) Schematic of the CVD technique, b) TEM image of a well-graphitised MWCNT produced by this technique[52].

The nanotube growth mechanism in a CVD process usually involves[53]:

Step 1) Dissociation of the hydrocarbons that are catalysed by the metal nanoparticles.

Step 2) Dissolution and diffusion of the carbon through the catalyst.

Step 3) Carbon precipitation from the saturated metal catalyst that leads to the formation of nanotubes.

Depending on the size of the catalyst particles and the substrate/catalyst interaction, two growth mechanisms can be described:

Mechanism 1) When the interaction between the catalyst and the substrate is weak, the carbon precipitation occurs below the catalyst particle, and the nanotube grows by pushing the catalyst away from the substrate (Figure 2-8a). The nanotube continues to grow as long as there is scope of further hydrocarbon decomposition on the catalyst surface and the growth ceases when the catalyst particle is covered with excess carbonaceous material. This is tip-growth.

Mechanism 2) When the catalyst particle strongly adheres to the substrate, the precipitated carbon cannot push the catalyst particle away from the substrate due to the strong interaction. Hence, the hydrocarbons are forced to eject from the top part of catalyst, which then extends to form a nanotube. This is base-growth (Figure 2-8b).

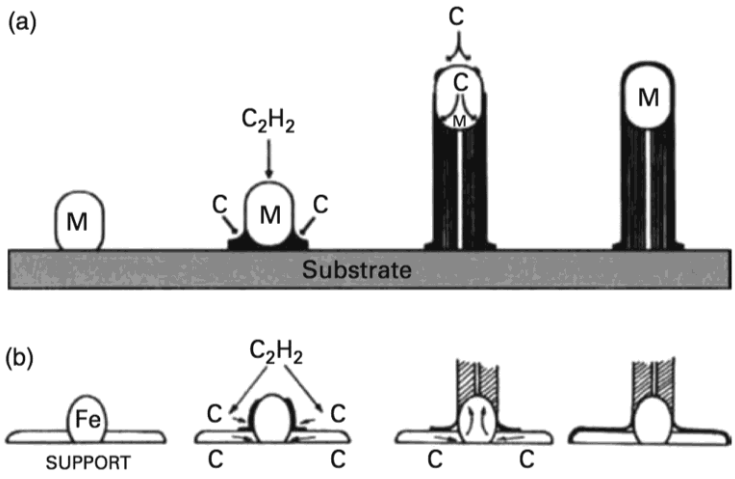


Figure 2-8. Illustration of the nanotube growth mechanism: a) tip-growth, b) base-growth[13]; C- Carbon, M- Metal catalyst particle.

Whether to use tip-grown or base-grown nanotubes depends on the application, especially for those applications where the presence of the metal particle in a certain

location is crucial. Sohn *et al*.[54] reported 80 mA/cm^2 field emission current density at 3 V/μm in their CVD-produced MWCNTs and attributed these properties to the base-growth of the nanotubes. The authors suggested that the open tip structure of the nanotubes, their strong adhesion to the substrate via the catalyst particles, and their good electrical contact with the electrode due to the metal catalyst at the bottom of the nanotube helped in improving the field emission properties.

It should be noted that most of the CVD-produced nanotubes are a combination of tip- and base- grown nanotubes. Whether a nanotube grows by tip- or base- growth is difficult to control and techniques for achieving purely tip-grown or base-grown nanotubes have not been successful till date. Furthermore, it is difficult to comprehend whether the catalyst remains in a solid state or transforms to a liquid state during the carbon precipitation. Due to the nano size of most of the metal catalyst particles (*ca*. 10 nm) it is likely that their melting points are lowered (*ca*. 600 – 900 °C) than usual (*ca*. 1500 °C), thus suggesting the possibility of their transformation to liquid state. Despite intensive research, it is still not clear if the diffusion of the carbon occurs in bulk or if it pertains to just the catalyst surface. *In situ* studies have revealed instances of pure bulk diffusion[55] and pure surface diffusion[56] through high-resolution TEM imaging. However, the environment in a TEM is not comparable to that of a reactor, making it difficult to extend these results to reactor synthesis. Moreover, the possibility of a combination of both bulk and surface diffusion cannot be ruled out as well. It is important to determine the key mechanisms in the nanotube growth as a better understanding of the mechanisms will certainly help in producing well-defined homogeneous nanotubes on a larger scale with reproducible and desired structures. Thus, this area requires further investigation and is beyond the scope of this thesis.

In order to upscale the production of nanotubes, several methods based on CVD have been reported in recent years: spray pyrolysis[57], catalytic CVD (CCVD)[58], aerosol assisted CVD (AACVD)[46], and plasma-enhanced CVD[59]. In most of these techniques, nanotubes are produced by pyrolysis of hydrocarbons in the gas phase. The hydrocarbons can be introduced into the CVD reactor from a liquid precursor that can be injected into the reactor through atomisation, in which case the technique is called AACVD. If the liquid precursor is instead sprayed using a spray injector, it is spray pyrolysis CVD. Introducing catalysts by depositing them on a substrate significantly enhances the hydrocarbon pyrolysis; this is CCVD. Alternatively, both the catalyst particles and the hydrocarbon feedstock can be simultaneously injected into the reactor, such as a combination of CCVD and AACVD – AACCVD, which has several advantages over the other CVD techniques[60]:

a) Compared to other CVD routes AACCVD simplifies the process of generating and delivering the vapour precursor to the reactor, hence reducing the costs involved in the deposition process.

b) The chemical precursors are usually combined into a single source precursor in AACCVD, which allows production of materials with controlled stoichiometry.

c) In this technique, the catalyst particles are produced *in situ*, thus eliminating the catalyst preparation step.

d) It uses mild synthesis conditions for the nanotube production (*ca*. 600–900 °C for MWCNTs and *ca*. 1000–1200 °C for SWCNTs) with the possibility of continuous production. Moreover, unlike other CVD techniques, AACCVD does not require sophisticated reactors; hence it is a relatively low cost process.

e) It has the potential for upscale production, which is beneficial for commercialisation.

f) It aids in producing clean and aligned nanotubes along with doped nanotubes without employing flammable or corrosive gases[42], which is a major advantage over other techniques.

g) There have been reports of efficiently controlling the morphology and the structure of the doped nanotubes using this technique by merely using different precursors[32,42] or by adding specific dopant containing hydrocarbons[46] to the precursors.

Hence, AACCVD was chosen to be the best-suited technique for producing the nanotubes required for this work. Conventional MWCNTs synthesised by AACCVD can be up to 1 cm in length and usually possess large diameters of up to 100 nm and 3 to > 100 inner walls[42,46]. However the AACCVD-produced MWCNTs usually present some structural disorder. A typical Raman spectrum of an AACCVD-produced MWCNTs is shown in Figure 2-9, where the intensities of different peaks in the spectrum can be related to the defects in the nanotubes. A strong D peak (at *ca*. 1338 cm^{-1}) that signifies the defect quantity[45] in the nanotubes can be clearly seen in this spectrum, along with a strong G peak (at *ca*. 1570 cm^{-1}) that relates to the degree of graphitisation[61]. A 2D peak (at *ca*. 2676 cm^{-1}) that indicates long-range ordering[61] in the nanotubes can also be seen.

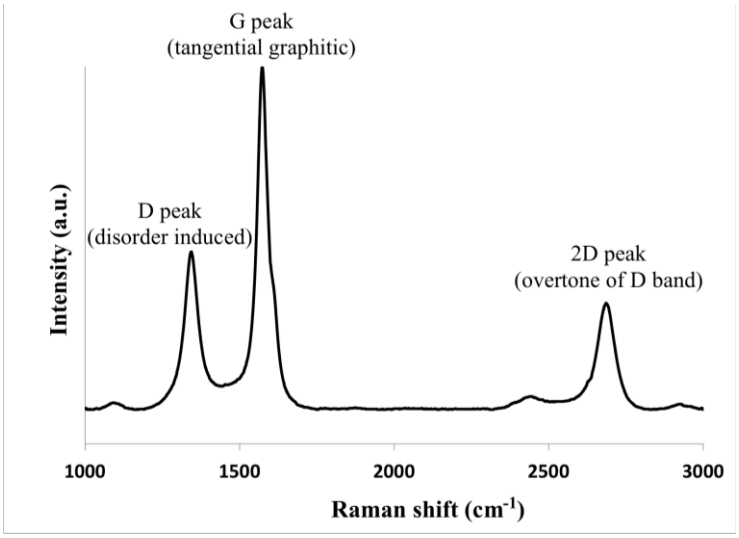


Figure 2-9. Typical Raman spectrum of AACCVD-produced MWCNTs.

2.4. Insulating carbon nanotubes

When nanotubes are used as reinforcements in polymer composites, the nanotube/polymer interface becomes crucial for the composite performance. When applications of such composites involve dielectrics, the conducting nature of the nanotubes can be disadvantageous. Nanotubes are effective in improving the dielectric properties of the nanotube/polymer systems until their concentration reaches a certain critical value (generally referred to as percolation threshold) beyond which they form a conducting path that results in a dielectric breakdown along with an increase in the dielectric losses[62–64]. However, there is a significant improvement in the dielectric constant at the percolation threshold due to interfacial polarisation effects arising from the nanotube/polymer interfaces[64,65]. Hence, forming an insulating layer on the individual nanotubes can avoid the formation of a conductive path and can aid in accommodating more nanotubes in the polymer matrix without causing capacitor failure.

A widely used technique to achieve this is to wrap the individual nanotubes with insulating polymers[66], inorganic metal oxides or hydroxides[67]. Wrapping of both SWCNTs and MWCNTs with polymers has been widely studied due to its potential for creating a variety of hybrid nanostructures. However, its application is limited due to the agglomeration of polymers and formation of irregular deposits. On the other hand, inorganic metal oxides such as aluminium oxide and silicon oxide offer better long-term stability and relatively superior insulating properties. In this work, silicon oxide coatings were deposited over the nanotubes in order to benefit from the inherent electrical insulation and dielectric strength of silicon oxide (5 – 10 MV/cm)[68].

2.5. Experimental procedure and characterisation

2.5.1. Synthesis of conventional, doped, and silica covered MWCNTs

AACCVD was used for synthesising conventional and doped MWCNTs (N, B). The experimental set-up comprised of an aerosol generator driven by a piezo (RBI Pyrosol 7901), a single zone horizontal tubular electric furnace (Elite Thermal Systems, 60 cm long, and 4 cm internal diameter), an n-type thermocouple, a temperature controller (Eurotherm 2416), and a quartz tube (Robson Scientific, 80 cm long, and 2.1 cm internal diameter) (Figure 2-10). The aerosol unit was firstly filled with the required precursor and was connected to one end of the quartz tube that was previously cleaned with ethanol and dried. The other end of the quartz tube was connected to an acetone trap to capture any by-products from the reactions such as soot or liquid hydrocarbons. The acetone trap was further connected to an exhaust. Once all the connections were sealed, the furnace was heated to the required temperature. The system was simultaneously flushed with argon for 10 minutes to remove any unwanted oxygen from the reactor. Once the desired temperature was reached, the amplitude and frequency of the aerosol generator were adjusted till a visually dense aerosol was generated. The aerosol was then directed into the reactor using argon as a carrier gas at a flow rate of 2.5 l/min. After the required synthesis time, the aerosol flow was stopped and the furnace was left to cool to room temperature under reduced argon flow. The quartz tube was then carefully removed and the nanotubes were gently scraped from the inner cylindrical wall of the quartz tube using a metallic spatula. From previous research[69], it has been realised that a small area at the start and end of the quartz tube usually consists of liquefied aerosol and amorphous carbon respectively. Hence, care was taken to avoid materials from a

10 cm long area after and before the start and end points of the tube (indicated as 'a' and 'b' in Figure 2-10 respectively).

The work of Koós *et al.*,[32,42,46] was used as a guideline for selecting the MWCNT synthesis parameters. Table 2-1 lists the precursors used for producing different MWCNTs along with their synthesis details.

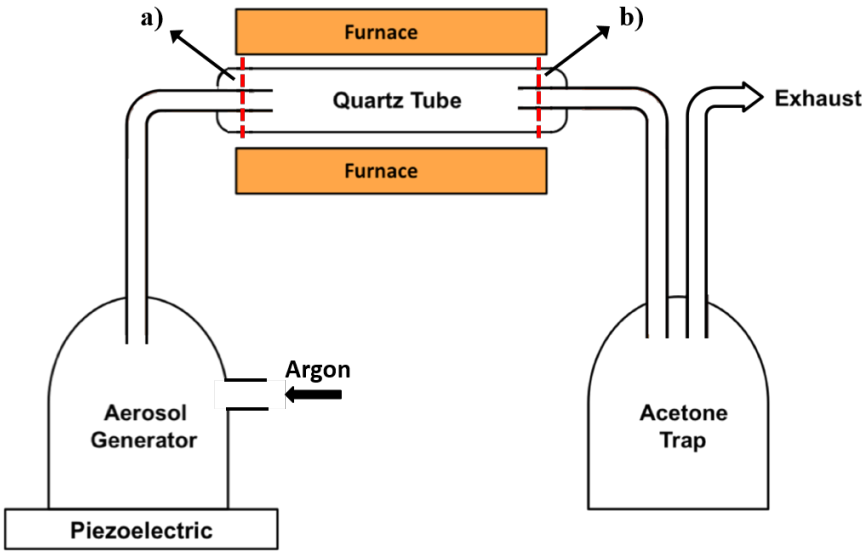


Figure 2-10. Schematic of the AACCVD setup used in this work. The area between 10 cm after the start position 'a' and 10 cm before the end position 'b' was considered for collecting the nanotubes.

MWCNT type	**Precursor**	**Synthesis temperature (°C)**	**Synthesis time, (minutes)**
Conventional MWCNTs	95 wt.% Toluene ($C_6H_5CH_3$, Fluka, 99.7%), 5 wt.% Ferrocene ($Fe(C_5H_5)_2$, Sigma-Aldrich, 98.0%; post-purified by sublimation at 95 °C)	800	30
N-MWCNTs	95 wt.% Benzylamine ($C_6H_5CH_2NH_2$; Fluka; 99.7%), 5 wt.% Ferrocene	800	30
B-MWCNTs	90 wt.% toluene, 1 M Triethylborane in hexanes ($(C_2H_5)_3B$, $CH_3(CH_2)_4CH_3$; Aldrich), 5 wt.% Ferrocene	1000	10

Table 2-1. List of precursors used for the synthesis of conventional and doped MWCNTs along with the synthesis parameters

A portion (*ca*. 30 mg) of the as-synthesised conventional and doped MWCNTs was further processed for depositing a silica coating over the nanotubes. This was accomplished through the sol-gel technique proposed by Seeger *et al*.[67]:

Step1) 1 mg/ml nanotube dispersions were formed in 0.1% aqueous polyethylenimine (PEI) (Sigma Aldrich, average M_w – 25,000) by sonicating them for 24 hours using an Ultrawave U1250D ultrasonic bath (200 W, 30–40 kHz). Any residual PEI was separated using a Rotanta 460R centrifuge (3250 rpm, 4 hours).

Step 2) A sol was formed by mixing Tetraethylorthosilicate (TEOS) (Sigma Aldrich 98.0%), Ethanol (EtOH) (Sigma Aldrich 99.5%), and water (pH – 6) in a mass ratio of 2:1:4.

Step 3) After 48 hours the sol was mixed with the nanotube dispersion in a mass ratio of 1:5 and was sonicated for 8 hours to avoid any phase separation. The mixture was then heated at 300 ^{o}C for 1 hour in argon atmosphere to allow adsorption of TEOS on the nanotube surface. It should be noted that the heat treatment procedure further decomposes TEOS into silica (Equation 2-1), resulting in a silica coating on the MWCNTs. From here on, the non-silica coated MWCNTs will be addressed as pristine MWCNTs.

$$Si(OC_2H_5)_4 \rightarrow SiO_2 + 2\,C_2H_5OH + 2\,C_2H_4 \qquad \text{Equation 2-1}$$

2.5.2. Characterisation of conventional and doped MWCNTs

Jeol JSM-840F and Jeol 6500F scanning electron microscopes (SEMs) in secondary electron imaging mode at 5–10 kV acceleration voltages were used for determining the lengths of the nanotubes. Samples for SEM were prepared by sprinkling the MWCNTs on conductive carbon tabs that were mounted on aluminium stubs. On the other hand, the nanotube internal structure and diameters were examined using a Jeol JEM-2000FX transmission electron microscope (TEM) at 200

kV acceleration voltage. Samples for TEM were prepared by sonicating few milligrams of MWCNTs in acetone for 30 seconds and drop casting 3–4 droplets of the dispersion onto lacey carbon copper grids and drying them overnight. The lengths and diameters were calculated from the micrographs using the ImageJ software. An average of 100 nanotubes was used to estimate the MWCNT lengths and outer diameters.

The defects in the nanotubes were studied using a Horiba Jobin Yvon LabRam Aramis Raman spectrometer (532 nm green laser) at room temperature. Samples for Raman were prepared by placing few drops of the nanotube dispersions in acetone on clean microscopy glass slides and drying them overnight. The defect peak intensity ratios were manually calculated from the Raman spectra and were used for understanding the defects. An average of 7 spectra was taken to calculate the intensity ratios for every batch of nanotubes. Additionally, the oxidation resistance of the nanotubes and their iron catalyst content was investigated using a Perkin Elmer Pyris thermogravimetric analyser (TGA) by heating *ca*. 4 mg of each type of MWCNTs in air from 50–900 °C at a rate of 10 °C/min. 3 TGA runs were conducted on each batch of nanotubes, and the oxidation resistance values were averaged.

2.5.3. Characterisation of silica covered MWCNTs

The extent of the silica coverage on the nanotubes was studied using a Jeol 2010 TEM (200 kV accelerating voltage) equipped with an Oxford Instruments LZ5 windowless energy dispersive X-ray (EDX) spectrometer. Furthermore, a VG HB501A scanning transmission electron microscope (STEM; 100 kV accelerating voltage) with a Gatan 666 EELS spectrometer with a spot size of 1 nm was used to conduct electron energy loss spectroscopy (EELS) line scans to evaluate the composition of the coating. The small spot size of STEM allowed local spectroscopy

of the sample and provided accurate chemical composition of the coating. The sample preparation for these studies was similar to the TEM sample preparation discussed in §2.5.2.

2.6. Results and discussion

2.6.1. Length analysis by SEM

Table 2-2 lists out the lengths of pristine conventional, N-, and B- MWCNTs produced using AACCVD and Figure 2-11 shows the respective SEM images. It can be observed from the SEM images that the nanotubes predominantly agglomerated into bundles. Moreover, it was found that bundles from the same batch exhibited a large distribution of lengths. This is due to the variation of growth parameters, especially temperature and catalyst concentration in various parts of the quartz tube. When an aerosol is directed into the quartz tube, it decomposes unevenly due to the variation in temperature along the quartz tube, resulting in different catalyst concentration in different parts of the quartz tube[45]. As the nanotube growth mechanism in AACCVD is based on nucleation from the catalyst particles, the rate of nanotube growth is different in different parts of the quartz tube. Furthermore, MWCNT doping had a drastic effect on its length and structure. Figure 2-11a,b shows bundles of wavy conventional MWCNTs containing many kinks, lengths of which were calculated to be 200±28 μm. However, nitrogen doping reduced the nanotube length to almost a quarter of the conventional MWCNT length, *i.e.*, 51±12 μm (Figure 2-11c,d). Moreover, N-MWCNTs appeared to be straighter with fewer kinks. During the nanotube growth, nitrogen atoms in the growing edge are likely to be more stable than the ones within the hexagonal carbon lattice[41]. This causes the nanotube edge to be filled with nitrogen atoms, thereby saturating it. For the nanotube

to grow any further, the nitrogen atoms saturating the tube edge need to be replaced by carbon atoms or form defects. This results in inhibition of the nanotube growth, resulting in shorter nanotubes in N-MWCNTs. On the contrary, B-MWCNTs formed wool-like long structures (Figure 2-11e), which made the identification of nanotubes and their length calculation difficult. Hence, a definite nanotube length for the B-MWCNTs could not be established. B-MWCNTs were of spongy nature and appeared relatively thick (Figure 2-11f). Unlike nitrogen, boron promotes nanotube growth by acting as a surfactant (as explained in §2.2). Boron atoms preferentially substitute carbon atoms at the end of nanotubes during the growth and form pentagons leading to a partial closure of the nanotube[43]. However, the boron bonds break easily resulting in the re-opening of the nanotube structure. This allows the pentagons at the end of the tube to form hexagons when exposed to carbon atoms from the vapour phase, which allows the nanotubes to grow further. Consequentially, an increase in the length is observed for B-MWCNTs.

Type of MWCNTs	**Length (µm)**	**Diameter (nm)**
Conventional MWCNTs	200 ± 28	67 ± 14
N-MWCNTs	51 ± 12	25 ± 6
B-MWCNTs	-	88 ± 22

Table 2-2. Lengths and diameters of pristine MWCNTs produced by AACCVD.

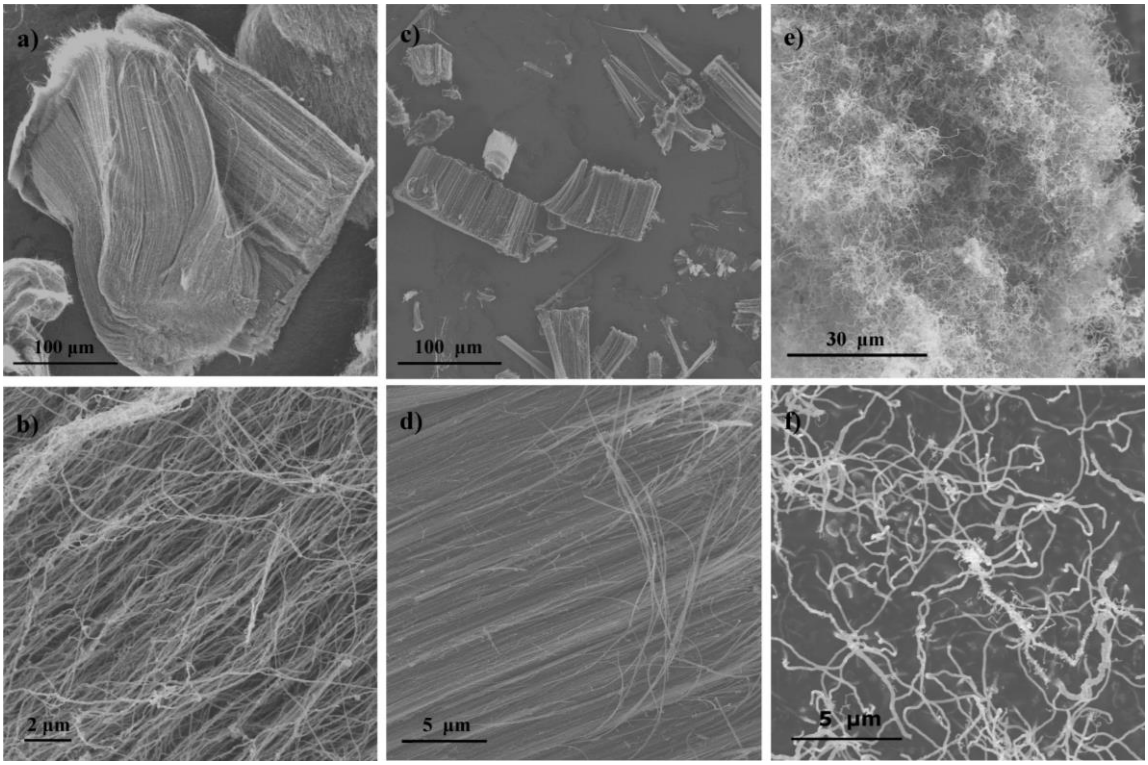


Figure 2-11. Low and high resolution SEM images of pristine MWCNTs produced by AACCVD: (a,b) Conventional MWCNTs, (c,d) N-MWCNTs, (e,f) B-MWCNTs.

2.6.2. Structural and diameter analysis by TEM

TEM images of pristine conventional and doped MWCNTs (Figure 2-12a-f) showed no signs of amorphous carbon implying that the nanotubes were clean. However, a number of iron catalyst particles seemed to be encapsulated in the inner core of the nanotube structure or attached to the surface, which is typical to AACCVD[70,71]. TEM studies of conventional MWCNTs (Figure 2-12a,b) revealed that the inner structure of these nanotubes was hollow and clearly showed evidence of many kinks. The average outer diameter of conventional MWCNTs was measured to be 67±14 nm. Comparing these to the TEM images of N- and B- MWCNTs (Figure 2-12c,e), a significant change in the internal structure of the nanotubes can be observed. N-MWCNTs (Figure 2-12c,d) exhibited straighter tubes with corrugated walls, and a stacked cone structure. Such structures are also known as 'bamboo-like' structures, where the internal part of the tube is separated into a series of

compartments. During the nanotube growth, nitrogen promotes nanotube closure (as explained in §2.2) and leads to an increase in defect density that induces curvature in the graphitic layers resulting in the bamboo-like structure[41,46,72]. The outer diameter of the N-MWCNTs was 25±6 nm; clearly the N-MWCNTs were narrower than the conventional MWCNTs. On the other hand, B-MWCNTs (Figure 2-12e,f) exhibited a curvy and distorted structure with many knees, along with a nested-cone shaped internal structure with entrapped iron particles. Unlike N-MWCNTs, the outer diameter of B-MWCNTs increased to 88±22 nm when compared to conventional MWCNTs. This is because boron promotes nanotube formation as discussed earlier. Furthermore, according to literature, the core cone-structure of the B-MWCNTs is well-defined and consists of boron while the outer structure is disordered and consists of only carbon[29,73]. Also, the concentration of boron within these cores can vary along the nanotube, thereby introducing changes in its physical and chemical properties locally within the nanotube[73].

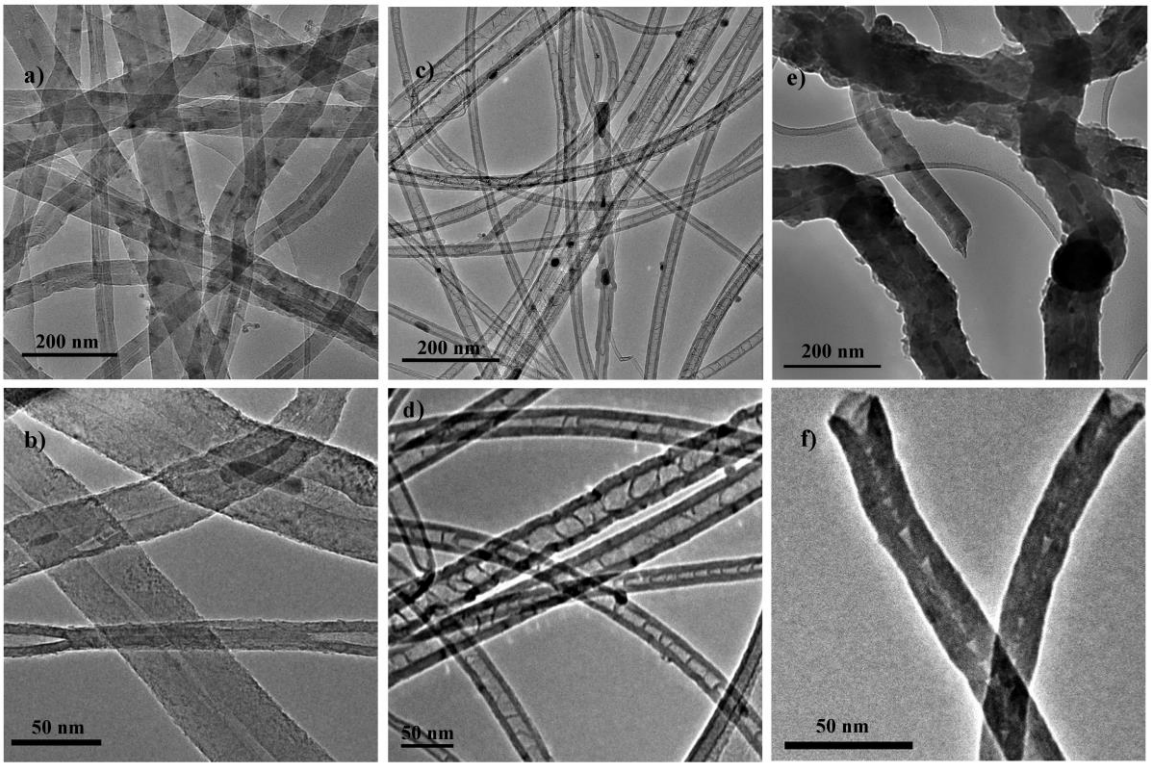


Figure 2-12. TEM images of pristine MWCNTs produced by AACCVD: (a,b) Conventional MWCNTs, (c,d) N-MWCNTs, (e,f) B-MWCNTs.

2.6.3. Defect analysis by Raman spectroscopy

In a typical Raman spectrum of MWCNTs (Figure 2-9), three major peaks are generally observed:

a) D peak at *ca*. 1350 cm^{-1}, which relates to the disorder in the structure. The D peak is associated with the defect quantity and size of crystallites in the MWCNTs[45].

b) G peak at *ca*. 1550–1600 cm^{-1}, which is a characteristic of sp^2 carbon networks and can be associated with in-plane hexagonal ordering of the carbon atoms. The G peak suggests the graphitisation of the MWCNTs[61].

c) The overtone or second-order harmonic of the D peak – the 2D peak at *ca*. 2700 cm^{-1}, which is a result of a double-resonance scattering process involving two phonons and the creation of inelastic phonons. The 2D peak is specifically sensitive to the number of graphitic layers and nanotube walls; indicating long-range ordering[61].

Figure 2-13 shows the original Raman spectra of the pristine conventional and doped MWCNTs used in this work. Table 2-3 lists out their respective I_D/I_G and I_{2D}/I_G Raman intensity ratios. It can be observed from Table 2-3 that nitrogen and boron doping resulted in an increase in the I_D/I_G and a decrease in I_{2D}/I_G intensity ratios. These intensity ratios are associated with defects and impurities in the nanotubes, therefore it can be confirmed that doping resulted in an increase in the defect density. This can also be seen in Figure 2-13, where the Raman spectra of N-, B- MWCNTs show an increase in the intensity of the D line and decrease in the intensity of the 2D line compared to their conventional counterpart. The increase in the I_D/I_G intensity ratio indicates an increase in the disorder and corrugated nature of nanotube walls. Also, the monotone increase in the intensity of the D line and decrease in the intensity of the 2D line of N-MWCNTs suggests an evident degradation of the carbon hexagonal lattice[74]. Moreover, the I_D/I_G intensity ratio of N-MWCNTs was almost close to 1, which signifies a decrease in its crystallinity. This

effect was stronger in N-MWCNTs than in B-MWCNTs, contradicting the observations of Koós *et al*.[42], where B-MWCNTs had a stronger effect on defect density compared to N-MWCNTs. However, it should be noted that the difference in the intensity ratios reported by Koós *et al*. and in this work is not more than 0.1 units.

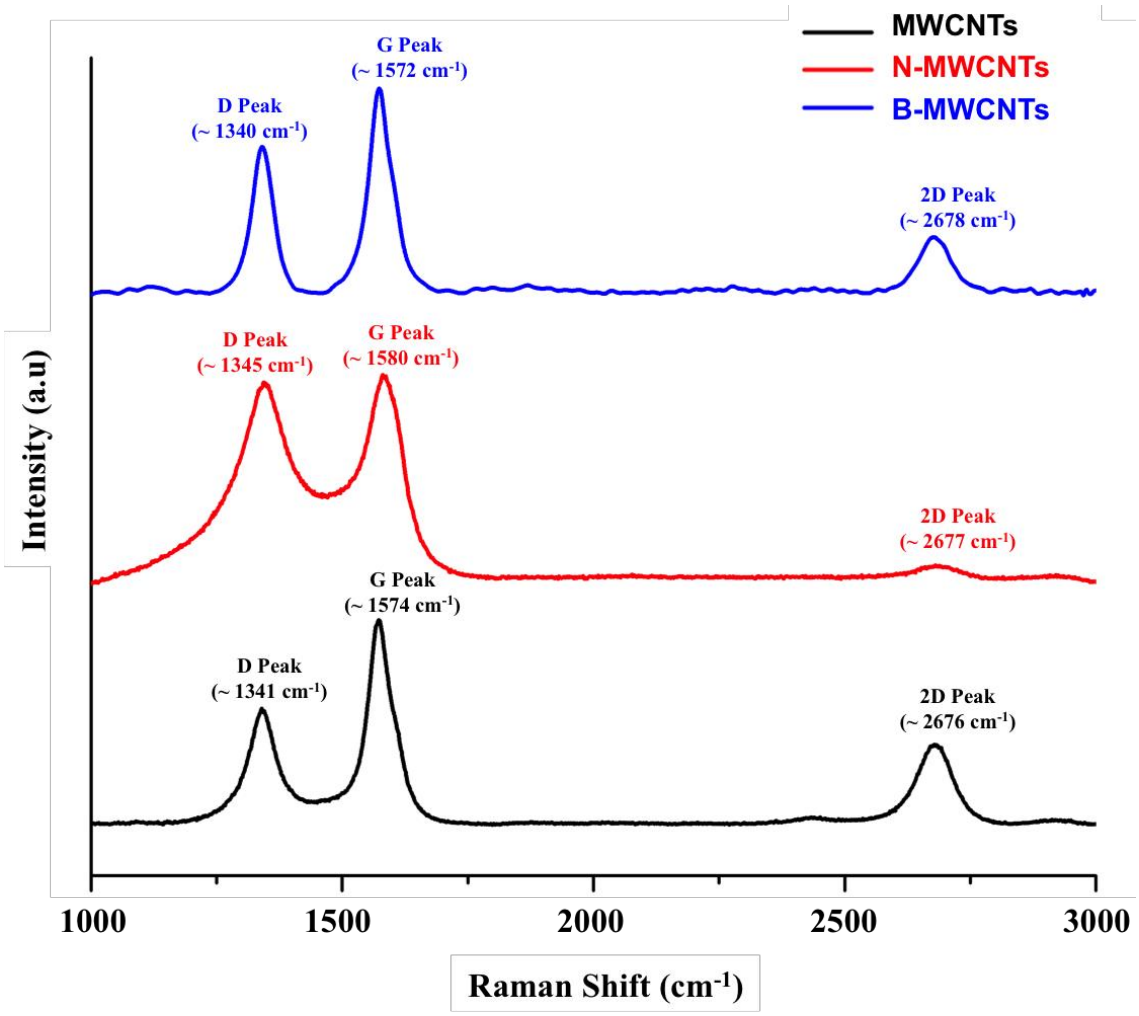


Figure 2-13. Raman spectra of pristine MWCNTs showing the variation in the defect peaks in different nanotubes. All spectra are normalised with respect to the G band intensity.

Type of MWCNT	I_D/I_G	I_{2D}/I_G
Conventional MWCNTs	0.56 ± 0.01	0.36 ± 0.02
N-MWCNTs	0.90 ± 0.03	0.12 ± 0.04
B-MWCNTs	0.75 ± 0.02	0.26 ± 0.04

Table 2-3. Raman intensity ratios: I_D/I_G and I_{2D}/I_G of pristine MWCNTs.

2.6.4. Oxidation studies using TGA analysis

In this work, the oxidation resistance of the MWCNTs is defined as the temperature range where 20–80% mass loss of the sample occurs ($T_{20\%}$, $T_{80\%}$ respectively). The calculated oxidation resistance values of pristine MWCNTs are listed in Table 2-4. Also, the amount of residual catalyst was calculated using Equation 2-2 and the calculated values are listed in Table 2-4.

$$\%\ \text{residual catalyst} = \frac{\text{Final Weight}}{\text{Initial Weight}}\ 100 \qquad \text{Equation 2-2}$$

It can be observed that the oxidation resistance of N-MWCNTs decreased compared to that of conventional MWCNTs. This can also be seen from the TGA graphs in Figure 2-14, where a sharp decrease in % weight can be observed in the spectra of N-MWCNTs. This could be due to the change in nanotube structure (as seen in Figure 2-12) that results in an increased reactivity of the nanotube walls, in addition to the increased number of defects in the N-MWCNTs as confirmed by the Raman studies (Table 2-3). Also, the TGA behaviour of N-MWCNTs suggests that oxidisation perhaps occurs along the entire nanotube surface, unlike conventional MWCNTs that oxidise just at the tips or at randomly distributed defects[42]. On the

contrary, presence of boron seemed to have inhibited nanotube oxidation and resulted in an increase in oxidation resistance (Table 2-4). Based on similar results reported in literature, this effect can be explained by the following theories:

i) Influence of boron on the electron structure of carbonaceous material[75]: the substitutional nature of boron atoms re-distributes the π electrons in the nanotube, which changes the number of charge carriers, lowering the Fermi level of the nanotube. This is likely to inhibit desorption of CO and CO_2.

ii) An improvement in the graphitisation of the nanotubes by substitutional boron[75].

iii) Active site blocking[76]: Formation of oxides, such as B_2O_3, on the nanotube surface that acts as a diffusional barrier which delays oxidation.

Another distinct effect due to doping was that the amount of catalyst content in the nanotubes was lower in the doped MWCNTs.

Type of MWCNT	Oxidation temperature at 20% mass loss, $T_{20\%}$ (°C)	Oxidation temperature at 80% mass loss, $T_{80\%}$ (°C)	Residual catalyst (wt. %)
MWCNTs	546.74	643.72	15.0
N-MWCNTs	507.23	598.69	10.9
B-MWCNTs	651.27	746.30	6.8

Table 2-4. Temperatures at which 20% and 80% mass loss occurs in the MWCNTs along with their catalyst content.

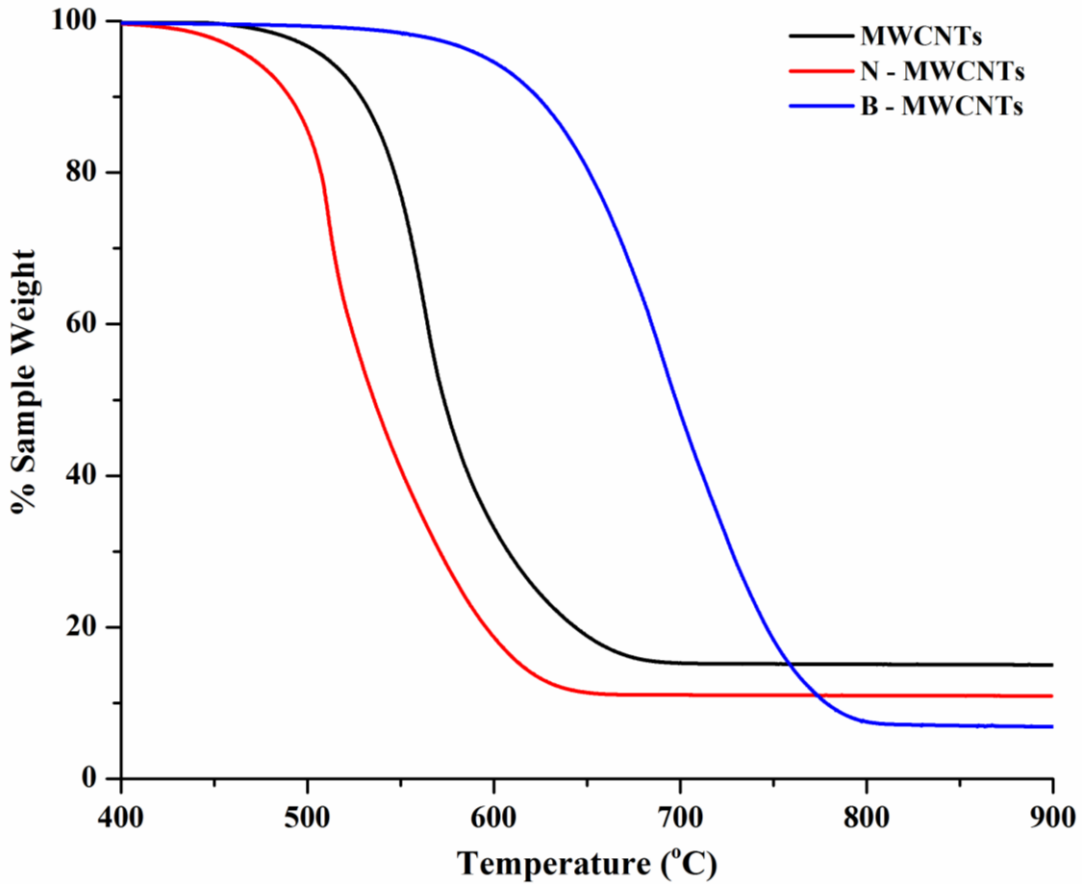


Figure 2-14. TGA measurements of pristine conventional and doped MWCNTs showing the effects of doping on the oxidation resistance.

2.6.5. Characterisation of silica coated MWCNTs

TEM studies coupled with EDX area scans were conducted on silica coated MWCNTs to understand the extent of silica coverage on the outer walls of the nanotubes. The extent of silica coverage was studied using TEM and the presence of silica coating was confirmed using EDX. Moreover, for accurate composition analysis of the coating, further investigations were conducted using STEM-EDX line scans and EELS.

a) TEM studies coupled with EDX

Figure 2-15 shows the TEM images and respective EDX area scans of silica coated MWCNTs (conventional and doped). From the TEM images (Figure

2-15a,c,e) it can be clearly seen that a rough non-uniform coating covered the surface of nanotubes. This coating appeared to have a strand-like structure and covered only parts of the nanotubes. Also, some nanotubes seemed to be not covered with any coating at all. However, even this amount of coverage was considered sufficient given the aim was to insulate the nanotubes from one another. The EDX area scans of all the three MWCNTs (Figure 2-15 b,d,f) revealed strong peaks of silicon, oxygen, iron, and copper. The peaks of silicon and oxygen confirm its presence in the coating. However, it is difficult to confirm its exact composition, but since silicon readily forms silicon oxide[77], it can be assumed that the coating was silica. The iron peaks relate to the encapsulated iron particles that served as a catalyst for the MWCNT synthesis, and the copper peaks relate to the lacey carbon copper grid. However, it should be noted that these EDX scans were area scans. Therefore, it is difficult to fully confirm whether the peaks relate purely to the coating over the nanotubes or from any silicon containing agglomerates in the neighbouring region.

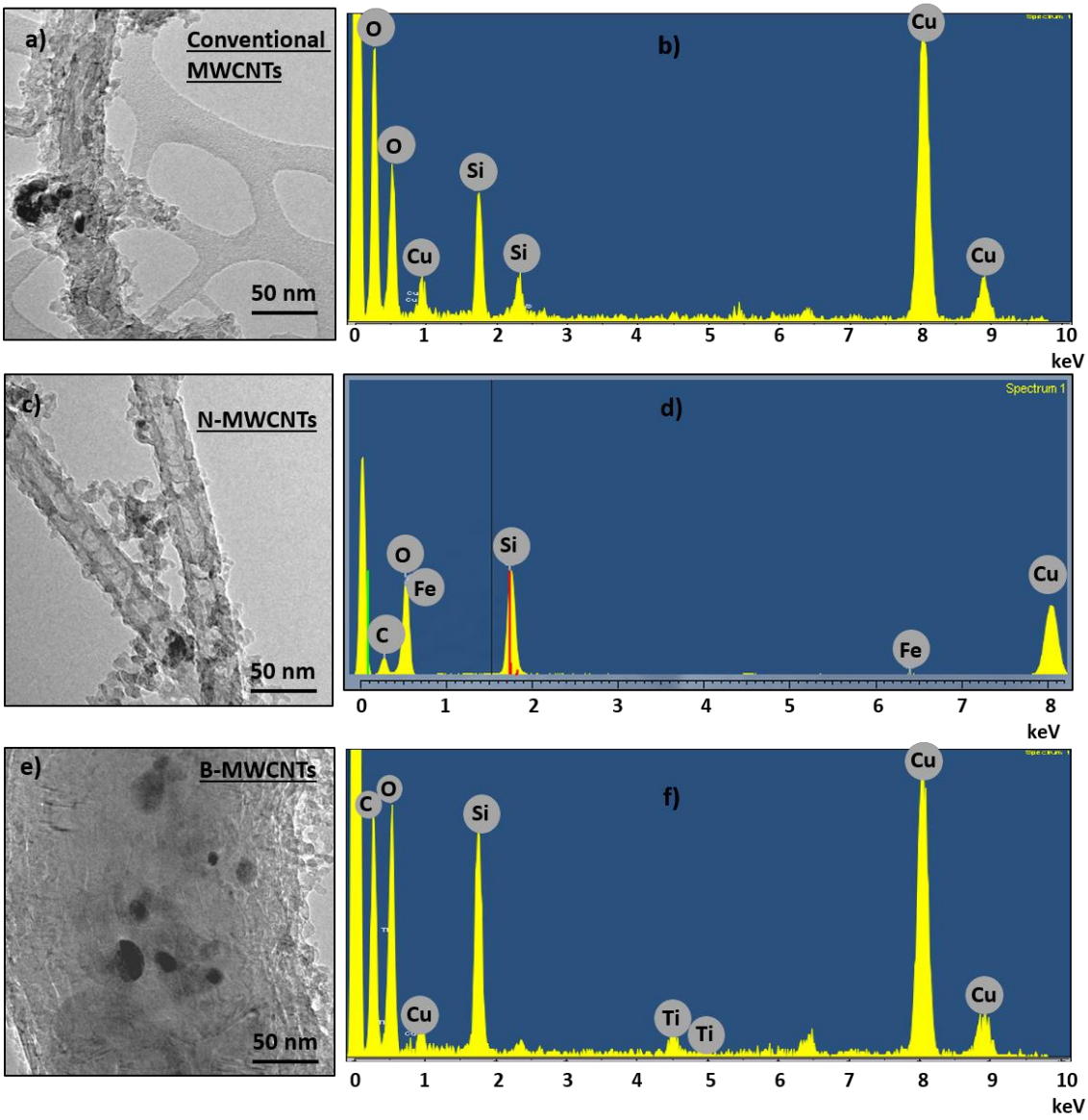


Figure 2-15. TEM images and their respective EDX area scans of silica covered MWCNTs: (a,b) Conventional MWCNTs, (c,d) N-MWCNTs, and (e,f) B-MWCNTs.

b) STEM and EELS

EELS line profiles coupled with STEM analysis were conducted in order to fully understand the composition of the coating covering the nanotubes. Due to the limited accessibility of the testing equipment, studies were conducted on silica covered conventional MWCNTs only. Figure 2-16 shows the STEM images of silica covered conventional MWCNTs at various locations of the sample along with their respective EELS line profiles. The STEM images show a non-contiguous particulate

coating surrounding the nanotubes that was roughly measured to be 5 nm thick. The blue and green lines in the EDX line scans correspond to silicon and oxygen, and the red line corresponds to carbon (*i.e.*, the MWCNT). It can clearly be seen that the silicon peaks were detected on both sides of the nanotubes, hence confirming the presence of silicon in the coating covering the nanotubes. On the other hand, presence of oxygen was detected all-along the nanotube, which is not unusual as oxygen could be present in the coating in the form of SiO_2 as well as within the nanotubes as iron oxide. Although, the STEM and EDX data confirm the presence of silicon and oxygen in the coating, the exact composition cannot be established from it. This ambiguity was solved by EELS studies. Figure 2-17 shows the EELS spectra from the particulate coating only. The green line corresponds to the spectrum from the coating and the blue line corresponds to a SiO_2 reference. An intensity peak at 106 eV corresponds to the contribution from SiO_2 (Si^{4+})[78], which can be evidently seen in both the reference sample and the coating. Moreover, the intensity peaks of the reference SiO_2 matches well with that of the coating. Hence, the composition of the coating around the conventional MWCNTs can be confirmed as SiO_2.

It should be noted that the same sol-gel recipe was followed for coating all the three types of MWCNTs (conventional and doped). Hence, it is only logical to extend the TEM, STEM, and EELS information from the silica covered conventional MWCNTs to the doped MWCNTs as well. Therefore, the coating covering the doped nanotubes (as seen in Figure 2-15c,e) is most likely to be SiO_2.

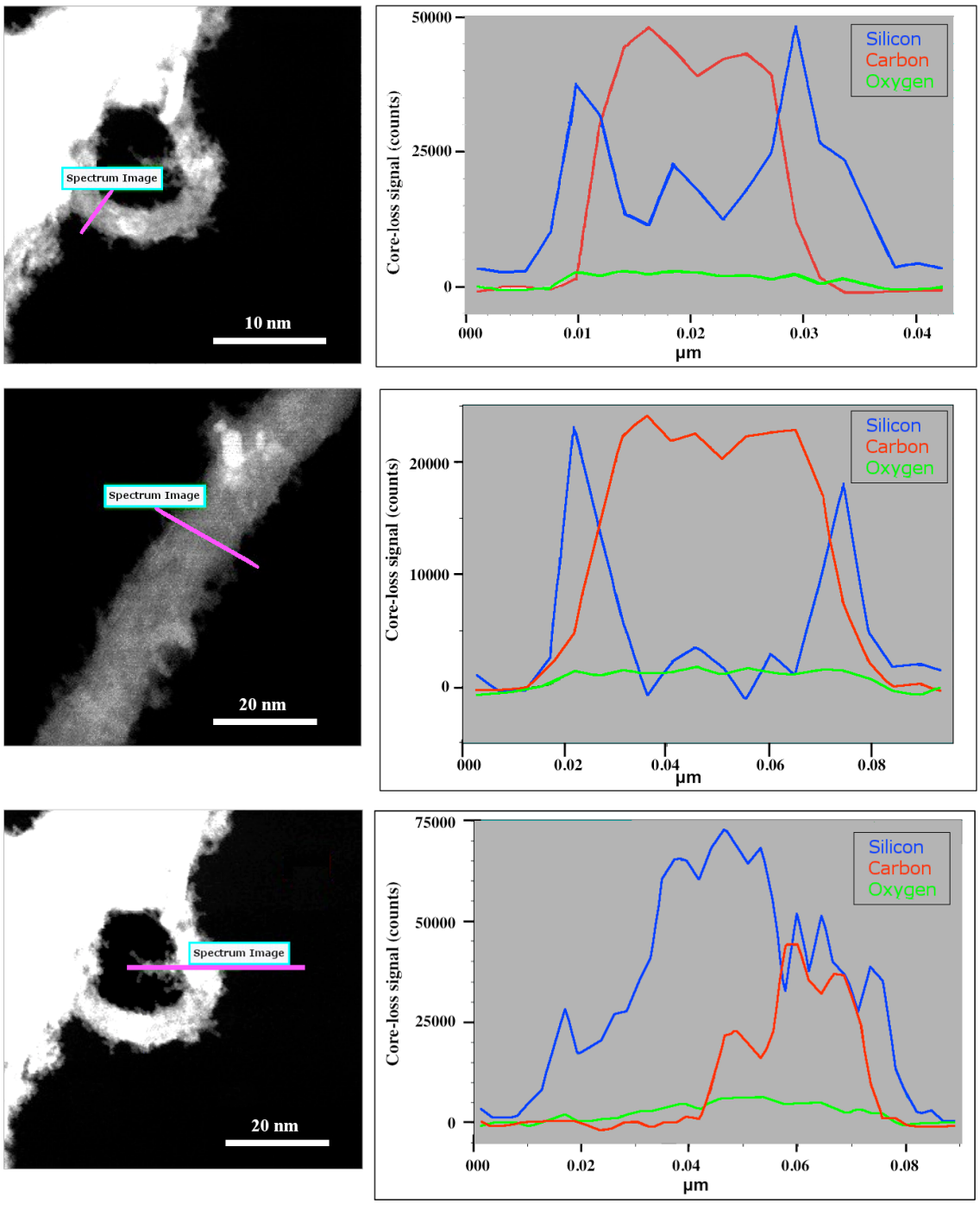


Figure 2-16. STEM images of silica coated conventional MWCNTs with their respective EDX line scans. The images belong to different areas of the same sample. (Scans conducted by Dr. Rebecca Nicholls.)

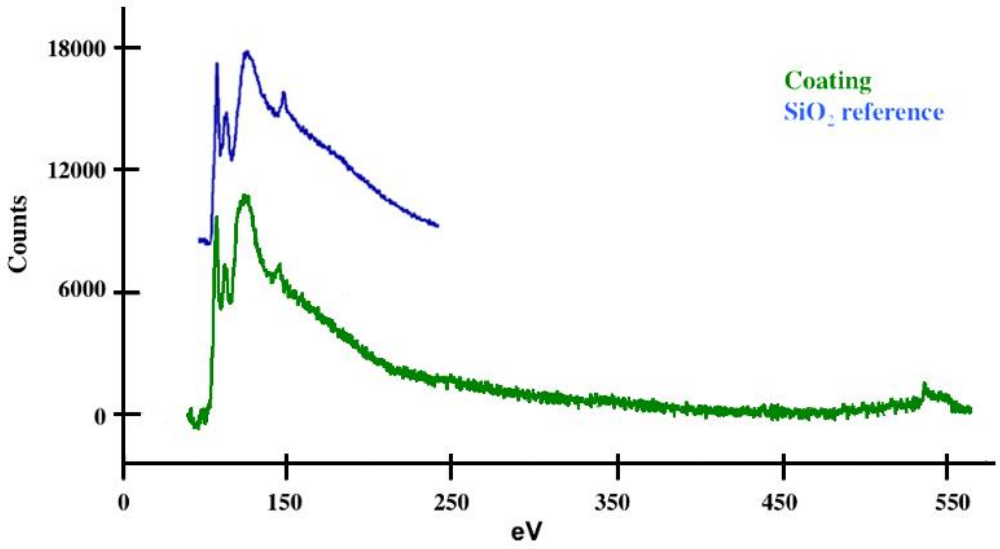


Figure 2-17. EELS spectra of the coating on the conventional MWCNTs. (Scan conducted by Dr. Rebecca Nicholls.)

2.7. Summary

The structural quality (such as short, long, coiled, aligned, curly, single-wall, and multi-wall) plays a key role in the applications of nanotubes, especially as fillers in composites[79,80]. Additionally, the presence of any unnecessary materials (such as amorphous carbon) in the nanotubes can potentially impede the composite properties. Hence, it is not only important to employ a set of well-defined nanotubes as fillers for composite applications but also to make sure they are clean from by-products. However, commercially available nanotubes are mostly inferior in quality as they contain a variety of nanotube structures along with carbonaceous by-products[7]. Hence, to control the type of nanotubes used in this thesis, they were synthesised in-house through AACCVD. The synthesis parameters presented in this chapter were carefully chosen and evaluated in order to produce larger batches (at least 300 mg) of well-defined clean nanotubes. The synthesis parameters, which are usually not presented in many research articles, are listed in detail in this chapter. The effect of variation in parameters was related to the difference in morphology of the resulting nanotubes.

These results provide a direct platform for tuning the structure with synthesis parameters and provide opportunities for synthesising nanotubes with specific morphologies for several applications.

Conventional, nitrogen, and boron doped MWCNTs that were required for this work were successfully synthesised using the AACCVD technique. It was observed that the produced nanotubes were agglomerated into aligned bundles and had a broad range of lengths and diameters, which is characteristic to AACCVD-produced MWCNTs. It would have been ideal to have a narrow range of lengths and diameters, however this was difficult to achieve due to the variation in synthesis parameters such as temperature and catalyst concentration along the length of the furnace. With respect to quality, the nanotubes were free from carbonaceous by-products such as amorphous carbon but seemed to have trapped many iron catalyst particles. Nonetheless, the synthesised MWCNTs were superior in quality to the commercially available MWCNTs and were considered acceptable for further dispersion studies and composite work reported in subsequent chapters.

Conventional MWCNTs were measured to be 200±28 μm in length with outer diameters of 67±14 nm. Upon doping with nitrogen, the lengths and diameters of the nanotubes decreased to 51±12 μm and 25±6 nm respectively. Moreover, nitrogen doping resulted in nanotubes with a bamboo-like internal structure. On the other hand, boron doping resulted in long, agglomerated nanotubes with increased outer diameters of 88±22 nm along with a nested-cone internal structure; the exact lengths of these nanotubes could not be measured due to agglomeration. Raman studies revealed an increase in the I_D/I_G and a decrease in the I_{2D}/I_G intensity ratios for N-, B-MWCNTs. The Raman intensity ratios usually relate to the defect densities and impurities in the nanotubes, which indicated an increase in the defect densities due to doping in this case. However, contrary to literature[42], nitrogen doping seemed to have

had a stronger effect on the defects than boron doping. TGA studies revealed that the oxidation resistance of N-MWCNTs decreased while that of B-MWCNTs increased, which was related to the structural changes induced by doping. Also, the amount of residual catalyst in the nanotubes decreased in doped MWCNTs.

The synthesised nanotubes were further processed for an insulation cover by depositing a silica coating over the nanotubes through sol-gel route. TEM studies with EDX area scans, and STEM studies with EELS line scans were performed on the silica covered nanotubes to understand the structure and composition of the coating. These studies confirmed the presence of silicon and oxygen in the coating. Furthermore, EELS studies accurately confirmed the composition of the coating as SiO_2. The silica coating was particulate in nature, approximately 5 nm thick, and covered the nanotubes non-uniformly.

2.8. References

[1] Krätschmer, W., Lamb, L. D., Fostiropoulos, K., and Huffman, D. R., "Solid C60: a new form of carbon," Nature, 1990, **347**(6291), pp. 354–358.

[2] Kroto, H. W., Heath, J. R., O'Brien, S. C., Curl, R. F., and Smalley, R. E., "C60: Buckminsterfullerene," Nature, 1985, **318**(6042), pp. 162–163.

[3] Iijima, S., "Helical microtubules of graphitic carbon," Nature, 1991, **354**(6348), pp. 56–58.

[4] Khan, Z. H., and Husain, M., "Carbon nanotube and its possible applications," Indian Journal of Engineering and Materials Sciences, 2005, **12**, pp. 529–551.

[5] Popov, V., "Carbon nanotubes: properties and application," Materials Science and Engineering: R: Reports, 2004, **43**(3), pp. 61–102.

[6] Bianco, A., Kostarelos, K., and Prato, M., "Applications of carbon nanotubes in drug delivery," Current Opinion in Chemical Biology, 2005, **9**(6), pp. 674–679.

[7] Grobert, N., "Carbon nanotubes – becoming clean," Materials Today, 2007, **10**(1-2), pp. 28–35.

[8] Grobert, N., "Nanotubes – grow or go?," Materials Today, 2006, **9**(10), p. 64.

[9] Oberlin, A., and Endo, M., “Filamentous growth of carbon through benzene decomposition,” Journal of Crystal Growth, 1976, **32**(3), pp. 335–349.

[10] Bacon, R., “Growth, structure, and properties of graphite whiskers,” Journal of Applied Physics, 1960, **31**(2), p. 283.

[11] Ebbesen, T. W., “Carbon nanotubes,” Annual Review of Materials Science., 1994, **24**, p. 235.

[12] Treacy, M. M. J., Ebbesen, T. W., and Gibson, J. M., “Exceptionally high Young’s modulus observed for individual carbon nanotubes,” Nature, 1996, **381**(6584), pp. 678–680.

[13] Harris, P. J. F., "Carbon nanotube science", 2009, Cambridge University Press, Cambridge, p. 179.

[14] Ebbesen, T. W., Lezec, H. J., Hiura, H., Bennett, J. W., Ghaemi, H. F., and Thio, T., “Electrical conductivity of individual carbon nanotubes,” Nature, 1996, **382**(6586), pp. 54–56.

[15] O’Connell, M. J., "Carbon nanotubes: properties and applications", 2006, CRC Press, Florida, p. 251.

[16] Collins, P. G., and Avouris, P., “Nanotubes for electronics,” Scientific American, 2000, **283**(62).

[17] Jorio, A., Dresselhaus, G., and Dresselhaus, M. S., eds., "Carbon nanotubes - advanced topics in the synthesis, structure, properties and applications", 2008, Topics in Applied Physics, New York.

[18] Baughman, R. H., Cui, C., Zakhidov, A. A., Iqbal, Z., Barisci, J. N., Spinks, G. M., Wallace, G. G., Mazzoldi, A., Rossi, D. D., Rinzler, A. G., Jaschinski, O., Roth, S., and Kertesz, M., “Carbon nanotube actuators,” Science, 1999, **284**(5418), pp. 1340–1344.

[19] Tans, S. J., Verschueren, A. R. M., and Dekker, C., “Room-temperature transistor based on a single carbon nanotube,” Nature, 1998, **393**(6680), pp. 49–52.

[20] Frackowiak, E., and Béguin, F., “Carbon materials for the electrochemical storage of energy in capacitors,” Carbon, 2001, **39**(6), pp. 937–950.

[21] Zhao, X., Hinchliffe, C., Johnston, C., Dobson, P., and Grant, P., “Spray deposition of polymer nanocomposite films for dielectric applications,” Materials Science and Engineering: B, 2008, **151**(2), pp. 140–145.

[22] Jung, Y. J., Kar, S., Talapatra, S., Soldano, C., Viswanathan, G., Li, X., Yao, Z., Ou, F. S., Avadhanula, A., Vajtai, R., Curran, S., Nalamasu, O., and Ajayan, P. M., “Aligned carbon nanotube-polymer hybrid architectures for diverse flexible electronic applications,” Nano Letters, 2006, **6**(3), pp. 413–8.

[23] Peigney, A., Laurent, C., Dumortier, O., and Rousset, A., "Carbon nanotubes–Fe–alumina nanocomposites. Part I: influence of the Fe content on the synthesis of powders," Journal of the European Ceramic Society, 1998, **18**(14), pp. 1995–2004.

[24] Lala, N. L., Thavasi, V., and Ramakrishna, S., "Preparation of surface adsorbed and impregnated multi-walled carbon nanotube/nylon-6 nanofiber composites and investigation of their gas sensing bility," Sensors, 2009, **9**(1), pp. 86–101.

[25] Zhang, G., Duan, W., and Gua, B., "Effect of substitutional atoms in the tip on field-emission properties of capped carbon nanotubes," Applied Physics Letters, 2002, **80**(14), pp. 2589–2591.

[26] Choi, W. B., Chung, D. S., Kang, J. H., Kim, H. Y., Jin, Y. W., Han, I. T., Lee, Y. H., Jung, J. E., Lee, N. S., Park, G. S., and Kim, J. M., "Fully sealed, high-brightness carbon-nanotube field-emission display," Applied Physics Letters, 1999, **75**(20), pp. 3129–3231.

[27] Hafner, J. H., Cheung, C. L., Woolley, A. T., and Lieber, C. M., "Structural and functional imaging with carbon nanotube AFM probes.," Progress in Biophysics and Molecular Biology, 2001, **77**(1), pp. 73–110.

[28] Planeix, J. M., Coustel, N., Coq, B., Brotons, V., Kumbhar, P. S., Dutartre, R., Geneste, P., Bernier, P., and Ajayan, P. M., "Application of carbon nanotubes as supports in heterogeneous catalysis," Journal of the American Chemical Society, 1994, **116**(17), pp. 7935–7936.

[29] Nicholls, R. J., Aslam, Z., Sarahan, M. C., Koós, A., Yates, J. R., Nellist, P. D., and Grobert, N., "Boron-mediated nanotube morphologies.," ACS nano, 2012, **6**(9), pp. 7800–5.

[30] Lolli, G., Zhang, L., Balzano, L., Sakulchaicharoen, N., Tan, Y., and Resasco, D. E., "Tailoring (n,m) structure of single-walled carbon nanotubes by modifying reaction conditions and the nature of the support of CoMo catalysts.," Journal of Physical Chemistry B, 2006, **110**(5), pp. 2108–15.

[31] Latil, S., Roche, S., Mayou, D., and Charlier, J. C., "Mesoscopic transport in chemically doped carbon nanotubes," Physical Review Letters, 2004, **92**(25), pp. 26805–1–4.

[32] Koós, A. A., Nicholls, R. J., Dillon, F., Kertész, K., Biró, L. P., Crossley, A., and Grobert, N., "Tailoring gas sensing properties of multi-walled carbon nanotubes by in situ modification with Si, P, and N," Carbon, 2012, **50**(8), pp. 2816–2823.

[33] Burch, H. J., Davies, J. A., Brown, E., Hao, L., Contera, S. A., Grobert, N., and Ryan, J. F., "Electrical conductance and breakdown in individual CN[sub x] multiwalled nanotubes," Applied Physics Letters, 2006, **89**(14), pp. 143110–1 – 143110–3.

[34] Duclaux, L., "Review of the doping of carbon nanotubes (multiwalled and single-walled)," Carbon, 2002, **40**(10), pp. 1751–1764.

[35] Terrones, M., Ajayan, P. M., Banhart, F., Blase, X., Carroll, D. L., Charlier, J. C., Czerw, R., Foley, B., Grobert, N., Kamalakaran, R., Redlich, P. K., Rühle, M., Seeger, T., and Terrones, H., "N-doping and coalescence of carbon nanotubes: synthesis and electronic properties," Applied Physics A-Materials, 2002, **74**(3), pp. 355–361.

[36] Hsu, W. K., Firth, S., Redlich, P., Terrones, M., Terrones, H., Zhu, Y. Q., Grobert, N., Schilder, A., Clark, R. J. H., Kroto, H. W., and Walton, D. R. M., "Boron-doping effects in carbon nanotubes," Journal of Materials Chemistry, 2000, **10**(6), pp. 1425–1429.

[37] Chen, A. Q., Shao, Q. Y., and Lin, Z. C., "Effects of phosphorus-doping upon the electronic structures of single wall carbon nanotubes," Science in China Series G: Physics Mechanics and Astronomy, 2009, **52**(8), pp. 1139–1145.

[38] Maurin, G., Henn, F., Simon, B., Colomer, J.-F., and Nagy, J. B., "Lithium doping of multiwalled carbon nanotubes produced by catalytic decomposition," Nano Letters, 2001, **1**(2), pp. 75–79.

[39] Lee, R. S., Kim, H. J., Fischer, J. E., Thess, A., and Smalley, R. E., "Conductivity enhancement in single-walled carbon nanotube bundles doped with K and Br," 1997, **388**(6639), pp. 255–257.

[40] Glerup, M., Ewels, C., Holzinger, M., and Val Lier, G., "Doping of carbon nanotubes" in Doped Nanomaterials and Nanodevices, Volume 3, American Scientific Publishers.

[41] Sumpter, B. G., Meunier, V., Romo-Herrera, J. M., Cruz-Silva, E., Cullen, D. A., Terrones, H., Smith, D. J., and Terrones, M., "Nitrogen-mediated carbon nanotube growth: diameter reduction, metallicity, bundle dispersability, and bamboo-like structure formation.," ACS Nano, 2007, **1**(4), pp. 369–75.

[42] Koós, A. A., Dillon, F., Obraztsova, E. A., Crossley, A., and Grobert, N., "Comparison of structural changes in nitrogen and boron-doped multi-walled carbon nanotubes," Carbon, 2010, **48**(11), pp. 3033–3041.

[43] Blase, X., Charlier, J. ., De Vita, A., Car, R., Redlich, P., Terrones, M., Hsu, W., Terrones, H., Carroll, D., and Ajayan, P. M., "Boron-mediated growth of long helicity-selected carbon nanotubes," Physical Review Letters, 1999, **83**(24), pp. 5078–5081.

[44] Lowell, C. E., "Solid solution of boron in graphite," Journal of the American Ceramic Society, 1967, **50**(3), pp. 142–144.

[45] Meysami, S. S., Dillon, F., Koós, A. A., Aslam, Z., and Grobert, N., "Aerosol-assisted chemical vapour deposition synthesis of multi-wall carbon nanotubes: I. Mapping the reactor," Carbon, 2013, **58**, pp. 151–158.

[46] Koós, A. A., Dowling, M., Jurkschat, K., Crossley, A., and Grobert, N., "Effect of the experimental parameters on the structure of nitrogen-doped carbon nanotubes produced by aerosol chemical vapour deposition," Carbon, 2009, **47**(1), pp. 30–37.

[47] Adjizian, J. J., Leghrib, R., Koós, A. A., Suarez-Martinez, I., Crossley, A., Wagner, P., Grobert, N., Llobet, E., and Ewels, C. P., "Boron- and nitrogen-doped multi-wall carbon nanotubes for gas detection," Carbon, 2014, **66**, pp. 662–673.

[48] S Loiseau, A., Launois, P., Petit, P., Roche, and Salvetat, J. P., "Understanding carbon nanotubes: from basics to applications", 2006, Springer, New York.

[49] Bhushan, B., ed., "Springer Handbook of Nanotechnology", 2004, Spinger-Verlag, Berlin, Heidelberg.

[50] Kim, H. H., and Kim, H. J., "The preparation of carbon nanotubes by DC arc discharge using a carbon cathode coated with catalyst," Materials Science and Engineering: B, 2006, **130**(1-3), pp. 73–80.

[51] Lebedkin, S., Schweiss, P., Renker, B., Malik, S., Hennrich, F., Neumaier, M., Stoermer, C., and Kappes, M. M., "Single-wall carbon nanotubes with diameters approaching 6 nm obtained by laser vaporization," Carbon, 2002, **40**(3), pp. 417–423.

[52] Andrews, R., Jacques, D., Qian, D., and Rantell, T., "Multiwall carbon nanotubes: synthesis and application," Accounts of Chemical Research, 2002, **35**(12), pp. 1008–1017.

[53] Jorio, A., Dresselhaus, G., and Dresselhaus, M. S., eds., "Carbon nanotubes - advanced topics in the synthesis, structure, properties and applications", 2008, Topics in Applied Physics, New York.

[54] Sohn, J. I., Lee, S., Song, Y.-H., Choi, S.-Y., Cho, K.-I., and Nam, K.-S., "Large field emission current density from well-aligned carbon nanotube field emitter arrays," Current Applied Physics, 2001, **1**(1), pp. 61–65.

[55] Rodríguez-Manzo, J. A., Terrones, M., Terrones, H., Kroto, H. W., Sun, L., and Banhart, F., "In situ nucleation of carbon nanotubes by the injection of carbon atoms into metal particles.," Nature Nanotechnology, 2007, **2**(5), pp. 307–11.

[56] Helveg, S., López-Cartes, C., Sehested, J., Hansen, P. L., Clausen, B. S., Rostrup-Nielsen, J. R., Abild-Pedersen, F., and Nørskov, J. K., "Atomic-scale imaging of carbon nanofibre growth.," Nature, 2004, **427**(6973), pp. 426–429.

[57] Incze, P. N., Daróczi, N., Sárközi, Z., Koós, A. A., Kertész, K., Ţiprigan, O., Horváth, Z. E., Darabont, A. L., and Biró, L. P., "Synthesis of bamboo–structured multiwalled carbon nanotubes by spray pyrolysis method, using a

mixture of benzene and pyridine," Journal of Optoelectronics and Advanced Materials, 2007, **9**(5), pp. 1525–1529.

[58] Maruyama, S., Kojimaa, R., Miyauchia, Y., Chiashia, S., and Kohno, M., "Low-temperature synthesis of high-purity single-walled carbon nanotubes from alcohol," Chemical Physics Letters, 2002, **360**(3-4), pp. 229–234.

[59] Zhong, G., Iwasaki, T., Honda, K., Furukawa, Y., Ohdomari, I., and Kawarada, H., "Low temperature synthesis of extremely dense and vertically aligned single-walled carbon nanotubes," Japanese Journal of Applied Physics, 2005, **44**(4a), pp. 1558–1561.

[60] Choy, K., "Chemical vapour deposition of coatings," Progress in Materials Science, 2003, **48**(2), pp. 57–170.

[61] Lehman, J. H., Terrones, M., Mansfield, E., Hurst, K. E., and Meunier, V., "Evaluating the characteristics of multiwall carbon nanotubes," Carbon, 2011, **49**(8), pp. 2581–2602.

[62] Ameli, A., Nofar, M., Park, C. B., Pötschke, P., and Rizvi, G., "Polypropylene/carbon nanotube nano/microcellular structures with high dielectric permittivity, low dielectric loss, and low percolation threshold," Carbon, 2014, **71**, pp. 206–217.

[63] Zhao, X., Koos, A. A., Chu, B. T. T., Johnston, C., Grobert, N., and Grant, P. S., "Spray deposited fluoropolymer/multi-walled carbon nanotube composite films with high dielectric permittivity at low percolation threshold," Carbon, 2009, **47**(3), pp. 561–569.

[64] Wang, L., and Dang, Z.-M., "Carbon nanotube composites with high dielectric constant at low percolation threshold," Applied Physics Letters, 2005, **87**(4), p. 042903.

[65] Psarras, G. ., Manolakaki, E., and Tsangaris, G. ., "Electrical relaxations in polymeric particulate composites of epoxy resin and metal particles," Composites Part A: Applied Science and Manufacturing, 2002, **33**(3), pp. 375–384.

[66] Pumera, M., Smíd, B., Peng, X., Golberg, D., Tang, J., and Ichinose, I., "Spontaneous coating of carbon nanotubes with an ultrathin polypyrrole layer.," Chemistry (Weinheim an der Bergstrasse, Germany), 2007, **13**(27), pp. 7644–9.

[67] Seeger, T., Redlich, P., Grobert, N., Terrones, M., Walton, D. R. M., Kroto, H. W., and Rühle, M., "SiOx-coating of carbon nanotubes at room temperature," Chemical Physics Letters, 2001, **339**(1-2), pp. 41–46.

[68] Osburn, C. M., and Ormond, D. W., "Dielectric breakdown in silicon dioxide films on silicon," Journal of The Electrochemical Society, 1972, **119**(5), p. 597.

[69] Meysami, S. S., "Development of an aerosol-CVD technique for the production of CNTs with integrated online control", 2013, D.Phil dissertation, University of Oxford.

[70] Castro, C., Pinault, M., Reynaud, C., and Mayne-L'Hermite, M., "Dynamics of catalyst particle formation and multi-walled carbon nanotube growth in aerosol-assisted catalytic chemical vapor deposition," Carbon, 2010, **48**(13), pp. 3807–3816.

[71] Deck, C. P., and Vecchio, K., "Growth mechanism of vapor phase CVD-grown multi-walled carbon nanotubes," Carbon, 2005, **43**(12), pp. 2608–2617.

[72] Mandumpal, J., Gemming, S., and Seifert, G., "Curvature effects of nitrogen on graphitic sheets: Structures and energetics," Chemical Physics Letters, 2007, **447**(1), pp. 115–120.

[73] Satishkumar, B., Govindaraja, A., Harikumara, K. R., Zhangc, J. P., Cheetham, A. K., and Rao, C. N. R., "Boron–carbon nanotubes from the pyrolysis of C2H2–B2H6 mixtures," Chemical Physics Letters, 1999, **300**(3-4), pp. 473–477.

[74] Dutta, M., Nicolosi, V., Obratzsova, E., Koós, A. A., Crossley, A., and Grobert, N., "Stable dispersions of nitrogen containing multi-walled carbon nanotubes," Materials Express, 2011, **1**(3), pp. 201–209.

[75] Labruquère, S., Blanchard, H., Pailler, R., and Naslain, R., "Enhancement of the oxidation resistance of interfacial area in C/C composites. Part I: oxidation resistance of B–C, Si–B–C and Si–C coated carbon fibres," Journal of the European Ceramic Society, 2002, **22**(7), pp. 1001–1009.

[76] Jones, L. E., and Thrower, P. A., "Influence of boron on carbon fiber microstructure, physical properties, and oxidation behavior," Carbon, 1991, **29**(2), pp. 251–269.

[77] Salonen, J., Lehto, V. P., and Laine, E., "The room temperature oxidation of porous silicon," Applied Surface Science, 1997, **120**(3-4), pp. 191–198.

[78] Batson, P. E., "Simultaneous STEM imaging and electron energy-loss spectroscopy with atomic-column sensitivity," Nature, 1993, **366**(6457), pp. 727–728.

[79] Bose, S., Khare, R. A., and Moldenaers, P., "Assessing the strengths and weaknesses of various types of pre-treatments of carbon nanotubes on the properties of polymer/carbon nanotubes composites: A critical review," Polymer, 2010, **51**(5), pp. 975–993.

[80] Esawi, A. M. K., and Faraga, M. M., "Carbon nanotube reinforced composites: potential and current challenges," Materials and Design, 2007, **28**(9), pp. 2394–2401.

Chapter 3. Sonication effects on carbon nanotubes

Carbon nanotubes are unique materials, possessing extraordinary properties with a potential for a multitude of applications. Most of these properties, especially the electronic ones, can only be exploited when they exist as individual nanotubes. Their tendency to agglomerate or form bundles due to strong intrinsic Van der Waals attraction forces poses a major limitation for their commercial use. Though the exact physics behind these attraction forces remains unclear, it is commonly believed that they arise from the π–π interactions between the adjacent tubes[1] and their high aspect ratios. It should be noted that the agglomeration exists regardless of the synthesis route followed[2–4]; although the type of agglomeration might vary. Figure 3-1 shows an example of few types of agglomerations in CVD-produced nanotubes. Hence, it is essential to individually separate the nanotubes (debundle) to utilise their full potential.

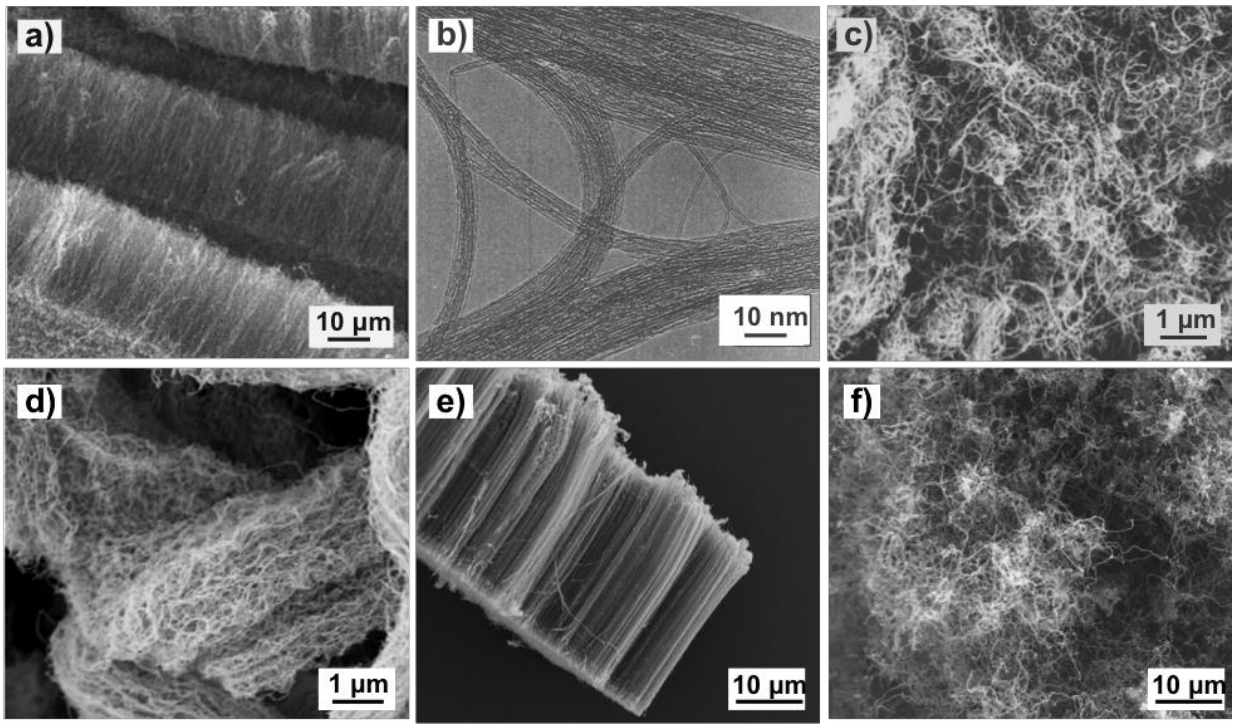


Figure 3-1. Agglomeration types of various CVD-produced nanotubes: a) Aligned MWCNT bundles grown via spray pyrolysis[3], b) SWCNT bundles grown via CCVD[2], c) Baytubes® C150P grown via floating catalyst CVD[4], d) Nanocyl™ NC7000 grown via CCVD[4], e) An aligned N-MWCNTs bundle grown via AACVD, f) An agglomerate of B-MWCNTs grown via AACVD.

There are many examples in literature describing numerous techniques for efficiently separating nanotubes, some of which include oxidative acid treatment[5], functionalisation using polymers[6], surface modification using surfactants[7], and dispersion forming in organic solvents through high energy routes[8]. Irrespective of the technique followed, sonication is the first and most common step used for separating nanotubes from their respective bundles. Sonication treatments involve application of excessive energies for longer time scales, which deeply affects the nanotube structure responsible for its outstanding properties. Although several theoretical[9–11] and experimental studies[12–15] have tried to explain the sonication mechanics, the actual effects still remain unclear. Despite this, the sonication approach has been widely adopted without the full understanding of its effects. Moreover, the existing reports in the literature mostly employed SEM, TEM, and atomic force microscopy to analyse the sonication effects. Unfortunately, these techniques do not give much insight into the defect densities induced by sonication.

This chapter presents the studies conducted to understand the effects of sonication on the nanotube lengths, diameters, and most importantly the defect densities. As one can imagine, the list of possible parameters involved in conducting such a study are vast. Hence, selected parameters were considered and the approach to conquer the problem was divided into two studies:

Sonication study I) Analysing and understanding the effects of various ultrasonic probes on MWCNTs using SEM, TEM, and Raman spectroscopy.

Sonication study II) Development of a ‘destruction reduced’ sonication protocol for dispersing MWCNTs through a combination of ultrasonic probe, ultrasonic bath, and centrifugation.

It should be noted that this chapter addresses only the effects of sonication on MWCNTs. However, the development of nanotube dispersions is discussed in Chapter 4.

3.1. Introduction to sonication theories and literature review

3.1.1. Sono-physical and sono-chemical reactions

In sonication, a high frequency current is used to oscillate piezoelectric crystals that are attached to a probe. The probe can be immersed into a liquid medium (solvent or polymer) that is mixed with the nanotubes. The oscillating crystals produce vibrations in the liquid that form vacuum cavities (bubbles) that implode within the liquid creating sono-physical reactions such as microscopic shock waves[16], microjets[17], microturbulence and microstreaming[18]. This mechanism is known as 'cavitation'. Cavitations occur in the order of microseconds releasing tremendous amount of energy that is strong enough to break the Van der Waals attraction forces between the nanotubes, causing fracture and separation of the nanotubes. The amount of energy generated via cavitation depends on the size of the bubble, which is determined by the ultrasound frequency. Lower ultrasound frequencies produce a long acoustic cycle that results in larger bubbles that release high energies on collapse. On the other hand, higher frequencies reduce the bubble size, thereby reducing the cavitation energy.

Bubble collapse also gives rise to sono-chemical mechanisms such as localised heating in the solvent and free radical formation. These mechanisms can be explained by the widely accepted 'hot-spot theory'[19], which describes each micro-bubble as a micro-reactor that undergoes adiabatic heating and creates extreme local conditions. The temperatures inside the micro-bubbles can rise to 1700–4700 °C and reach pressures of 1000–4000 atm. A study on the effect of a 3 MHz sound wave on a cavitation bubble was described by Apfel[20] and some of his findings are listed in Table

3-1. Such extreme conditions in the bubble can lead to the formation of free radicals (primary radicals) from the vapour/volatile compounds in the liquid[19]. These primary radicals can further catalyse secondary reactions such as conversion to other radicals, initiation of a radical chain, reaction with substrates or the solvent itself, and attack or recombine with other radicals.

Parameter	**Initial (Before collapse)**	**Final (After collapse)**
Radius	1 μm	3 μm (max.) 0.14 μm (min.)
Internal Pressure	1 atm	4140 atm
Internal Temperature	20 °C	2900 °C
Energy Density	1 MeV/μm^3	383 MeV/μm^3

Table 3-1: Energy concentration in a cavitation bubble (before and after collapse) caused by a 3 MHz sound wave[20].

3.1.2. Sonication effects

When the nanotube aggregates are mixed in a solvent medium and mechanical energy is applied via sonication, shear stresses are exerted through the medium on the aggregates[21]. These stresses lead to the separation of nanotubes from the aggregates and shorten the nanotubes (known as 'scission'). For successful separation, it is important that the energy supplied be more than the opposing binding energy of the aggregates. It is also important that the supplied energy shortens the nanotubes to avoid re-entangling and re-aggregation. However, it is critical that the supplied energy does not cause excessive nanotube fracturing or form new defects as this would only damage the nanotube's structure.

Extensive studies have been conducted to understand the sonication mechanisms precisely[9,11,13–15,22,23], especially the nanotube scission. However, due to the lack of detailed understanding of the various key factors occurring at such micro-scale, the nanotube scission mechanics remain unclear to date. Nevertheless, in a way it can be related to the polymer chain shortening mechanism[13]: Polymer chains tend to break at their centre of mass during sonication and the shortening kinetics depend on the polymer chain length. A similar behaviour can be expected from the nanotubes and it can be assumed that its length decrease during sonication follows a power law:

$$l \sim t^{-m} \qquad \text{Equation 3-1}$$

where, l is the nanotube length, t is the sonication time, and m is the power law exponent that usually varies between 0.2–0.5[13]. It should be noted that assigning a specific value to m is difficult, as it depends on the nanotube stiffness and distance between the nanotube and the collapsing bubble[13,14].

Although the power law gives a vague idea of the effect of sonication time on the nanotube length, the influence of various other parameters on the law makes it challenging to predict the effect exactly. Recently, Pasquali *et al*.[9] showed theoretically that the nanotube length plays a key role in its scission. Shorter nanotubes (length ≤ 3 μm) in ambient fluids behave as rigid rods[11] (assuming that only Brownian forces exist), and demonstrate diffusion through translation or rotation only and break via stretching[9]. On the other hand, longer nanotubes undergo excessive bending and break via buckling[9]. A model of the nanotube buckling due to compressive forces and torque is shown in Figure 3-2. It is usually assumed that sonication time plays a major role in the nanotube scission, but in certain sonication treatments sonication energy could instead be the most influencing parameter[12,24,25]. To add to the complexity, the wide range of nanotube lengths, diameters, defect densities, chiralities, and surface

properties makes it difficult to follow one standard sonication theory. Nevertheless, attempts are ongoing to understand the real science behind the nanotube scission.

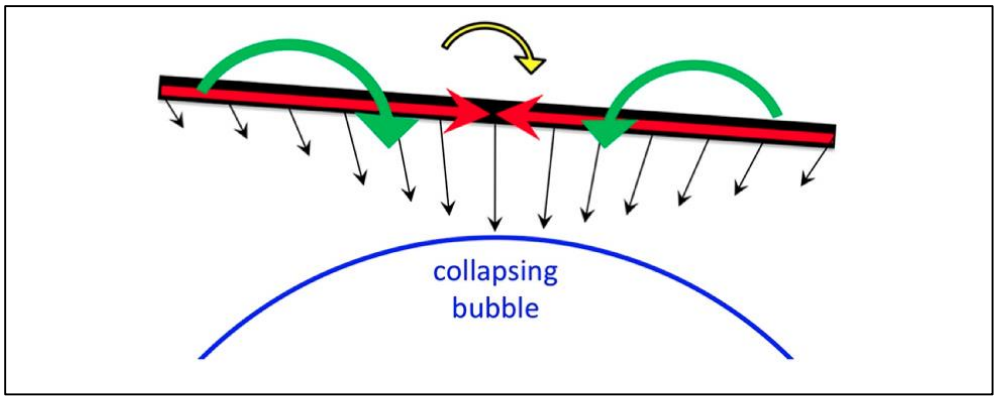


Figure 3-2. A schematic showing the forces acting on a nanotube near a collapsing bubble. The compressive forces (red) and the inward torque (green) result in the nanotube buckling. If the torque imbalance is sufficiently large, the nanotube rotates radially i.e., clockwise (yellow)[9].

There are two major ways of supplying the ultrasonic energy to the nanotubes:

a) Ultrasonic baths (US baths): US baths usually consist of a stainless steel tank base, an attached transducer that induces vibrations from the base of the tank, and an optional heating element (Figure 3-3a). They typically have high frequencies (*ca.* 40–50 kHz), a better distribution of acoustic field, and can treat larger batches of samples[26]. However, the amount of power dissipation in an US bath is not large (usually < 5 Wcm^{-2}) and is difficult to control. Therefore, a defined cavitation zone cannot be maintained. Moreover, controlling the bath temperature is not easy.

b) Ultrasonic probes (US probes): US probes, unlike the US baths, deliver the energy directly into the system. A US probe consists of a generator that can provide an alternating electrical frequency (*ca.* 20 kHz) to a transducer, which is attached to a specifically designed metal horn (Figure 3-3b). The metal horn, usually made of titanium alloy, amplifies the ultrasonic energy. When the tip of the horn is immersed in the liquid, energy is directly delivered to the required liquid mixture. Therefore, the

US probe can create a defined cavitation zone but cannot maintain uniformity of the energy dispersed through the liquid.

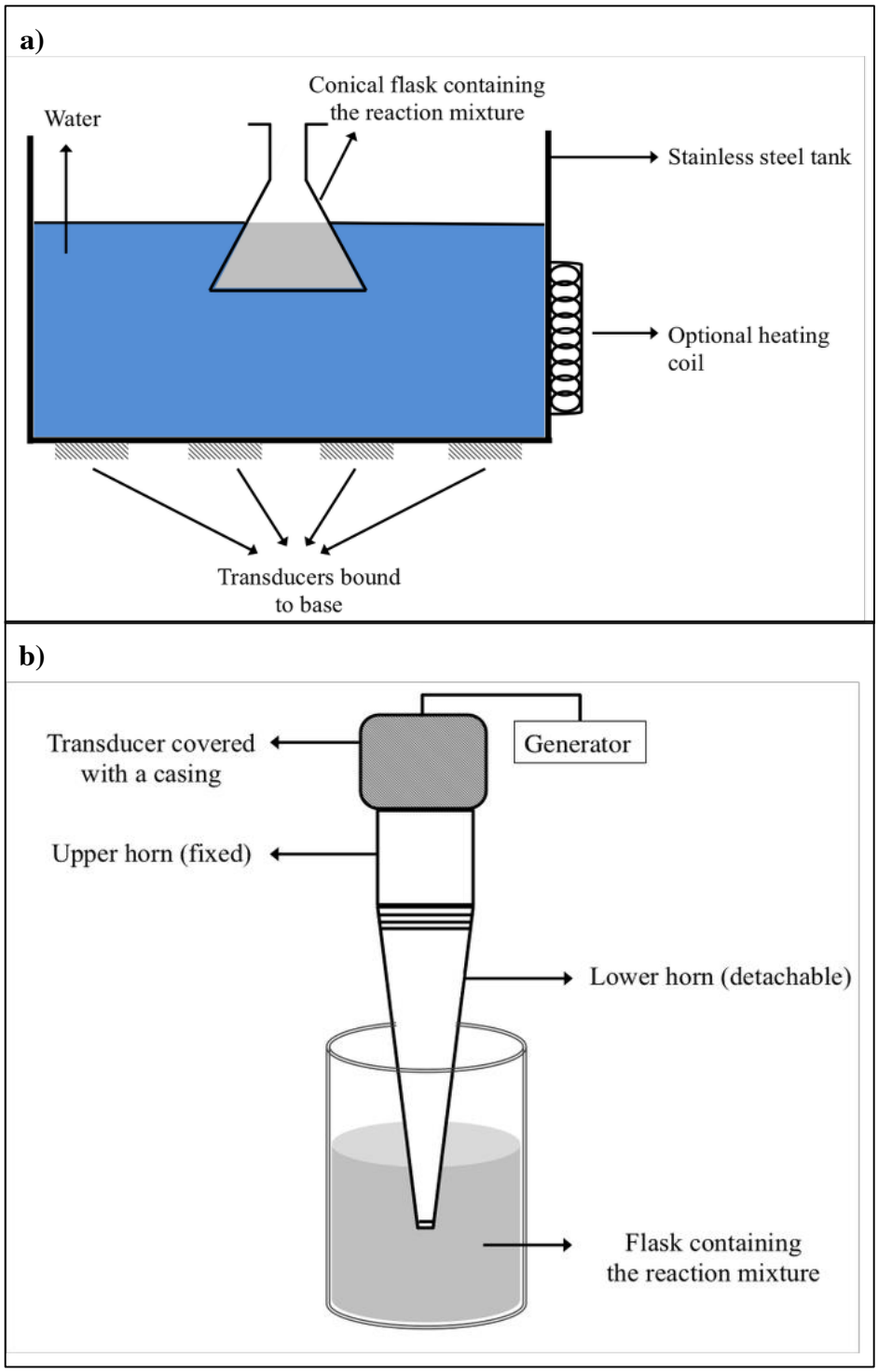


Figure 3-3. Schematic of: a) An US Bath, b) An US Probe.[19]

3.2. Experimental procedure

Conventional, N-, and B- MWCNTs synthesised through the AACCVD technique were used for studying the sonication effects. MWCNTs used for this sonication study were produced using the synthesis parameters discussed in Chapter 2 and were provided by Dr Antal Koós and Dr Frank Dillon. The related synthesis parameters along with the respective precursor details are also listed in Table 3-2.

MWCNT type	Synthesis temperature (°C)	Precursor solution	Synthesis time (minutes)	Gas
MWCNTs	800	Toluene (Fluka 99.7%)	30	2500 sccm Argon
N-MWCNTs	800	Benzylamine (Fluka 99%)	30	2500 sccm Argon
B-MWCNTs	1000	[10 vol.% of 1 M Triethylborane in Hexane (Aldrich)] in Toluene (Fluka 99.7%)	10	2500 sccm Argon

Table 3-2. Synthesis parameters used for synthesising MWCNTs for the sonication studies.

Sonication study I)

Three different types of US probes with varying powers and frequencies were selected for the first sonication study – Hielscher UP 100H (100 W, 30 kHz), Hielscher UP 200S (200 W, 24 kHz), and Branson 450D (400 W, 20 kHz). 7 ml MWCNT dispersions of concentration 1 mg/ml were prepared by dispersing each type of MWCNT in anhydrous Dimethylformamide (DMF) (Fluka 98.0%), Ethanol (EtOH) (Sigma Aldrich 99.5%), and Hexafluoroisopropanol (HFIP) (Apollo Scientific 99.0%). Sonication time scales of 1, 2, and 5 minutes were used in combination with continuous and pulsed modes of the US probes. In order to maintain consistency in the studies, it

was made sure that a single batch of each type of MWCNT was used throughout the sonication studies. It should be noted that due to limited quantity of MWCNTs and B-MWCNTs, studies using the Branson 450D were conducted only on the N-MWCNTs. Furthermore, due to the high power of Branson 450D US probe, sonication time-scales on it were limited to 1 and 2 minutes only. The complete list of testing parameters used for sonication study I is listed in Table 3-3. Hereon, the ultrasonic probe treated MWCNTs will be referred as 'MWCNTs-SP'. It should also be noted that the MWCNTs-SP dispersions were a thick mass of inhomogeneous aggregates. This was because the aim of sonication study I was to only understand the effects of sonication and not form homogeneous dispersions.

UP 100H US Probe	**UP 200S US Probe**	**Branson 450D US Probe**
MWCNTs: Conventional, N-, B-MWCNTs	MWCNTs: Conventional, N-, B-MWCNTs	MWCNTs: N-MWCNTs
Solvents: DMF, EtOH, HFIP	Solvents: DMF, EtOH, HFIP	Solvents: DMF, EtOH, HFIP
Time Scales: 1min, 2min, 5min	Time Scales: 1min, 2min, 5min	Time Scales: 1min, 2min
Mode: Continuous, Pulsed	Mode: Continuous, Pulsed	Mode: Continuous, Pulsed

Table 3-3. List of parameters used for sonication study I.

Sonication study II)

The aim of sonication study II was to develop a protocol for minimising the damage usually caused to the nanotubes during dispersion forming. This protocol was to be used to form homogeneous nanotube dispersions for developing polymer matrix

composites (discussed in Chapters 4 and 5). For this, a Hielscher UP 100H (100 W, 30 kHz) US probe was used in combination with an Ultrawave U1250D (200 W, 30–40 kHz) US bath, and a Sciquip 1-6P centrifuge. Clearly, the number of experimental variables in this study was enormous, therefore, based on literature and the results from sonication study I, a mild sonication regime was proposed and its effects were studied. The sonication regime was established from the work of Bergin *et al*[27,28], Cheng *et al*[29], Hennrich *et al*[13], Giordani *et al*[8], Ham *et al*[30] and is as follows:

Step 1) 2 minutes US Probe (continuous mode),

Step 2) 2 hours US Bath (room temperature),

Step 3) 2 minutes US Probe (continuous mode),

Step 4) 95 minutes Centrifugation (5000 rpm, *ca*. 2380 g).

Conventional MWCNTs in N-Methyl Pyrrolidone solvent (Sigma Aldrich 99.5%) (NMP) were used for sonication study II as NMP is well-known for efficiently dispersing carbon nanotubes[8,28,30]. Raman studies were conducted after every step to understand the induced defects. TEM studies were conducted after step 4 to examine the resulting MWCNT structure.

3.3. Characterisation techniques

SEM and TEM studies were conducted to study the morphology of pristine and US probe treated MWCNTs. The sample preparation protocol discussed in §2.5.2 was used for preparing the SEM and TEM samples of pristine MWCNTs. On the other hand, the protocol followed for preparing samples of MWCNTs-SP is as follows:

a) SEM sample preparation: Firstly, 1 ml of each MWCNT dispersion was diluted with 5 ml of its respective solvent. Then, two drops of the diluted dispersions were carefully drop cast onto clean silicon wafers and were allowed to dry for at least 3 hours. The

silicon wafers were then glued to aluminium stubs using silver paste and were allowed to dry for at least a day before conducting the SEM studies.

b) TEM sample preparation: Three drops of the diluted dispersions were drop cast onto 400 mesh Cu lacey carbon TEM grids. The grids were then heated at 50 °C for 20 minutes to remove the solvent, and were allowed to dry overnight before conducting the TEM studies. At least 50 SEM micrographs and 20 TEM micrographs at various magnifications were taken for each sample. An average of 100 nanotubes was used to estimate the nanotube lengths and outer diameters using the ImageJ software.

Raman spectroscopy was conducted on pristine and US probe treated MWCNTs to study their defect densities. The Raman sample preparation method mentioned in §2.5.2 was used for preparing the pristine MWCNT samples. On the other hand, samples of the MWCNTs-SP were prepared by drop casting 5–6 drops of each dispersion on clean microscopy glass slides. The glass slides were then heated on a hot plate at 50 °C for 10 minutes to remove the solvent and dried overnight prior to testing.

3.4. Sonication study I: effect of US probes; results and discussion

3.4.1. Structural characterisation using SEM and TEM

a) Pristine MWCNTs

Firstly, SEM and TEM studies were conducted on pristine MWCNTs to understand their morphology before the sonication treatment. It was observed that the pristine MWCNTs used in sonication study I (Figure 3-4) were slightly different in morphology compared to the MWCNTs reported in chapter 2, and had a wider range of lengths and diameters. It should be noted that the MWCNTs in either case were synthesised using the same parameters, however they belonged to different batches. It is not unusual for AACCVD-produced MWCNTs to vary from batch to batch. This is due to the non-uniformity of the parameters along the CVD reactor, especially the

variation in catalyst content and the temperature along the length of the reactor[31]. Therefore, the MWCNT length and diameter values in the lower 75th percentile were considered more reliable and will be presented in '{}' in this chapter along-side the average values.

Table 3-4 lists out the lengths and diameters of the MWCNTs used for sonication study I. Conventional MWCNTs synthesised from pure toluene (Figure 3-4a,b) appeared similar in overall structure to the ones reported in Chapter 2 *i.e*., long, wavy tubes with kinks. However, the conventional MWCNTs used in sonication study I were relatively longer in length, 394±44 μm {443 μm} with outer diameters of 62±13 nm {77 nm}. Doping the MWCNTs with nitrogen and boron introduced significant changes:

1) N-MWCNTs were shorter and straighter than the conventional MWCNTs with fewer kinks (Figure 3-4c,d). This is due to the nanotube edge saturation by nitrogen, which prevents the tube growth[32] (as discussed in Chapter 2). The length of N-MWCNTs used for the sonication study I was 53±9 μm {55 μm}. They had outer diameters of 40±21 nm {55 nm} and exhibited a bamboo-like internal structure.

2) As discussed in Chapter 2, the addition of boron promotes nanotube growth by preferential substitution of carbon atoms[33]. This resulted in thick wool-like nanotubes as seen in Figure 3-4e. Due to the formation of thick agglomerates, it was difficult to calculate the lengths of B-MWCNTs. They exhibited a nested cone shaped internal structure (Figure 3-4f) with outer diameters of 61±24 nm {64 nm}.

Type of MWCNTs	Length (µm)	Diameter (nm)
Conventional MWCNTs	399 ± 44	62 ± 13
N-MWCNTs	53 ± 9	40 ± 21
B-MWCNTs	-	61 ± 24

Table 3-4. Lengths and diameters of pristine MWCNTs produced by AACCVD used for sonication study I.

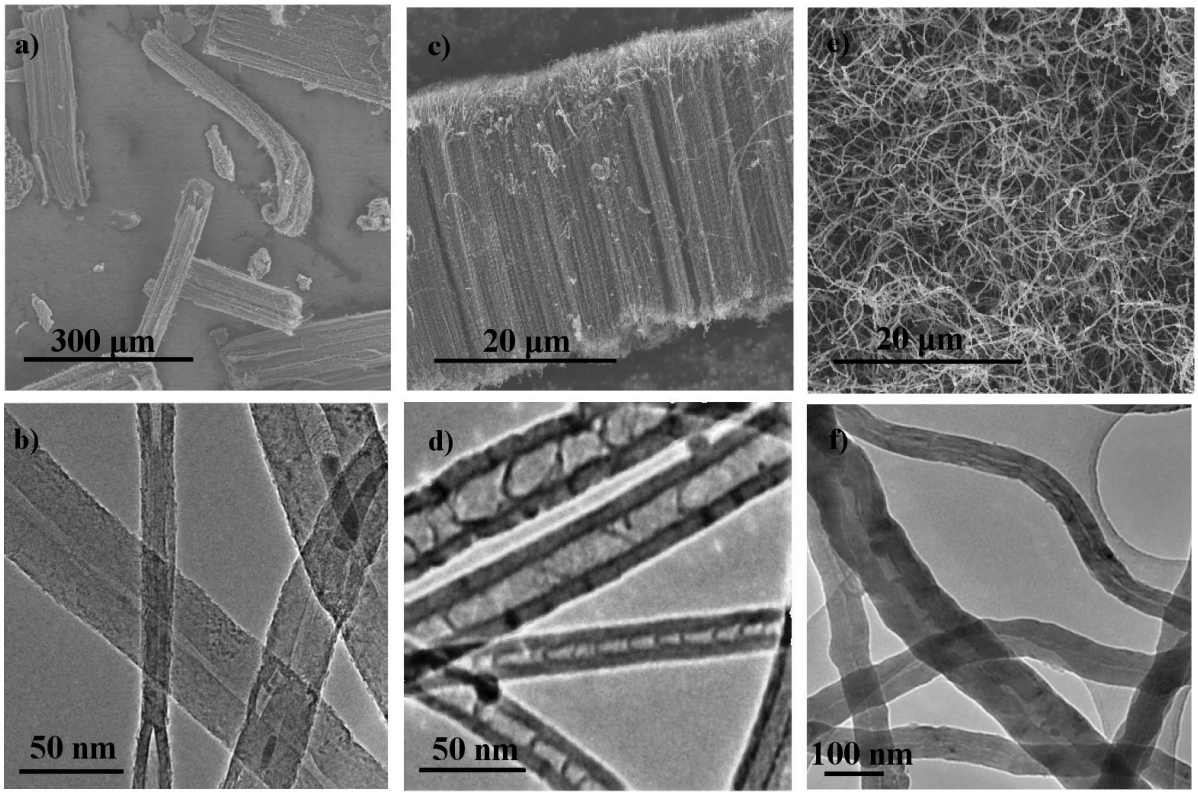


Figure 3-4. SEM and TEM images of pristine: a,b) Conventional MWCNTs, (c,d) N-MWCNTs, (e,f) B-MWCNTs respectively.

b) MWCNTs-SP

It should be noted that the TEM images of pristine MWCNTs from Figure 3-4b,d,f show individual nanotubes. The sample preparation protocol for these samples

involved 30 seconds US probe treatment, hence it can be assumed that the nanotube debundling occurred at as short as 30 seconds sonication time. However, it was observed that at least 1 minute of US probe treatment was required to see a significant effect on the nanotube scission. Due to the vast number of micrographs obtained during this study, SEM and TEM images of only two sample sets are presented in this chapter. Figure 3-5 shows the SEM and TEM images of N-MWCNTs-SP in HFIP treated with UP 100H (Figure 3-5a,b,c) and UP 200S (Figure 3-5d,e,f) for 2 minutes in pulsed mode. It appears from Figure 3-5 that the sonication treatment led to a notable nanotube scission, along with successful debundling. Moreover, the inhomogeneous energy distribution during the treatment (as explained in §3.1.2) seemed to have affected individual tubes differently. This can be attributed to the fact that the starting raw material consisted of nanotubes with different lengths, diameters, and defect densities. Therefore, the sonication effect on the tubes was obviously different. The average lengths of the N-MWCNTs-SP treated with UP 100H and 200S (as observed in Figure 3-5) were 10±7 μm {7.13 μm}, and 8±6 μm {7.5 μm}, respectively.

Figure 3-5c,f shows the TEM images of N-MWCNTs-SP treated with UP 100H and 200S, whose average outer diameters were 37±21 nm {50 nm} and 21±15 nm {40 nm}, respectively. The diameter range of the N-MWCNTs-SP roughly matched that of the pristine N-MWCNT (*i.e.*, 40±21 nm {55 nm}). This was true for all the MWCNTs-SP. This effect is discussed in detail in §3.4.2.b) through distribution graphs. Moreover, the TEM images of N-MWCNTs-SP showed no significant damage in the nanotubes. Micrographs similar to Figure 3-5 were taken for all the samples, and the respective nanotube lengths and diameters were calculated. Probability density curves were fitted to the data to further understand the sonication effects, which are discussed in §3.4.2.

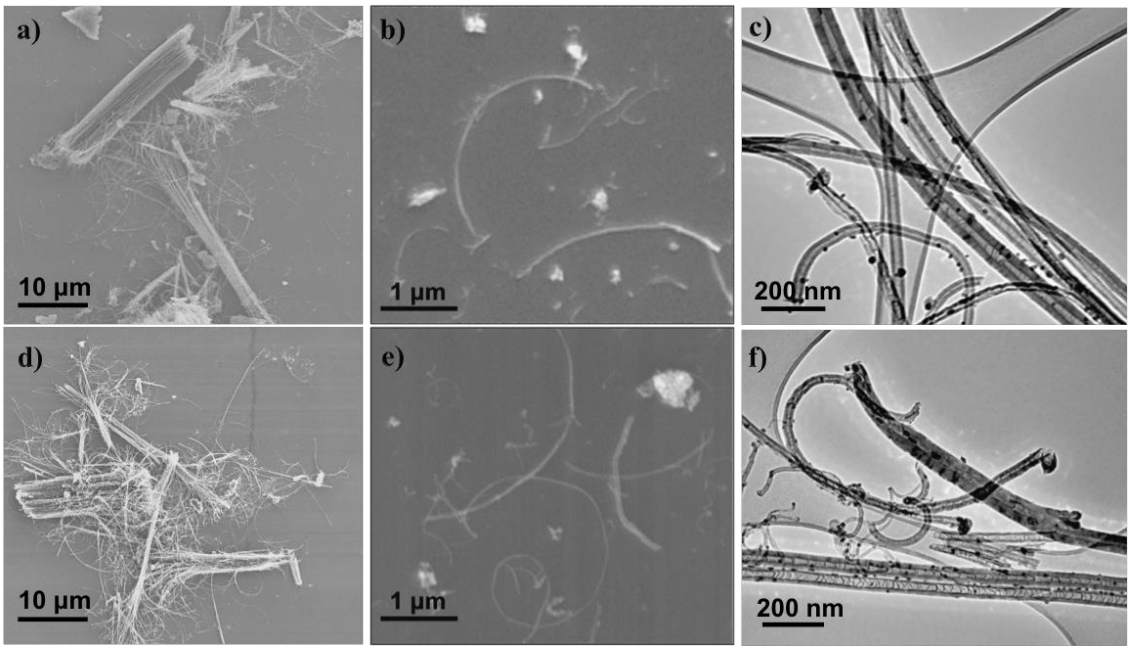


Figure 3-5. SEM and TEM micrographs of N-MWCNTs treated in HFIP for 2 min in pulsed mode using: (a,b,c) UP 100H, (d,e,f) UP 200S (Note: b,e are magnified SEM images of a,d respectively).

3.4.2. Analysis of length and diameter distributions

From the lengths and diameters data of pristine and US probe treated MWCNTs, it transpired that the distributions were wide and random. Therefore, fitting a standard distribution curve seemed to be an incorrect representation of the data. However, the lognormal model proved to be a more representative fit, hence probability density functions were plotted to help interpret the data. The lognormal probability densities were calculated in Microsoft Excel; the function can be represented as:

$$f(\ln(L)) = \frac{1}{\sigma\sqrt{2\pi}} e^{-\frac{1}{2}\left(\frac{\ln(L)-\mu}{\sigma}\right)^2} \qquad \text{Equation 3-2}$$

where: L is the value at which the function is evaluated, the fitting parameters σ and μ are the standard deviation and mean of ln(L) respectively.

a) Length distributions of pristine and US probe treated MWCNTs

Figure 3-6 compares the length distributions of pristine and US probe treated conventional MWCNTs. It can be seen from Figure 3-6a that the distribution of pristine conventional MWCNTs was very wide and it consisted of nanotubes twice as long as the ones reported in chapter 2. This is an interesting example of how small variations in the synthesis parameters can sometimes result in significantly different MWCNTs, hence requiring extensive studies to understand the nanotube growth mechanisms. From the distribution of pristine conventional MWCNTs it was expected that the MWCNTs-SP would follow the same behaviour, which is confirmed in Figure 3-6b,c. Lengths of the conventional MWCNTs-SP varied between *ca*. 0.2–80 μm, but lengths of 80% of the conventional MWCNTs-SP lay within 0.2–10 μm, indicating successful debundling. However, no significant trend with varying sonication parameters such as solvents, US probes and sonication time was observed. This was unexpected, especially with the varying solvents, as the nature of solvents used in this study was different in terms of viscosity, surface tension, and vapour pressures. Hence, the cavitation process should have occurred differently in the three solvents and should have had a significant effect on the nanotube fracture[19], which clearly is not the case. A possible explanation for this could be that the sonication timescales were perhaps too short to observe the effect of the solvent. Additionally, another explanation is that an average of 100 nanotubes might not have been a sufficient representation for the samples. Hence, a definite conclusion for the effects of sonication could not be established. Therefore, to further understand the effect, the nanotube lengths in the lower 75th percentile were plotted against varying sonication parameters (Figure 3-7). It can be seen from Figure 3-7a that the lengths of MWCNTs-SP were in the same range for all three sonication times. Hence, the scission mechanism in this study didn't follow the power law and an increase in the sonication time did not necessarily cause a significant increase in the

scission. Moreover, it can be seen from Figure 3-7b that there was no trend with the change in solvents either. However, irrespective of the sonication parameters, considering the lengths in the lower 75th percentile, it can be realised that the lengths of conventional MWCNTs-SP decreased to 1–4% of the original lengths of their pristine counterparts.

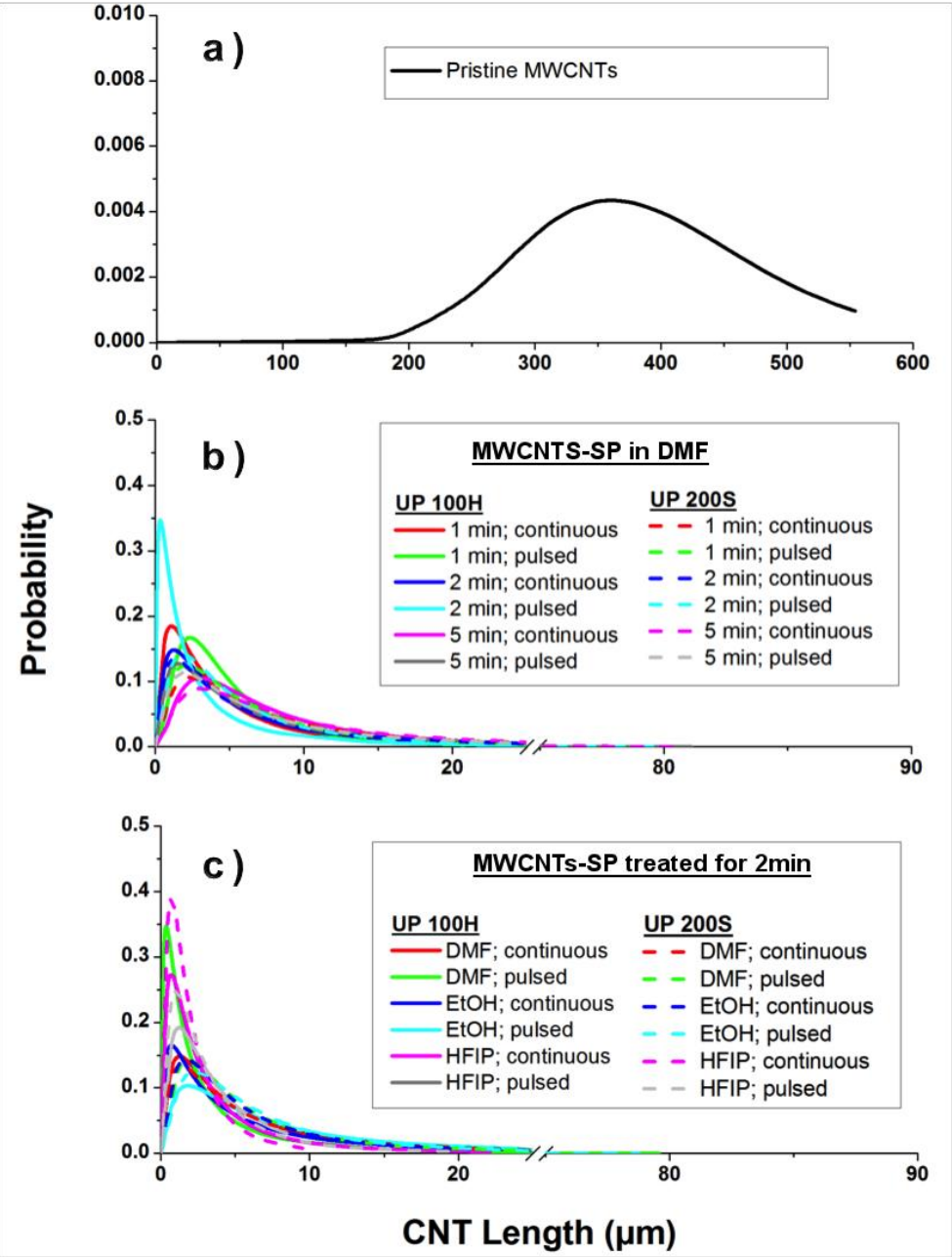


Figure 3-6. Lognormal probability density functions of conventional MWCNT lengths: (a) Pristine MWCNTs, (b) MWCNTs-SP in DMF with varied US probes, sonication times and modes, (c) MWCNTs-SP treated for 2 minutes with varied US probes, sonication modes and solvents.

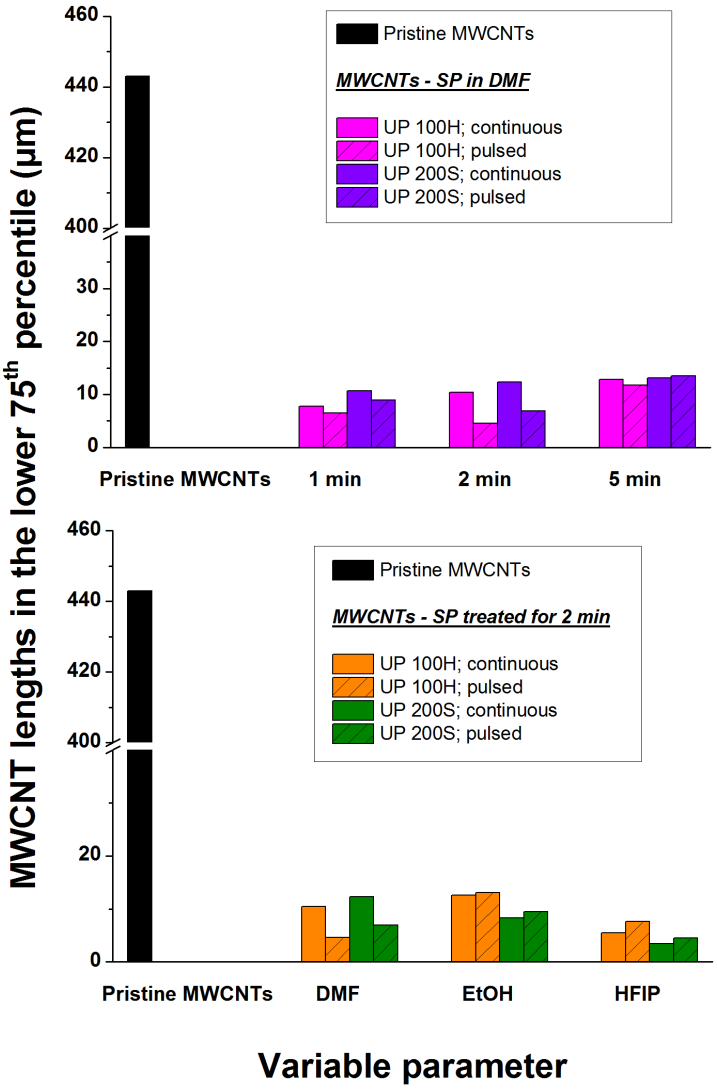


Figure 3-7. Comparison of conventional MWCNT lengths in the lower 75th percentile with variable sonication parameters:
(a) Conventional MWCNTs-SP in DMF treated with varying US probes, sonication modes and times,
(b) Conventional MWCNTs-SP treated for 2 minutes in different solvents with varying US probes, and sonication modes.

Unlike the conventional MWCNTs, the length distribution of pristine N-MWCNTS was not wide (Figure 3-8a); the lengths were relatively uniform with majority between 40–65 µm. However, N-MWCNTs-SP did have a wider range lengths *ca*. 0.2–80 µm (Figure 3-8b,c) with 80% lengths within 0.2–7 µm. Similar to the MWCNTs-SP, there was no trend in the effect of various sonication parameters over the nanotube lengths. However, a significant observation was that the sonication parameters used in this study resulted in successful debundling and scission of N-

MWCNTs without causing major damage to the N-MWCNTs (as seen from the TEM micrographs in Figure 3-5c,f). However, a suitable analysis technique for understanding the nanotube damage is Raman studies, which is discussed in §3.4.3. Considering the N-MWCNT lengths in the lower 75th percentile (Figure 3-9), it can be observed that irrespective of the sonication parameters the lengths of N-MWCNTs-SP decreased to 5–15% of their original lengths.

The higher decrease in length for MWCNTs-SP can be explained by the fact that the MWCNTs produced by AACCVD contain many kinks. These kinks can act as stress raisers during sonication, and fracture might occur primarily at the kinks[10,34]. Doping of MWCNTs with N decreases the number of kinks[32], therefore more energy is required to fracture the N-MWCNTs having fewer kinks. Also, breaking the longer MWCNTs is easier compared to the relatively shorter and thinner N-MWCNTs.

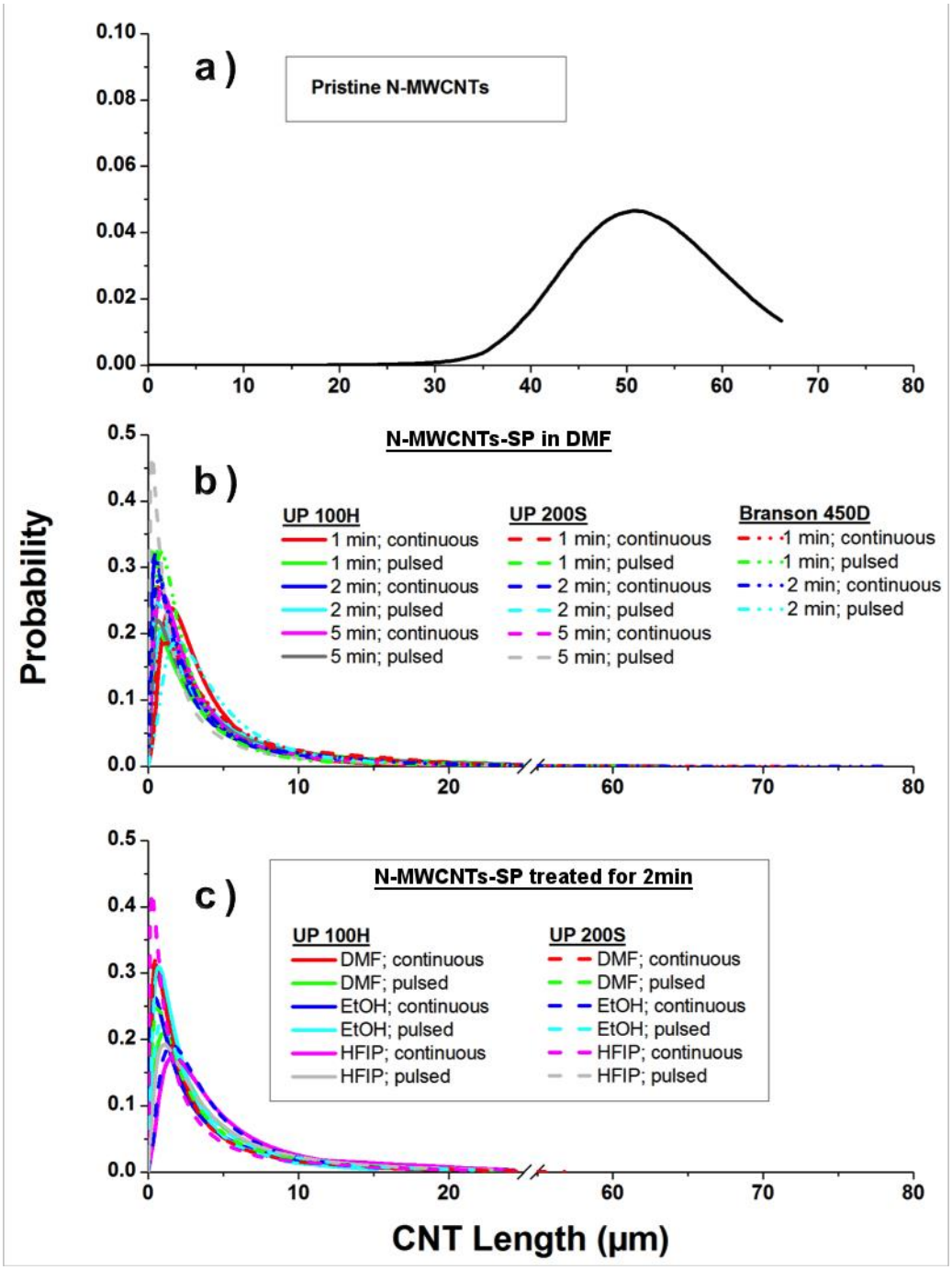


Figure 3-8. Lognormal probability density functions of N-MWCNT lengths:
(a) Pristine N-MWCNTs,
(b) N-MWCNTs-SP in DMF with varied US probes, sonication times and modes,
(c) N-MWCNTs-SP treated for 2 minutes with varied US probes and sonication modes and solvents.

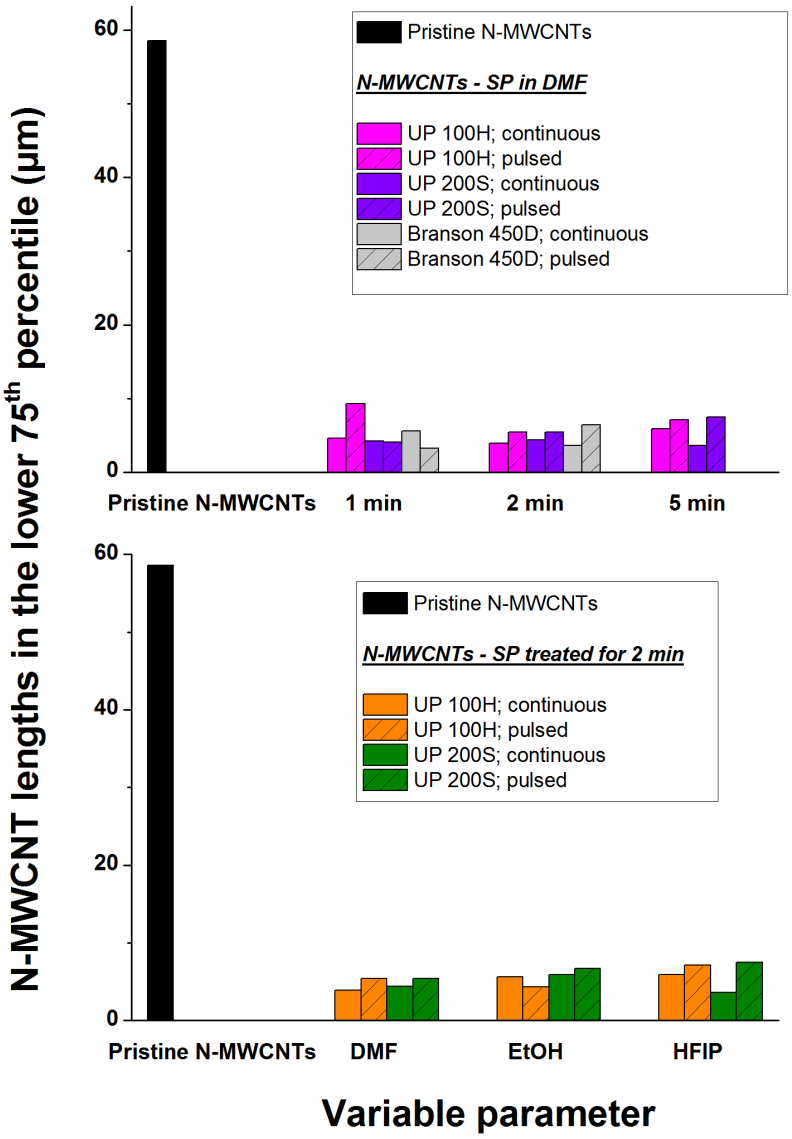


Figure 3-9. Comparison of N-MWCNT lengths in the lower 75th percentile with variable sonication parameters:
(a) N-MWCNTs-SP in DMF treated with varying US probes, sonication modes and times,
(b) N-MWCNTs-SP treated for 2 minutes in different solvents with varying US probes, and sonication modes.

b) Diameter distributions of pristine and US probe treated MWCNTs

Figure 3-10a,b compares the probability distributions of conventional MWCNT diameters (pristine and US probe treated) in varying sonication parameters. The solid black line in the Figure 3-10 represents the pristine conventional MWCNTs and the coloured lines represent various conventional MWCNTs-SP. It can be seen in Figure

3-10a,b that the diameter distributions of conventional MWCNTs-SP approximately match that of their pristine counterparts, signifying no specific effect on the MWCNT diameters. However, a noteworthy observation is that the distribution of the pristine conventional MWCNTs is wider than that of the conventional MWCNTs-SP. Also, the probability of the nanotubes having diameters within 20–60 nm is high. This could signify that not only most of the nanotubes debundle successfully after the sonication treatment, but that they are also mostly distributed in 20–60 nm diameter range, resulting in a fairly uniform spread. Figure 3-11 shows the outer diameters of pristine and US probe treated conventional MWCNTs in the lower 75th percentile with varying sonication parameters. Similar to the nanotube lengths, a clear trend could not be observed with the diameters of the nanotubes either. Complementary to this, no significant effect on the diameters or thinning of the nanotubes was observed in the TEM studies.

Figure 3-12a,b compares the diameter distributions of N-MWCNTs (pristine and US probe treated) with varying sonication parameters (including the three US probes: UP 100H, UP 200S, and 450D). Unlike the MWCNTs, there seemed to be a slight shift of diameters in the N-MWCNTs-SP. Diameters of majority of the N-MWCNTs-SP seemed to have shifted to 10–30 nm diameter range while the diameters of their pristine counterparts majorly lay within 20–50 nm. However, the overall distribution range of the N-MWCNTs-SP was similar to that of the pristine N-MWCNTs. Therefore it cannot be definitely established whether the sonication parameters actually had a significant effect on the diameters. Figure 3-13a,b shows the outer diameters of pristine and US probe treated N-MWCNTs in the lower 75th percentile with respect to the varying sonication parameters. Similar to the MWCNTs, no clear trend could be observed for N-MWCNT diameters either. However, a decrease in the diameters for N-MWCNTs-SP with no evident wall thinning/damage could suggest pure debundling.

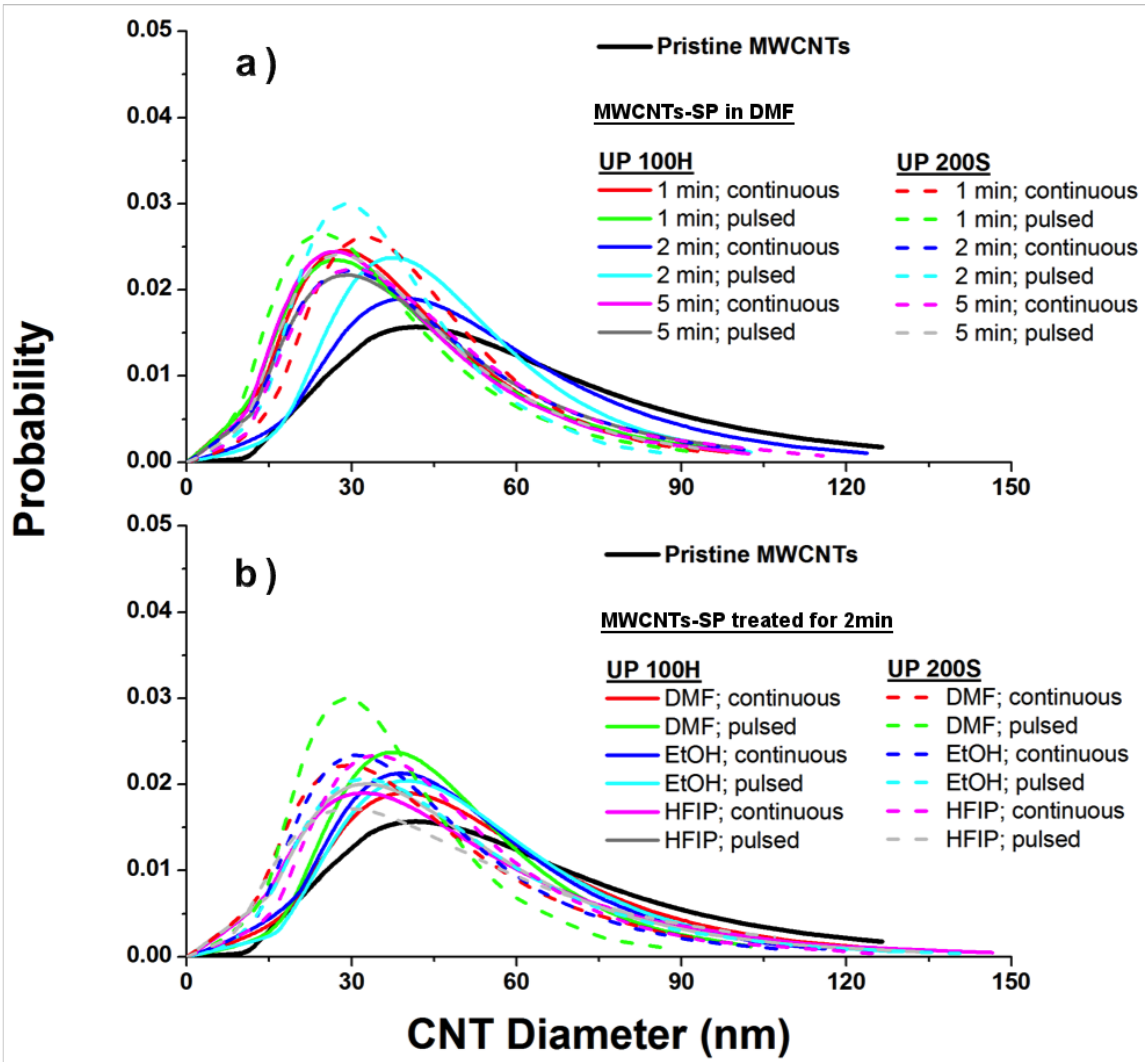


Figure 3-10. Lognormal probability density functions of conventional MWCNT outer diameters (pristine and US probe treated):
(a) Treated in DMF with varied US probes, sonication times and modes,
(b) Treated for 2 minutes in different solvents with varying US probes, and sonication modes.

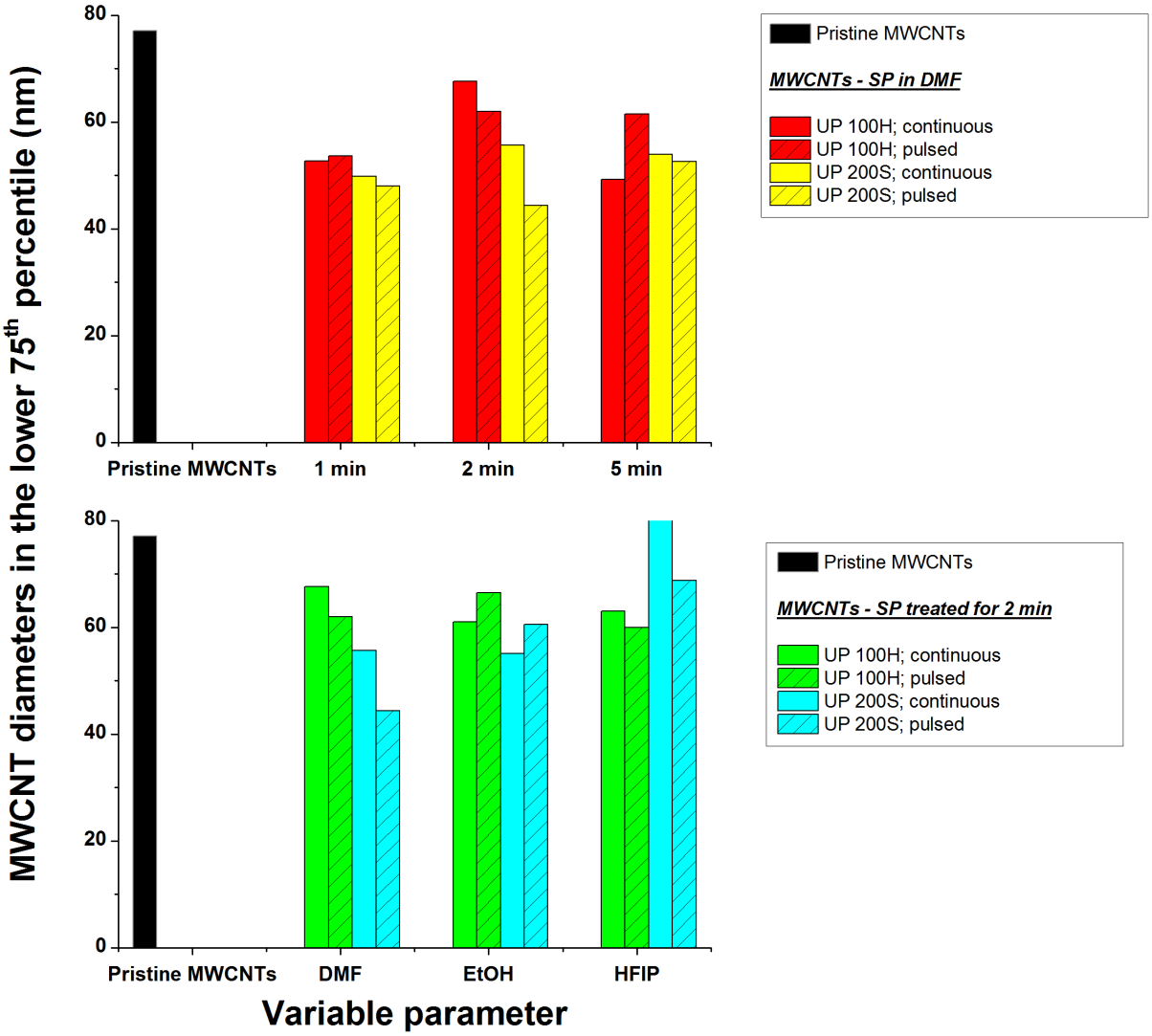


Figure 3-11. Comparison of conventional MWCNT outer diameters (pristine and US probe treated) in the lower 75th percentile with variable sonication parameters:
(a) Treated in DMF with varying US probes, sonication modes and times,
(b) Treated for 2 minutes in different solvents with varying US probes, and sonication modes.

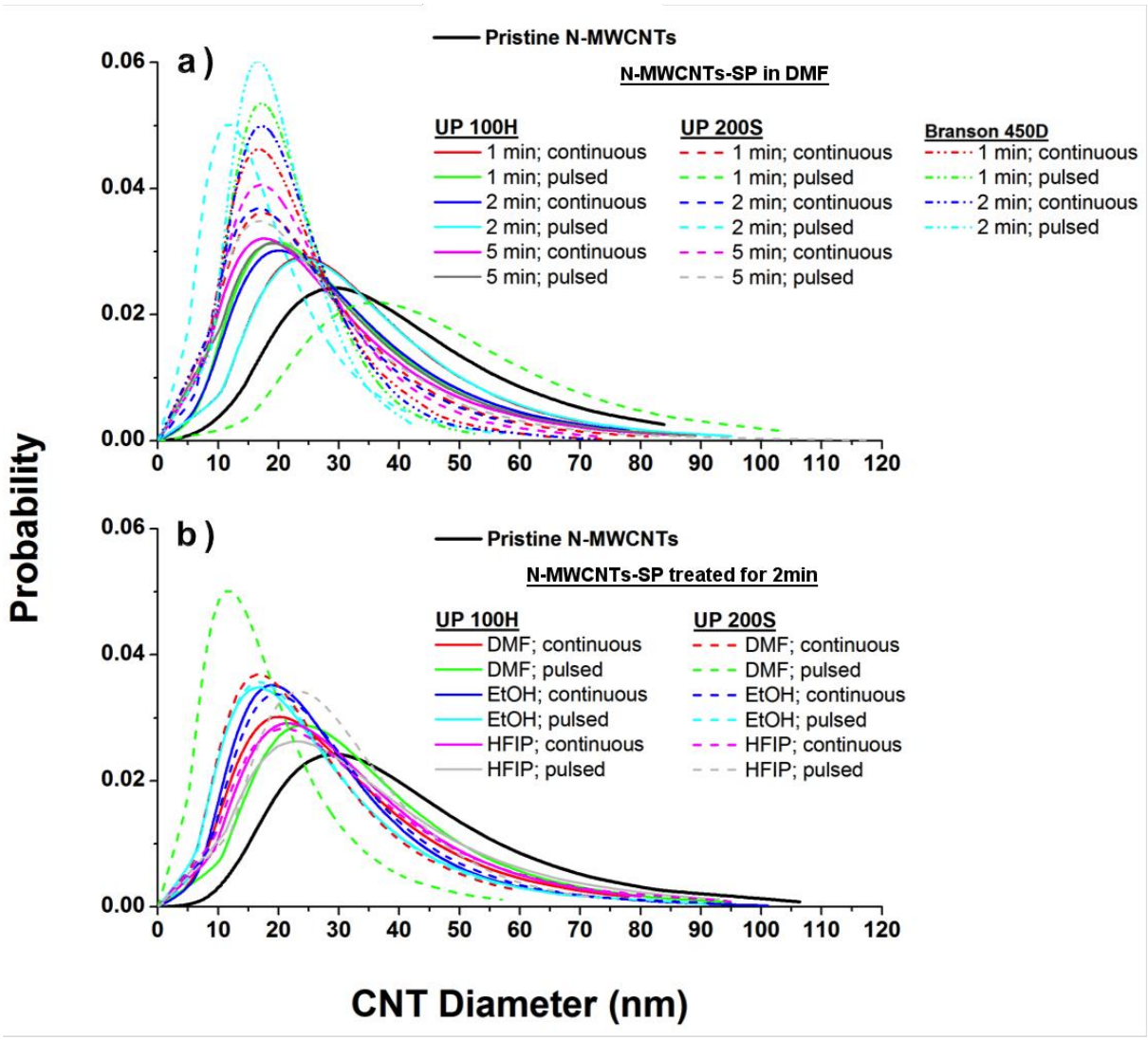


Figure 3-12. Lognormal probability density functions N-MWCNT outer diameters (pristine and US probe treated):
(a) Treated in DMF with varied US probes, sonication times and modes,
(b) Treated for 2 minutes in different solvents with varying US probes, and sonication modes.

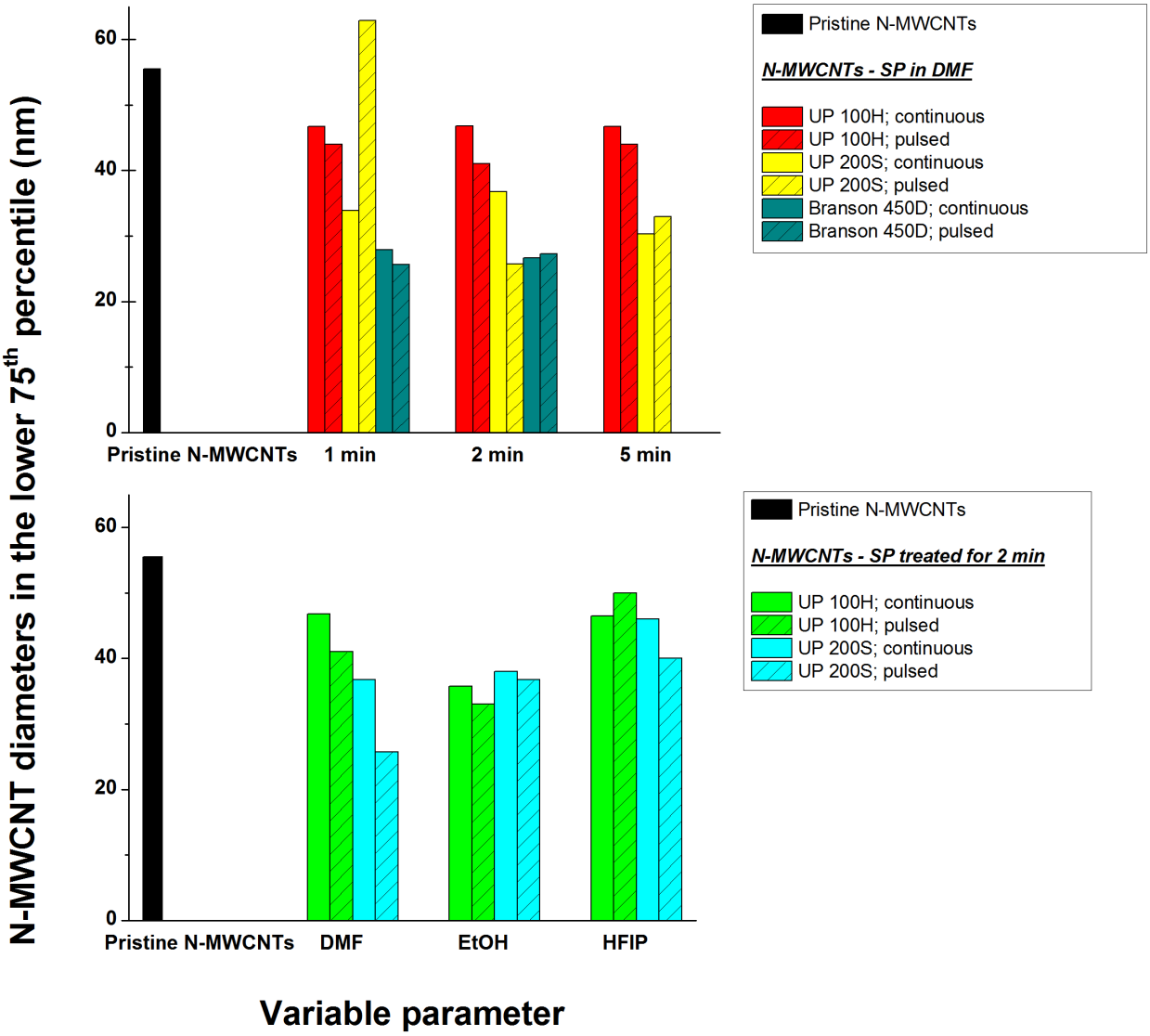


Figure 3-13. Comparison of the N-MWCNT outer diameters (pristine and US probe treated) in the lower 75th percentile with variable sonication parameters:
(a) Treated in DMF with varying US probes, sonication modes and times,
(b) Treated for 2 minutes in different solvents with varying US probes, and sonication modes.

The length and diameter distribution analysis suggest that the sonication parameters (including the power of the US probes, sonication timescales, sonication modes, and dispersing solvents) used in this study were within the limiting parameters that could damage the MWCNTs. However, a significant trend in the effect of varying sonication parameters could not be observed. Moreover, since there was no particular trend in the data of conventional MWCNTs-SP and N-MWCNTs-SP, considering the

time and efforts in obtaining and analysing the SEM and TEM data, further studies on the B-MWCNTs were not conducted.

3.4.3. Analysis of the induced defects

By comparing the Raman spectra of pristine MWCNTs and N-MWCNTs (Figure 3-14), a change in the I_D/I_G and I_{2D}/I_G intensity ratios due to nitrogen doping can be observed. As discussed in Chapter 2, these intensity ratios are widely used to quantify the defects in the MWCNTs and their long-range order. The monotone increase of the I_D/I_G and decrease of the I_{2D}/I_G in N-MWCNTs suggests an obvious degradation of the carbon hexagonal lattice in these nanotubes. The effect of nitrogen doping on the defect densities has been discussed in detail in Chapter 2.

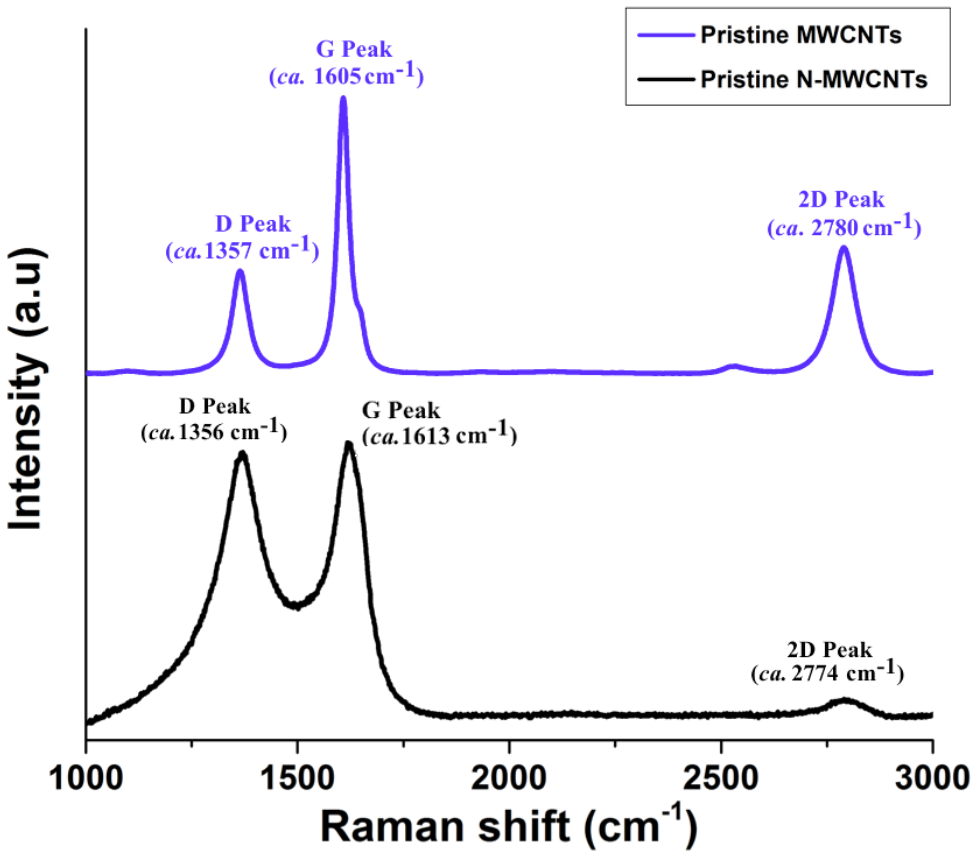


Figure 3-14. Raman spectra of pristine conventional and N- MWCNTs used for sonication study I; all spectra are normalised with respect to the G band intensity.

Figure 3-15 – Figure 3-18 compare the Raman spectra of pristine and US probe treated conventional and N- MWCNTs with varying sonication parameters. It can be seen that no significant effect on the D, G or 2D lines was caused by any of the ultrasonic probes. Even for the longest treatment time, *i.e.*, 5 minutes, the nanotubes seemed to have had minimal damage (Figure 3-16, Figure 3-18). This is a noteworthy result and the reasons for this could be:

a) Low energy US probes: It is reported in literature that the high-energy sonication treatment (both US probe and bath) not only causes nanotube scission but could potentially cause serious damage to the nanotubes[23,29,35,36]. As discussed in 3.4.2.a), the length of the nanotubes decreased significantly, hence it can be confirmed that all the three US probes resulted in successful scission. It can be proposed that the power of the US probes (especially UP 100H and UP 200S) was not high enough to cause damage to the MWCNTs as even the high powered US probe – Branson 450D did not cause damage to the MWCNTs.

b) Lower sonication time-scales: The sonication time plays an equally important role during a sonication treatment. Hence, the lower power of the US probes cannot be given the total credit for not damaging the nanotubes. It has been previously observed that a longer sonication time gives rise to a better quality MWCNT dispersions when suspended in the presence of a surfactant such as sodium dodecylbenzene sulfonate [24,37]. However, it also induces new defects and damages the nanotubes due to the generation of excessive energy[38]. However, in this dissertation work, the sonication time-scales were $\leq$ 5 min. Since these time-scales did not seem to influence the defect densities, it can be assumed that 1–5 min is a safe time range for forming dispersions using any of the above discussed ultrasonic tips.

c) Less harsh nature of the solvents: The deformation caused to the nanotubes can also be solvent dependent. Such behaviour was observed by Green *et al*.[35] who reported less

damage to the MWCNTs in polar solvents such as water and ethanol. Dispersing solvent plays an important role in the transfer of excessive heat and energy to the nanotubes. The structural damage caused is usually significant diameter thinning or induced dislocation defects due to the inefficiency of energy transfer during cavitation. Furthermore, extreme sonication regimes can also result in the increase in the disorder of the CNT structure and result in the formation of amorphous carbon. Such behaviour was not observed in this study (Figure 3-5c,f).

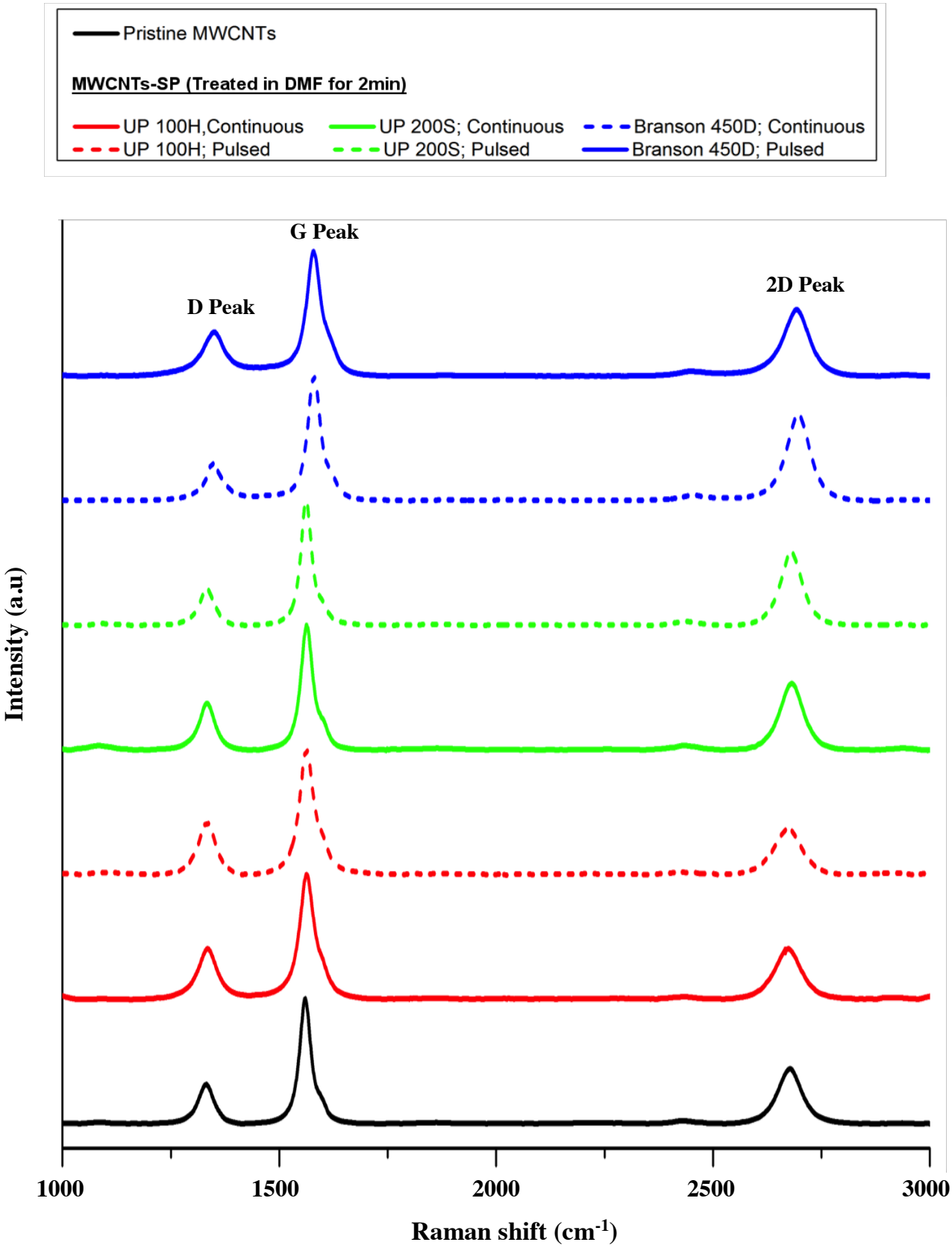


Figure 3-15. Raman spectra of the conventional MWCNTs (pristine and US probe treated) in DMF treated for 2 minutes using three different US probes in continuous and pulsed modes; All spectra are normalised with respect to the G band intensity.

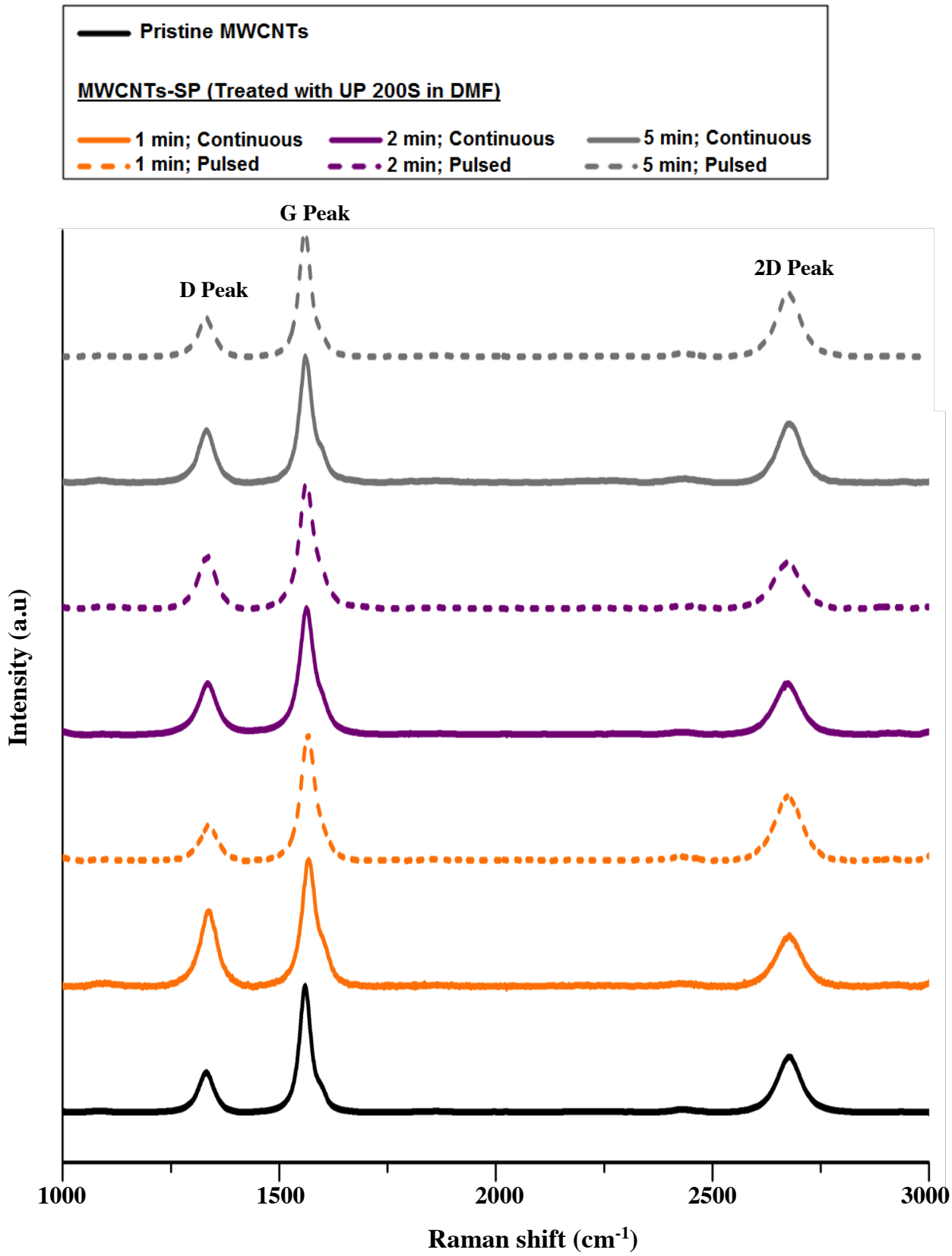


Figure 3-16. Raman spectra of the conventional MWCNTs (pristine and US probe treated) in DMF treated with UP 200S for various times and modes; All spectra are normalised with respect to the G band intensity.

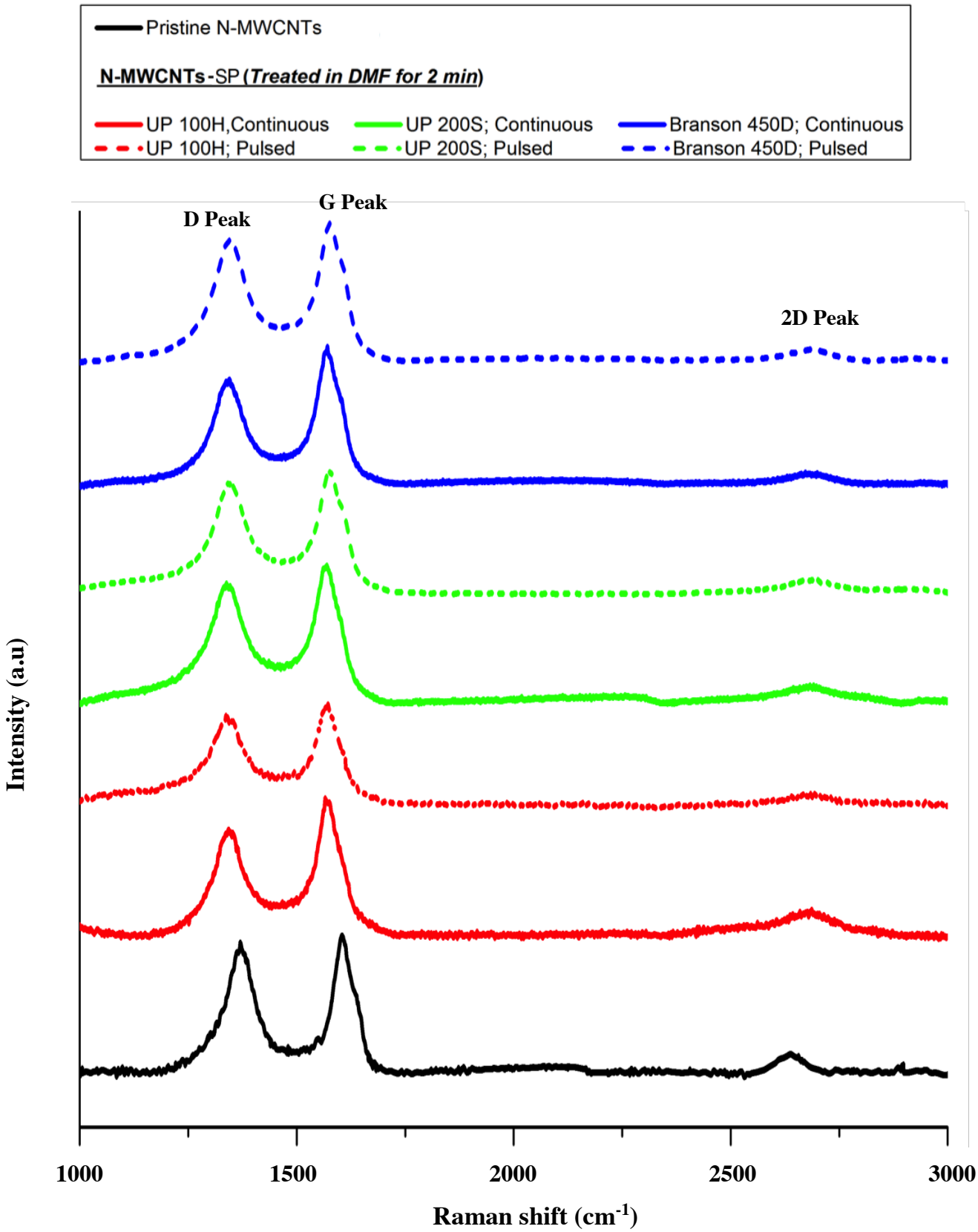


Figure 3-17. Raman spectra of the N-MWCNTs (pristine and US probe treated) in DMF treated for 2 minutes using the three different US probes in continuous and pulsed modes; All spectra are normalised with respect to the G band intensity.

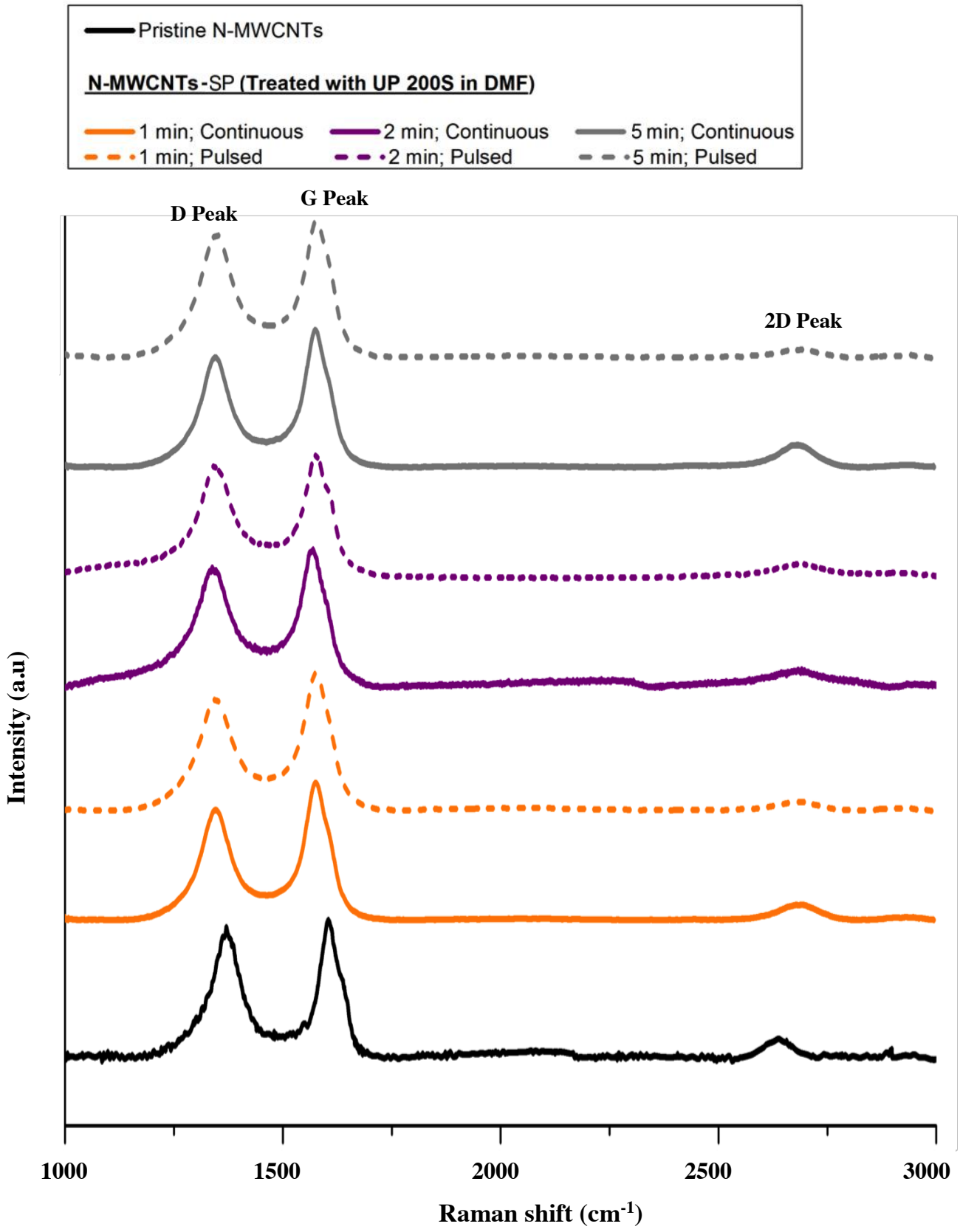


Figure 3-18. Raman spectra of the N-MWCNTs (pristine and US probe treated) in DMF treated with UP 200S for various times and modes; All spectra are normalised with respect to the G band intensity.

3.5. Sonication study II: Development of a sonication protocol; results and discussion

From the results of sonication study I, it was understood that the sonication parameters used were well within the limiting values that could damage the MWCNTs. However, a trend in the effect with respect to changing parameters could not be observed. Based on these results, sonication study II was conducted to develop a protocol mainly to:

1) Efficiently disperse MWCNTs in solvents via sonication.

2) Avoid the use of a surfactant or surface modification of the MWCNTs.

3) Cause least possible damage to the MWCNTs during sonication.

Unlike sonication study I, in the second study the MWCNT lengths and diameters were of less concern. The main concern in study II was the effect on defects, which was analysed through TEM and Raman studies.

3.5.1. Structural characterisation using TEM

Figure 3-19a,b shows the TEM images of the pristine and dispersed conventional MWCNTs in NMP. For a better understanding, the TEM images of as-synthesised and acid treated MWCNTs from the work of Buang *et al*.[39] have also been presented in Figure 3-19c,d. It can be clearly seen that the sonication regime did not have any severe effect on the MWCNT structure. Usually, treatments such as acid treatments that are commonly used for dispersing nanotubes, have a detrimental effect on their structure as can be seen in Figure 3-19d. In this case, straight MWCNTs transformed into twisted structures after the acid treatment, which can potentially affect the nanotube properties. However, the sonication regime used in this study had no such effect, on the contrary, the MWCNTs looked similar to their pristine form.

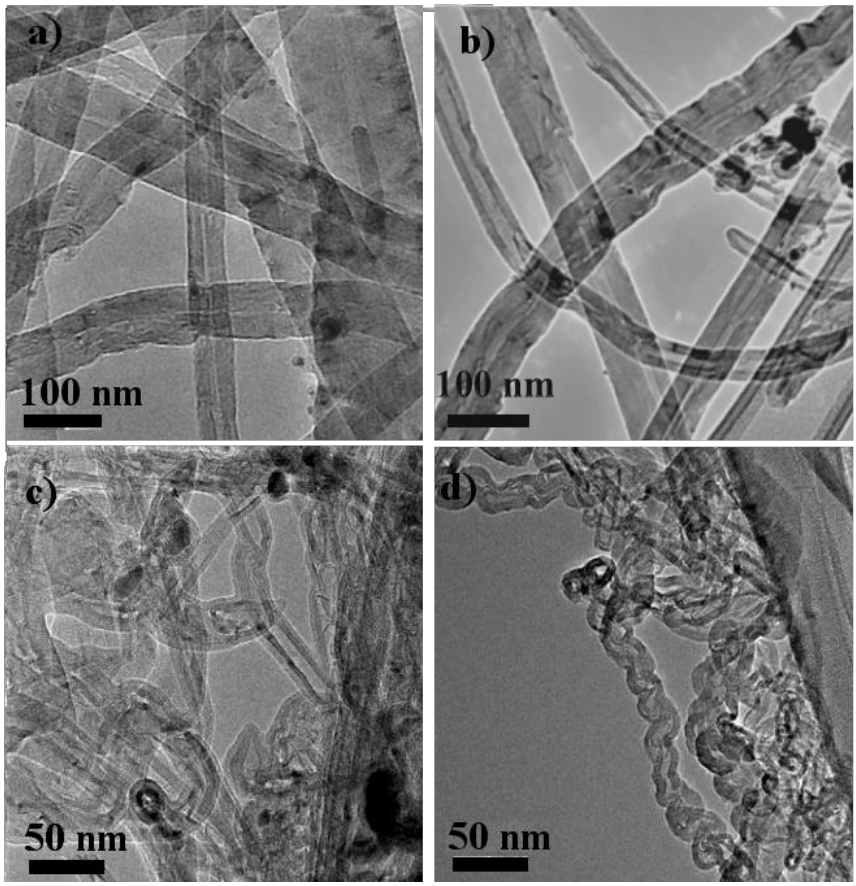


Figure 3-19. TEM images of: a) Pristine conventional MWCNTs, (b) Dispersed conventional MWCNTs in NMP after step 4 of the sonication regime, (c, d) As synthesised and acid treated MWCNTs from the work of Buang et al.[39]

3.5.2. Defect analysis using Raman spectroscopy

Figure 3-20 shows the Raman spectra of the conventional MWCNTs after every step of the sonication regime. The calculated I_D/I_G and I_{2D}/I_G intensity ratios of the conventional MWCNTs after every step of the sonication regime are listed in Table 3-5. It can be seen from Figure 3-20 and Table 3-5 that the sonication regime used in the sonication study II did not induce any significant or new defects in the nanotubes. The I_D/I_G and I_{2D}/I_G intensity ratios were mostly similar to that of the pristine nanotubes; although a small variation after every step of the sonication regime can be observed. This is a noteworthy result confirming the 'destruction reduced' nature of the proposed sonication protocol.

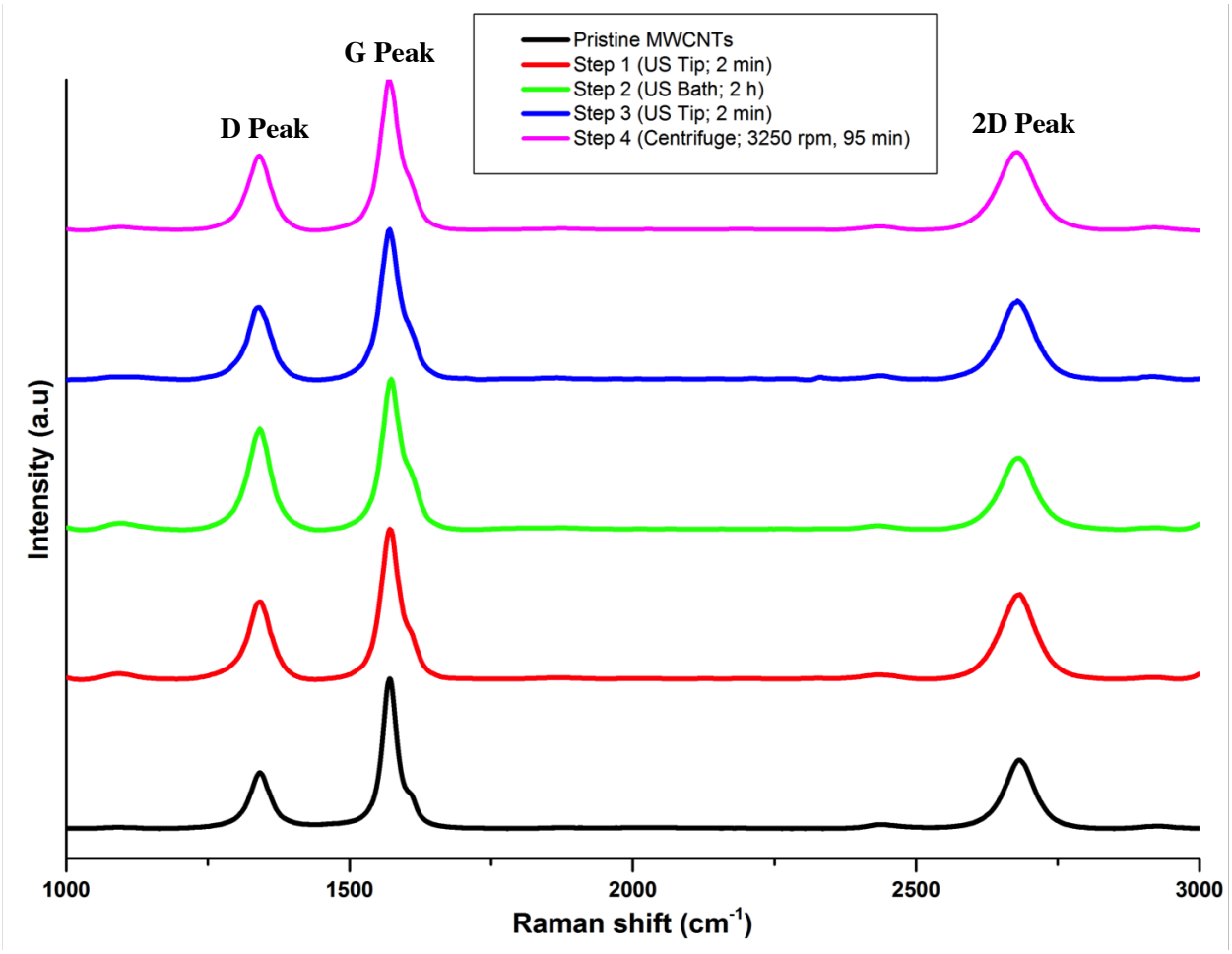


Figure 3-20. Raman spectra of conventional MWCNTs in NMP after every step of the sonication regime.

Sonication Step	I_D/I_G	I_{2D}/I_G
Pristine MWCNTs	0.6 ± 0.10	0.4 ± 0.07
2 min US Probe	0.6 ± 0.06	0.4 ± 0.08
2 h US Bath	0.5 ± 0.10	0.5 ± 0.08
2 min US Probe	0.5 ± 0.04	0.5 ± 0.02
95 min Centrifuge	0.5 ± 0.05	0.4 ± 0.10

Table 3-5. Raman I_D/I_G and I_{2D}/I_G intensity ratios of conventional MWCNTs in NMP after every step of the sonication regime.

3.6. Summary

Sonication studies were conducted to understand the effects of sonication treatments on the MWCNTs. Sonication study I was used to understand the effect of various US probes on the lengths, diameters, and defect densities of conventional MWCNTs, and N-, B- MWCNTs. For this, a combination of sonication parameters was used including varying times (1, 2, and 5 minutes), modes (continuous and pulsed) and dispersing solvents (NMP, EtOH, and HFIP).

Definite debundling of nanotubes occurred for as short as 1 minute sonication intervals. However, the debundling was not uniform and some MWCNT bundles existed even after the sonication treatment. Understanding the sonication effects on the MWCNTs was challenging, as the length and diameter distributions of the pristine raw material MWCNTs were wide to begin with. Therefore, a similarly wide distribution was expected for MWCNTs-SP; this was confirmed through probability length distribution curves. After being treated with various US probes, the conventional MWCNTs and N-MWCNTs decreased to 1–4% and 5–15% of their original lengths respectively with no particular trend by any of the US probes. Though a clear debundling was observed, a difference in the effect of varying sonication parameters could not be established. On the contrary, all treatments presented a wide distribution of MWCNT lengths. Therefore, the MWCNT scission in this study for short intervals (≤ 5 min) did not follow the power law, rather could have followed the theory proposed by Yang *et al*.[25] that the degree of MWCNT suspension is dependent on the sonication energy. However, the sonication times used in this study were perhaps too low to present any specific effects based on either the sonication energy or time or dispersing solvents. Also, the diameter distribution of the MWCNTs subjected to the sonication treatment roughly matched the diameter distribution of their pristine counterparts,

suggesting that thinning of nanotubes did not occur even at the longest sonication time used in this study, *i.e*., 5 minutes. It was also observed from Raman analysis that the parameters used for this study did not introduce any significant defects in the nanotubes and that no major damage was caused to them even after 5 minutes sonication time. Moreover, the TEM studies of the US probe treated MWCNTs confirmed that no major damage was caused to the nanotubes by the sonication treatment. Based on the results from MWCNTs and N-MWCNTs, and having taken into consideration the large amount of characterisation time required to study such samples, it was decided to conduct no further sonication studies on B-MWCNTs. This sonication study gives an approximate estimate of the MWCNT structural properties when treated with US probes, especially the final lengths (reduction to 1–15% of original lengths depending on the type of MWCNT). This estimation can be a useful tool while understanding the properties of composites with MWCNT fillers, where an approximate length of the nanotubes can be estimated based on the sonication treatment. Most importantly, this study was a foundation for the sonication study II that was conducted for developing a 'destruction reduced' sonication regime.

A second sonication study was used to develop a sonication regime to form MWCNT dispersions through pure sonication methods that caused minimum nanotube damage. The aim of the study was also to develop a technique of dispersion forming by avoiding surfactants or any MWCNT surface modification technique. Conventional MWCNTs were dispersed in a common organic solvent – NMP using a combination of US probe, US bath and centrifugation. The proposed regime was based on the work of various researchers in the field of nanotube dispersions. Raman studies were conducted at every step of the sonication regime to understand the effect on the defect densities. Based on the I_D/I_G and I_{2D}/I_G Raman intensity ratios it was confirmed that no

significant defects were introduced in the nanotubes during the sonication regime. This was further confirmed through TEM studies on the MWCNTs at the end of treatment, which showed no noteworthy damage. This sonication regime opens the doors for developing MWCNT dispersions in regular organic solvents solely through mild sonication, without altering the inherent nanotube structure or using a third-phase (such as a surfactant). This helps in retaining the inherent properties of MWCNTs whilst processing for composites.

3.7. References

[1] Simmons, T. J., "Carbon nanotube suspensions, dispersions, & composites," 2008, D.Phil dissertation, Rensselaer Polytechnic Institute.

[2] Maruyama, S., Kojimaa, R., Miyauchia, Y., Chiashia, S., and Kohno, M., "Low-temperature synthesis of high-purity single-walled carbon nanotubes from alcohol," Chemical Physics Letters, 2002, **360**(3-4), pp. 229–234.

[3] Deck, C. P., and Vecchio, K., "Growth mechanism of vapor phase CVD-grown multi-walled carbon nanotubes," Carbon, 2005, **43**(12), pp. 2608–2617.

[4] Krause, B., Mende, M., Pötschke, P., and Petzold, G., "Dispersability and particle size distribution of CNTs in an aqueous surfactant dispersion as a function of ultrasonic treatment time," Carbon, 2010, **48**(10), pp. 2746–2754.

[5] Esumi, K., Ishigami, M., Nakajima, Z., Sawada, K., and Honda, H., "Chemical treatment of carbon nanotubes," Carbon, 1996, **34**(2), pp. 279–281.

[6] O'Connell, M. J., Boul, P., Ericson, L. M., Huffman, C., Wang, Y., Haroz, E., Kuper, C., Tour, J., Ausman, K. D., and Smalley, R. E., "Reversible water-solubilization of single-walled carbon nanotubes by polymer wrapping," Chemical Physics Letters, 2001, **342**(3-4), pp. 265–271.

[7] Park, J. E., Kim, G. R., Yoon, D. J., Sin, C. H., Park, I. S., Bea, T. S., and Lee, M. H., "The Effect of Dispersed MWCNTs Using SDBS Surfactant on Bacterial Growth," World Academy of Science, Engineering & Technology, 2012, (70), pp. 743–746.

[8] Giordani, S., Bergin, S. D., Nicolosi, V., Lebedkin, S., Kappes, M. M., Blau, W. J., and Coleman, J. N., "Debundling of single-walled nanotubes by dilution: observation of large populations of individual nanotubes in amide solvent dispersions," Journal of Physical Chemistry B, 2006, **110**(32), pp. 15708–15718.

[9] Pagani, G., Green, M. J., Poulin, P., and Pasquali, M., "Competing mechanisms and scaling laws for carbon nanotube scission by ultrasonication.," Proceedings of the National Academy of Sciences of the United States of America, 2012, **109**(29), pp. 11599–604.

[10] Tang, C., Guo, W., and Chen, C., "Bending manipulation induced sp^2–sp^3 bond transition in carbon nanotubes," Journal of Applied Physics, 2010, **108**(2), p. 026108.

[11] Fakhri, N., Tsyboulski, D. A., Cognet, L., Weisman, R. B., and Pasquali, M., "Diameter-dependent bending dynamics of single-walled carbon nanotubes in liquids.," Proceedings of the National Academy of Sciences of the United States of America, 2009, **106**(34), pp. 14219–23.

[12] Garg, P., Alvarado, J. L., Marsh, C., Carlson, T. A., Kessler, D. A., and Annamalai, K., "An experimental study on the effect of ultrasonication on viscosity and heat transfer performance of multi-wall carbon nanotube-based aqueous nanofluids," International Journal of Heat and Mass Transfer, 2009, **52**(21), pp. 5090–5101.

[13] Hennrich, F., Krupke, R., Arnold, K., Rojas Stütz, J. A., Lebedkin, S., Koch, T., Schimmel, T., and Kappes, M. M., "The mechanism of cavitation-induced scission of single-walled carbon nanotubes," Journal of Physical Chemistry B, 2007, **111**(8), pp. 1932–1937.

[14] Lucas, A., Zakri, C., Maugey, M., Pasquali, M., van der Schoot, P., and Poulin, P., "Kinetics of nanotube and microfiber scission under sonication," Journal of Physical Chemistry C, 2009, **113**(48), pp. 20599–20605.

[15] Hilding, J., Grulke, E., George Z, Z., and Lockwood, F., "Dispersion of carbon nanotubes in liquids," Journal of Dispersion Science and Technology, 2003, **24**(1), pp. 1–41.

[16] Wu, T. Y., Guo, N., Teh, C. Y., and Hay, J. X. W., "Advances in ultrasound technology for environmental remediation," 2013 Springer Netherlands, Dordrecht.

[17] Pang, Y. L., Abdullah, A. Z., and Bhatia, S., "Review on sonochemical methods in the presence of catalysts and chemical additives for treatment of organic pollutants in wastewater," Desalination, 2011, **277**(1), pp. 1–14.

[18] Kuppa, R., and Moholkar, V. S., "Physical features of ultrasound-enhanced heterogeneous permanganate oxidation," Ultrasonics Sonochemistry, 2010, **17**(1), pp. 123–131.

[19] Mason, T., and Peters, D., " Practical sonochemistry : power ultrasound uses and applications," 2nd Edition, 2002, Woodhead Publishing Limited, Cambridge, p. 12.

[20] Apfel, R. E., "Sonic effervescence: A tutorial on acoustic cavitation," Journal of the Acoustical Society of America, 1997, **101**(3), p. 1227.

[21] Huang, Y. Y., and Terentjev, E. M., "Dispersion of carbon nanotubes: mixing, sonication, stabilization, and composite properties," Polymers, 2012, **4**(4), pp. 275–295.

[22] Glory, J., Mierczynska, A., Pinault, M., Hermite, M. M. L., and Reynaud, C., "Dispersion study of long and aligned multi-walled carbon nanotubes in water," Journal of Nanoscience and Nanotechnology, 2007, **7**(10), pp. 3458–3462.

[23] Dumée, L., Sears, K., Schütz, J., Finn, N., Duke, M., and Gray, S., "Influence of the Sonication Temperature on the Debundling Kinetics of Carbon Nanotubes in Propan-2-ol," Nanomaterials, 2013, **3**(1), pp. 70–85.

[24] Yu, J., Grossiord, N., Koning, C. E., and Loos, J., "Controlling the dispersion of multi-wall carbon nanotubes in aqueous surfactant solution," Carbon, 2007, **45**(3), pp. 618–623.

[25] Yang, Y., Grulke, E. A., Zhang, Z. G., and Wu, G., "Thermal and rheological properties of carbon nanotube-in-oil dispersions," Journal of Applied Physics, 2006, **99**(11), p. 114307.

[26] Journet, C., Maser, W. K., Bernier, P., Loiseau, A., Chapelle, M. L., Lefrant, S., Deniard, P., Lee, R., and Fischer, J. E., "Large-scale production of single-walled carbon nanotubes by the electric-arc technique," Nature, 1997, **388**(6644), pp. 756–758.

[27] Bergin, S. D., Nicolosi, V., Giordani, S., Gromard, A., Carpenter, L., Blau, W. J., and Coleman, J. N., "Exfoliation in ecstasy: liquid crystal formation and concentration-dependent debundling observed for single-wall nanotubes dispersed in the liquid drug γ-butyrolactone," Nanotechnology, 2007, **18**(45), p. 455705.

[28] Bergin, S. D., Sun, Z., Streich, P., Hamilton, J., and Coleman, J. N., "New solvents for nanotubes: approaching the dispersibility of surfactants," Journal of Physical Chemistry C, 2010, **114**(1), pp. 231–237.

[29] Cheng, Q., Debnath, S., Gregan, E., and Byrne, H. J., "Ultrasound-assisted SWNTs dispersion: effects of sonication parameters and solvent properties," Journal of Physical Chemistry C, 2010, **114**(19), pp. 8821–8827.

[30] Ham, H. T., Choi, Y. S., and Chung, I. J., "An explanation of dispersion states of single-walled carbon nanotubes in solvents and aqueous surfactant solutions using solubility parameters.," Journal of Colloid and Interface Science, 2005, **286**(1), pp. 216–23.

[31] Meysami, S. S., Dillon, F., Koós, A. A., Aslam, Z., and Grobert, N., "Aerosol-assisted chemical vapour deposition synthesis of multi-wall carbon nanotubes: I. Mapping the reactor," Carbon, 2013, **58**, pp. 151–158.

[32] Koós, A. A., Dowling, M., Jurkschat, K., Crossley, A., and Grobert, N., "Effect of the experimental parameters on the structure of nitrogen-doped carbon nanotubes produced by aerosol chemical vapour deposition," Carbon, 2009, **47**(1), pp. 30–37.

[33] Blase, X., Charlier, J. ., De Vita, A., Car, R., Redlich, P., Terrones, M., Hsu, W., Terrones, H., Carroll, D., and Ajayan, P. M., "Boron-mediated growth of long helicity-selected carbon nanotubes," Physical Review Letters, 1999, **83**(24), pp. 5078–5081.

[34] Poncharal, P., Berger, C., Yi, Y., Wang, Z. L., and de Heer, W. A., "Room temperature ballistic conduction in carbon nanotubes," Journal of Physical Chemistry B, 2002, **106**(47), pp. 12104–12118.

[35] Lu, K., Lago, R. M., Chen, Y. K., Green, M. L. H., Harris, P. J. F., and Tsan, S. C., "Mechanical damage of carbon nanotubes by ultrasound," Carbon, 1996, **34**(6), pp. 814–816.

[36] Ma, P.-C., Siddiqui, N. A., Marom, G., and Kim, J.-K., "Dispersion and functionalization of carbon nanotubes for polymer-based nanocomposites: A review," Composites Part A: Applied Science and Manufacturing, 2010, **41**(10), pp. 1345–1367.

[37] Yang, K., Yi, Z., Jing, Q., Yue, R., Jiang, W., and Lin, D., "Sonication-assisted dispersion of carbon nanotubes in aqueous solutions of the anionic surfactant SDBS: The role of sonication energy," Chinese Science Bulletin, 2013, **58**(17), pp. 2082–2090.

[38] Shi, Y., "Optimization conditions for single-walled carbon nanotubes dispersion," Journal of Surface Engineered Materials and Advanced Technology, 2013, **03**(01), pp. 6–12.

[39] Buang, N. A., Fadil, F., Majid, Z. A., and Shahir, S., "Characteristic of mild acid functionalized multiwalled carbon nanotubes towards high dispersion with low structural defects," Digest Journal of Nanomaterials & Biostructures, 2012, **7**(1), p. 33.

Chapter 4. Development of stable MWCNT dispersions

4.1. Introduction

As discussed in chapter 3, sonication of MWCNTs allows individual separation of nanotubes from their respective bundles and presents opportunities for fully exploiting their potential. However, individual separation of the nanotubes is not the only limitation towards their commercial use in composites. Due to their agglomerating nature, there is a possibility for re-agglomeration to occur during the composite processing, which can result in inferior properties of the composite. One solution to this problem is to form nanotube dispersions in solvents that can keep the individual nanotubes separated for a long time, thus allowing easier processing[1–5]. Literature suggests various techniques for developing such dispersions, most of which include functionalisation or surface treatments of the nanotubes along with high-energy methods. These techniques usually degrade the nanotube structure, which consequently deteriorates its physical and electrical performance[6–10]. Fewer strategies have been developed for forming high quality MWCNT dispersions whilst retaining their remarkable intrinsic properties. Moreover, limited research has been reported in the field of dispersions of doped MWCNTs in their pristine form.

This chapter presents a technique to form uniform and homogeneous MWCNT dispersions, whilst overcoming the above-mentioned issues. The 'destruction reduced sonication protocol' presented in chapter 3 was used for developing dispersions of conventional, N-, and B- MWCNTs in organic solvents. For this purpose, the studies were divided into two parts:

Dispersion study I) Development of MWCNT dispersions at labscale.

Dispersion study II) Development of MWCNT dispersions at upscale.

It should be noted that the term 'dispersion' in Chapters 4 and 5 refers to individually separated and homogeneously distributed MWCNT suspensions in organic or aqueous solvents.

4.2. Dispersion strategies

Most of the existing dispersion forming techniques include treating the nanotubes covalently[11–14] or non-covalently[1,3,5,15–20]. These treatments employ dangerous materials, alter the nanotube structure, and/or use high sonication treatments. An assessment of the existing treatments is given below, indicating their limitations in utilising the full potential of MWCNTs, and showing the need for more research in developing MWCNT dispersions with less damage in a safer environment.

4.2.1. Covalent approach

Ability of carbon to widely interact chemically allows the addition of various functional groups with ease, *i.e.*, functionalisation of the nanotubes. Some of the commonly used approaches are briefly discussed here.

a) *Acid functionalisation*

Functionalising nanotubes covalently with oxidative acids is a well-established technique and is one of the foremost methods proposed for readily forming dispersions. It involves either treating the nanotubes with acid solutions at high temperatures or sonicating them at room temperature. The first reports addressing this technique were reported by Smalley *et al*.[21] and Esumi *et al*.[22] who treated SWCNTs and MWCNTs with a mixture of concentrated nitric acid and sulphuric acid (1:3 concentration mixture). The mixture of these acids results in nitronium ions (NO_2^+) (Equation 4-1), which on heating interact with the electron-rich nanotubes and forms carboxylic or oxygen containing functional groups with the nanotubes. Functionalisation primarily

occurs at the tube ends or at the nanotube sidewalls. These functional groups allow the nanotube to readily disperse in regular solvents such as water or ethanol.

$$2\,H_2SO_4 + HNO_3 \rightleftharpoons 2\,HSO_4^- + NO_2^+ + H_3O^+ \qquad \text{Equation 4-1}$$

The oxidation process usually varies with the nanotube type, *i.e.*, SWCNTs undergo tip opening and sidewall degradation, MWCNTs on the other hand are less reactive due to their less curved tips. Furthermore, the functionalisation process can also vary with the type of defects present in the nanotube. The generally occurring defects in the nanotubes can be classified as[23,24]: topological (anomaly in the regular six-membered carbon ring structure, such as an inclusion of five or seven membered rings) (Figure 4-1a), re-hybridisation (such as sp^3 hybridised defects) (Figure 4-1b), and incomplete bonding defects (such as vacancies or dislocations). These inherently occurring defects can degrade the nanotube properties, such as the nanotube strength[6] or a change in the metallic or semiconducting behaviour[24]. To add to this, the functionalisation process creates new defects in the nanotubes, such as holes created due to oxidation (Figure 4-1c) or opening of the tube end and formation of terminal groups (COOH, OH, H, *etc*.) (Figure 4-1d) that can cause further damage to the nanotube properties.

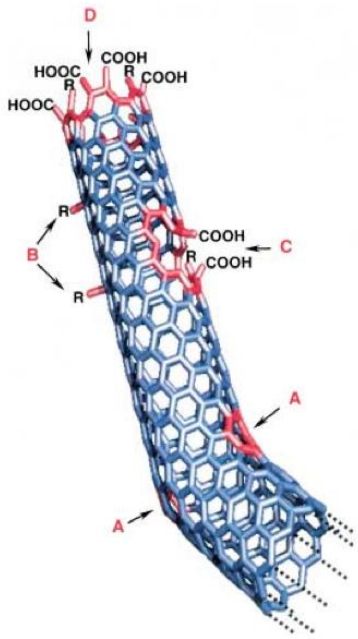


Figure 4-1. A model showing some typical inherent defects and those arising from functionalisation in a SWCNT: A) A topological anomaly in the regular six-membered carbon ring that results in bending of the tube, B) sp^3-hybridised defects (R=H and OH), C) Damage in the SWCNT structure due to the oxidative acid treatment, which also results in a hole lined with -COOH groups, and D) -COOH terminal groups at the open end of the nanotube caused due to the oxidative treatment.[23]

Acid functionalisation of the nanotubes helps in creating a strong interfacial interaction between the functional moieties attached to the nanotubes and the functional groups in the polymer matrix. This aids in an efficient interfacial load transfer that has a profound positive effect on the mechanical and thermal properties of the composites. For example, Zou *et al*.,[25] observed an improvement of 45% and 90% in the tensile strength and modulus respectively of acid treated MWCNT/epoxy composites at a low nanotube concentration of 0.1 wt.%. This improvement was attributed to the covalent bond formation between the functional groups attached to the MWCNTs and the polymer matrix. Similarly, Ramanathan *et al*.,[26] observed an increase in the thermal degradation temperature and storage modulus in functionalised SWCNTs/PMMA composites due to an improved interfacial interaction between the nanotubes and the PMMA matrix. However, the acid functionalisation has sometimes proven to be

disadvantageous due to its adverse effect on the electrical properties[27,28] of the nanotubes as it causes disruption in the nanotube structure[10]. For instance, Bose *et al*.,[27] reported that the addition of functionalised MWCNTs to polyamide and acrylonitrile–butadiene–styrene blends lowered the dielectric constants of the system due to a decrease in the aspect ratios of the functionalised nanotubes. Hence, acid treatments are immensely useful when an application demands for excellent mechanical or thermal properties but can be equally detrimental for electrical applications.

b) *Secondary acid-functionalisation*

Further functionalisation following the previously mentioned acid treatment has also been proven to improve the dispersibility of the nanotubes. Examples of such secondary functionalisation techniques are conversion of the carboxylic and alcohol groups into acyl chlorides[29] or covalently attaching diamine terminated chains of polyethyleneglycol[30]. These functional groups can further be substituted with different nucleophiles. Such secondary functionalisation enables the nanotubes to form high quality dispersions, especially polyethylene glycol substitutions have proven to produce high quality dispersions[30]. However, the secondary functionalisation treatments involve use of corrosive and toxic chemicals (such as thionyl chloride[30]) and are unable to yield economically feasible products. This poses a major limitation for this technique.

4.2.2. Non-covalent approach

The non-covalent approach offers more benefits than the covalent approach as no harsh or dangerous chemicals are involved in this approach; making it relatively safe to use. Moreover, the non-covalent approach helps in preserving the intrinsic properties of nanotubes. Additionally, some of these techniques employ low-energy processes that minimise the damage caused to the nanotubes during dispersion forming.

a) Surfactant Assisted

The amphiphilic nature of surfactants, *i.e.*, the hydrophilic/polar head group and the hydrophobic/tail group, makes them a candidate for improving the aqueous dispersibility of nanotubes. The hydrophobic molecules of the surfactants adsorb onto the nanotube sidewalls through the Van der Waals attractions and the π–π and CH–π interactions[31]. On the other hand, the hydrophilic molecules of the surfactant facilitate the dispersibility in an aqueous medium. This process is usually combined with sonication so that exfoliation and adsorption can occur simultaneously improving the quality of the dispersion. Sonication causes separation of individual nanotubes from bundles that can act as sites for surfactant adsorption. The stability of these surfactant-coated individual nanotubes is maintained by electrostatic repulsions (in the case of ionic surfactants)[32] or steric repulsions (in the case of non-ionic surfactants)[19].

Various surfactants (both ionic and non-ionic) have been reported in the literature for effectively dispersing nanotubes. Some examples are: sodium dodecyl sulfate (SDS)[4,33], sodium dodecylbenzene sulfonate (SDBS)[5,34], triton X-100[35], tween 20[35], tween 80[35], dodecyltrimethylammonium bromide[36], and hexadecyltrimethylammonium bromide[37]. Amongst these, the interactions of SDS and SDBS with the nanotubes have been well studied. It has been reported that SDS has the ability to disperse both SWCNTs[38,39] and MWCNTs[4,33]. However, the interactions between the alkyl chains of SDS and the nanotubes are non-specific. This results in a weak packing of the chains around the nanotubes and formation of unstable micelles[40]. SDBS, on the other hand, has proven to be more efficient due to the presence of a phenyl ring (as seen in Figure 4-2). Surfactants with such aromatic rings have the ability to form specific and directional π–π stacking with the nanotubes and increase the surfactant adsorption ratio[19].

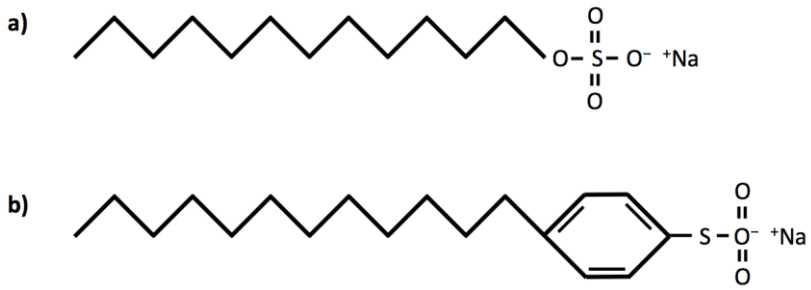


Figure 4-2. Structures of: a) Sodium dodecyl sulfate and b) Sodium dodecylbenzene sulfonate with the additional aromatic ring.

Alternatively, the efficiency of these surfactants can be explained by the 'crowning effect' caused due to the formation of surfactant micelles on the nanotube surface[41]. The hydrophobic alkyl chains of the surfactants can easily pack along the nanotube surface. But the terminating hydrophilic sulfate and sulfonate groups are mutually repellent and do not pack closely. Hence, the molecules form a crown shape that reduces the dispersibility of the nanotubes as it decreases the accessibility of the hydrophilic groups of the chain to the aqueous solvent. The additional phenyl ring in the SDBS forces the alkyl chains to be separated more widely, thereby reducing the crowning effect in the case of SDBS (as seen in Figure 4-3), and making it more efficient. This has been confirmed experimentally in the literature, with various reports confirming higher dispersibility concentration of nanotubes by SDBS[41].

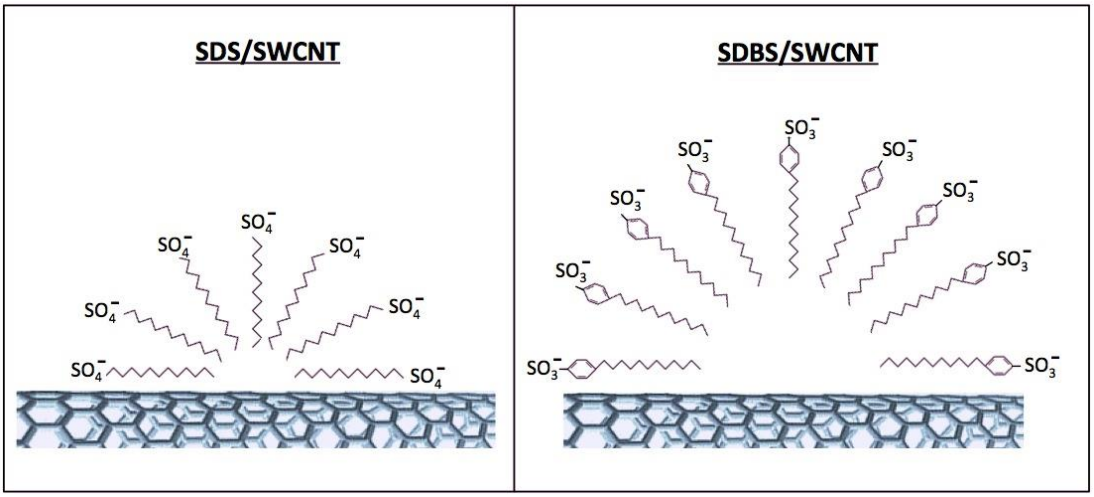


Figure 4-3. An illustration of the crowning effect due to the interaction between the SDS, SDBS surfactants and the nanotube.[41]

Similar to the acid functionalisation, surfactants improve the interfacial adhesion between the nanotubes and the polymer matrix by forming hydrogen bonds between the hydrophilic segments of the surfactant and the hydrophilic segments in the polymer. Such bonding improves the wettability of the nanotubes in the polymer and creates efficient load transfer interfaces[7]. This can help in improving the flexural strength, flexural modulus, storage modulus, and glass transition temperature in the composites[7,10]. However, such bonding has also proven to deteriorate the impact properties in composites due to a cross-linking induced brittleness[7]. Moreover, the presence of ionic surfactants on the nanotube surface has proven to deteriorate the thermal conductivity in MWCNT/silicone composites due to phonon scattering[8]. Additionally, the presence of surfactants has also proven to degrade the electrical properties of the composites[9].

b) Polymer functionalisation

Wrapping nanotubes with polymers non-covalently is another technique that can successfully solubilise them. Given the wide compositional variation of the polymers, this technique offers a broad research area. The idea of polymer wrapping was first inspired by the reports of nanotube dispersions formed using gum arabic[42], which has been long known for its efficiency in suspending carbon black. Regev *et al*.[42] were able to disperse SWCNT concentrations of up to 3 wt.% in aqueous gum arabic ($C_{26}H_{34}N_2O_{13}$) solutions, however the stability of these dispersions proved to be bad. This paved path for new studies, such as polymer wrapping. Some of the commonly used polymers for wrapping nanotubes are polyvinyl pyrrolidone (PVP)[16,39], polystyrene sulfonate[16,43], polyaniline[44], polyethylene[45], poly(methyl methacrylate)[46], and poly(phenylene vinylene)[47].

Smalley *et al*.[16] proposed that the phenomenon of polymer wrapping is based on the elimination of the hydrophobic interface between the nanotubes and the aqueous medium. This creates a thermodynamic drive to minimise the strain in the polymer conformations whilst interacting with the mechanically rigid nanotubes. It is believed that the wrapping occurs uniformly around the nanotube in an orderly manner usually as a helical motif, and is only occasionally random. Let us consider the case of PVP that has a hydrophobic alkyl backbone along with hydrophilic pyrrolidone groups. Upon interacting with a nanotube in an aqueous medium, PVP wraps around the nanotube with its alkyl chain in contact with the nanotube surface, while the pyrrolidone groups are exposed to the water. Figure 4-4 illustrates the different wrapping arrangements that are possible in such an interaction.

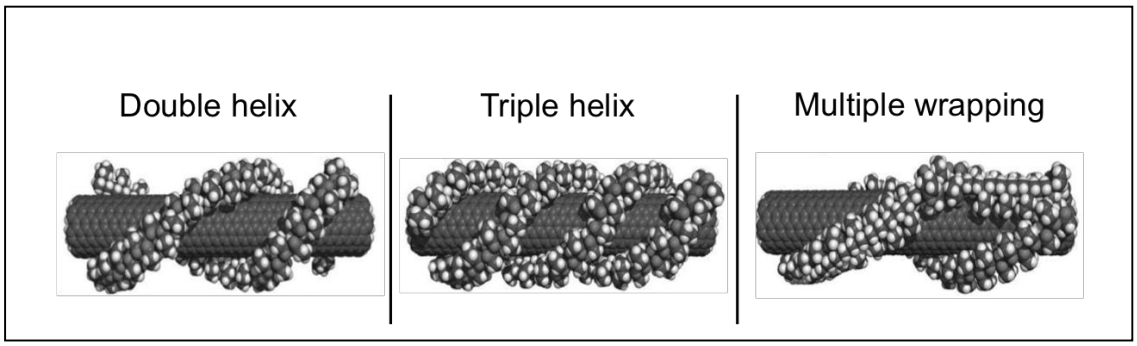


Figure 4-4. A molecular simulation showing the possible wrapping arrangements of PVP polymer around a SWCNT (8,8)[16].

Additionally, polymer functionalised nanotubes have been realised to be dispersible in a variety of solvents. Hong *et al*.[48] successfully dispersed poly(2-ethyl-2-oxazoline) functionalised MWCNTs in both aqueous and organic solvents such as ethanol and dimethylformamide. The quality of these dispersions was excellent and the stability could be maintained even after 642 hours. Similarly, Tang *et al*.[49] conducted *in situ* polymerisation of MWCNTs with poly(phenylacetylene) and successfully formed dispersions in tetrahydrofuran, toluene, chloroform, and 1,4-dioxane.

Functionalisation of this type creates a possibility for macroscopic manipulation of nanotubes, extends the list of potential applications, and thus opens a new area of research. However, the number of polymers that can form efficient functionalisation are limited, which poses a major limitation to this technique.

c) Non-aqueous dispersions in organic solvents

The technique of forming nanotube dispersions in organic solvents avoids the implementation of a third phase (such as a surfactant) in the system that can have a detrimental effect on the final properties. It also prevents the alteration of the intrinsic nanotube structure that affects its electronic performance. It is for these reasons that this technique is of interest for this doctoral work. This section discusses the various theories and possibilities for forming such non-aqueous nanotube dispersions.

A systematic study conducted by Landi *et al*.,[50] revealed the favourable interactions between SWCNTs and alkyl amide solvents that allow dispersion forming. These interactions can be attributed to the high polarisability of the nanotubes and their suitable optical geometries such as bond lengths and bond angles. In addition to the amides, aromatic solvents such as chlorinated[51,52] and fluorinated[53] aromatic solvents, have also been reported to efficiently disperse nanotubes. The effectiveness of these solvents is determined from the dispersion states of the nanotubes, which in turn depends on the intrinsic Van der Waals forces and the nanotube/solvent interactions. These dispersion states can be explained using the Hildebrand and Hansen solubility parameters. The Hildebrand solubility parameter (δ) was proposed by Joel Hildebrand and Robert Scott in 1950[54] in their work on solubility of non-electrolytes. It gives a numerical estimate of the degree of intermolecular interactions of a solvent and is derived from the cohesive energy density of a solvent, which depends on its heat of vaporisation. It can be described as:

$$\delta = \sqrt{c} = \sqrt{\frac{\Delta H - RT}{V_m}} \qquad \text{Equation 4-2}$$

where: c is the cohesive energy density, ΔH is the enthalpy of vaporisation, R is the gas constant, T is the temperature, and V_m is the molar volume.

The total energy of vaporisation consists of several individual forces, *i.e.*, dispersion forces between the molecules (δ_D), dipolar intermolecular forces (δ_P), and molecular hydrogen bonding (δ_H). During a solvent/solute interaction, one or more of these individual forces can be dominant. This means that two solvents can have similar Hildebrand values but might show completely different solubility behaviour. Since the total cohesive energy on its own cannot give an accurate idea of the solubility behaviour, it is important to know which of the individual forces are dominant during such an interaction. Hence, this restricts the universal applicability of the Hildebrand values. This resulted in the three-dimensional Hansen parameters proposed by Charles Hansen in 1967 in his doctoral dissertation[64]. Hansen's parameters take into consideration all the three energy components (δ_D, δ_P, δ_H) and relate them to the total Hildebrand value (δ_T), which can be described as:

$$\delta_T^2 = \delta_D^2 + \delta_P^2 + \delta_H^2 \qquad \text{Equation 4-3}$$

Materials having similar Hansen solubility parameters interact well with each other and are expected to have high affinity. Therefore, by matching the Hansen solubility parameters of the nanotubes with that of the solvents, one can predict the suitable solvents for the nanotubes. However, the reports by Coleman *et al.*,[3,55] suggest the possibility of the nanotube surface energy as a fundamental parameter for finding suitable solvents. Coleman's team used the thermodynamic theories of free energy of mixing to explain the dispersibility of SWCNTs in solvents such as N-Methyl Pyrrolidone. The free energy of mixing (ΔG_{mix}) is given by:

$$\Delta G_{mix} = \Delta H_{mix} - T\Delta S_{mix}$$ Equation 4-4

where: ΔH_{mix} is the enthalpy of mixing, ΔS_{mix} is the entropy of mixing, and T is the temperature.

The solubilisation of the nanotubes in a particular solvent is thermodynamically possible only if ΔG_{mix} is negative, which is possible when ΔH_{mix} is small. ΔH_{mix} is related to the balance of the surface energies of the nanotubes and the dispersing solvent and is minimal when both the surface energies match[1,3,55]. Furthermore, Coleman *et al*.,[55] also reported that a number of solvents in the Hansen parameter region fail to disperse nanotubes. Hence, it can be presumed that the Hansen solubility parameters can sometimes be used for finding suitable solvents for the nanotubes but they cannot be treated as fundamental parameters to understand the nanotube/solvent interactions.

Various studies have reported a variety of solvents suitable for dispersing SWCNTs, some based on Hansen solubility parameters, and others based on surface energy calculations, while some found through traditional trial and error. Some of these solvents are N-Methyl Pyrrolidone[3], Dimethylformamide[56], Cyclohexyl pyrrolidone[57], 1-Benzyl-2-Pyrrolidinone[57], Hexafluoroisopropanol[53], γ-Butyrolactone[58], N,N-Dimethylacetamide[50], 1,2-Dichlorobenze[51], Chloroform[51], and Toluene[59]. However, the efficiency of the dispersing solvent depends on the type of nanotube, which varies widely with different synthesis methods and precursors used (as discussed in Chapter 2)[60,61]. Moreover, the surface characteristics change completely for MWCNTs and all the solvents used for dispersing SWCNTs might not be suitable for MWCNTs. Furthermore, very few reports[1,62,63] address the dispersibility behaviour of conventional and doped MWCNTs in organic solvents, therefore requiring further research into the development of such techniques.

4.3. Materials and equipment used

Conventional, N-, and B- MWCNTs produced by the AACCVD technique were used for both studies I and II. For study I, 22 different organic solvents were used (see Table 4-1) for dispersing the MWCNTs. Hielscher UP 100H (100 W, 30 kHz) US probe, Ultrawave U1250D (200 W, 30–40 kHz) US bath, and Sciquip 1-6P centrifuge were used for preparing the dispersions.

Based on the results from study I, selected solvents were used for dispersing the MWCNTs in study II: N-Methyl Pyrrolidone (NMP; Sigma Aldrich 99.5%) for dispersing conventional MWCNTs, Benzyl alcohol (Sigma Aldrich 99.0%) and Dimethylacetamide (DMA; Sigma Aldrich 99.0%) for dispersing N-MWCNTs, and γ-Butyrolactone (GBL; Fluka 99.5%) for dispersing B-MWCNTs. Upscale production of the MWCNT dispersions was conducted at Bayer Technology Services, Germany during my secondment programme. A Branson 450D (400 W, 20 kHz) US probe, Bandelin Sonorex RK 510/H (400 W, 35 kHz) US bath, and Avanti J-30I centrifuge were used for forming these dispersions.

Solvent	Surface Energy (mJ/m^2)	Boiling Point at 760 mm Hg (^oC)	Retained final concentration, $\chi_{retained}$ (%)	
			Conventional MWCNTs	***N-MWCNTs***
Diethyl Ether (Romil 99.9%)	45.8	34.6	0.5	0.4
Iso-Propyl Alcohol (Sigma Aldrich 99.5%)	51	82.2	0.4	0.3
Acetone (Sigma Aldrich 99.0%)	53	56.5	0.2	0.4
Tetrahydrofuran (Romil 99.9%)	55.7	66	0.3	1
Dichloromethane (Sigma Aldrich 99.8%)	57.19	38.7	0.6	0.3
Chloroform (Sigma Aldrich 99.8%)	58.4	62	0.3	2
Propionitrile (Aldrich 99.0%)	58.9	109	1.1	5
Toluene (Sigma Aldrich 99.9%)	60.2	110.5	0.4	9
Cyclopentanone (Fluka 99.0%)	64.85	49.2	0.3	56
Dimethylacetamide (Sigma Aldrich 99.0%)	66	166.1	2	82
Dimethylformamide (Romil 99.9%)	66.4	152.9	11	61
Benzyl alcohol (Sigma Aldrich 99.0%)	68.3	204.7	14	59
Acetophenone (Fluka 99.5%)	69.1	201.9	46	43
N-methyl-Pyrrolidone (Sigma Aldrich 99.5%)	70	202	56	41
Dimethyl-imidazolidinone (Aldrich 99.5%)	71.8	220.3	52	11
Dimethyl Sulfoxide (Sigma Aldrich 99.9%)	72.28	189	9	13
Triethanolamine (Sigma 99.9%)	74.54	335	4.8	6
Benzyl Benzoate (Sigma 99.0%)	75.25	323	1	5
γ-Butyrolactone (Fluka 99.0%)	75.8	205	14	8
Diiodomethane (Sigma Aldrich 99.0%)	80.1	182	0.8	0.1
Formamide (Sigma 99.5%)	87.5	210.5	0.2	0
Water	102.3	100	0.2	0.1

Table 4-1. List of the solvents along with their properties used for study I for dispersing conventional and N-MWCNTs. Also listed is the percentage of retained MWCNT concentration in the supernatant dispersion after CF ($\chi_{retained}$) calculated using UV-Vis-NIR studies.

4.4. Experimental procedure and characterisation

4.4.1. Labscale production

In order to develop efficient non-aqueous MWCNT dispersions containing pristine nanotubes, it was important to understand their dispersing mechanisms in various solvents. Moreover, it was critical to choose the best suitable solvent that not only dispersed maximum amount of MWCNTs but also maintained the dispersion stability for a long time. Therefore, the labscale production study was further divided into two steps:

Step 1) Choosing the best solvent.

Step 2) Forming MWCNT dispersions.

Step 1: Firstly, 7 mg of each MWCNT was mixed with solvents from Table 4-1 (concentration – 1 mg/ml) and was sonicated for 2 minutes using the US probe in continuous mode. The US probe aids in the disruption of the MWCNT bundles and promotes intercalation of the solvent between the nanotubes. The dispersions were then placed in the US bath for 30 minutes to further homogenise the mixture. The dispersions were then centrifuged for 95 minutes at 5000 rpm. Finally, the supernatant dispersion was carefully separated from its sediment. UV-Vis-NIR absorption studies were performed on the dispersions using Varian Cary 5000 spectrometer before and after centrifugation (CF) to estimate the final MWCNT concentration. It should be noted that a summer student – Mr. Richard Franzese, conducted a part of the dispersion preparation.

Step 2: Based on the results of step 1, 10 ml dispersions (concentration – 1 mg/ml) of conventional MWCNTs in NMP, N-MWCNTs in DMA, and B-MWCNTs in GBL were prepared using the sonication protocol proposed in Chapter 3, *i.e.*, 2 minutes US probe in continuous mode, 2 hours US bath, 2 minutes US probe in continuous mode,

and 95 minutes CF. UV-Vis-NIR absorption studies were performed on the dispersions before and after CF to measure the final concentration and the extinction coefficients of the MWCNTs. Raman studies were also performed on the final dispersions for understanding the defect densities in the MWCNTs. The dispersions were monitored visually to study their stability over time.

4.4.2. Upscale production

150 ml MWCNT dispersions (concentration – 1 mg/ml) were prepared by dispersing 150 mg each of conventional MWCNTs in NMP, N-MWCNTs in Benzyl alcohol, and B-MWCNTs in GBL. It should be noted that due to the unavailability of DMA at the time of preparation, Benzyl alcohol, which has a similar surface energy as DMA, was used for dispersing the N-MWCNTs. Also, the high power of the Branson 450D US probe resulted in overheating of the dispersions, therefore the sonication procedure was slightly modified for the upscale production. The procedure followed was 2 minutes US probe treatment in pulsating mode, 2 hours US bath treatment at room temperature, 2 minutes US probe treatment in pulsating mode, followed by 90 minutes of CF at 5000 rpm. UV-Vis-NIR absorption and Raman studies were performed on the final dispersions to measure the final MWCNT concentrations and to study the defect densities.

4.5. Results and discussion

4.5.1. UV-Vis-NIR spectroscopy of MWCNT dispersions

UV-Vis-NIR spectroscopy was used to determine the efficiency of the 22 organic solvents (listed in Table 4-1) in dispersing the MWCNTs. It was also used to understand the effect of nitrogen doping on the dispersing behaviour of the nanotubes. Dispersions of higher concentrations tend to contain larger nanotube aggregates that are usually removed after CF. Hence, the concentration of the nanotubes in the

dispersions after CF is always less than the initial concentration. The UV-Vis-NIR spectra at a particular wavelength can be used to calculate the retained nanotube concentration in the final dispersions[2]. In this case the spectra at 660 nm were taken before and after CF and the percentage of final retained nanotube concentration after CF ($\chi_{retained}$) was calculated using:

$$\chi_{retained} = \frac{A_{660,F}}{A_{660,I}} 100 \qquad \text{Equation 4-5}$$

where: $A_{660,I}$ and $A_{660,F}$ are the absorbance at 660 nm before and after CF respectively. Table 4-1 also lists the $\chi_{retained}$ for the conventional and N-MWCNT dispersions and Table 4-2 lists the Hansen and Hildebrand solubility parameters of the 22 dispersing solvents. A plot of the $\chi_{retained}$ against the surface energy of the dispersing solvent provides a better understanding of the efficiency of the various dispersing solvents and the effect of nitrogen doping on the dispersion behaviour (Figure 4-5).

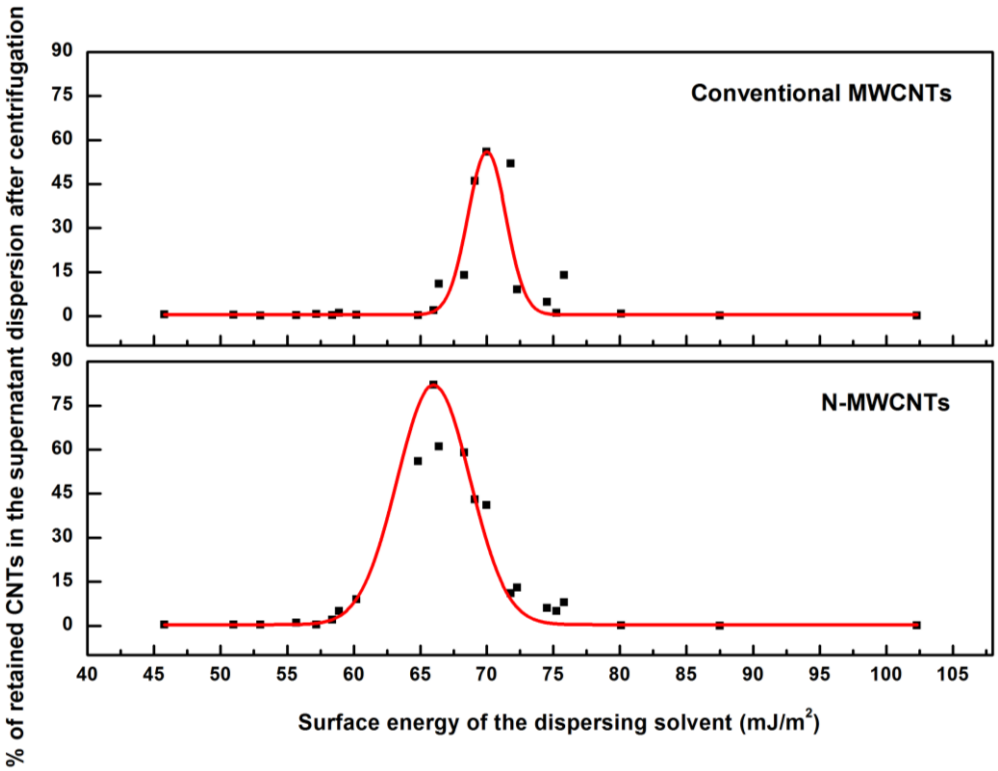


Figure 4-5. Graphs showing the % of MWCNTs retained after centrifugation as a function of the surface energy of the dispersing solvent. A Gaussian curve (in red) fitted to the data clearly shows a shift in the dispersing ability of the N-MWCNTs towards the lower surface energy solvents.[1]

Solvent	δ_D (mJ/m^2)	δ_P (mJ/m^2)	δ_H (mJ/m^2)	δ_T (mJ/m^2)
Diethyl Ether	14.5	2.9	5.1	15.8
Iso-Propyl Alcohol	15.8	6.1	16.4	23.6
Acetone	15.5	10.4	7.0	19.9
Tetrahydrofuran	16.8	5.7	8.0	19.5
Dichloromethane	18.2	6.3	6.1	20.2
Chloroform	17.8	3.1	5.7	18.9
Propionitrile	15.3	14.3	5.5	22.1
Toluene	18.0	1.4	2.0	18.2
Cyclopentanone	17.9	11.9	5.2	22.1
Dimethylacetamide	16.8	11.5	10.2	22.8
Dimethylformamide	17.4	17.4	11.3	24.9
Benzyl alcohol	18.4	6.3	13.7	23.8
Acetophenone	19.6	8.6	3.7	21.8
N-methyl-Pyrrolidone	18	12.3	7.2	23.0
Dimethyl-imidazolidinone	18.0	10.5	9.7	23.0
Dimethyl Sulfoxide	18.4	16.4	10.2	26.7
Triethanolamine	17.3	22.4	23.3	36.7
Benzyl Benzoate	20.0	5.1	5.2	21.3
γ-Butyrolactone	19.0	16.5	7.3	26.2
Diiodomethane	17.8	3.9	5.5	19.0
Formamide	17.2	26.2	19.0	36.6
Water	15.5	16.0	42.3	47.8

Table 4-2. Hansen and Hildebrand solubility parameters of the 22 solvents used for nanotube dispersibility test. *The Hansen parameters were taken from the book - Hansen's handbook on solubility parameters*[64].

It can be seen from Figure 4-5 that the solvents with surface energies in the range of 69–72 mJ/m^2 effectively dispersed a large amount of conventional MWCNTs, with the most efficient being N-Methyl Pyrrolidone (NMP; $\chi_{retained}$ = 56%) and Dimethyl-imidazolidinone (DMEU; $\chi_{retained}$ = 52%). A number of reports have shown that SWCNTs can be efficiently dispersed in amide solvents, such as NMP[2,55,56,65], Dimethylformamide[50,52,55,66], and DMEU[55]. This behaviour can be attributed to their high electron pair donicity, low hydrogen bond donation parameter, and a high solvatochromic parameter. The same argument can be applied to the MWCNTs due to the similarity in their surface properties. Moreover, Coleman *et al*.,[3] demonstrated that the SWCNT/NMP interactions result in an extremely small or negative ΔH_{mix} leading to a negative ΔG_{mix}, which is ideal for successful debundling and dispersion of nanotubes. Additionally, NMP and DMEU have similar Hildebrand parameter – 23.0 mJ/m^2 and Hansen solubility parameters that approximately match with that of SWCNTs[55] (*i.e.,* δ_D – 17.8 mJ/m^2, δ_P – 7.5 mJ/m^2, and δ_H – 7.6 mJ/m^2). This explains the successful dispersion of conventional MWCNTs in NMP and DMEU.

On the other hand, N-MWCNTs were effectively dispersed in solvents with relatively lower surface energies (65–70 mJ/m^2) and the most effective solvent being DMA ($\chi_{retained}$ = 82%). Such a high amount of dispersibility has not been achieved before for pristine MWCNTs; the highest reported in the literature is 70% for SWCNTs dispersions in NMP[3]. Fitting a Gaussian curve through the dispersibility data (red curve in Figure 4-5) reveals a clear peak shift towards the lower surface energy solvents in the case of N-MWCNTs. This is an interesting result that gives information of the effect of nitrogen doping on the MWCNT surface properties. By applying the theory discussed above for dispersing conventional MWCNTs in solvents with matching surface energy, it can be deduced that the ability of N-MWCNTs to disperse in lower

surface energy solvents is indicative of a lower surface energy of the nanotubes themselves due to nitrogen doping. Therefore, it can be established that nitrogen doping leads to the lowering of nanotube surface energy, which results in the successful dispersion of N-MWCNTs in lower surface energy solvents (65–70 mJ/m^2).

From the above results the best dispersing solvents were selected: NMP for conventional MWCNTs, and DMA for N-MWCNTs. Additionally, similar dispersion tests were conducted for finding the best dispersing solvent for B-MWCNTs. However, considering the number of experiments and characterisation time, only three solvents (based on their high surface energy) were tested for dispersibility of B-MWCNT – Dimethylsulfoxide (DMS; 72.28 mJ/m^2), Benzyl benzoate (75.25 mJ/m^2) and γ-Butyrolactone (GBL; 75.8 mJ/m^2). Based on the structure of the B-MWCNTs derived from their SEM and TEM images (as seen in Chapter 2 – §2.6.1 and §2.6.2), it was suspected that boron doping could lead to an increase in the nanotube surface energy. Therefore, the dispersion tests of B-MWCNTs were conducted in high surface energy solvents. It could be concluded that GBL was the most effective among the three solvents for dispersing B-MWCNTs ($\chi_{retained}$ = 55.6%).

Once the best solvents for each type of MWCNT were established, further dispersion tests were conducted to calculate the extinction coefficient of these MWCNTs that are useful for calculating the nanotube concentration in the final dispersions after CF. For this, varying concentrations of conventional, N-, and B-MWCNTs (0.0003–0.02 mg/ml) were prepared in NMP, DMA, and GBL respectively. UV-Vis-NIR spectra were collected before and after CF and the data at 660 nm was used for calculating the extinction coefficients using the Lambert-Beer law (Equation 4-6). According to the Lambert-Beer law, in an ideal molecular solution the absorbance of a material (A) is proportional to the molar concentration (C), and the sample

thickness (L; in this case the path length of the quartz cuvette used for UV-Vis-NIR studies):

$$A = \varepsilon C L \qquad \text{Equation 4-6}$$

where: ε is the molar extinction coefficient that is wavelength dependent and is constant for a given material.

Figure 4-6 shows the normalised absorption spectra of each MWCNT in its respective best solvents in the UV-Vis-NIR region (300–1800 nm). It is usually assumed that the peak intensity and sharpness are a measure of the extent of MWCNT debundling. However, this has been contradicted by Coleman *et al*.,[2] who observed that instead the peak width can depend on the interactions between the nanotube and dispersing medium. Amidst these contradicting theories, it is difficult to entirely confirm the debundling efficiency based on the peak sharpness. However, the former theory of peak sharpness as a measure of debundling complies well with the data reported in this work. Furthermore, a slight red shift (shift to longer wavelengths) of the peaks, along with broadening can be observed in the S_{22} band for all the after CF spectra. This could indicate the presence of debundled nanotubes after CF[67]. A small blue shift (shift to shorter wavelengths) in the S_{11} band in the after CF spectra of all the dispersions corresponds to the presence of nanotubes with different diameters. Moreover, the fine and sharper structure of the peaks of the after CF spectra could represent the presence of individual nanotubes and unbinding process of the bundles in the isolated nanotubes[20,68]. It can also be seen that a strong absorption peak at 1430 nm is present in almost all the spectra, which possibly corresponds to the presence of absorbed moisture in the dispersions[69] due to the hygroscopic nature of the solvents.

By comparing the before CF spectra of the conventional MWCNTs to that of the N-MWCNTs, a slight blue shift in the S_{11} peaks can be observed at 1400 nm and 1720

nm, which could be due to the smaller diameters of the N-MWCNTs[70]. Also, on careful examination, it can be seen that many peak positions of the conventional and N-MWCNT dispersions (before CF) roughly match. However, the peaks of the latter are sharper, which perhaps indicates effective debundling of the N-MWCNTs in DMA. On the other hand, the absorption peaks of B-MWCNT dispersion before CF have no significant peaks, which can be attributed to the presence of bundles that have a broader range of absorption. It should be noted that a direct comparison between the absorption spectra of different MWCNTs might not be entirely logical due to the differences in the dispersing solvents that give rise to different nanotube/solvent interactions.

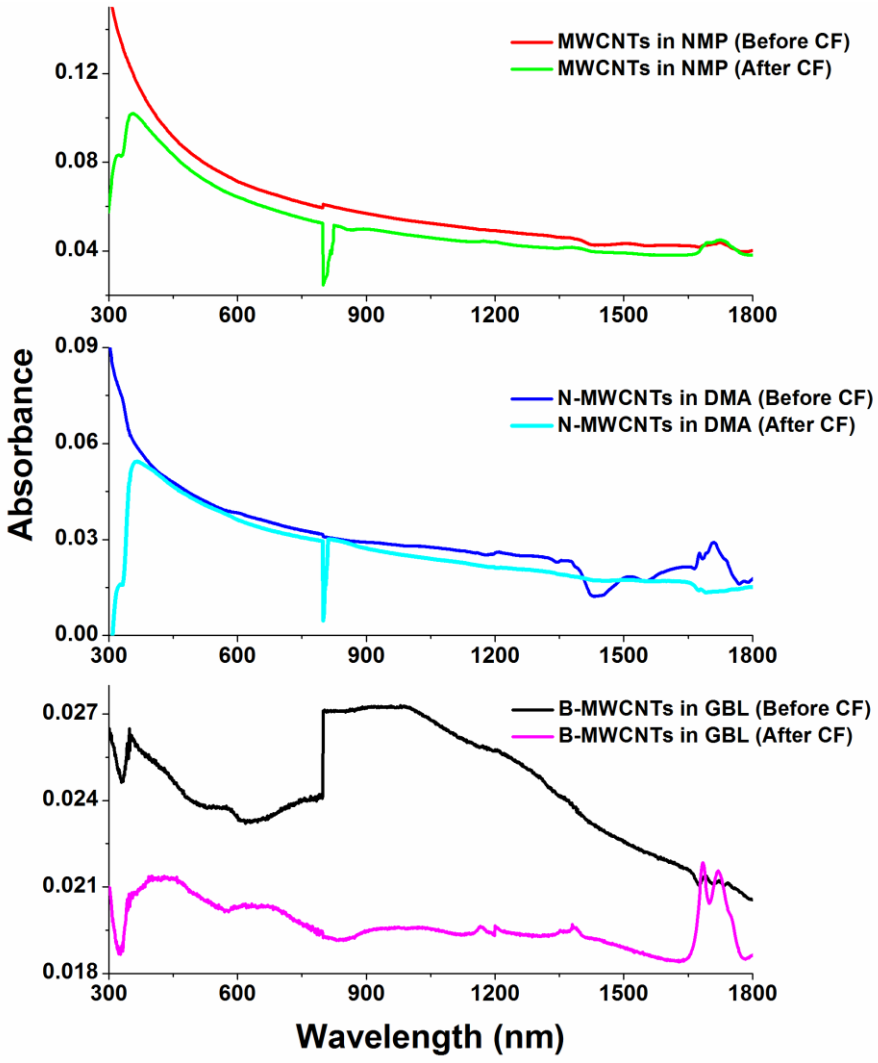


Figure 4-6. UV-Vis-NIR absorbance spectra of dispersions of MWCNTs in NMP, N-MWCNTs in DMA, B-MWCNTs in GBL (concentration – 0.01 mg/ml). Spectra of the dispersions before and after centrifugation (CF) are shown.

The extinction coefficients (ε) of the MWCNTs were calculated at λ = 660 nm from the slope of the absorbance per unit length (A/L) graph as a function of the initial nanotube concentration (Figure 4-7). The extinction coefficients (ε) of conventional, N-, and B- MWCNTs (at λ = 660 nm) was calculated to be 4903 ml mg^{-1} m^{-1}, 4436 ml mg^{-1} m^{-1}, 1903 ml mg^{-1} m^{-1} respectively. The ε values of the conventional MWCNTs comply well with the values reported by Foldvari *et al*.[71], who reported ε values of 4900 – 5300 ml mg^{-1} m^{-1} for CVD produced MWCNTs. It should be noted that the value of ε differs for every nanotube and is sensitive to various factors such as the synthesis route, purity, chirality, and diameter of the nanotube. Hence, a single value of ε cannot be universally used for all the MWCNTs. Therefore, it is critical that the ε is calculated for each batch of nanotubes to accurately calculate the final concentrations in the dispersions after CF. Furthermore, the extinction coefficients of N-, B-MWCNTs in their pristine form have never been reported in the literature. Although the values for ε reported for the doped MWCNTs in this work may not be applicable for nanotubes produced through other synthesis routes, they can be certainly be used as guidance for future work on doped MWCNT dispersions.

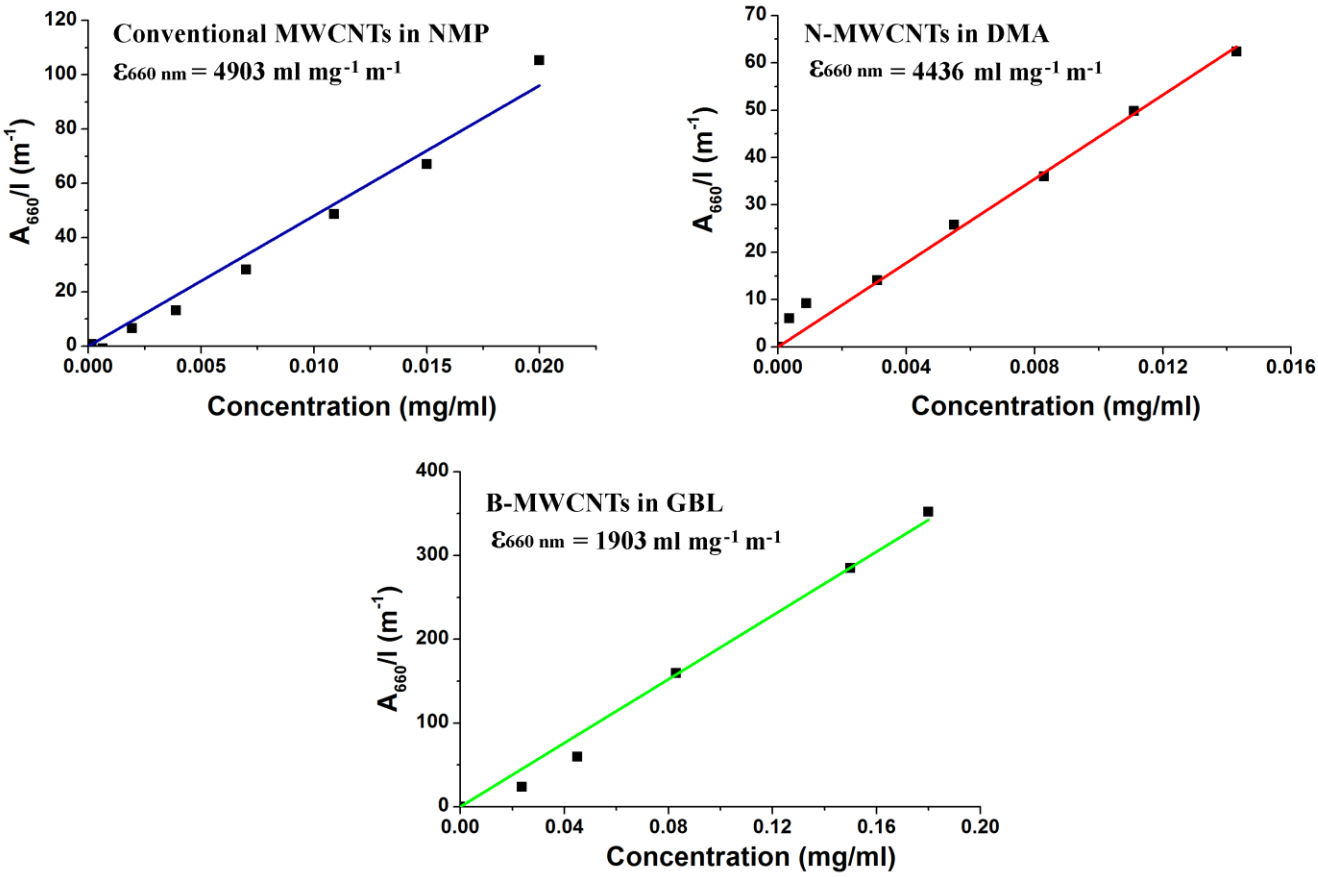


Figure 4-7. Extinction coefficients of conventional, N-, and B- MWCNTs at 660 nm.

The extinction coefficients were further used to calculate the concentrations of the dispersions using Equation 4-6. The concentrations at the time of manufacture and after a period of 3 years were compared (Table 4-3) to evaluate the sedimentation in the dispersions, evaporation of the dispersing solvents, and the dispersion stability. It can be seen from Table 4-3 that there was minimal sedimentation in all the dispersions over the 3 year duration. However, the stability of the B-MWCNT dispersions seemed to have reduced much faster than the conventional and N- MWCNT dispersions. This could be due to the ability of B-MWCNTs to easily agglomerate compared to the other MWCNTs (as discussed in Chapter 2). Furthermore, the N-MWCNTs dispersion in Benzyl alcohol completely sedimented after 3 months. It should be noted that NMP, DMA, GBL and Benzyl alcohol are all hygroscopic solvents and exposure to moisture

can potentially alter their surface energies and render them unsuitable for dispersing the nanotubes. Except the N-MWCNTs dispersion in Benzyl alcohol, no other dispersions exhibited such behaviour despite being exposed to atmosphere occasionally. Additionally, the cause of destabilisation in this case could have also been due to any contamination during sample transport or due to the presence of residual chemicals in the glass container prior to cleaning. Nonetheless, it can be confirmed that the concentration of the nanotubes in the dispersions was fairly consistent over the 3 year duration, implying the high stability of these dispersions.

Technique	**Dispersion**	**Concentration on the date of manufacture (mg/ml)**	**Concentration after 3 years (mg/ml)**
Labscale	Conventional MWCNTs in NMP	0.58	0.45
	N-MWCNTs in DMA	0.82	0.69
	B-MWCNTS in GBL	0.58	0.42
Upscale	Conventional MWCNTs in NMP	0.50	0.46
	N-MWCNTs in Benzyl alcohol	0.52	-
	B-MWCNTS in GBL	0.56	0.50

Table 4-3. Concentrations of the labscale and upscale MWCNT dispersions over a period of 3 years.

4.5.2. Defect density characterisation using Raman

Raman spectroscopy was used to analyse the defect densities of the MWCNTs in their dispersed form. The main objective was to understand if any new defects were induced in the nanotubes due to the labscale and upscale sonication treatments. Table 4-4 lists out the Raman intensity ratios (I_D/I_G, I_{2D}/I_G) of the pristine and dispersed MWCNTs. It can be seen that the intensity ratios of the pristine MWCNTs used for preparing the dispersions were similar to the results from Chapter 2, though they belonged to different batches. This confirms the homogeneity in the nanotube quality used in this work. It can be seen from Table 4-4 that the sonication treatment in either case did not cause any major changes in the intensity ratios compared to their pristine counter parts, therefore it can be confirmed that a minimal damage was caused to the nanotubes. Such a result was anticipated from the labscale dispersions due to the low power sonication treatment. However, a similar result from the upscale dispersions was unexpected due to the high-power sonication treatment, especially the powerful Branson W-450D US probe. This could have been possible due to[72]:

1) Limitation of the sonication parameters to minimal values that caused successful scission and debundling of the MWCNTs but did not cause damage to them.

2) Ability of the dispersing solvents to transfer sufficient energy to overcome the binding energy of the MWCNT aggregates, but restrict excessive nanotube fracture.

The Raman spectra of the labscale and upscale are shown in Figure 4-8 and Figure 4-9 respectively. It can be seen that although a significant change in the intensity of the peaks could not be observed, a small shift of the peaks in the dispersed MWCNTs to lower wave numbers was observed. This effect was more pronounced in the case of upscale dispersions, which is an unusual result because the Raman peaks of dispersed MWCNTs generally shift to higher wave numbers due to fewer tube-tube

interactions[73,74]. The unusual shifting of the Raman peaks in this case can be attributed to the following factors:

1) Loss of the Van der Waals interactions that are responsible for causing a frequency upshift due to the changes in the tube-tube interactions in the dispersed MWCNTs[75].

2) Thermal effects induced by irradiation of the incident laser that can occasionally cause frequency downshifts[76].

Technique	**Type of Dispersion**	**Pristine**		**Dispersed**	
		I_D/I_G	**I_{2D}/I_G**	**I_D/I_G**	**I_{2D}/I_G**
Labscale	Conventional MWCNTs in NMP	0.56 ± 0.1	0.44 ± 0.07	0.53 ± 0.05	0.45 ± 0.11
	N-MWCNTs in DMA	0.93 ± 0.07	0.07 ± 0.02	0.89 ± 0.04	0.03 ± 0.02
	B-MWCNTs in GBL	0.87 ± 0.04	0.27 ± 0.03	0.94 ± 0.21	0.27 ± 0.04
Upscale	Conventional MWCNTs in NMP	0.44 ± 0.09	0.48 ± 0.08	0.36 ± 0.08	0.48 ± 0.04
	N-MWCNTs in Benzylalcohol	0.84 ± 0.04	0.13 ± 0.02	0.79 ± 0.15	0.18 ± 0.05
	B-MWCNTs in GBL	0.75 ± 0.05	0.26 ± 0.03	0.87 ± 0.11	0.25 ± 0.02

Table 4-4. List of the Raman intensity ratios of labscale and upscale dispersions and their respective pristine counterparts.

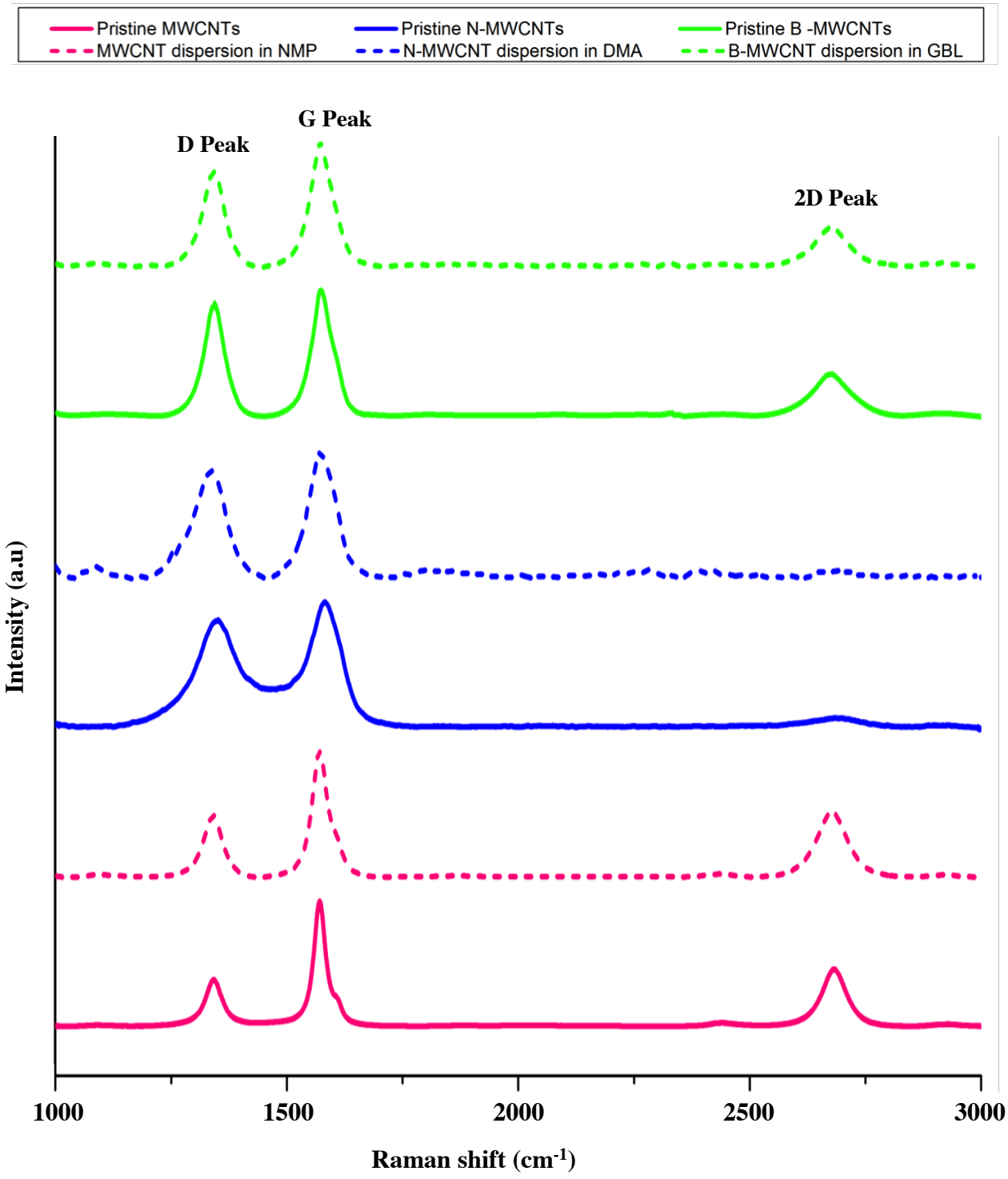


Figure 4-8. Raman spectra of the pristine MWCNTs and their respective labscale dispersions. All spectra are normalised with respect to the G band intensity.

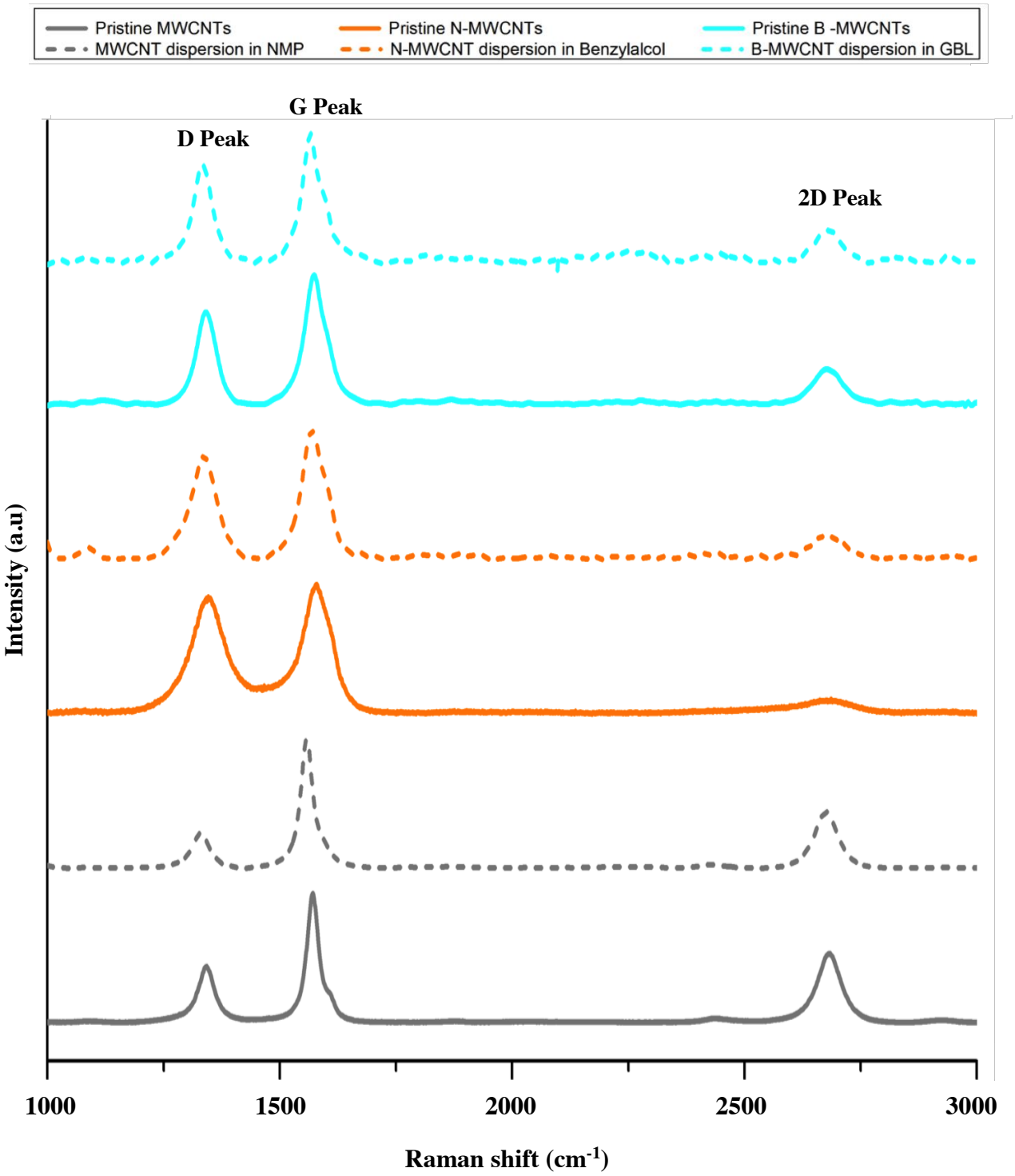


Figure 4-9. Raman spectra of the pristine MWCNTs and their respective upscale dispersions. All spectra are normalised with respect to the G band intensity.

4.5.3. Visual inspection of MWCNT dispersions

All MWCNT dispersions (both labscale and upscale) were monitored visually for sedimentation and photographs were taken periodically to evaluate the quality. Minimal sedimentation was observed for most of the dispersions over a period of 2.5–3 years with no evident solvent evaporation. The stability of the labscale dispersions was fairly high (Figure 4-10) over the 3-year duration, and among the upscale dispersions (Figure 4-11), conventional MWCNTs in NMP and B-MWCNTs in GBL were stable for at least 2.5 years, however the N-MWCNTs dispersion in Benzyl alcohol showed sedimentation after 3 months (as discussed in §4.5.1). It should be noted that the labscale stability test samples were sealed throughout the testing period. However, the upscale dispersions were used for composite processing and were therefore constantly exposed to atmosphere. Despite this, the conventional and B-MWCNT upscale dispersions maintained their stability. However, the N-MWCNT dispersion in Benzyl alcohol seems to have suffered from the atmospheric exposure.

The visual analysis in combination with the UV-Vis-NIR studies confirms that the general stability of these dispersions in their respective best solvents was excellent over a period of at least 2.5–3 years. It has to be noted that such long-term stability for pristine MWCNT dispersions has never been reported before. This allows batch preparation of conventional and doped MWCNT dispersions for composite forming and aids in fabrication of composites with uniform concentration.

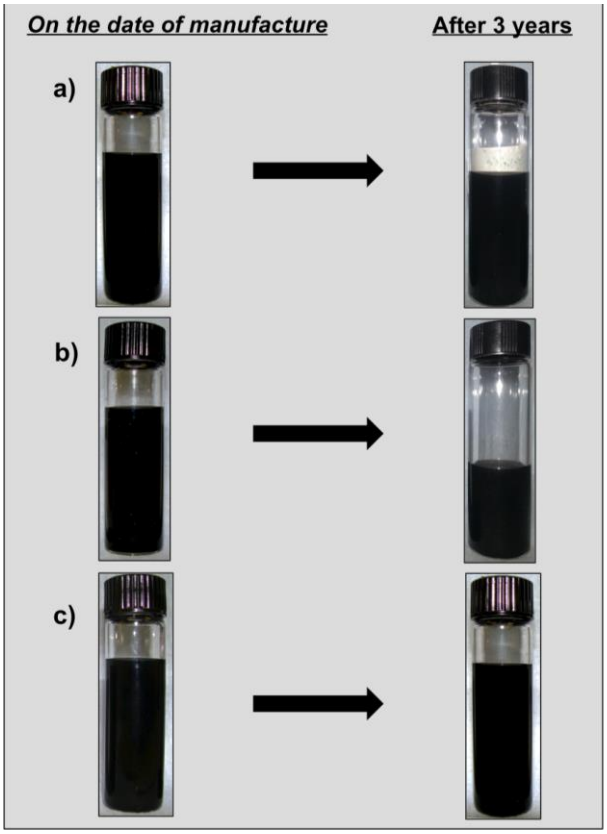


Figure 4-10. Photographs of the lab scale dispersions: a) Conventional MWCNTs in NMP, b) N-MWCNTs in DMA, c) B-MWCNTs in GBL. The stability of the dispersions over a period of 3 years can be observed. Volume of the dispersions - 10 ml.

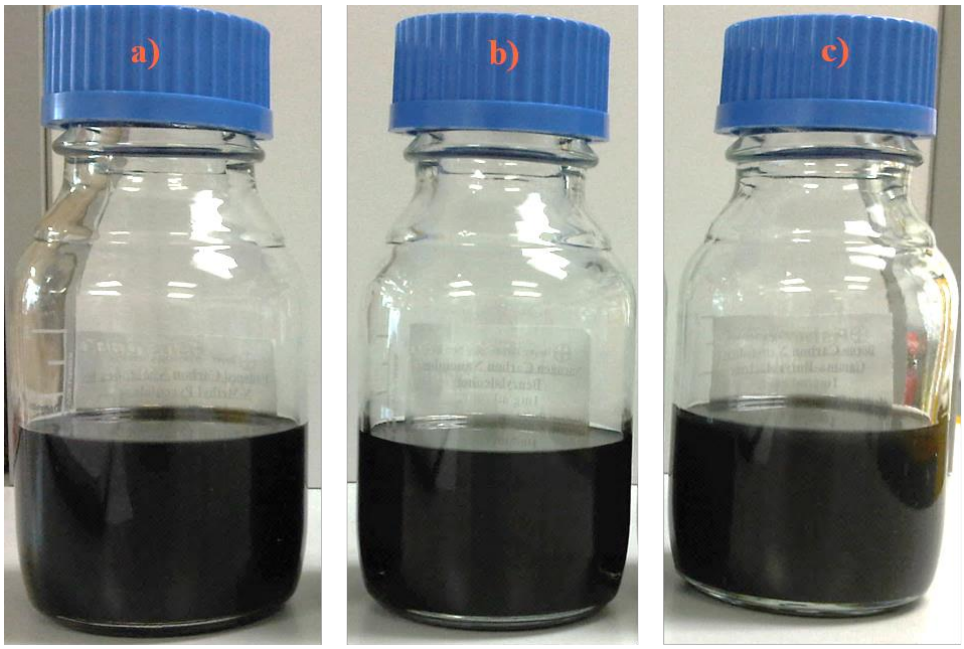


Figure 4-11. Photographs of the upscale dispersions on the date of manufacture: a) Conventional MWCNTs in NMP, b) N-MWCNTs in Benzyl alcohol, c) B-MWCNTs in GBL. Volume of the dispersions - 150 ml.

4.6. Summary

The sonication protocol established in Chapter 3 was used for understanding the dispersibility behaviour of conventional, N-, and B- MWCNTs in different organic solvents (surface energies: 45.8–10.3 mJ/m^2). It was observed that the alterations in the nanotube structure arising from doping greatly affected their dispersibility behaviour. N-MWCNTs could be dispersed in solvents possessing lower surface energies, while B-MWCNTs could be dispersed only in higher surface energy solvents. UV-Vis-NIR spectroscopy results showed that 82% of the initial nanotube concentration could be retained for N-MWCNT dispersions in DMA. This is the highest level of concentration ever attained for pristine MWCNTs in common organic solvents. Based on thermodynamics theories it was confirmed that MWCNTs could be successfully dispersed by matching the surface energy of the solvent with that of the nanotube, *i.e.*, by maintaining the $\Delta G_{mix} < 0$. Stable and homogeneous dispersions of conventional MWCNTs in NMP, N-MWCNTs in DMA and Benzyl alcohol, and B-MWCNTs in GBL were prepared both at labscale and upscale. The dispersions appeared to have stability of more than 2.5 years, except the N-MWCNT dispersion in Benzyl alcohol which sedimented after 3 months. Raman characterisation of the dispersions confirmed minimal damage to the MWCNTs after the dispersion treatments.

These results open opportunities for new techniques to tune the surface energy of the MWCNTs through doping in order to achieve high quality dispersions in chosen solvents with minimal damage. Furthermore, the expansion of the number of efficient solvents for dispersing MWCNTs is crucial to allow a much wider choice for experimentation towards application that require specific solvents. These results could also be useful for *in situ* manipulation of the surface chemistry of nanotubes to allow spontaneous dispersibility in aqueous solutions. The list of the 22 solvents studied in

this work include both high (> 200°C) and low (< 70°C) boiling point solvents, which add versatility to the range of possible applications.

It should be noted that an analysis of the dispersion behaviour of AACCVD produced pristine MWCNTs (both conventional and doped) has not been looked into before. Researchers have mainly studied the applications of functionalised nanotube dispersions or surfactant aided dispersions. However, such treatments usually degrade the nanotube properties, especially when used in composites. Hence, the actual potential of the nanotubes in improving the composite properties could not be clearly understood so far. However, the dispersion studies reported in this dissertation can help in exploiting the full potential of the intrinsic properties of conventional and doped MWCNTs towards various composite applications.

4.7. References

[1] Dutta, M., Nicolosi, V., Obratzsova, E., Koós, A. A., Crossley, A., and Grobert, N., "Stable dispersions of nitrogen containing multi-walled carbon nanotubes," Materials Express, 2011, **1**(3), pp. 201–209.

[2] Giordani, S., Bergin, S. D., Nicolosi, V., Lebedkin, S., Kappes, M. M., Blau, W. J., and Coleman, J. N., "Debundling of single-walled nanotubes by dilution: observation of large populations of individual nanotubes in amide solvent dispersions," Journal of Physical Chemistry B, 2006, **110**(32), pp. 15708–15718.

[3] Bergin, S. D., Nicolosi, V., Streich, P. V, Giordani, S., Sun, Z., Windle, A. H., Ryan, P., Niraj, N. P. P., Wang, Z. T., Carpenter, L., Blau, W. J., Boland, J. J., Hamilton, J. P., and Coleman, J. N., "Towards solutions of single-walled carbon nanotubes in common solvents," Advanced Materials, 2008, **20**(10), pp. 1876–1881.

[4] Glory, J., Mierczynska, A., Pinault, M., Hermite, M. M. L., and Reynaud, C., "Dispersion study of long and aligned multi-walled carbon nanotubes in water," Journal of Nanoscience and Nanotechnology, 2007, **7**(10), pp. 3458–3462.

[5] Yang, K., Yi, Z., Jing, Q., Yue, R., Jiang, W., and Lin, D., "Sonication-assisted dispersion of carbon nanotubes in aqueous solutions of the anionic surfactant SDBS: The role of sonication energy," Chinese Science Bulletin, 2013, **58**(17), pp. 2082–2090.

[6] Yu, M. F., Lourie, O., Dyer, M. J., Moloni, K., Kelly, T. F., and Ruoff, R. S., "Strength and breaking mechanism of multiwalled carbon nanotubes under tensile load," Science, 2000, **287**(5453), pp. 637–640.

[7] Kaleemullah, M., Khan, S. U., and Kim, J.-K., "Effect of surfactant treatment on thermal stability and mechanical properties of CNT/polybenzoxazine nanocomposites," Composites Science and Technology, 2012, **72**(16), pp. 1968–1976.

[8] Vilčáková, J., Moučka, R., Svoboda, P., Ilčíková, M., Kazantseva, N., Hřibová, M., Mičušík, M., and Omastová, M., "Effect of surfactants and manufacturing methods on the electrical and thermal conductivity of carbon nanotube/silicone composites," Molecules, 2012, **17**(12), pp. 13157–13174.

[9] Yu, X., and Kwon, E., "A carbon nanotube/cement composite with piezoresistive properties," Smart Materials and Structures, 2009, **18**(5), p. 055010.

[10] Bose, S., Khare, R. A., and Moldenaers, P., "Assessing the strengths and weaknesses of various types of pre-treatments of carbon nanotubes on the properties of polymer/carbon nanotubes composites: A critical review," Polymer, 2010, **51**(5), pp. 975–993.

[11] Sun, J., Wang, Y., Liu, Y., Kajiura, H., Li, Y., and Noda, K., "Debundling of single-walled carbon nanotubes by a nanoball-penetrating method," Journal of Physical Chemistry C, 2008, **112**(6), pp. 1789–1794.

[12] Xie, H., Lee, H., Youn, W., and Choi, M., "Nanofluids containing multiwalled carbon nanotubes and their enhanced thermal conductivities," Journal of Applied Physics, 2003, **94**(8), pp. 4967–4971.

[13] Zhao, X., Chu, B. T. T., Ballesteros, B., Wang, W., Johnston, C., Sykes, J. M., and Grant, P. S., "Spray deposition of steam treated and functionalized single-walled and multi-walled carbon nanotube films for supercapacitors," Nanotechnology, 2009, **20**(6), p. 065605.

[14] Otieno, G., "Processing and properties of aligned carbon nanotube/glass ceramic composite", 2012, D.Phil dissertation, University of Oxford.

[15] Star, A., Steuerman, D. W., Heath, J. R., and Stoddart, J. F., "Starched carbon nanotubes.," Angewandte Chemie International Edition, 2002, **41**(14), pp. 2508–12.

[16] O'Connell, M. J., Boul, P., Ericson, L. M., Huffman, C., Wang, Y., Haroz, E., Kuper, C., Tour, J., Ausman, K. D., and Smalley, R. E., "Reversible water-solubilization of single-walled carbon nanotubes by polymer wrapping," Chemical Physics Letters, 2001, **342**(3-4), pp. 265–271.

[17] Hama, H. T., Choib, Y. S., and Chung, I. J., "An explanation of dispersion states of single-walled carbon nanotubes in solvents and aqueous surfactant solutions

using solubility parameters," Journal of Colloid and Interface Science, 2005, **286**(1), pp. 216–223.

[18] Gong, X., Liu, J., Baskaran, S., Voise, R. D., and Young, J. S., "Surfactant-assisted processing of carbon nanotube/polymer composites," Chemistry of Materials, 2000, **12**(4), pp. 1049–1052.

[19] Islam, M. F., Rojas, E., Bergey, D. M., Johnson, A. T., and Yodh, A. G., "High weight fraction surfactant solubilization of single-wall carbon nanotubes in water," Nano Letters, 2003, **3**(2), pp. 269–273.

[20] Yu, J., Grossiord, N., Koning, C. E., and Loos, J., "Controlling the dispersion of multi-wall carbon nanotubes in aqueous surfactant solution," Carbon, 2007, **45**(3), pp. 618–623.

[21] Liu, J., Rinzler, A. G., Dai, H., Hafner, J. H., Bradley, R. K., Boul, P. J., Lu, A., Iverson, T., Shelimov, K., Huffman, C. B., Rodriguez-Macias, F., Shon, Y.-S., Lee, T. R., Colbert, D. T., and Smalley, R. E., "Fullerene pipes," Science, 1998, **280**(5367), pp. 1253–1256.

[22] Esumi, K., Ishigami, M., Nakajima, Z., Sawada, K., and Honda, H., "Chemical treatment of carbon nanotubes," Carbon, 1996, **34**(2), pp. 279–281.

[23] Hirsch, A., "Functionalization of single-walled carbon nanotubes," Angewandte Chemie International Edition, 2002, **41**(11), pp. 1853–1859.

[24] Charlier, J.-C., Ebbesen, T. W., and Lambin, P., "Structural and electronic properties of pentagon-heptagon pair defects in carbon nanotubes," Physical Review B, 1996, **53**(16), pp. 11108–11113.

[25] Zou, W., Du, Z., Liu, Y., Yang, X., Li, H., and Zhang, C., "Functionalization of MWNTs using polyacryloyl chloride and the properties of CNT–epoxy matrix nanocomposites," Composites Science and Technology, 2008, **68**(15-16), pp. 3259–3264.

[26] Ramanathan, T., Liu, H., and Brinson, L. C., "Functionalized SWNT/polymer nanocomposites for dramatic property improvement," Journal of Polymer Science Part B: Polymer Physics, 2005, **43**(17), pp. 2269–2279.

[27] Bose, S., Bhattacharyya, A. R., Bondre, A. P., Kulkarni, A. R., and Pötschke, P., "Rheology, electrical conductivity, and the phase behavior of cocontinuous PA6/ABS blends with MWNT: Correlating the aspect ratio of MWNT with the percolation threshold," Journal of Polymer Science Part B: Polymer Physics, 2008, **46**(15), pp. 1619–1631.

[28] Ma, P. C., Kim, J.-K., and Tang, B. Z., "Effects of silane functionalization on the properties of carbon nanotube/epoxy nanocomposites," Composites Science and Technology, 2007, **67**(14), pp. 2965–2972.

[29] Gao, C., Jin, Y. Z., Kong, H., Whitby, R. L. D., Acquah, S. F. A., Chen, G. Y., Qian, H., Hartschuh, A., Silva, S. R. P., Henley, S., Fearon, P., Kroto, H. W., and Walton, D. R. M., "Polyurea-functionalized multiwalled carbon nanotubes: synthesis, morphology, and Raman spectroscopy.," Journal of Physical Chemistry B, 2005, **109**(24), pp. 11925–32.

[30] Huang, W., Fernando, S., Allard, L. F., and Sun, Y.-P., "Solubilization of single-walled carbon nanotubes with diamine-terminated oligomeric poly(ethylene glycol) in different functionalization reactions," Nano Letters, 2003, **3**(4), pp. 565–568.

[31] Kocharova, N., Aäritalo, T., Leiro, J., Kankare, J., and Lukkari, J., "Aqueous dispersion, surface thiolation, and direct self-assembly of carbon nanotubes on gold.," Langmuir : The ACS Journal of Surfaces And Colloids, 2007, **23**(6), pp. 3363–71.

[32] Strano, M. S., Moore, V. C., Miller, M. K., Allen, M. J., Haroz, E. H., Kittrell, C., Hauge, R. H., and Smalley, R. E., "The role of surfactant adsorption during ultrasonication in the dispersion of single-walled carbon nanotubes.," Journal of Nanoscience and Nanotechnology, **3**(1-2), pp. 81–6.

[33] Assael, M. J., Chen, C. F., Metaxa, I., and Wakeham, W. A., "Thermal conductivity of suspensions of carbon nanotubes in water," International Journal of Thermophysics, 2004, **25**(4), pp. 971–985.

[34] Park, J. E., Kim, G. R., Yoon, D. J., Sin, C. H., Park, I. S., Bea, T. S., and Lee, M. H., "The effect of dispersed MWCNTs using sdbs surfactant on bacterial growth," World Academy of Science, Engineering & Technology, 2012, (70), pp. 743–746.

[35] Rastogi, R., Kaushal, R., Tripathi, S. K., Sharma, A. L., Kaur, I., and Bharadwaj, L. M., "Comparative study of carbon nanotube dispersion using surfactants.," Journal of Colloid and Interface Science, 2008, **328**(2), pp. 421–8.

[36] Whitsitt, E. A., and Barron, A. R., "Silica coated single walled carbon nanotubes," Nano Letters, 2003, **3**(6), pp. 775–778.

[37] Ryabenko, A. G., Dorofeeva, T. V., and Zvereva, G. I., "UV–VIS–NIR spectroscopy study of sensitivity of single-wall carbon nanotubes to chemical processing and Van-der-Waals SWNT/SWNT interaction. Verification of the SWNT content measurements by absorption spectroscopy," Carbon, 2004, **42**(8-9), pp. 1523–1535.

[38] Zhang, Q., Rastogi, S., Chen, D., Lippits, D., and Lemstra, P. J., "Low percolation threshold in single-walled carbon nanotube/high density polyethylene composites prepared by melt processing technique," Carbon, 2006, **44**(4), pp. 778–785.

[39] O'Connell, M. J., Bachilo, S. M., Huffman, C. B., Moore, V. C., Strano, M. S., Haroz, E. H., Rialon, K. L., Boul, P. J., Noon, W. H., Kittrell, C., Ma, J., Hauge, R. H., Weisman, R. B., and Smalley, R. E., "Band gap fluorescence from

individual single-walled carbon nanotubes.," Science, 2002, **297**(5581), pp. 593–6.

[40] Hu, C., Xu, Y., Duo, S., Zhang, R., and Li, M., "Non-covalent functionalization of carbon nanotubes with surfactants and polymers," Journal of the Chinese Chemical Society, 2009, **56**(2), pp. 234–239.

[41] Simmons, T. J., "Carbon Nanotube Suspensions, Dispersions, & Composites", 2008, D.Phil dissertation, ProQuest.

[42] Bandyopadhyaya, R., Nativ-roth, E., Regev, O., and Yerushalmi-rozen, R., "Stabilization of individual carbon nanotubes in aqueous solutions," Nano Letters, 2002, **2**(1), pp. 25–28.

[43] Kongkanand, A., Vinodgopal, K., Kuwabata, S., and Kamat, P. V, "Highly dispersed Pt catalysts on single-walled carbon nanotubes and their role in methanol oxidation.," Journal of Physical Chemistry B, 2006, **110**(33), pp. 16185–8.

[44] Kar, P., and Choudhury, A., "Electrical and Dielectric Properties of Polyaniline Doped with Carboxyl-Functionalized Multiwalled Carbon Nanotube," Advances in Polymer Technology, 2013, **32**(S1), pp. E760–E770.

[45] McNally, T., Pötschke, P., Halley, P., Murphy, M., Martin, D., Bell, S. E. J., Brennan, G. P., Bein, D., Lemoine, P., and Quinn, J. P., "Polyethylene multiwalled carbon nanotube composites," Polymer, 2005, **46**(19), pp. 8222–8232.

[46] Jia, Z., Wang, Z., Xu, C., Liang, J., Wei, B., Wu, D., and Zhu, S., "Study on poly(methyl methacrylate)/carbon nanotube composites," Materials Science and Engineering: A, 1999, **271**(1-2), pp. 395–400.

[47] Mc Carthy, B., Coleman, J. N., Czerw, R., Dalton, A. B., Carroll, D. L., and Blau, W. J., "Microscopy studies of nanotube-conjugated polymer interactions," Synthetic Metals, 2001, **121**(1-3), pp. 1225–1226.

[48] Tan, S. H., Goak, J. C., Lee, N., Kim, J.-Y., and Hong, S. C., "Functionalization of multi-walled carbon nanotubes with poly(2-ethyl-2-oxazoline)," Macromolecular Symposia, 2007, **249-250**(1), pp. 270–275.

[49] Tang, B. Z., and Xu, H., "Preparation, alignment, and optical properties of soluble poly(phenylacetylene)-wrapped carbon nanotubes," Macromolecules, 1999, **32**(8), pp. 2569–2576.

[50] Landi, B. J., Ruf, H. J., Worman, J. J., and Raffaelle, R. P., "Effects of alkyl amide solvents on the dispersion of single-wall carbon nanotubes," Journal of Physical Chemistry B, 2004, **108**(44), pp. 17089–17095.

[51] Bahr, J. L., Mickelson, E. T., Bronikowski, M. J., Smalley, R. E., and Tour, J. M., "Dissolution of small diameter single-wall carbon nanotubes in organic solvents?," Chemical Communications, 2001, (2), pp. 193–194.

[52] Cheng, Q., Debnath, S., Gregan, E., and Byrne, H. J., "Ultrasound-assisted SWNTs dispersion: effects of sonication parameters and solvent properties," Journal of Physical Chemistry C, 2010, **114**(19), pp. 8821–8827.

[53] Fifield, L. S., and Grate, J. W., "Hydrogen-bond acidic functionalized carbon nanotubes (CNTs) with covalently-bound hexafluoroisopropanol groups," Carbon, 2010, **48**(7), pp. 2085–2088.

[54] Hildebrand, J. H., and Scott, R. L., "The solubility of nonelectrolytes", 3rd Edition, 1950, Reinhold, New York.

[55] Bergin, S. D., Sun, Z., Rickard, D., Streich, P. V, Hamilton, J. P., and Coleman, J. N., "Multicomponent solubility parameters for single-walled carbon nanotube-solvent mixtures.," ACS Nano, 2009, **3**(8), pp. 2340–2350.

[56] Liu, J., Casavant, M. J., Cox, M., Walters, D. A., Boul, P., Lu, W., Rimberg, A. J., Smith, K. A., Colbert, D. T., and Smalley, R. E., "Controlled deposition of individual single-walled carbon nanotubes on chemically functionalized templates," Chemical Physics Letters, 1999, **303**(1-2), pp. 125–129.

[57] Bergin, S. D., Sun, Z., Streich, P., Hamilton, J., and Coleman, J. N., "New solvents for nanotubes: approaching the dispersibility of surfactants," Journal of Physical Chemistry C, 2010, **114**(1), pp. 231–237.

[58] Bergin, S. D., Nicolosi, V., Giordani, S., Gromard, A., Carpenter, L., Blau, W. J., and Coleman, J. N., "Exfoliation in ecstasy: liquid crystal formation and concentration-dependent debundling observed for single-wall nanotubes dispersed in the liquid drug γ-butyrolactone," Nanotechnology, 2007, **18**(45), p. 455705.

[59] Schadler, L. S., Giannaris, S. C., and Ajayan, P. M., "Load transfer in carbon nanotube epoxy composites," Applied Physics Letters, 1998, **73**(26), pp. 3842–3844.

[60] Meysami, S. S., "Development of an aerosol-CVD technique for the production of CNTs with integrated online control", 2013, D.Phil dissertation, University of Oxford.

[61] Koós, A. A., Dillon, F., Obraztsova, E. A., Crossley, A., and Grobert, N., "Comparison of structural changes in nitrogen and boron-doped multi-walled carbon nanotubes," Carbon, 2010, **48**(11), pp. 3033–3041.

[62] Buang, N. A., Fadil, F., Majid, Z. A., and Shahir, S., "Characteristic of mild acid functionalized multiwalled carbon nanotubes towards high dispersion with low structural defects," Digest Journal of Nanomaterials & Biostructures, 2012, **7**(1), p. 33.

[63] Hilding, J., Grulke, E., George Z, Z., and Lockwood, F., "Dispersion of carbon nanotubes in liquids," Journal of Dispersion Science and Technology, 2003, **24**(1), pp. 1–41.

[64] Hansen, C. M., "Hansen Solubility Parameters: A User's Handbook," 2000, CRC Press.

[65] Ausman, K. D., Piner, R., Lourie, O., Ruoff, R. S., and Korobov, M., "Organic solvent dispersions of single-walled carbon nanotubes: toward solutions of pristine nanotubes," Journal of Physical Chemistry B, 2000, **104**(38), pp. 8911–8915.

[66] Furtado, C. A., Kim, U. J., Gutierrez, H. R., Pan, L., Dickey, E. C., and Eklund, P. C., "Debundling and dissolution of single-walled carbon nanotubes in amide solvents.," Journal of the American Chemical Society, 2004, **126**(19), pp. 6095–105.

[67] Arnold, M. S., Green, A. A., Hulvat, J. F., Stupp, S. I., and Hersam, M. C., "Sorting carbon nanotubes by electronic structure using density differentiation.," Nature Nanotechnology, 2006, **1**(1), pp. 60–5.

[68] Kataura, H., Kumazawa, Y., Maniwa, Y., Umezu, I., Suzuki, S., Ohtsuka, Y., and Achiba, Y., "Optical properties of single-wall carbon nanotubes," Synthetic Metals, 1999, **103**(1-3), pp. 2555–2558.

[69] Hasan, T., Scardaci, V., Tan, P. H., Rozhin, A. G., Milne, W. I., and Ferrari, A. C., "Stabilization and 'debundling' of single-wall carbon nanotube dispersions in N-methyl-2-pyrrolidone (NMP) by polyvinylpyrrolidone (PVP)," Journal of Physical Chemistry C, 2007, **111**(34), pp. 12594–12602.

[70] Wang, B., Ma, Y., Wu, Y., Li, N., Huang, Y., and Chen, Y., "Direct and large scale electric arc discharge synthesis of boron and nitrogen doped single-walled carbon nanotubes and their electronic properties," Carbon, 2009, **47**(8), pp. 2112–2115.

[71] Ivanova, M. V, Lamprecht, C., Loureiro, M. J., Huzil, J. T., and Foldvari, M., "Pharmaceutical characterization of solid and dispersed carbon nanotubes as nanoexcipients.," International Journal of Nanomedicine, 2012, **7**, pp. 403–15.

[72] Huang, Y. Y., and Terentjev, E. M., "Dispersion of carbon nanotubes: mixing, sonication, stabilization, and composite properties," Polymers, 2012, **4**(4), pp. 275–295.

[73] Jespersen, T. S., "Raman scattering in carbon nanotubes", 2003 Ms.sc Thesis, University of Copenhagen.

[74] Utsumi, S., Kanamaru, M., Honda, H., Kanoh, H., Tanaka, H., Ohkubo, T., Sakai, H., Abe, M., and Kaneko, K., "RBM band shift-evidenced dispersion mechanism of single-wall carbon nanotube bundles with NaDDBS.," Journal of colloid and interface science, 2007, **308**(1), pp. 276–84.

[75] Rao, A., Chen, J., Richter, E., Schlecht, U., Eklund, P., Haddon, R., Venkateswaran, U., Kwon, Y.-K., and Tománek, D., "Effect of van der Waals interactions on the raman modes in single walled carbon nanotubes," Physical Review Letters, 2001, **86**(17), pp. 3895–3898.

[76] Bokobza, L., and Zhang, J., "Raman spectroscopic characterization of multiwall carbon nanotubes and of composites," eXPRESS Polymer Letters, 2012, **6**(7), pp. 601 – 608.

Chapter 5. MWCNT/polymer dielectrics

The current catastrophic climate change calls for a pressing need for the development of greener technologies. Unquestionably, the next few years will see a significant transformation from the conventional form of energy consumption, such as fossil fuel-run automobiles to fully electric powered[1]. This means that there is a massive demand for new energy storage materials that can store large amounts of energy and efficiently release it, *i.e.*, we need new generation capacitors[2,3]. It is not just the high efficiency that is required in these new capacitors, but also a smaller size[4]. Therefore, research and money are being invested to develop nanomaterials to match these requirements.

Carbon nanotube/polymer composites are one such class of attractive materials for this purpose. Polymers are one of the best dielectric materials with low density, high durability and flexibility, and easy processability[5]. However, their low dielectric constants impede their potential dielectric applications[6,7]. Hence, reinforcing them with nanomaterial fillers is an ideal way of achieving the required blend of properties. Nanotubes present superior combination of strength, Young's modulus, thermal and electrical conductivities along with high aspect ratios and low densities and have proven to be potential reinforcements for polymers[8–10]. Experimental studies have demonstrated that relatively low nanotube loadings can result in a significant improvement in the mechanical and electrical behaviour of the polymers[11–13]; giving rise to highly efficient, yet light weight composites for both structural and electrical applications. Both SWCNTs[14] and MWCNTs[12] have been realised to be useful for improving the properties of polymer composites. However, SWCNTs are more efficient in improving the mechanical properties due to their larger aspect ratios that aids in better stress transfer[15]. On the other hand, MWCNTs are better for electrical and

thermal properties due to their larger diameters, relatively lower specific surface area, and higher phonon scattering ability[16].

However, to date, commercial fabrication of such composites, especially as dielectric thin films, has been challenging due to the nanotube agglomeration[17–19] that arises from their high aspect ratios and the strong intrinsic Van der Waals forces. Their inability to disperse homogeneously within a polymer matrix in its pristine form is an additional challenge[20]. Furthermore, the difficulties in forming strong interfacial bonds and load transfer between the nanotubes and the polymer matrix, and the uniaxial alignment of the nanotubes cause further complications. Examples of some of these issues are shown in Figure 5-1. Although various techniques have been proposed in the literature for overcoming these challenges, no single technique has been able to solve all the issues and form large area nanotube/polymer films with good homogeneity[20–22]. This chapter presents the various techniques used in this doctoral work to form uniform and homogeneous MWCNT/polymer dielectric films, and the steps that were undertaken to select the best technique to form such films at a larger scale.

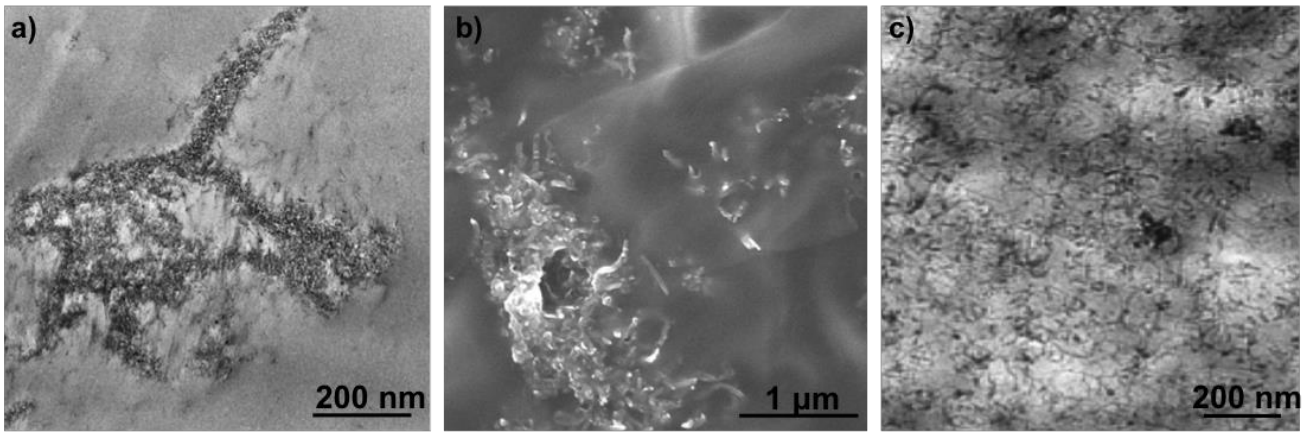


Figure 5-1. TEM images showing the nanotube agglomerations in various polymer composites: a) MWCNTs/epoxy[20], b) MWCNTs/poly(vinyl alcohol)[23], and c) MWCNTs/ polycarbonate[24].

It should be noted that the homogeneous MWCNT dispersions discussed in Chapter 4, along with aqueous MWCNT dispersions with SDBS surfactant were used for forming the composite films. A strategic approach was followed for identifying the best technique, and this is discussed in detail in this chapter. The structural and electrical characterisation of the composite films, especially analysis of their dielectric properties is also discussed in this chapter.

5.1. Capacitors and current technologies

5.1.1. Capacitors

Capacitors are used in electronic applications for storing, filtering, and regulating electrical energy and current flow. They basically consist of two conducting metal electrode plates separated by a non-conductive medium (known as dielectric), as seen in Figure 5-2. When a voltage is applied across the capacitor, positive and negative charges form on the plates and an electric field is created in the dielectric medium, and energy is stored in it.

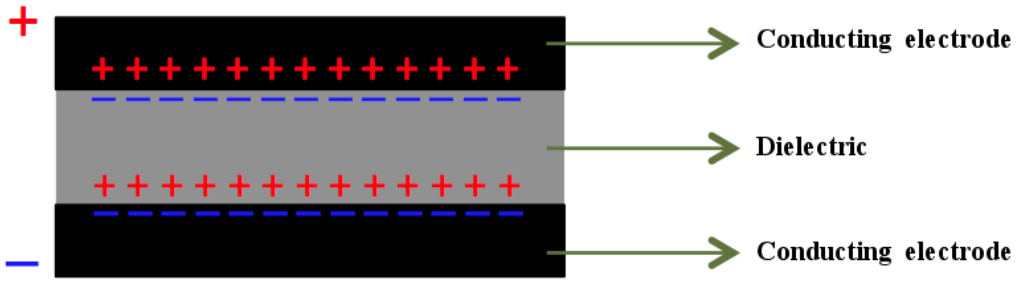


Figure 5-2. Schematic of a traditional parallel plate capacitor showing the charge accumulation when a voltage is applied.

The efficiency of a capacitor can be represented by capacitance (C); in a simple scenario where the capacitor comprises of two parallel conducting plates separated by a dielectric medium, the capacitance can be described as:

$$C = \frac{\varepsilon \, x \, A}{d}$$ Equation 5-1

where: A is the area of the plates, d is the distance between the plates *i.e.*, the thickness of the dielectric, and ε is the dielectric permittivity of the dielectric material.

ε of the dielectric material can also be described as:

$$\varepsilon = \varepsilon_o \, x \, \varepsilon_r$$ Equation 5-2

where: ε_o is the permittivity of free space (vacuum) and is 8.854 x 10^{-12} Fm^{-1}, and ε_r is the relative permittivity or the dielectric constant of the material and gives the extent to which the material can be polarised.

It can be seen from Equation 5-1 that capacitance can be improved by:

1. Increasing the area of the plates.
2. Reducing the distance between the plates, *i.e.*, by using thin dielectric materials.
3. Using materials that inherently possess high dielectric constants.

Ideally, the new generation capacitors would combine all these three points. They are similar to a conventional capacitor in structure but have plates with higher surface area, and employ extremely thin dielectrics. The plates of these capacitors are surface treated such as an activated charcoal coating to maximise the surface area. On the other hand, the conventional plastic dielectrics are replaced with new nano-composites that can significantly decrease the distance between the plates and possess inherently superior dielectric properties. This enables the capacitors to store much more charge than the conventional ones. Also, dielectrics of composite materials such as polymers with nanomaterials (such as SWCNTs[14,25], MWCNTs[12,26], and barium titanate[27,28]) have proven to significantly improve the capacitance. This is because the nanomaterial reinforcements within the polymer matrix act as micro-capacitors within the dielectric (Figure 5-4), which drastically increases the amount of energy storage[13].

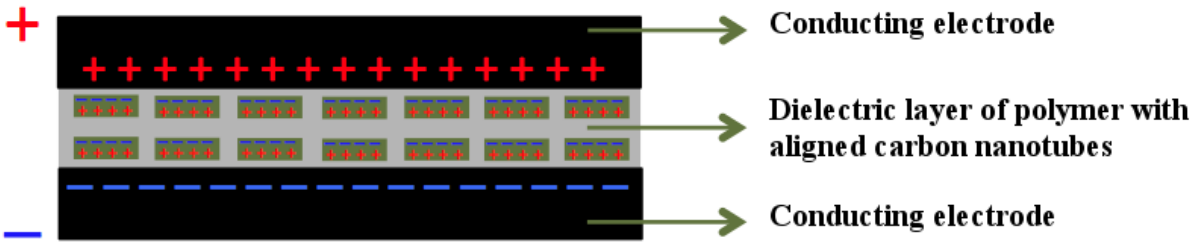


Figure 5-3. Schematic of a new generation capacitor with a composite dielectric containing aligned MWCNTs showing increased charge accumulation on application of voltage.

5.1.2. Capacitor technologies

Based on the dielectric film, capacitors can be broadly classified into three categories:

1. Electrolytic capacitors (such as aluminium oxide and tantalum pentoxide).

2. Ceramic capacitors (such as titanium oxide, barium titanate).

3. Film capacitors (such as paper, mica, polymers such as polypropylene, and polyethylene terephthalate).

The selection of a certain type of capacitor mostly depends on the application requirements. However, the common criteria for selection are: small size, low dissipation factor, good capacitance stability, cost, and low temperature and frequency dependence. Film capacitors, especially polymer films, are considered well-suited for various applications due to their low cost, low densities, high stability over a range of frequencies, high capability for handling higher current per unit volume, low ageing rate, and ability to resist mechanical stress[5,29]. A general comparison of some common capacitors is shown in Table 5-1.

Capacitor type	Dielectric Material	Thickness (µm)	Operating Temperature (°C)	Dielectric Constant	Capacitance	Working voltage (VDC)	Dissipation Factor	Advantages	Disadvantages
Electrolytic Capacitors	Aluminium Electrolytic	0.03 – 0.7	- 40 – 85	8 – 10	0.5 µF – 1 F	5 – 500	8	Inexpensive, self-healing, high voltage stability	High dependence on temperature and frequency, high leakage, limited lifetime
	Tantalum Electrolytic	0.04 – 0.5	-55 – 125	23 – 27	10 nF – 1000 µF	5 – 125	10 – 20	High reliability, low temperature dependence, long life	Violent failure, expensive
Ceramic Capacitors	Multi-layer Ceramics (X7R)	0.1 – 150 (Depending on construction)	-55 – 125	1400 – 2270	10 µF – 100 µF	6.3 – 100	2.5 – 5	High thermal stability and reliability	Aging, Mechanically fragile
	Ceramic Disc	4 – 22	-25 – 85	10 – 15000	1.5 pF – 68 pF	100 – 1000	2.5 – 5	Less expensive, High thermal stability, easy production	Mechanically fragile
Film Capacitors	Polypropylene Films	3 – 20	-55 – 85	2.1 – 2.2	1 µF – 1000 µF	50 – 600	0.35	Low moisture absorption, self-healing, low temperature and frequency dependence	Unsuitable for high temperatures
	Polystyrene Films	8 – 25	-55 – 70	2.5	100 pF – 33 nF	16 – 600	0.1	Low moisture absorption, high thermal stability, moderate cost	Unsuitable for high temperatures, limited availability

Table 5-1. Comparison of some of the commonly available capacitors.[5,30–37]

The current day microelectronics industry demands miniaturised dielectrics that can be manufactured economically and can store a large amount of energy relative to their volume[2,38]. Such requirements put pressure on the dielectric material to inherently possess high dielectric constants and efficiently function at high stresses at minimal thickness and with minimal losses. The conventional dielectrics are unsuitable for this purpose due to the high temperature processing conditions (in the case of ceramic capacitors[39]), low dielectric constants (in the case of film capacitors[5]), and high charge leakage and polarity sensitive nature (in the case of electrolytic capacitors[37]). Therefore, new materials need to be formulated to comply with the current market requirements. Polymer film dielectrics reinforced with high dielectric constant materials combine the advantages of the high dielectric values of the fillers with the flexibility and high dielectric strength of the polymers. Research has confirmed that carbon nanotubes and ceramic materials[27,28], especially ferroelectric ceramics such as barium titanate ($BaTiO_3$) and lead zirconium titanate are effective fillers for improving the dielectric properties[13,25,40].

Choi *et al*.[41] reported a dielectric constant of 19.03 (100 kHz, 50 vol.% ceramic filler) with a loss of 0.0109 in $BaTiO_3$/polyimide composites by treating the ceramic particles with isopropyl tris(N-amino-ethyl aminoethyl) titanate. However, an agglomeration of the $BaTiO_3$ was observed in these composites that can potentially result in a weak interfacial interaction. Ding *et al*.[7] tried to address the issue of agglomeration by combining several techniques such as electrospinning, electrospraying, and hot pressing. They developed homogeneous $BaTiO_3$/polyimide composites with improved dielectric constants from 3.71 to 28.13 (100 kHz, 50 vol.% ceramic filler) with a low dielectric loss of 0.0053. However, the electric breakdown strength and the tensile strength of these composites were low due to the presence of the ceramic phase. Several other reports similar to these studies have reported improved

dielectric properties in ceramic/polymer systems[8,28,42]. However, the amount of ceramic fillers required to achieve these values is high, making it difficult to process such composites due to the brittle nature of ceramics. Moreover, electromechanical effects such as piezoelectric effects arising from the ferroelectric ceramics induce a mechanical resonance in the system that limits its reliability[6]. Arbatti *et al*.[6] instead incorporated a semiconductor like ceramic – calcium copper titanate (CCTO) in irradiated poly(vinylidene fluoride-trifluoroethylene) and achieved significantly high dielectric constants of 240 with a dielectric loss of 0.32 at room temperature at 1 kHz. The CCTO unlike conventional ceramics does not exhibit piezoelectric effect, hence improving the breakdown strength of the system. However, the dielectric properties of such composites are highly temperature dependent.

On the other hand, conductive fillers such as MWCNTs can significantly improve the dielectric constants at relatively low loading due to their exceptionally high aspect ratios. Therefore, the flexibility of the composite can be maintained unlike the ceramic reinforced polymer composites. The improvement in the dielectric properties in the nanotube/polymer composites is associated with interfacial polarisation, also known as Maxwell-Wagner-Sillars effect[10,40,43]. In a multiphase system that consists of electrically heterogeneous materials with different dielectric properties and relaxation times, charge storage occurs at the interfaces, in this case the nanotube/polymer interface[44]. When the concentration of nanotubes approaches a critical value (generally referred to as percolation threshold), there is an increase in the nanotube/polymer interfaces that leads to an increase in the interfacial polarisation resulting in a sharp improvement in the dielectric constant. At the percolation threshold, the naturally conducting nanotubes are in very close proximity to each other and are separated by fine regions of the insulating polymer, thereby creating several micro-capacitors within the film. Hence, the cumulative polarisation effect from all the micro-capacitors results

in a significant increase in the dielectric constants[13]. However, when the nanotube concentration is below the percolation threshold, this phenomenon becomes obscure due to insufficient number of interfaces. Wang *et al*.[10] reported an improvement in the dielectric constant from 10 to 300 at 1000 Hz in poly (vinylidene fluoride) polymer, by incorporating as little as 2.0 vol.% pristine MWCNTs with a high dielectric loss of 0.4 along with low dielectric breakdown strength. On the other hand, Li *et al*.[40] achieved extremely high dielectric constants of 1700 and 3600 at 1 kHz in the same polymer by incorporating 6.0 vol.% of pristine MWCNTs and 8.0 vol.% acid-functionalised MWCNTs respectively. The improvement in the dielectric constants of such composites is attributed to the interfacial polarisation between the nanotubes and the polymer matrix. However, the excessive improvement in the case of acid-functionalised nanotubes in the work of Li *et al*.[40] resulted from the increased interfacial polarisation due to the presence of relatively shorter nanotubes resulting from the acid treatment, and the presence of electron withdrawing carboxylic groups in the functionalised nanotubes. However, the improvement in the dielectric constant of these composites is always coupled with an increase in the dielectric loss and degradation in the dielectric breakdown strength. The conducting nature of the nanotubes and the close proximity to each other at the percolation threshold can allow electron hopping between the nanotubes (also known as tunnelling effect), and cause a leakage of current[28]. Moreover, the efficiency of these fillers is optimal only when they are uniformly dispersed in the polymer matrix. If the nanotubes are individually separated and homogeneously aligned in the polymer matrix, then significantly higher dielectric constants with very low dielectric losses can be achieved at low percolation thresholds. Moreover, MWCNTs containing hetero-atoms (such as nitrogen and boron doped MWCNTs) that possess inherent electrical properties (as discussed in Chapter 2) could further alter the dielectric properties of these composites. However, the use of

doped MWCNT containing polymer composites as dielectric films has received less attention due to the technical difficulties with creating large amounts of uniformly doped MWCNTs, and dispersing them homogeneously in the polymer matrix.

5.2. Introduction to composite film forming techniques

Although nanotube/polymer composites are promising dielectrics, the development of such composites, especially as films, has always been associated with certain challenges:

(1) Separation of individual nanotubes.

(2) Production of uniform and reproducible dispersions.

(3) Orientation/alignment of the nanotubes in the polymer matrix.

Almost all film forming techniques follow the solution processing route that helps in overcoming some of these issues. The first step in this route is the preparation of the nanotube dispersions in solvents via energetic agitation (mechanical stirring or sonication). This helps in breaking the nanotubes from their agglomerates or bundles, and disperses the individual nanotubes in the solvent. The next step is mixing of the polymer with the nanotube dispersions either in their pure form or already dissolved in the same solvent to facilitate intercalation of the polymer chains with the nanotubes. The final step is the formation of composite films and evaporation of the solvent. Although the dispersion-forming step is common for all techniques, depending on the techniques used for forming the final film, they can be broadly classified into the following categories[27]:

- Pre-metered: Film quality is controlled by regulating the amount of material delivered to the applicator. E.g., extrusion, spray coating.

- Self-metered: Film quality is predominantly controlled by the process parameters (such as viscosity and processing speed). E.g., dip coating, direct rolling of hot melt.
- Doctored: A post-coating technique (such as a blade) is used to control the film quality. E.g., tape casting, doctor blade.
- Hybrid: Combination of the techniques from the above categories. E.g., meniscus coating, gravure coating.

There are more than 30 different film-forming techniques that fall in the above-listed categories. However, in the last 5 years much attention has been given to spray coating techniques[45–47] due to their ability to precisely control the parameters affecting the film. Some of these techniques are discussed below.

5.2.1. Drop casting and spin coating

Drop casting and spin coating of thin (thickness > 200 nm) and ultra-thin (thickness < 200 nm) polymer composite films from dilute polymer solutions are the most common traditional film forming techniques. Drop casting is the simplest of the film forming techniques in which a required amount of the dispersion is dropped carefully on a flat substrate and allowed to dry at a desired temperature to evaporate the solvent (Figure 5-4a). Despite its low complexity, drop casting is not the most chosen technique for developing films commercially as it has a low reproducibility factor and no precise control on the film thickness.

Spin coating, on the other hand, involves depositing the dispersion on a flat substrate and rapidly rotating the substrate at a certain speed. Due to the centrifugal force arising from the rotation, the dispersion flows radially, and any excess dispersion is spun off at the substrate edge, resulting in a thin film. Rotation is usually continued till the desired film thickness is achieved. Finally, the solvent is evaporated from the

film leaving behind a dry polymer film (Figure 5-4b). Regulating the rotation speed and evaporation temperature, and altering the substrate surface can usually control the film thickness. Spin coating results in a significant amount of wastage of the solution due to the radial spinning and cannot be upscaled due to the inconsistencies in the solvent evaporation. This is a bigger problem especially in the case of solvents with higher boiling points. Moreover, understanding the effect of process parameters on the film quality is extremely challenging due to the complex interactions between the dispersion rheology and the solvent evaporation.

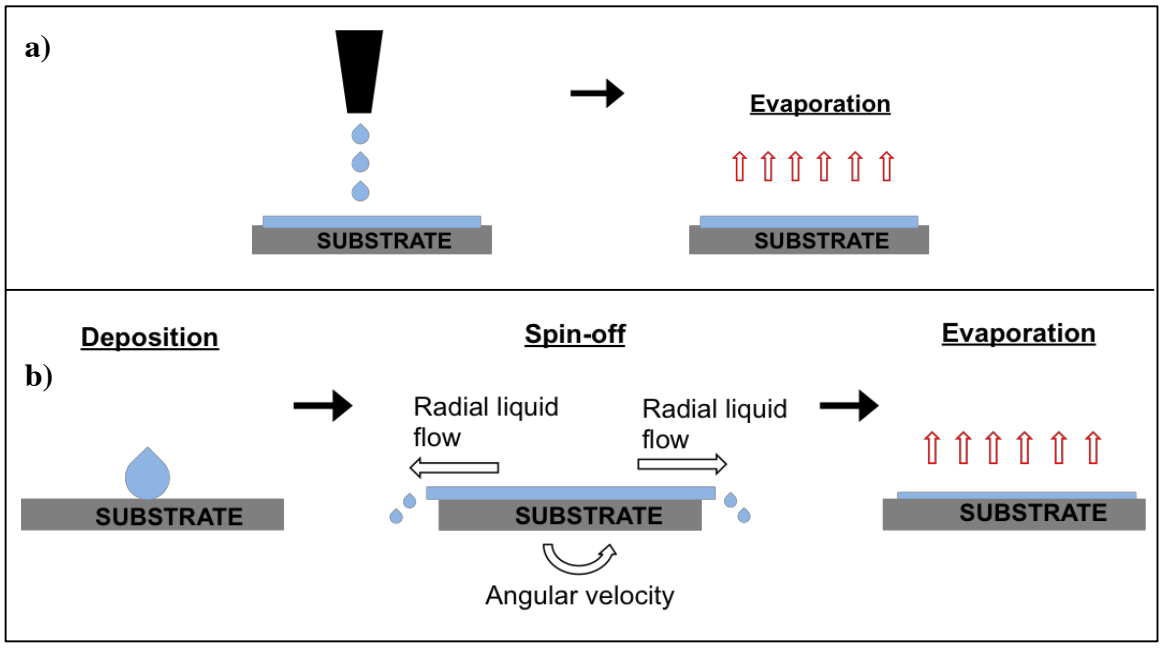


Figure 5-4. Schematic showing the various stages of: a) Drop casting, b) Spin coating.

5.2.2. Electrospraying

Electrospraying is mostly used industrially for dispersing paints and agricultural pesticides. It has also been applied for mass spectrometry of large biomolecules[48], protein viability studies[49], and for depositing nanoparticles[50]. This technique has the ability to form ultra-thin films that can be as thin as 300 nm[51]. Over the recent years there has been interest in this technique for spraying nanotube films because of its ability to spray individual nanotubes and avoid post-spraying agglomeration.

The process of electrospraying can be better understood by considering a spherically charged liquid droplet held in vacuum, as shown in Figure 5-5. The liquid droplet is affected by the electrostatic repulsive forces and the surface tension that tries to hold the droplet within the spherical shape. These two forces balance each other in equilibrium and can be described by:

$$\frac{1}{8\pi\varepsilon_o}\frac{Q^2}{R^2} = 8\pi\sigma_s R \qquad \text{Equation 5-3}$$

where: Q is the electrostatic charge on the surface of the droplet, R is the radius of the droplet, ε_o is the dielectric permeability of vacuum, and σ_s is the coefficient of surface tension.

As the strength of the electric field increases, the charge on the surface of the droplet increases too until it reaches a critical point when the electrostatic force overcomes the surface tension. At this point, the droplet disintegrates into fine droplets forming an electrospray.

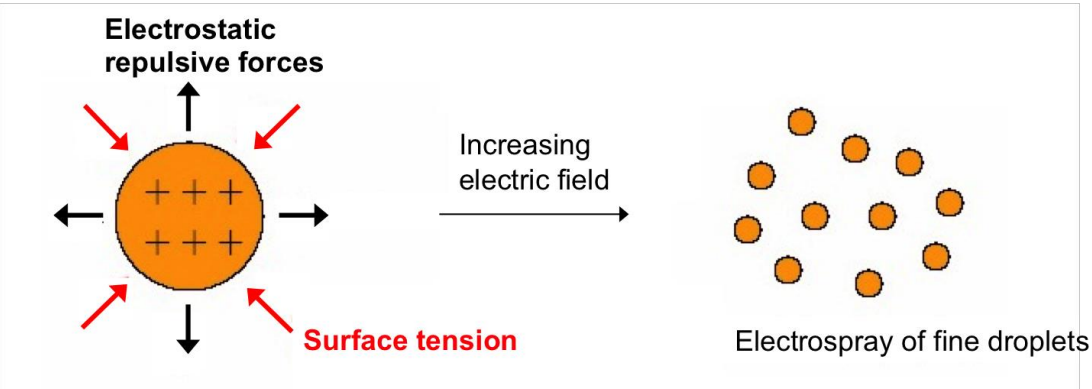


Figure 5-5. Schematic of the electrospray principle[70].

Due to the controlled deposition in electrospraying, it can produce consistent and highly homogeneous films, which can be used for numerous applications: CdS films for solar cells[52], Y_2O_3 -doped ZrO_2 thin films for fuel cells[53], cathode layers of $LiCoO_2$ for lithium batteries[54], and dielectric Al_2O_3 layers[55]. It is particularly useful for

synthesising MWCNT/polymer films, allowing simultaneous alignment of the nanotubes along a single axis. However, the properties of these films can be maintained only when they are nano-fabricated through electrospraying *i.e.*, by forming a nano-electrospray. This is possible only by precisely maintaining the flow-rate of the system in nano-litres per minute, which impedes industrial scale film forming. Moreover, additional problems of nano-fibre formation exist for nanotube/polymer composites due to the entanglement of polymer chains with the nanotubes. Moreover, the voltage required for the formation of the nano-electrospray is high (2–3 kV); requiring additional safety precautions. Therefore, this technique has received less attention for the purpose of forming nanotubes/polymer films, but it provides scope for further investigation. If one were to overcome the nano-fabrication and fibre formation issues by altering the design and tuning the electrospray parameters, this technique certainly has the possibility to emerge as a potential technique for forming nanotube/polymer films.

5.2.3. Aerosol spray deposition technique

Aerosol spray forming is a simple technique that allows formation of controlled films through solution processing in a safer environment, and therefore is of interest as a manufacturing technique. Unlike electrospraying, which requires high voltages to form droplets, this technique atomises a liquid stream into fine droplets by using inert gases. These droplets are then propelled away from the region of atomisation by the atomising gas and collected by a substrate, which solidifies them into a coherent and dense preform. The substrate can be pre-heated and/or post-heated as per the requirement of the sample. In a basic aerosol spray forming system developed by Dr Hinchliffe[27], aqueous $BaTiO_3$ suspensions in polymers were sprayed from a hypodermic needle at a high velocity (≥ 10 m/s), and the resulting droplets were

deposited onto heated substrates to produce uniform films. The thickness of these films varied from a few hundred nanometres to microns and the films presented porosity in some cases. This is one of the major issues in this technique, as it is critical to understand the spraying and curing parameters for forming high quality films. Zhao *et al.*[13,46] used a modified version of this setup for forming good quality SWCNT/polyelectrolyte and $BaTiO_3$/polydiacrylate films of thickness 150 nm – 5 μm and 5–30 μm respectively. A schematic of the setup along with an optical photograph of the SWCNT/polyelectrolyte film developed by Zhao *et al.*[9] is shown in Figure 5-6.

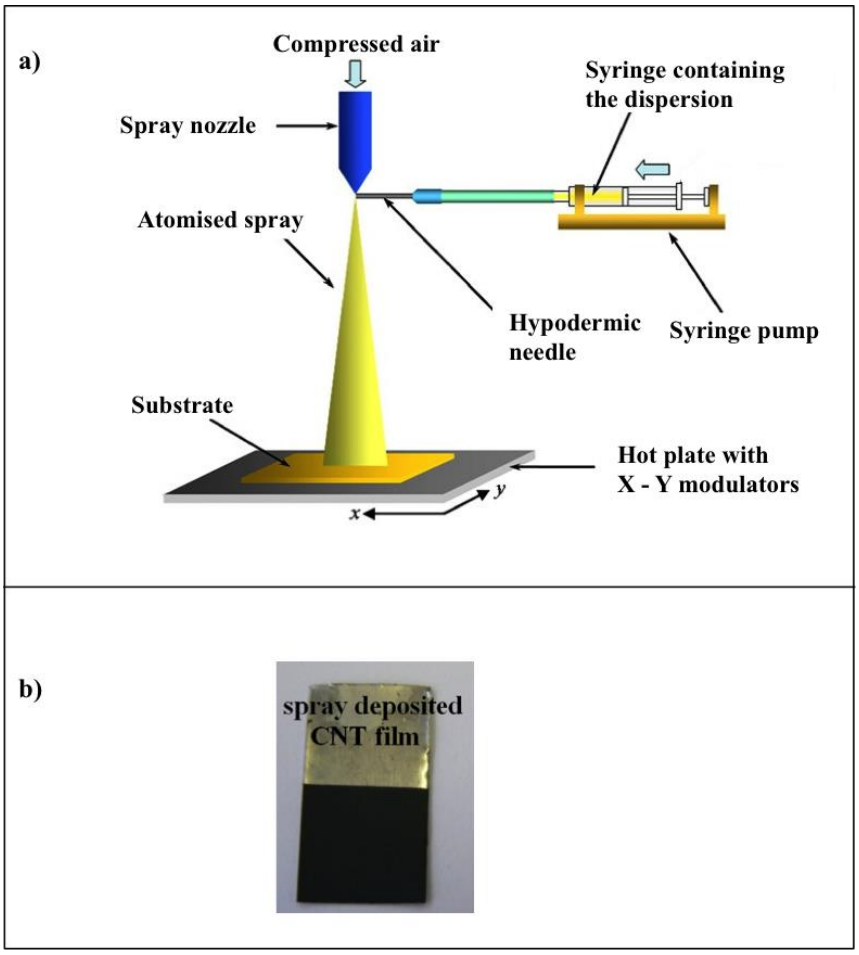


Figure 5-6. a) Schematic of a basic aerosol spray deposition technique[46], b) An optical photograph of a high quality SWCNT/polyelectrolyte film[9].

The main advantages of this technique are flexibility and scalability, elimination of macro-segregation and multiple processing steps such as heat treatment, refined microstructure, and formation of non-equilibrium phases (that in some cases can enhance mechanical properties)[27]. Despite this, the control on the atomisation parameters (including deposition height, surface chemistry of the substrate, and flow rate) that can significantly influence the film quality is a major concern. Moreover, the surface roughness of the films that can arise when spraying is conducted on heated substrates, and which can have detrimental effects on the final properties of the film is also an issue. Additionally, the efficiency of this technique to convert 100% feedstock to final product is usually low, which means that a considerable amount of the feedstock is wasted.

Spray techniques have the flexibility of forming films of a variety of materials (including polymers, polymer composites, and nanomaterials) provided they can be brought into a dispersion medium. Moreover, with substantial optimisation, these techniques can form large area films (20x20 cm) with uniform thickness (*ca*. 75 nm – 30 μm)[46,56] and homogeneity at a low cost, hence outdoing the conventional spin coating or drop casting techniques. Furthermore, with additional modifications it can also be used for forming patterned films or multi-component layered films, which makes it versatile.

5.3. Materials used for composite fabrication

Based on the film forming technique applied, two different polymers were used:

1) Polyester polyurethane elastomer (PU) – Poly(4,4'-methylenebis(phenyl isocyanate) alt-1,4-butanediol/poly(butylene adipate), Sigma Aldrich; Melt index – 224°C/1.2 kg, Density – 1.19 g/ml at 25 °C.

2) Perfluoro alkoxy fluoroplastic polymer (PFA), Dyneon™ PFA 6910GZ water based dispersion; Viscosity – 12 mPa.s, Melting point – 306 °C.

The PU polymer was chosen for its mechanical toughness, wear resistance, and flexibility[57,58], whereas the PFA polymer was chosen for its large operating temperature range and aqueous dispersibility[13,59].

The as-received PU polymer was in the form of pellets that readily dissolved in the same organic solvents as those suitable for conventional, N-, and B- MWCNTs. Therefore, 500 ml batch dispersions of PU in NMP, DMA, and GBL were prepared (concentration – 10 mg/ml) by sonicating the mixtures in an US bath (U1250D) for 5 hours. The batch was subsequently diluted and required quantities of the batch were then added to the nanotube dispersions as described in Chapter 4, *i.e.*, conventional MWCNT in NMP, N-MWCNTs in DMA, and B-MWCNTs in GBL. The mixtures were then used to form composite films. The dispersions for film forming were prepared one day before the experiments and were mixed on a roller mixer overnight for better homogeneity.

On the other hand, the as-received PFA polymer was a transparent water-based dispersion. Hence, the nanotube dispersions in organic solvents as mentioned in Chapter 4 could not be directly mixed with PFA as this resulted in phase separation. Therefore, aqueous nanotube dispersions were prepared using sodium dodecylbenzenesulfonate surfactant (SDBS, Aldrich; Molecular weight – 348.48 g/mol). For this, firstly a 500 ml batch of 0.1 wt.% SDBS was prepared in deionised water and was sonicated for 3 hours in an US bath (U1250 D), resulting in full dissolution of the SDBS. 500 mg of pristine MWCNTs (conventional and B- doped) in powder form were then added to the aqueous SDBS mixture and were further sonicated in the US bath for 8 hours. The dispersions were centrifuged (Rotanta 460R) at 3250 rpm for 95 minutes and the supernatant was carefully separated. The sediment was

further diluted and the sonication process was repeated. The aqueous MWCNT dispersions with the SDBS surfactant were dark, homogeneous mixtures with no visible aggregates.

5.4. Experimental procedure and characterisation

5.4.1. Fabrication of MWCNT/polymer composite films

a) *Spin coating and drop casting*

Spin coating[60,61] and drop casting[62,63] are the most commonly used techniques for producing polymer and polymer composite films due to their simple set-up and fabrication process. Moreover, it has been seen that spin coating allows alignment of nanotubes due to the hydrodynamic flow[61,64]. Hence, they were the first techniques to be studied to assess their suitability for this work. Dispersions of PU in NMP, DMA, and GBL with and without the nanotubes were used for preparing the films.

Drop Casting: 5 drops of the dispersion (*ca*. 1 ml) was put on a clean microscopy glass slide that was on a hotplate (IKA® Ret basic) at 100 °C (Figure 5-7a) and was allowed to dry for 2 hours. Samples of similar composition were also prepared at room temperature and were allowed to dry for 48 hours.

Spin coating: Clean microscopy glass slides were fixed onto the vacuum plate of the spin coater (assembled model from Headway Research Inc.) to facilitate a firm grip. 1 ml of each dispersion was dispensed drop by drop onto the glass substrates that were rotating at 200 rpm. Figure 5-7b shows the set-up used for spin coating. Two samples of each composition were prepared and dried at room temperature and 100 ^{o}C for 24 hours to remove the residual solvent.

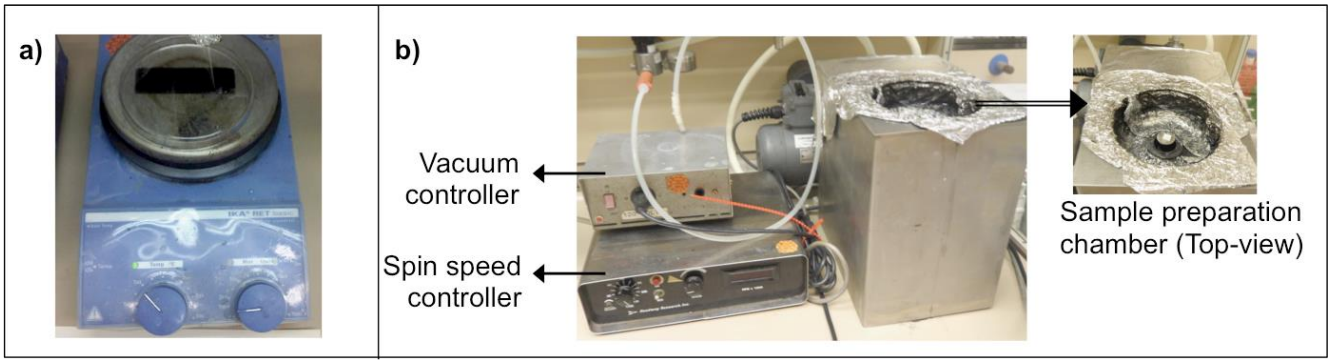


Figure 5-7. Experimental set-up used for: a) Drop casting, and b) Spin coating.

b) *Electrospraying*

The next technique that was studied for assessing the suitability for this work was electrospraying. A customised electrospray kit designed by Dr Peter Rockett at the Department of Engineering Science, University of Oxford was used for this purpose (Figure 5-8). The kit was modified to facilitate the spraying of MWCNT/PU dispersions in NMP, DMA, and GBL. Its special design consisted of a microscope and a camera system that provided comprehensive imaging of the fluid emission at the nozzle tip that was used for characterising the spraying mode, which is vital for an effective deposition process. The test chamber was designed to allow a controllable gas environment (in this case nitrogen) during spraying. Due to the reactive nature of the solvents used in this work, only glass syringes and PEEK capillary tubing (100 μm) were used for feeding the sample into the kit. Silica tip nozzles (New Objective; 30 μm) were found to be best suited for the flow rates used in this work.

An initial assessment was conducted with ethanol/water mixtures (50/50, 60/40, 70/30) to make sure that the modified version of the kit was fully functional and to deduce process windows. Once this was established, dispersions of MWCNT/PU dispersions were electrosprayed onto silica wafers. Before every spray run, 50/50 ethanol/water mixture was firstly sprayed for at least 20 minutes to clear residual debris from previous experiments and to detect blockages in the system. The operating

conditions usually varied for different dispersions based on their surface tensions, however the typical range is listed in Table 5-2. Figure 5-9 shows the stable Taylor cones of some of the dispersions; similar images were taken throughout every experiment and the voltage was tweaked until a stable spray was achieved.

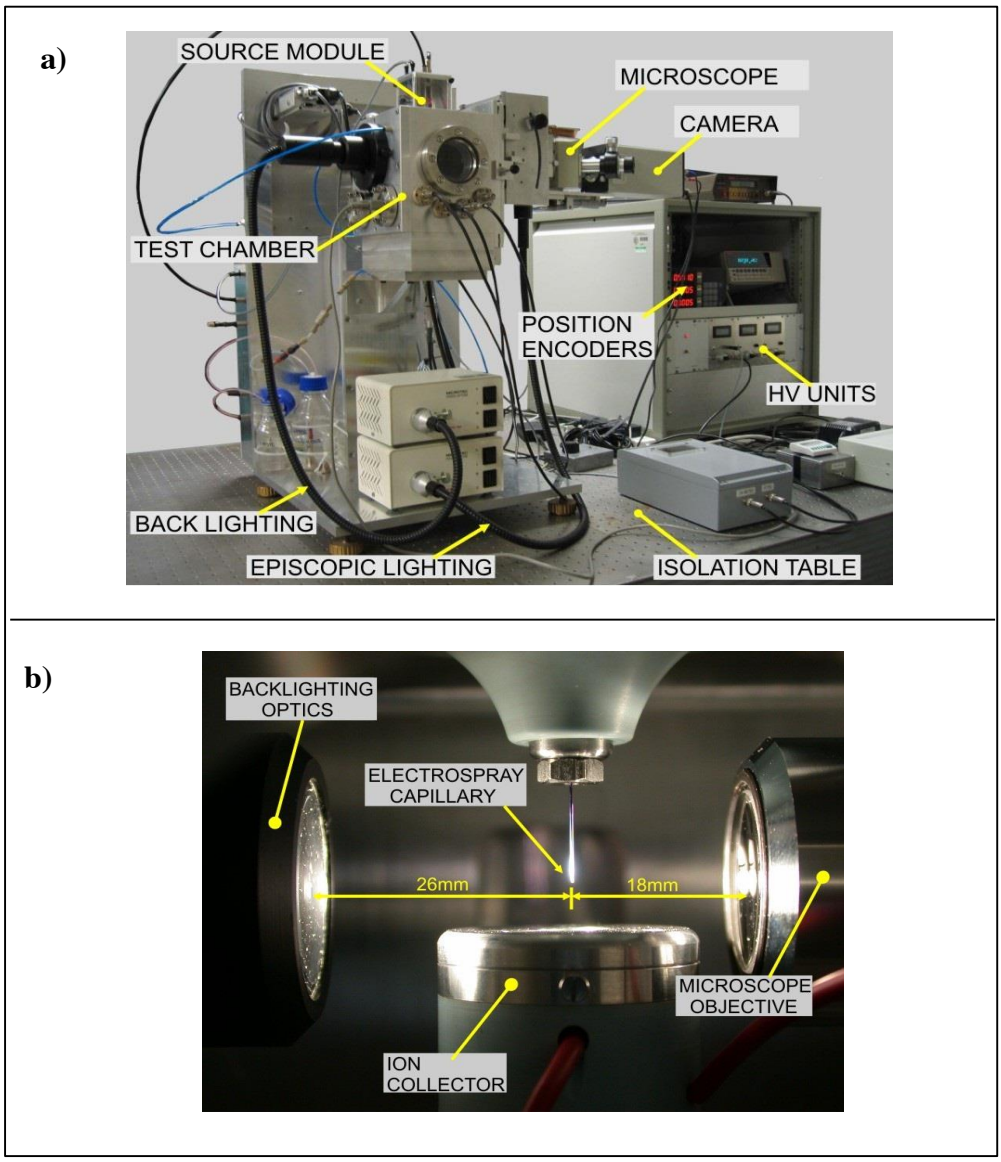


Figure 5-8. Photograph of the electrospray system as set-up in the lab: a) Details of the associated electronics and instrumentation, b) Capillary illumination. (Photo courtesy: Dr Peter Rockett)

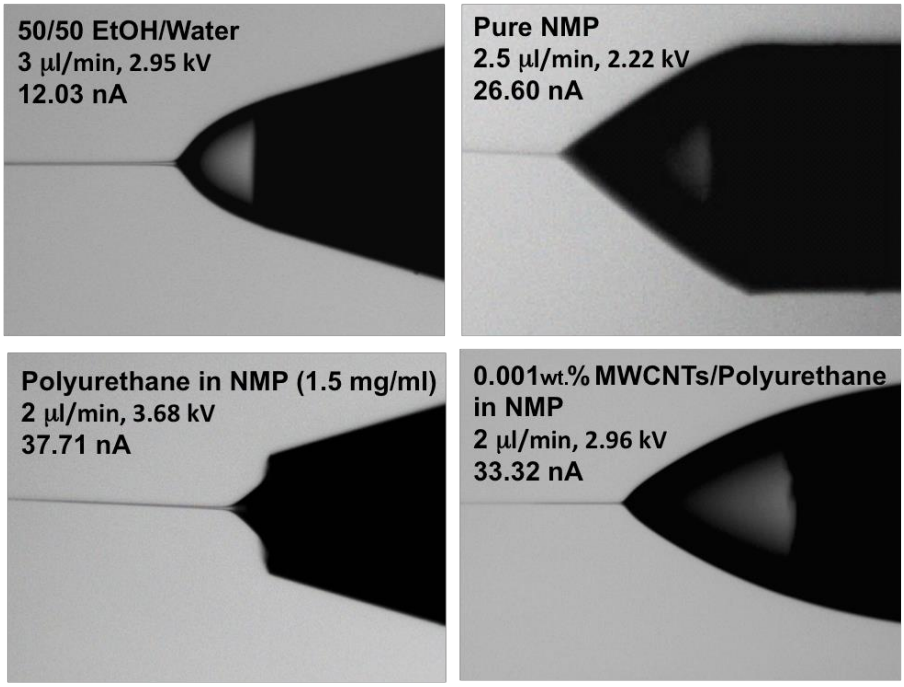


Figure 5-9. Photographs of stable electrospray cone jet modes of different types of dispersions along with their respective flow rates, applied voltages and collected currents.

Electrospray Parameter	**Typical range**
Flow rate	2.0–3.2 μl/min
Applied voltage	2.2–3.5 kV
Extraction gap	8–10 mm

Table 5-2. List of typical parameters used for electrospraying.

c) *Aerosol spraying*

Aerosol spraying was the last technique that was studied for the technique assessment. A basic aerosol spray kit developed by Dr Hinchliffe[27] at the Department of Materials, University of Oxford was modified to match the requirements of the materials used in this work. The set-up (Figure 5-10) consisted of a precision controlled

syringe pump (KDS Legato 200), which delivered the MWCNT/polymer dispersion to a customised nozzle (Viscomist 176 series, Lechler). The nozzle consisted of several inlets for atomising air and fluid injection and was designed in such a way that the atomising air was directly above the injection compartment filled with the dispersion. Therefore, when the compartment was filled with the required dispersion, by adjusting the pressure of the atomising air a fine aerosol was generated. This fine spray was collected onto substrates on a hot plate that was mounted on an X-Y-Z manipulator. This feature of the system allowed development of films in a 3-D manner. The spray experiments were conducted on 12 x 12 cm area.

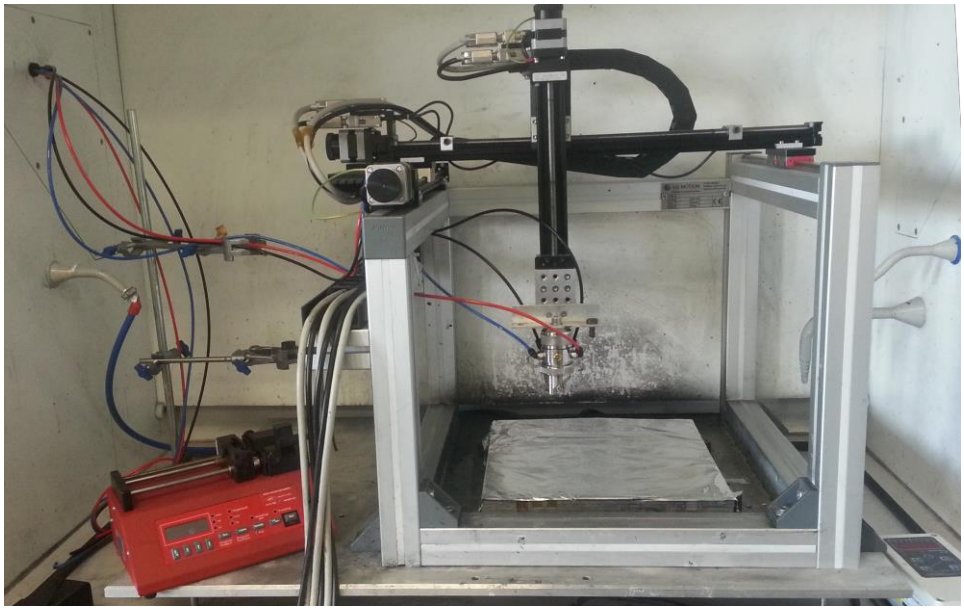


Figure 5-10. Photograph of the modified aerosol spray set-up used for forming nanotube/polymer composite films.

Due to the harsh nature of the dispersing solvents used in this work, proof of concept studies were conducted using aqueous MWCNT/polymer dispersions. Since PU was not soluble in water, the matrix polymer was changed to PFA that was readily available in an aqueous medium from the manufacturer. Aqueous dispersions of

conventional MWCNT/PFA and B-MWCNT/PFA were sprayed onto two different substrates: 1) Gold-coated glass slides and, 2) Plain microscopy glass slides.

Both substrates were firmly fixed to the hot plate at 100 °C using vacuum and the spraying was conducted. The sprayed films were cured in a belt furnace at 380 °C for 30 minutes. Once the films were cured, a masked top layer of gold was formed on substrate 1, which facilitated in forming model capacitors of the film. The gold coating was thermally evaporated onto the substrates using Edwards 306 (Moorfield) and Nano 36™ (Kurt J. Lesker) thermal evaporators; extreme care was taken to make sure that both top and bottom gold layers were roughly 70 nm thick. The gold layers on either side of the composite film acted as conductive electrodes for forming model capacitors and facilitated in electrical characterisation. On the other hand, films on plain glass slides were used for surface and microstructural characterisation. Figure 5-11 shows the procedure followed for film forming. The key parameters used for forming the films are as follows:

- Spray distance = 14 cm
- Flow rate = 1 ml/min
- Atomising air pressure = 2 bar
- Hot plate temperature = 100 °C
- Hot plate speed = 10 mm/min
- Belt furnace speed = 40 mm/min
- Curing temperature = 380 °C
- Curing hold time = 30 min
- Number of spray runs = 1–7 runs

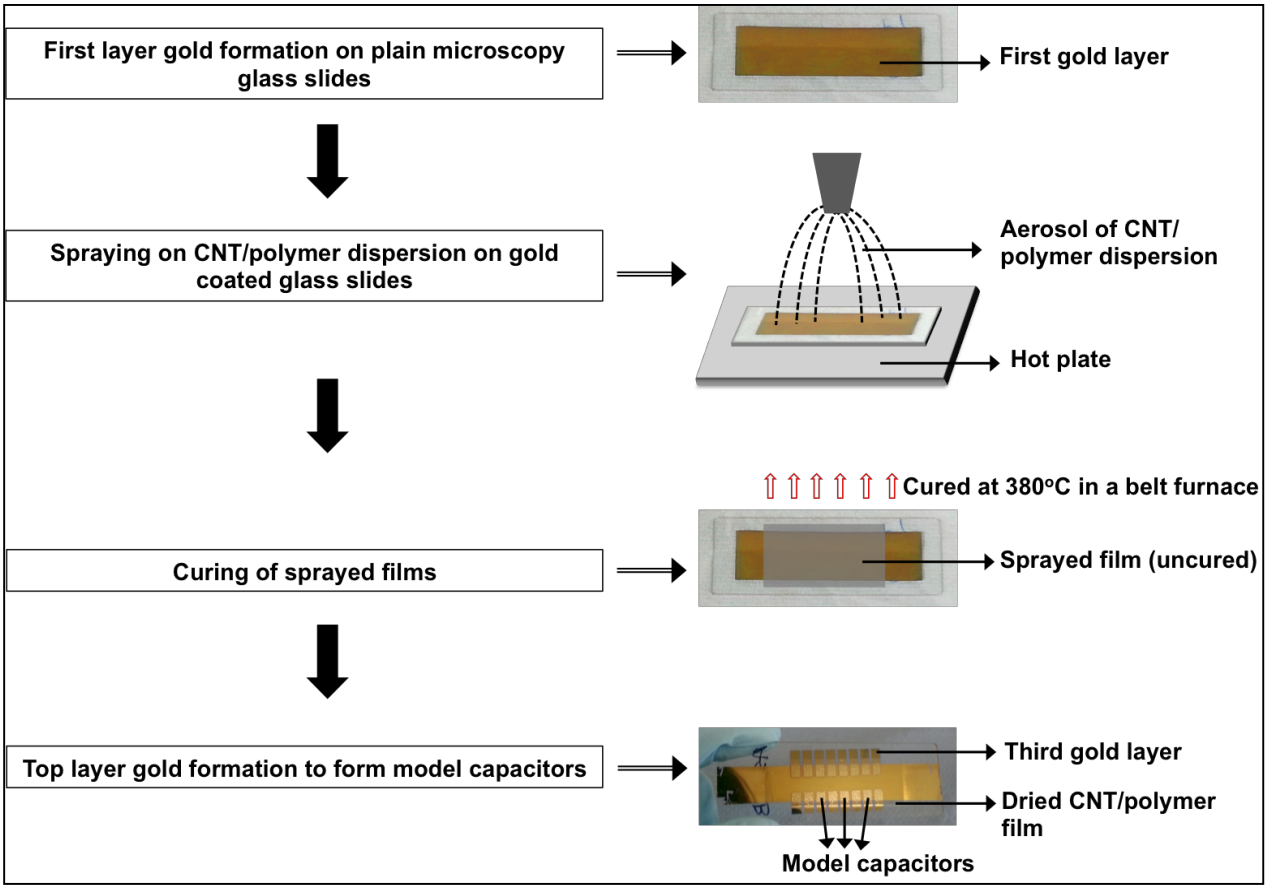


Figure 5-11. Flow chart showing the steps involved in the aerosol spraying for forming nanotube/PFA films. Also shown are optical photographs of the samples at every step.

5.4.2. Characterisation of MWCNT/PU and MWCNT/PFA films

a) *Surface characterisation*

Macroscopic and microscopic surface characterisations of the films were conducted using optical photography and SEM respectively. The optical photographs were taken with an 8 megapixel Samsung Galaxy S3 phone camera in a regular flash-free mode. SEM studies were conducted using a Jeol JSM-840F SEM in secondary electron mode at 3 kV over a range of magnifications. The glass-coated films were line-marked on the backside of the glass with a diamond pen and dipped in liquid nitrogen for 10 minutes to effectively fracture the film and form smaller pieces for cross-section analysis using SEM. The films were coated with 4 nm platinum to facilitate conduction and reduce charging during SEM studies.

b) *Thickness analysis*

The film thickness was calculated using a Veeco Dektak IIA surface profilometer using the step height method. Line scans were conducted across each film in 8 different places and the values were averaged. The thickness of the film at various places gave an idea of the uniformity of the film and also helped in understanding the dielectric behaviour of the films in various locations.

c) *Impedance spectroscopy*

Dielectric studies were conducted on the films using impedance spectroscopy for which a Solartron SI 1260 impedance analyser was used at different frequencies (100 Hz – 1 MHz) at an applied voltage of 1 V. The films were heated at 40 °C for 24 hours prior to testing to remove any absorbed moisture. Measurements were conducted on at least 6 model capacitors of every film, and the basic parallel plate capacitor formula as shown in Equation 5-4 was used for calculating the dielectric constants (k) of the films:

$$k = \frac{C\,d}{\varepsilon_o\,A} \qquad \text{Equation 5-4}$$

where: C is the effective capacitance of the capacitor that was directly obtained from the instrument, ε_o is the permittivity of free space (8.854 x 10^{-12} F/m), A is the cross-sectional area of one capacitor plate that was calculated using the dimensions of the capacitor, and d is the distance between the plates (*i.e.*, the thickness of the dielectric film) that was calculated using surface profilometry.

The dissipation factor, real and imaginary permittivities were calculated from the following equations:

$$DF = \mathrm{Tan}\,\delta \qquad \text{Equation 5-5}$$

$$\varepsilon' = k\,\varepsilon_o \qquad \text{Equation 5-6}$$

$$\varepsilon'' = \varepsilon' \text{Tan } \delta \qquad \text{Equation 5-7}$$

where: DF is the dissipation factor, δ is the loss tangent that was directly obtained from the equipment, ε' is the real dielectric permittivity, and ε" is the imaginary dielectric permittivity.

5.5. Results and discussion

5.5.1. Optical characterisation of composite films

Optical characterisation was the first characterisation test conducted to assess the film quality. It was realised that the high boiling points of the dispersing solvents (NMP – 202 °C, DMA – 166 °C, GBL – 204–205 °C, and Benzylalcohol – 203–205 °C) made it difficult to remove the solvent from the drop casted and spin coated films, resulting in poor quality and inhomogeneous films. Figure 5-12a,b shows the 0.01 wt.% conventional MWCNT/PU drop casted films dried at room temperature and at 100 °C. The drop casted film dried at room temperature appeared to be better than the film dried at 100 °C that showed a coffee stain effect. However, areas of dark and light regions existed in both the films signifying inhomogeneity within the film. On the other hand, 0.01 wt.% conventional MWCNT/PU spin coated films (Figure 5-12c,d) were of extremely poor quality and formed islands rather than a continuous film. In addition to the high boiling points of the solvents, the poor quality of the drop casted and spin coated films can be attributed to the inability of the dispersions to wet the glass surface. Dispersion interaction with the glass surface can usually be improved by surface treating the glass, such as salinisation, however salinisation did not prove useful either for these mixtures. Therefore, drop casting and spin coating proved to be unsuitable for this work.

Figure 5-12e,f shows the 0.1 wt.% conventional MWCNT/PU electrosprayed film before and after heating at 50 °C for 120 hours. Since the film was formed on a

silicon wafer, it was difficult to judge its optical quality due to reduced contrast from the background. Nevertheless, the film appeared to be optically uniform and had an average thickness of 10±4 μm. Despite the ability of electrospraying to form acceptable films, the set-up was incapable of forming large area films, hence this technique had to be ruled out too. The last technique that was explored was aerosol spraying, which produced high quality films, as shown in Figure 5-12g,h. The aerosol sprayed films appeared to be homogeneous, uniform and had an average thickness of 20–30 μm. Hence, this technique was chosen as the best suitable technique for this work.

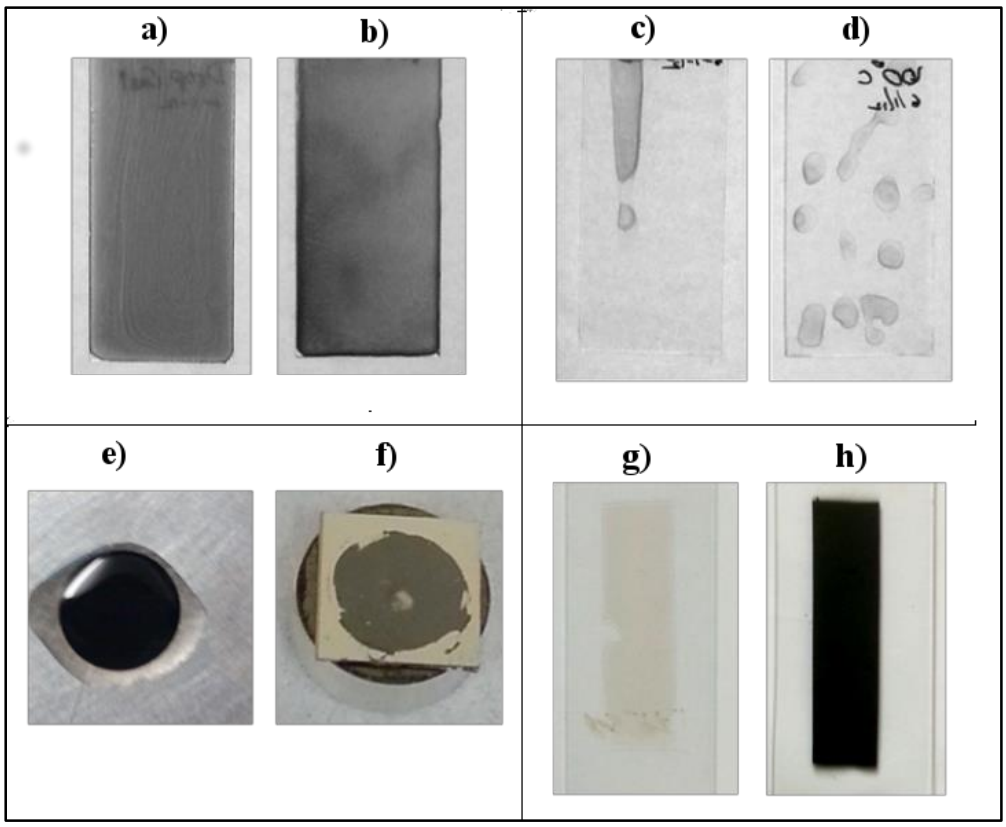


Figure 5-12. Optical photographs of composite films synthesised through different techniques:
a) Drop casted 0.01 wt.% conventional MWCNT/PU films dried at room temperature,
b) Drop casted 0.01 wt.% conventional MWCNT/PU films dried at 100 °C,
c) Spin coated 0.01 wt.% conventional MWCNT/PU films dried at room temperature,
d) Spin coated 0.01 wt.% conventional MWCNT/PU films dried at 100 °C,
e) Electrosprayed sample of 0.1 wt.% conventional MWCNT/PU film before drying,
f) Electrosprayed film of 0.1 wt.% conventional MWCNT/PU film after drying,
g) Aerosol sprayed plain PFA film after curing, and
h) Aerosol sprayed 0.5 wt.% conventional MWCNT/PFA film after curing.

5.5.2. Surface characterisation using SEM

SEM studies were conducted on the surface of electrosprayed and aerosol sprayed films to understand the distribution of nanotubes in the film. Ideally, cross-sectional analysis would have given a better idea of the nanotube distribution, however, attempts for perfectly fracturing the films cross-sectionally failed due to the elasticity of the polymer. Hence, only surface analysis of the films was conducted. The 0.1 wt.% conventional MWCNT/PU electrosprayed film (Figure 5-13a) showed no signs of MWCNTs on the surface. It could be that the MWCNTs were trapped within the film; however, the precise distribution of the nanotubes within the polymer matrix was unclear. Moreover, the electrosprayed films seemed to be porous and microscopically non-uniform. Therefore, electrospraying was decided to be unsuitable for this work. On the other hand, the presence of individual and separated nanotubes on the surface of 0.5 wt.% aerosol sprayed conventional MWCNT/PFA film (Figure 5-13b), confirms the ability of this technique to form agglomerate free films. However, it was difficult to understand the uniformity of the nanotubes within aerosol sprayed film from the SEM images. Nevertheless, aerosol spraying seemed to be the best suited film-forming technique for this work.

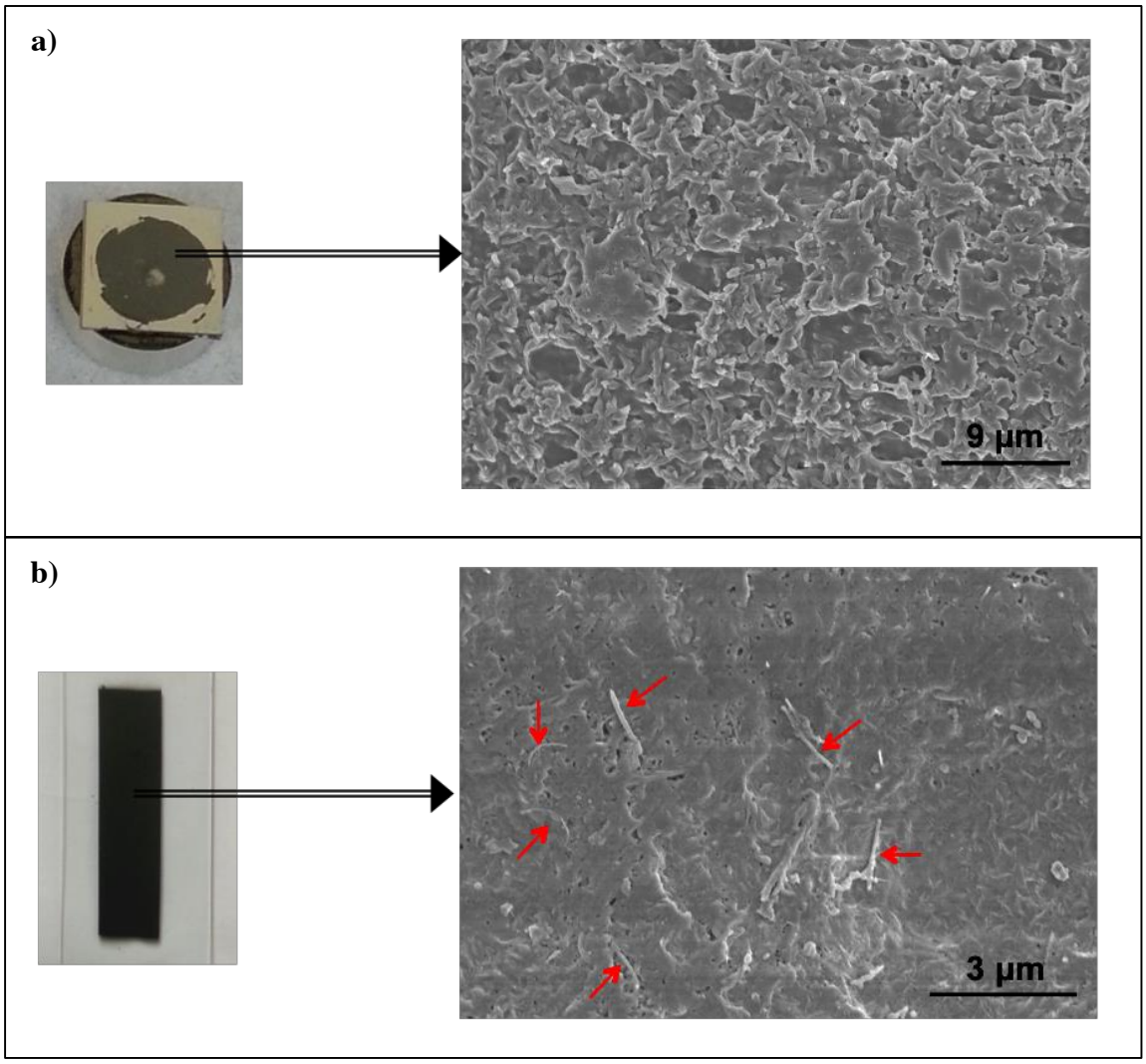


Figure 5-13. SEM images of:
a) 0.1 wt.% MWCNT/PU electrosprayed film that had no evident nanotubes on the surface,
b) 0.5 wt.% MWCNT/PFA aerosol sprayed film that shows the presence of individual nanotubes on the surface of the film.

5.5.3. Impedance spectroscopy of aerosol sprayed films

The Cole-plots of the conventional MWCNT/PFA composite films (Figure 5-14) showed that the films mostly behaved as lossy capacitors, however at higher nanotube concentrations (weight % ≥ 0.5%) a resistive behaviour was observed. This could have been due to the contribution of the pure capacitive elements for nanotube concentrations up to 0.5 wt.%. However, at 0.5 wt.% nanotube concentration there is perhaps a contribution from both the resistive and capacitive elements of the capacitor

due to an increase in the number of individual nanotubes that form micro-capacitors within the film.

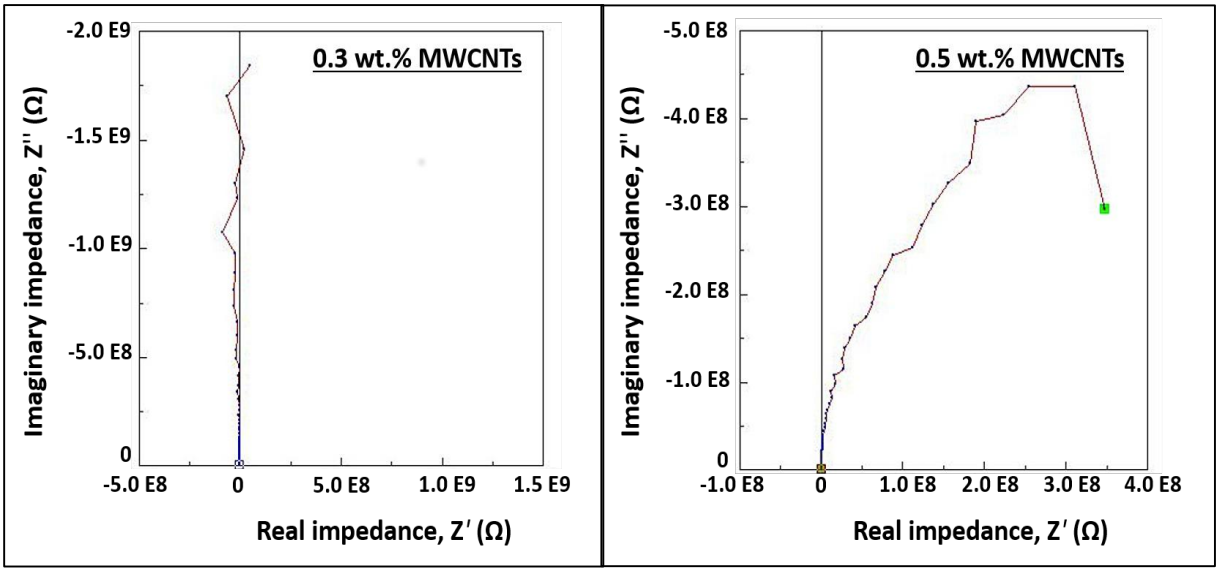


Figure 5-14. Cole-plots depicting the change from lossy to resistive behaviour in the capacitor containing conventional MWCNT/PFA dielectric films containing different nanotube concentrations.

Figure 5-15 shows the dielectric constants of conventional MWCNT/PFA and B-MWCNT/PFA films at varying nanotube concentrations at 10 kHz. The dielectric constant of plain PFA film at 10 kHz was measured to be 2.4 and an increase in the dielectric constant was observed with increasing nanotube concentration. This can be attributed to the interfacial polarisation[43] due to the difference in dielectric relaxation of the nanotubes and the PFA matrix. Since the charge storage occurs at the interfaces, the high aspect ratios of the nanotubes lead to a significant increase in the number of nanotube/PFA interfaces in both the conventional MWCNT/PFA and B-MWCNT/PFA films[44]. This contributes towards the overall increase of the dielectric constants of the films. Usually, when the amount of nanotube concentration approaches the percolation threshold, each nanotube surrounded by the insulating PFA matrix acts as a micro-capacitor. Hence, there is a cumulative polarisation contribution from all the micro-capacitors in the film that results in a sudden and sharp increase in the dielectric

constant of the system[13]. However, the concentration values reported in this dissertation were less than the percolation threshold values, hence such a sharp increase in the dielectric constants could not be observed in these samples.

It can also be observed in Figure 5-15 that for the same nanotube wt.%, films containing B-MWCNTs showed better improvement in dielectric constants compared to that containing conventional MWCNTs. Boron doping induces substantial number of defects in the nanotubes and hence significantly alters the nanotube structure (as discussed in Chapter 2). These defects, at room temperature, may not necessarily alter the electronic band structure of the nanotube but can act as polarised centres that contribute towards an improvement in the dielectric properties[65]. Similar results were reported by Son *et al*.,[66] who proposed theoretically that the presence of such defects in metallic SWCNTs improves the resistance of the nanotubes threefold. However, their study only looked into calculations with transverse electrical fields for metallic nanotubes. Nevertheless, it is reasonable to extend their theory to all types of nanotubes.

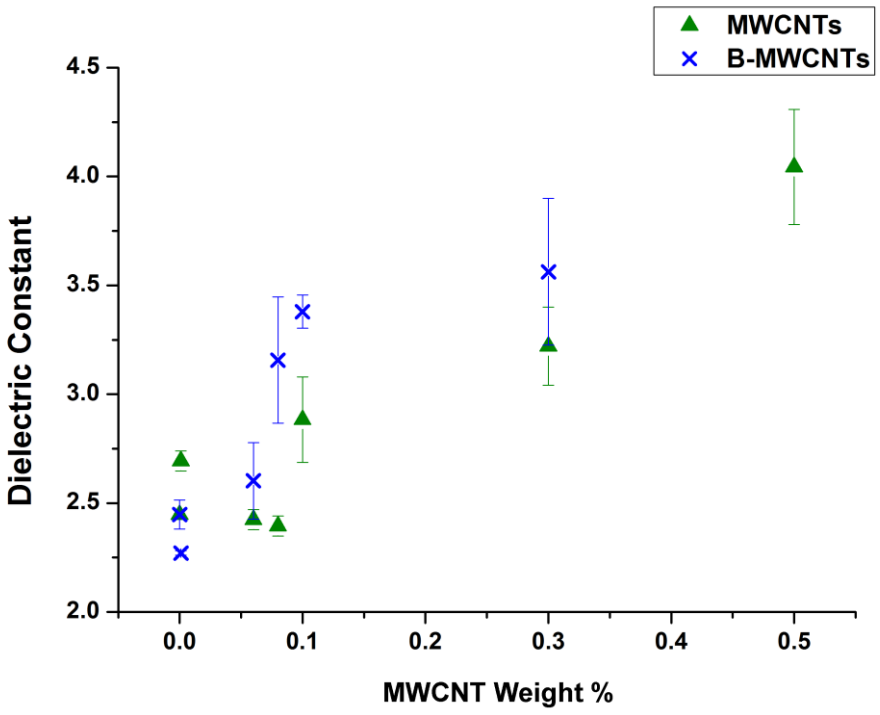


Figure 5-15. Dielectric constants of conventional MWCNT/PFA and B-MWCNT/PFA films as a function of nanotube wt.% at 10 kHz that show an improvement in the dielectric constant with increasing nanotube concentration.

Figure 5-16a,b shows the dielectric constants of both conventional MWCNT/PFA and B-MWCNT/PFA films with varying nanotube concentration as a function of frequency (100 Hz – 1 MHz). The dielectric constants of both the films increased with increasing nanotube wt.%, although for a given amount of nanotubes the dielectric constants of most of the films were fairly uniform over the entire frequency range. The 0.5 wt.% conventional MWCNT/PFA film showed an initial decrease followed by a subsequent increase in the dielectric constant with increasing frequency. This could be due to the predominant influence of interfacial polarisation at lower frequencies that is discussed later in this section. Furthermore, the dielectric constants were an averaged from 6 different locations from the films and the deviation in the values measured from different locations was < 0.5. This indicates a uniform distribution of nanotubes within the film, thereby confirming the efficiency of the aerosol spray technique in forming homogeneous films. However, the 0.001 wt.% B-MWCNT/PFA film (Figure 5-16b) exhibited dielectric constants lower than the plain PFA film along with an unusual increase at 1 MHz. This behaviour is perhaps not a real change in the dielectric nature of the film, but could be associated with external parasitic effects that can cause erroneous results. The parasitic effects can occur either due to contact electrification from contact between materials with dissimilar work functions, or gas discharge within the capacitor that can cause charge deposition on the dielectric material[67]. However, this is only a speculation and it is difficult to prove this result as no other samples exhibited similar behaviour.

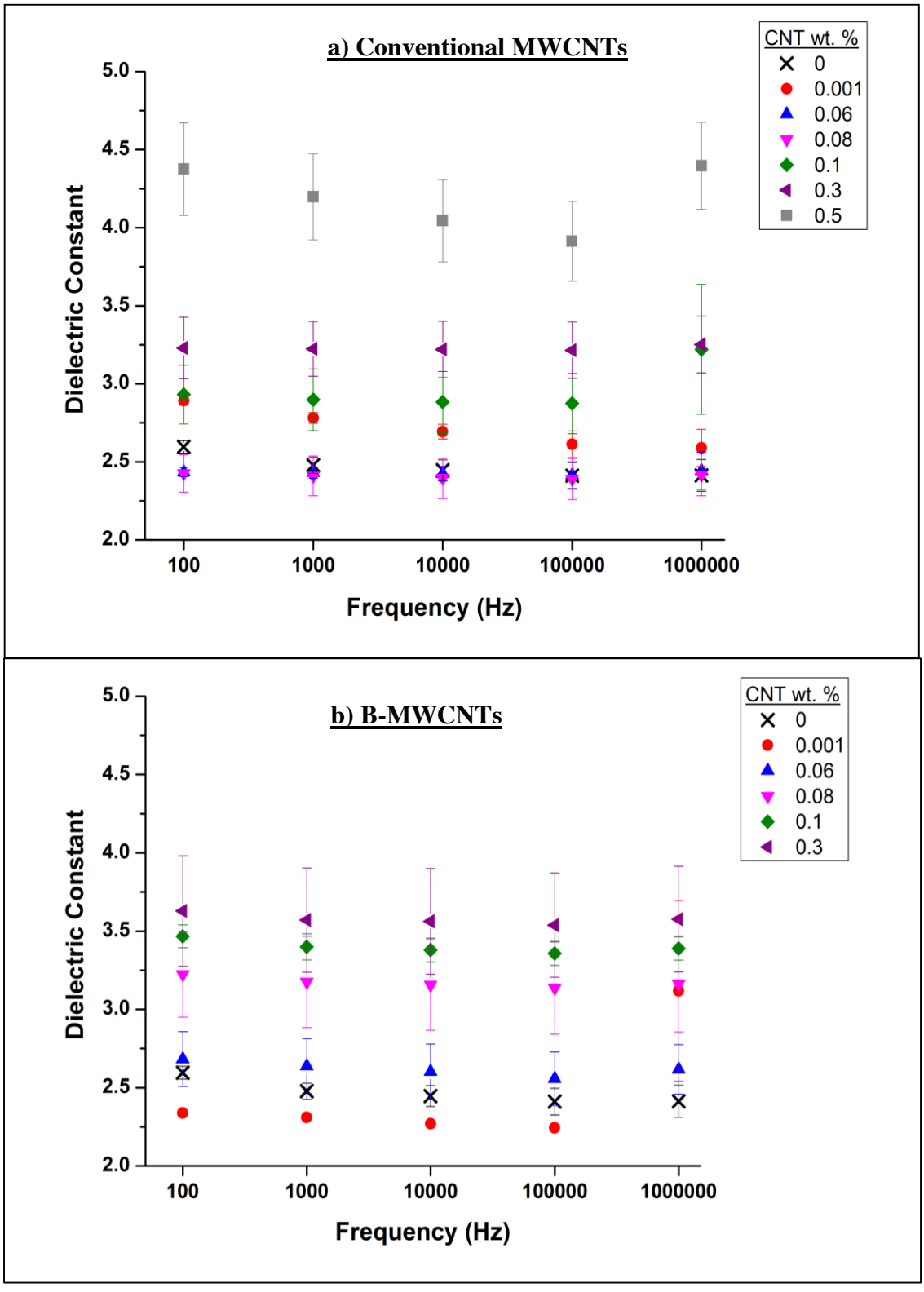


Figure 5-16. Dielectric constants of: a) Conventional MWCNT/PFA films, and b) B-MWCNT/PFA films with varying nanotube concentrations as a function of increasing frequency that show the stability of the dielectric values over a range of frequencies.

To understand the exact effect of the nanotubes on the dielectric properties, it is important to look into the individual components of the complex permittivity, *i.e.*, the real and imaginary permittivities. Figure 5-17a,b shows the real permittivities of PFA films containing conventional and B-MWCNTs as a function of frequencies for increasing nanotube concentrations. The real permittivities were mostly independent of the frequencies at lower nanotube concentrations for conventional MWCNT/PFA films, however an increase in the real permittivity was observed at concentrations > 0.08 wt.%. The 0.5 wt.% conventional MWCNT/PFA film showed a significant increase in the real permittivity at lower frequencies that decreased gradually with increasing frequency. The decrease in real permittivity with increasing frequency is expected in composite films due to the dielectric relaxation at higher frequencies[43], *i.e.*, at lower frequency the charges, accumulated at the nanotube/PFA interface, can readily redistribute in the applied electric field direction. However, at higher frequencies the charges cannot easily re-orient themselves in the direction of the electric field and get less time for re-orientation. Hence, the applied electric field tends to periodically alter, resulting in a reduction of dipole diffusion in the direction of applied electric field and accumulation of space charges that causes a significant decrease in the polarisation and the permittivity. Furthermore, the significant increase in real permittivity could signify the onset of the percolation threshold in the case of conventional MWCNTs at 0.5 wt.%. It can be expected that a further increase in the conventional MWCNT concentration could have led to an outstanding improvement in the real permittivity[13]. Additionally, for the same nanotube concentration, the improvement in the real permittivity for B-MWCNTs/PFA films was slightly higher than those with conventional MWCNTs. This could imply that for the same nanotube concentration the charge storage was much better for films with B-MWCNTs. For the same reason, it can also be expected that the

B-MWCNT/PFA films might have higher dielectric constants at relatively lower nanotube concentrations compared to conventional MWCNT/PFA films.

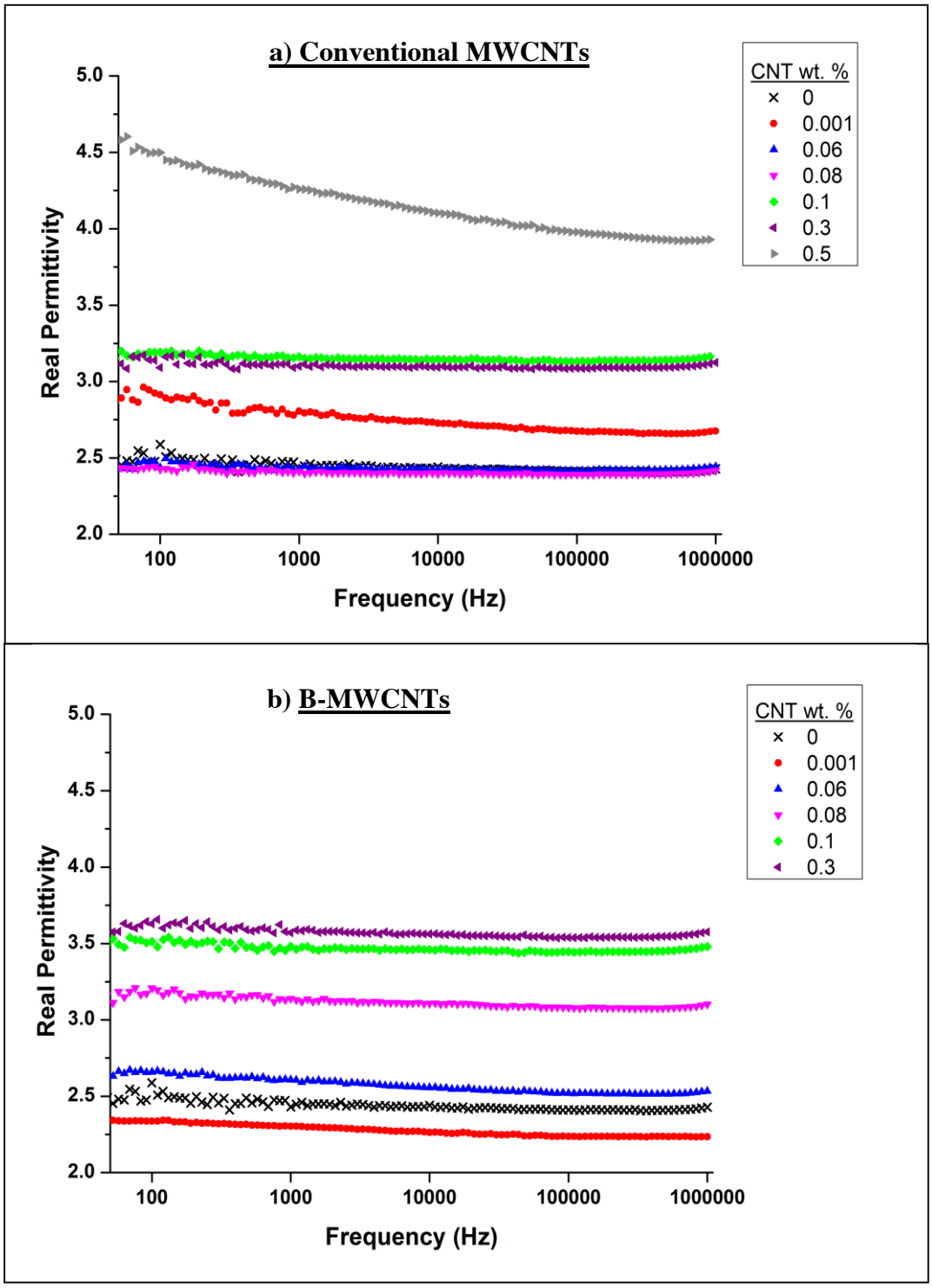


Figure 5-17. Real permittivities of: a) Conventional MWCNT/PFA films, and b) B-MWCNT/PFA films with varying concentrations of CNTs as a function of increasing frequency. The change in dielectric behaviour of the B-MWCNT containing films relative to films with conventional MWCNTs can be clearly observed.

Figure 5-18a,b show the imaginary permittivities of PFA films containing conventional and B-MWCNTs as a function of varying frequency at different nanotube concentrations. The imaginary permittivities remained fairly constant for most of the films indicating no significant dielectric losses. However, an increase in the imaginary permittivity at higher frequencies can be observed for all the films. It should be noted that the plain PFA film also followed the same trend, which indicates that this behaviour could have been contributed by the PFA rather than presence of nanotubes. A significant increase in the imaginary permittivity for the 0.5 wt.% conventional MWCNT/PFA film signifies the increase in the dielectric losses due to the increased number of nanotube/PFA interfaces. As discussed earlier, this concentration could be the onset of the percolation threshold in the conventional MWCNT/PFA films. The conventional MWCNTs are electrically conductive by nature; at higher concentrations (such as 0.5 wt.%) there exists a significantly higher number of individual nanotubes within close proximity to each other. This can induce a tunnelling effect and cause an increase in the dielectric losses[28]. Based on the earlier argument for real permittivities in the PFA films containing B-MWCNTs, if the presence of B-MWCNTs can improve the dielectric properties at low percolation threshold, then lower dielectric losses can also be expected from the B-MWCNT containing films at the percolation threshold. However, this cannot be confirmed from the current results as the percolation threshold could not be achieved in these samples, but hopefully will be confirmed in the future experiments.

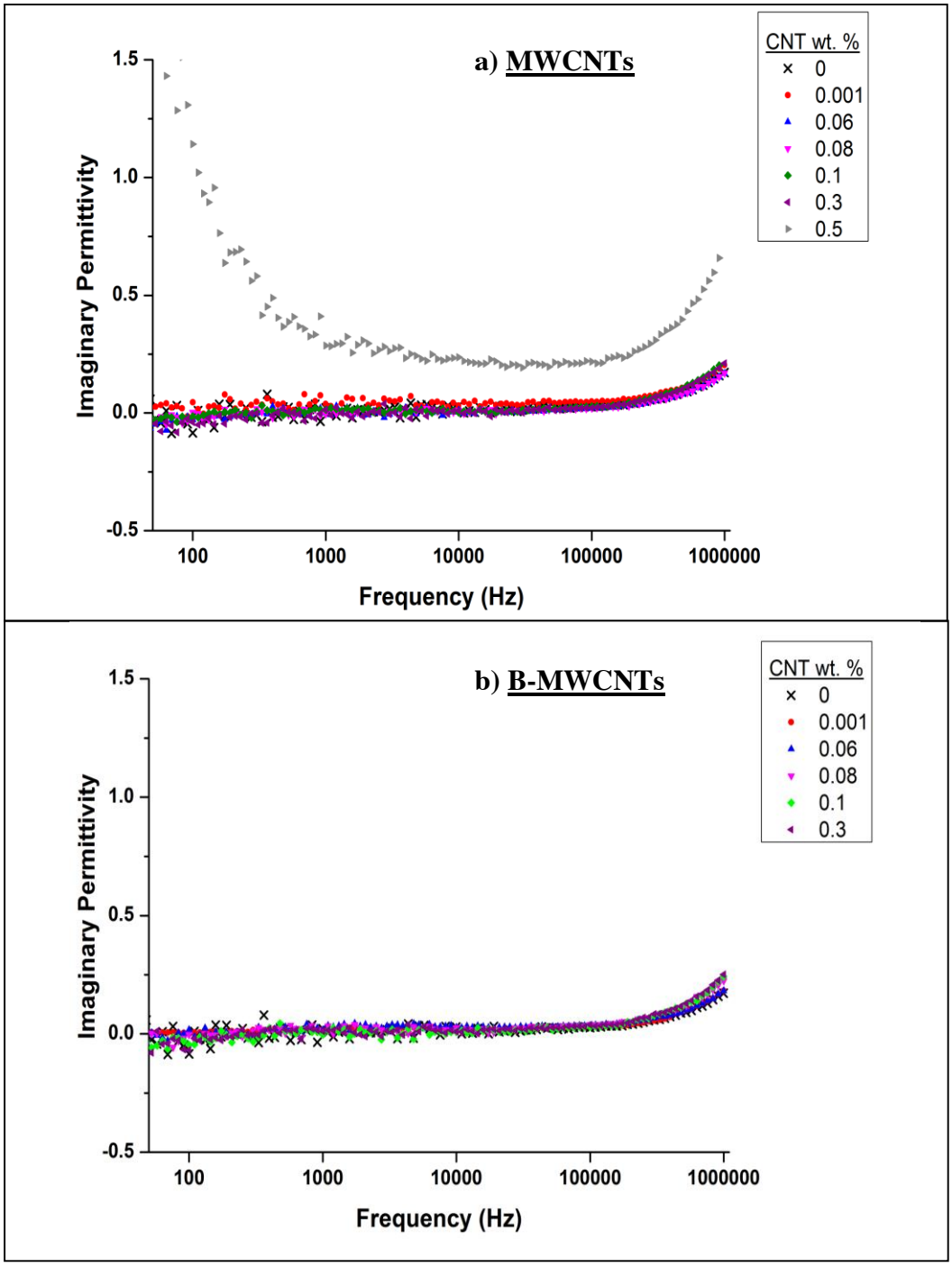


Figure 5-18. Imaginary permittivities of: a) Conventional MWCNT/PFA films, and b) B-MWCNT/PFA films with varying concentrations of CNTs as a function of increasing frequency. It can be seen that the imaginary permittivity was independent of nanotube concentration and frequency for most of the films.

The dissipation factors of the PFA films with conventional and B-MWCNTs at 10 kHz (Figure 5-19) showed a gradual decrease in the values with increasing nanotube concentration. A strong interfacial interaction between the fillers and the polymer matrix usually hinders the relaxation of the polymer chains and interferes with the

energy dissipation that can cause a decrease in the dissipation factors in polymer nano-composite systems[68]. A similar behaviour can be seen in Figure 5-19, which confirms the interfacial interaction between the nanotubes and the PFA matrix. However, an increase in the dissipation factor at 0.5 wt.% conventional MWCNTs indicates the start of formation of a conductive path between the nanotubes, and can be indicative to the onset of the percolation threshold. It can also be seen that the dissipation factors of PFA films with B-MWCNTs were relatively higher than those of conventional MWCNTs, which could be due to the additional defects in B-MWCNTs[69]. The dissipation factors at the percolation threshold could reveal interesting information.

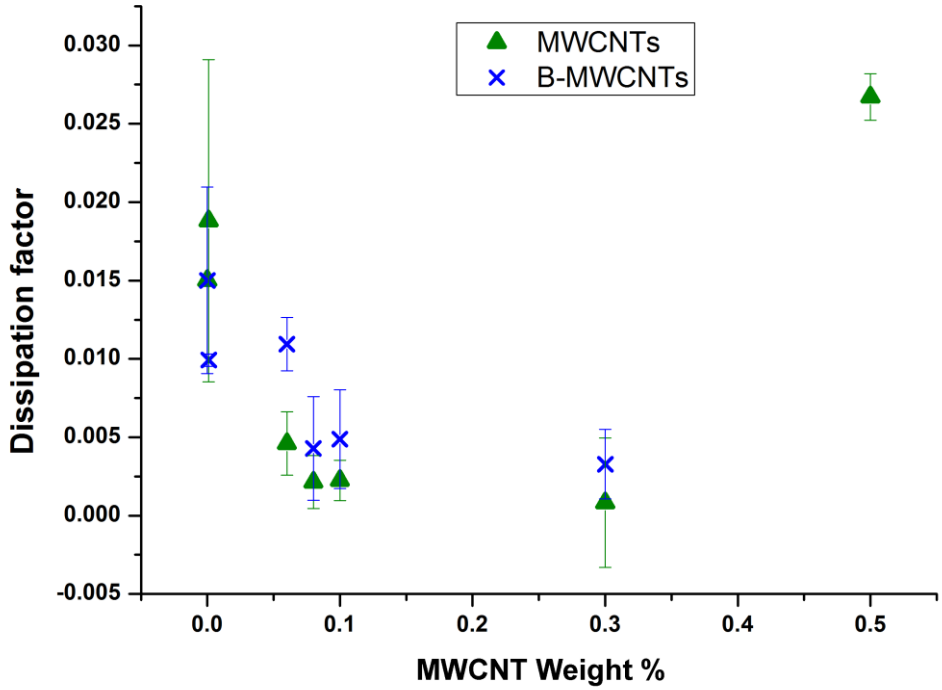


Figure 5-19. Dissipation factors of PFA films containing conventional and B-MWCNTs as a function of nanotube wt.% at 10 kHz. A decrease in the values with the increasing nanotube concentration signifies a strong interfacial interaction of the nanotubes with the PFA matrix.

The dissipation factors of the composite films over the entire frequency range (100Hz – 1 MHz) (Figure 5-20a,b) showed a similar behaviour to the imaginary permittivity. It was observed that the dissipation factors of the all the films remained fairly constant up to 100 kHz and gradually increased with the frequency thereafter. As

discussed earlier in the chapter, at lower frequencies the charges accumulated at the nanotube/PFA interface can easily redistribute, however at higher frequencies dielectric relaxation occurs due to the shorter re-orientation time[43]. Furthermore, a significant increase in the 0.5% MWCNT-PFA film could indicate the onset of percolation threshold. Nevertheless, the dissipation factors of all the films over the entire frequency range were still very low *i.e.*, < 0.2, which indicates improved efficiency over the films reported in literature.

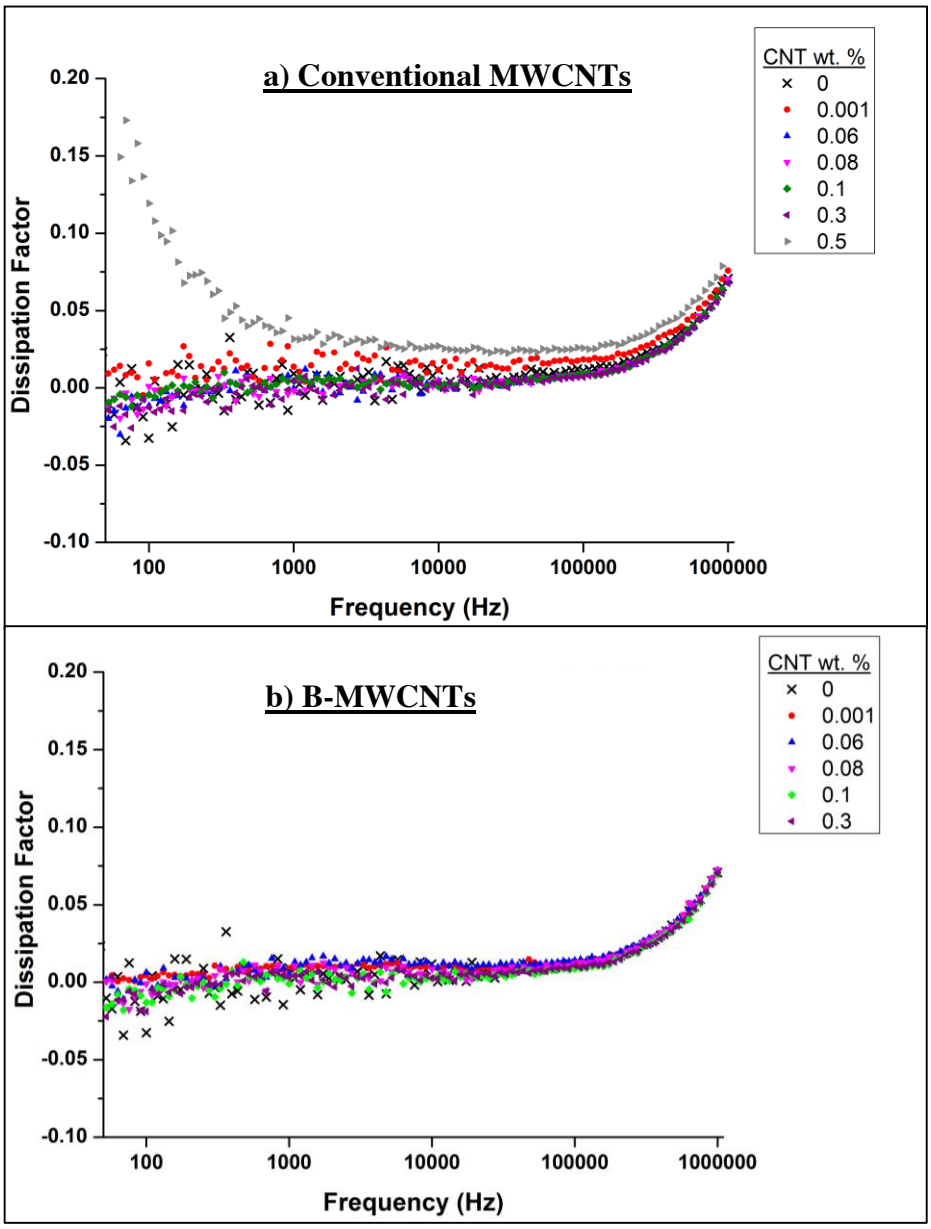


Figure 5-20. Dissipation factors of: a) MWCNT/PFA films, b) B-MWCNT/PFA films with varying nanotube concentration showing the consistency of the values with increasing frequency.

5.6. Summary

Four different techniques were studied in order to understand their suitability for forming large area nanotube/polymer dielectric films. The techniques used (in the order of study) were drop casting, spin coating, electrospraying, and aerosol spraying. Uniform and homogeneous MWCNT dispersions in organic solvents reported in previous chapters were used for forming the composite films. MWCNT dispersions in NMP, DMA, and GBL mixed with PU polymer were used as feedstock for the first three techniques. After conducting several experiments with drop casting and spin coating, it was realised that these techniques were unsuitable for the nature of the material used in this work. This was due to the high boiling points of the dispersing solvents, which made the solvent evaporation difficult. On the other hand, electrosprayed films were an improvement over the drop casted and spin coated films. However, due to the harsh nature of the dispersing solvents that caused damage to the internal parts of the electrospray system, and the complexity of the apparatus, which prevented it to be modified for large area film forming, the electrospraying technique was ruled out too. Aerosol spraying seemed to overcome the challenges of the first three techniques and proved to be the best. Initial testing of the aerosol set-up was done with surfactant assisted aqueous MWCNT dispersions mixed with PFA polymer. PFA films containing varying concentrations of MWCNTs and B-MWCNTs were developed and characterised for dielectric properties. The films were 20–30 μm thick and looked optically homogeneous. The dielectric constants of the films improved with increasing nanotube concentration as a result of interfacial polarisation induced by the nanotubes. Presence of conductive MWCNT fillers with high aspect ratios resulted in an increased interfacial polarisation at the nanotube/polymer interfaces and also increased the density of the interfacial polarisation. Moreover, for the same nanotube concentration, PFA films containing B-MWCNTs showed better dielectric properties

than those containing conventional MWCNTs. This was related to the increased defect density in B-MWCNTs that can potentially act as polarised centres and contribute towards an improvement in polarisation. Therefore, behaviour of B-MWCNT/PFA films at percolation threshold values could be of high interest for future work.

It was observed that the dielectric values recorded from different locations of the films deviated by a small number (< 0.5), which indicated a homogeneous distribution of the nanotubes within the polymer films. The presence of MWCNTs seemed to have affected the real permittivity more significantly than the imaginary permittivity. This is due to the fact that the real permittivity is related to the polarisation but the imaginary permittivity is related to the electric loss/dissipated energy. Therefore, whilst the increase in interfacial polarisation resulted in an increase in real permittivity, the low dissipation factors of these films caused no significant changes in the imaginary permittivity. A striking improvement in dielectric properties of 0.5 wt.% conventional MWCNT/PFA film was observed, which could signify the onset of the percolation threshold. However, the exact percolation threshold values could not be identified for these films.

The results reported in this chapter prove that it is critical to understand various film forming techniques, before choosing any particular technique for forming composite films, especially for films with nanomaterial fillers. Moreover, the suitability of any technique with respect to the nature of material is essential. This becomes even more important when considering upscaling. Additionally, the characterisation tests of nanotube/PFA films show a clear evidence of improvement in dielectric properties for films with B-MWCNTs. This creates new possibilities for doped filler materials in dielectric composite films. The simplified set-up of the aerosol spraying provides an additional option of studying the effects of pristine MWCNTs on dielectric properties, as it can allow spraying of MWCNT dispersions in organic

solvents. Consequently, this technique allows easier processing of a wider choice of nanomaterials for thin films.

5.7. References

[1] Hamilton, T., "Next stop: ultracapacitor buses," MIT Technology Review, 2009: *http://www.technologyreview.com/news/415773/next-stop-ultracapacitor-buses/*

[2] Coughlin, C., "Ultracapacitors: The next big thing in energy storage?," Green Biz, 2012: *http://www.greenbiz.com/blog/2012/06/10/ultracapacitors-next-big-thing-energy-storage*

[3] Kannappan, S., Kaliyappan, K., Manian, R. K., Pandian, A. S., Yang, H., Lee, Y. S., Jang, J.-H., and Lu, W., "Graphene based supercapacitors with improved specific capacitance and fast charging time at high current density," 2013.

[4] Whittingham, M. S., "Materials challenges facing electrical energy storage," MRS Bulletin, 2011, **33**(04), pp. 411–419.

[5] Charlton, C. B., and Shen, T. E., "Plastic-film-dielectric capacitors," Proceedings of the IEE - Part B: Electronic and Communication Engineering, 1962, **109**(22S), pp. 476–487.

[6] Arbatti, M., Shan, X., and Cheng, Z.-Y., "Ceramic–polymer composites with high dielectric constant," Advanced Materials, 2007, **19**(10), pp. 1369–1372.

[7] Ding, Y., Wu, Q., Zhao, D., Ye, W., Hanif, M., and Hou, H., "Flexible PI/BaTiO3 dielectric nanocomposite fabricated by combining electrospinning and electrospraying," European Polymer Journal, 2013, **49**(9), pp. 2567–2571.

[8] Su, C.-C., Wu, C.-C., and Yang, C.-F., "Developing the dielectric mechanisms of polyetherimide/multiwalled carbon nanotube/$(Ba_{0.8}Sr_{0.2})(Ti_{0.9}Zr_{0.1})O_3$ composites.," Nanoscale Research Letters, 2012, **7**(1), p. 132.

[9] Zhao, X., Chu, B. T. T., Ballesteros, B., Wang, W., Johnston, C., Sykes, J. M., and Grant, P. S., "Spray deposition of steam treated and functionalized single-walled and multi-walled carbon nanotube films for supercapacitors," Nanotechnology, 2009, **20**(6), p. 065605.

[10] Wang, L., and Dang, Z.-M., "Carbon nanotube composites with high dielectric constant at low percolation threshold," Applied Physics Letters, 2005, **87**(4), p. 042903.

[11] Ameli, A., Nofar, M., Park, C. B., Pötschke, P., and Rizvi, G., "Polypropylene/carbon nanotube nano/microcellular structures with high dielectric permittivity, low dielectric loss, and low percolation threshold," Carbon, 2014, **17,** pp. 206–217.

[12] Dang, Z.-M., Wang, L., Yin, Y., Zhang, Q., and Lei, Q.-Q., "Giant dielectric permittivities in functionalized carbon-nanotube/ electroactive-polymer nanocomposites," Advanced Materials, 2007, **19**(6), pp. 852–857.

[13] Zhao, X., Koos, A. A., Chu, B. T. T., Johnston, C., Grobert, N., and Grant, P. S., "Spray deposited fluoropolymer/multi-walled carbon nanotube composite films with high dielectric permittivity at low percolation threshold," Carbon, 2009, **47**(3), pp. 561–569.

[14] Ramanathan, T., Liu, H., and Brinson, L. C., "Functionalized SWNT/polymer nanocomposites for dramatic property improvement," Journal of Polymer Science Part B: Polymer Physics, 2005, **43**(17), pp. 2269–2279.

[15] Park, S., and Bandaru, P., "Improved mechanical properties of carbon nanotube/polymer composites through the use of carboxyl-epoxide functional group linkages," Polymer, 2010, **51**(22), pp. 5071–5077.

[16] Gojny, F. H., Wichmann, M. H. ., Fiedler, B., Kinloch, I. A., Bauhofer, W., Windle, A. H., and Schulte, K., "Evaluation and identification of electrical and thermal conduction mechanisms in carbon nanotube/epoxy composites," Polymer, 2006, **47**(6), pp. 2036–2045.

[17] Maruyama, S., Kojimaa, R., Miyauchia, Y., Chiashia, S., and Kohno, M., "Low-temperature synthesis of high-purity single-walled carbon nanotubes from alcohol," Chemical Physics Letters, 2002, **360**(3-4), pp. 229–234.

[18] Deck, C. P., and Vecchio, K., "Growth mechanism of vapor phase CVD-grown multi-walled carbon nanotubes," Carbon, 2005, **43**(12), pp. 2608–2617.

[19] Krause, B., Mende, M., Pötschke, P., and Petzold, G., "Dispersability and particle size distribution of CNTs in an aqueous surfactant dispersion as a function of ultrasonic treatment time," Carbon, 2010, **48**(10), pp. 2746–2754.

[20] Ma, P.-C., Siddiqui, N. A., Marom, G., and Kim, J.-K., "Dispersion and functionalization of carbon nanotubes for polymer-based nanocomposites: A review," Composites Part A: Applied Science and Manufacturing, 2010, **41**(10), pp. 1345–1367.

[21] Gong, X., Liu, J., Baskaran, S., Voise, R. D., and Young, J. S., "Surfactant-assisted processing of carbon nanotube/polymer composites," Chemistry of Materials, 2000, **12**(4), pp. 1049–1052.

[22] Seyhan, A. T., Gojny, F. H., Tanoğlu, M., and Schulte, K., "Critical aspects related to processing of carbon nanotube/unsaturated thermoset polyester nanocomposites," European Polymer Journal, 2007, **43**(2), pp. 374–379.

[23] Zhao, B., Wang, J., Li, Z., Liu, P., Chen, D., and Zhang, Y., "Mechanical strength improvement of polypropylene threads modified by PVA/CNT composite coatings," Materials Letters, 2008, **62**(28), pp. 4380–4382.

[24] Jogi, B. F., "Dispersion and performance properties of carbon nanotubes (cnts) based polymer composites: A Review," Journal of Encapsulation and Adsorption Sciences, 2012, **02**(04), pp. 69–78.

[25] Clayton, L. M., Sikder, A. K., Kumar, A., Cinke, M., Meyyappan, M., Gerasimov, T. G., and Harmon, J. P., "Transparent poly(methyl methacrylate)/single-walled carbon nanotube (PMMA/SWNT) composite films with increased dielectric constants," Advanced Functional Materials, 2005, **15**(1), pp. 101–106.

[26] Khajehpour, M., Arjmand, M., and Sundararaj, U., "Dielectric properties of multiwalled carbon nanotube/clay/polyvinylidene fluoride nanocomposites: Effect of clay incorporation," Polymer Composites, 2014.

[27] Hinchliffe, C., "Processing and properties of nanocomposite dielectric films," 2006, D.Phil dissertation, University of Oxford.

[28] Hayashida, K., and Matsuoka, Y., "Highly enhanced dielectric constants of barium titanate-filled polymer composites using polymer-grafted carbon nanotube matrix," Carbon, 2013, **60**, pp. 506–513.

[29] Barber, P., Balasubramanian, S., Anguchamy, Y., Gong, S., Wibowo, A., Gao, H., Ploehn, H. J., and zur Loye, H.-C., "Polymer composite and nanocomposite dielectric materials for pulse power energy storage," Materials, 2009, **2**(4), pp. 1697–1733.

[30] Clelland, I. W., and Price, R. A., "Polymer film capacitors," Special session 1.3.4, 2011, Applied Power and Energy Conversion Conference.

[31] Roederstein, V., "Film capacitors," 2012, Vishay, General Technical Information:
http://www.vishay.com/docs/26033/gentechinfofilm.pdf

[32] Kazuyuki, K., Nishiyama, S., and Malhotra, K., "Ceramic capacitors aid high voltage designs.pdf," Power Electronics Today, 2004, pp. 14–23.

[33] Darfon - MLCC X5R/X7R Series approval sheet:
http://www.darfon.com/cn/Folder/MLCC/MLCC/X5R%20X7R%20sreies.pdf

[34] Liu, X., Cheng, S., and Randall, C., "The Core-shell Structure in Ultrafine X7R Dielectric Ceramics," Journal of the Korean Physical Society, 1998, **32**, pp. S312 – S315.

[35] Cain, J., Comparison of multilayer ceramic and tantalum capacitors:
h*ttp://www.avx.com/docs/techinfo/mlc-tant.pdf*

[36] "Capacitor dielectric comaprison, HolystoneCaps Technical Notes: *http://www.holystonecaps.com/PDF/TechNotes/20140116144107O.Capdielectriccomp3.pdf*

[37] *http://industrial.panasonic.com/lecs/www-data/pdf/ABA0000/ABA0000TE1.pdf*

[38] University College London, Case Study 2014 – Enabling SEMATECH and industrial member companies to improve their transistor technology: *http://impact.ref.ac.uk/casestudiesapi/refservice.svc/GetCaseStudyPDF/34176*

[39] Bertram, B. D., and Gerhardt, R. A., "Frequency-dependent dielectric properties and percolation behavior of alumina-silicon carbide whisker composites": *http://www.acm-usa.com/site/user/files/0/frequency_dependent_dielectrics.pdf*

[40] Li, Q., Xue, Q. Z., Gao, X. L., and Zheng, Q. B., "Temperature dependence of the electrical properties of the carbon nanotube/polymer composites," eXPRESS Polymer Letters, 2009, **3**(12), pp. 769–777.

[41] Choi, S.H., Kim, I.D., Hong, J.M., Park, K.H., and Oh, S.G., "Effect of the dispersibility of $BaTiO_3$ nanoparticles in $BaTiO_3$/polyimide composites on the dielectric properties," Materials Letters, 2007, **61**(11-12), pp. 2478–2481.

[42] Bowen, C. P., Newnham, R. E., and Randall, C. A., "Dielectric properties of dielectrophoretically assembled particulate-polymer composites," Journal of Materials Research, 1998, **13**(1), pp. 205–210.

[43] Psarras, G. ., Manolakaki, E., and Tsangaris, G. ., "Electrical relaxations in polymeric particulate composites of epoxy resin and metal particles," Composites Part A: Applied Science and Manufacturing, 2002, **33**(3), pp. 375–384.

[44] Kar, P., and Choudhury, A., "Electrical and dielectric properties of polyaniline doped with carboxyl-functionalized multiwalled carbon nanotube," Advances in Polymer Technology, 2013, **32**(S1), pp. E760–E770.

[45] Huang, C., Young, N. P., and Grant, P., "Spray processing of TiO_2 nanoparticle/ionomer coatings on carbon nanotube scaffolds for solid-state supercapacitors," Journal of Materials Chemistry A, 2014, **2**, pp. 11022–11028.

[46] Zhao, X., Hinchliffe, C., Johnston, C., Dobson, P., and Grant, P., "Spray deposition of polymer nanocomposite films for dielectric applications," Materials Science and Engineering: B, 2008, **151**(2), pp. 140–145.

[47] Ahn, J. Y., Kim, J. H., Kim, J. M., Lee, D., and Kim, S. H., "Multiwalled carbon nanotube thin films prepared by aerosol deposition process for use as highly efficient Pt-free counter electrodes of dye-sensitized solar cells," Solar Energy, 2014, **107**, pp. 660–667.

[48] Fenn, J. B., Mann, M., Meng, C. K., Wong, S. F., and Whitehouse, C. M., "Electrospray ionization for mass spectrometry of large biomolecules," Science, 1989, **246**(4926), pp. 64–71.

[49] Mao, S., Lu, G., Yu, K., and Chen, J., "Protein viability on Au nanoparticles during an electrospray and electrostatic-force-directed assembly process," Journal of Nanomaterials, 2010, **2010**, pp. 1–7.

[50] Salata, O. V, Dobson, P. J., Hull, P. J., and Hutchison, J. L., "Fabrication of PbS nanoparticles embedded in a polymer film by a gas-aerosol reactive electrostatic deposition technique," Advanced Materials, 1994, **6**(10), pp. 772–775.

[51] Hoyer, B., Sørensen, G., Jensen, N., Nielsen, D. B., and Larsen, B., "Electrostatic spraying: a novel technique for preparation of polymer coatings on electrodes," Analytical Chemistry, 1996, **68**(21), pp. 3840–3844.

[52] Choy, K. L., and Su, B., "Growth behavior and microstructure of CdS thin films deposited by an electrostatic spray assisted vapor deposition (ESAVD) process," Thin Solid Films, 2001, **388**(1-2), pp. 9–14.

[53] Neagu, R., Djurado, E., Ortega, L., and Pagnier, T., "ZrO_2-based thin films synthesized by electrostatic spray deposition: effect of post-deposition thermal treatments," Solid State Ionics, 2006, **177**(17-18), pp. 1443–1449.

[54] Chen, C. H., Kelder, E. M., Jak, M. J. G., and Schoonman, J., "Electrostatic spray deposition of thin layers of cathode materials for lithium battery," Solid State Ionics, 1996, **86-88**(2), pp. 1301–1306.

[55] Jayasinghe, S. N., and Edirisinghe, M. J., "Electrostatic atomization of a ceramic suspension at pico-flow rates," Applied Physics A-Materials, 2003, **80**(2), pp. 399–404.

[56] Trottier, C. M., Glatkowski, P., Wallis, P., and Luo, J., "Properties and characterization of carbon-nanotube-based transparent conductive coating," Journal of the Society for Information Display, 2005, **13**(9), p. 759.

[57] Sen, R., Zhao, B., Perea, D., Itkis, M. E., Hu, H., Love, J., Bekyarova, E., and Haddon, R. C., "Preparation of single-walled carbon nanotube reinforced polystyrene and polyurethane nanofibers and membranes by electrospinning," Nano Letters, 2004, **4**(3), pp. 459–464.

[58] Sigma Aldrich Technical Information - Poly[4,4′-methylenebis(phenyl isocyanate)-alt-1,4-butanediol/poly(butylene adipate)]: *http://www.sigmaaldrich.com/catalog/product/aldrich/430188?lang=en&region=GB*

[59] 3M^{TM} Product Data Sheet of Fluoroplastic PFA 6910GZ: *http://catalogue.3m.eu/en_EU/eu-Dyneon/3M%E2%84%A2_Dyneon%E2%84%A2_Dispersion/3M%E2%84%A2_Dyneon%E2%84%A2_Fluoroplastic_Dispersion/Dyneon%E2%84%A2~Fluoroplastic~PFA_6910GZ/Fluoroplastic~PFA_6910GZ*

[60] Hall, D. B., Underhill, P., and Torkelson, J. M., "Spin coating of thin and ultrathin polymer films," Polymer Engineering and Science, 1998, **38**(12), pp. 2039–2045.

[61] Pradhan, B., Kohlmeyer, R. R., and Chen, J., "Fabrication of in-plane aligned carbon nanotube–polymer composite thin films," Carbon, 2010, **48**(1), pp. 217–222.

[62] Li, S., Qin, Y., Shi, J., Guo, Z. X., Li, Y., and Zhu, D., "Electrical properties of soluble carbon nanotube/polymer composite films," Chemistry of Materials, 2005, **17**(1), pp. 130–135.

[63] Jiang, L., Zhang, C., Liu, M., Yang, Z., Tjiu, W. W., and Liu, T., "Simultaneous Reinforcement and Toughening of Polyurethane Composites with Carbon Nanotube / Halloysite Nanotube Hybrids," Composites Science and Technology, 2013, **91**, pp. 98–103.

[64] LeMieux, M. C., Roberts, M., Barman, S., Jin, Y. W., Kim, J. M., and Bao, Z., "Self-sorted, aligned nanotube networks for thin-film transistors.," Science, 2008, **321**(5885), pp. 101–4.

[65] Watts, P. C. P., Hsu, W.-K., Barnes, A., and Chambers, B., "High permittivity from defective multiwalled carbon nanotubes in the X-Band," Advanced Materials, 2003, **15**(78), pp. 600–603.

[66] Son, Y.-W., Ihm, J., Cohen, M., Louie, S., and Choi, H., "Electrical switching in metallic carbon nanotubes," Physical Review Letters, 2005, **95**(21), p. 216602.

[67] Wibbeler, J., Pfeifer, G., and Hietschold, M., "Parasitic charging of dielectric surfaces in capacitive microelectromechanical systems (MEMS)," Sensors and Actuators A: Physical, 1998, **71**(1-2), pp. 74–80.

[68] McNally, T., Pötschke, P., Halley, P., Murphy, M., Martin, D., Bell, S. E. J., Brennan, G. P., Bein, D., Lemoine, P., and Quinn, J. P., "Polyethylene multiwalled carbon nanotube composites," Polymer, 2005, **46**(19), pp. 8222–8232.

[69] Chanmal, C. V, and Jog, J. P., "Dielectric relaxations in PVDF/$BaTiO_3$ nanocomposites," eXPRESS Polymer Letters, 2008, pp. 294–301.

[70] Romeo, V., "Preparation and characterization of polymer nanocomposites with new techniques," 2006, D.Phil dissertation, University of Salerno.

Chapter 6. Summary and future work

6.1. Summary

A spray process for forming MWCNT/polymer dielectric films was successfully developed. The role of MWCNTs, especially doped MWCNTs, as fillers in dielectric films has been studied in this research work. The importance of well-defined MWCNT fillers in composites and homogeneous solution-based feed materials for forming composite films was realised early in this study. Due to the inferior quality of commercially available MWCNTs, the nanotubes required for this study were synthesised in-house using AACCVD. Novel nanotube-dispersing methods for forming dispersions of pristine MWCNTs in organic solvents were developed by avoiding nanotube surface treatments and without the aid of any third-phase materials such as surfactants. Also, the dispersibility behaviour of different MWCNTs (conventional, nitrogen doped, and boron doped) in a range of organic solvents was studied. The structural changes induced in the nanotubes due to doping played a key role in the dispersibility behaviour of the nanotubes. Understanding this behaviour helped in developing techniques for forming uniform, homogeneous, and stable dispersions of MWCNTs in organic solvents, which were directly mixed with polymers and processed into composite films. Studies were conducted on different film-forming techniques and aerosol spraying was chosen as a potential technique for forming high quality films with a uniform nanotube distribution. Preliminary film forming experiments with conventional and boron doped MWCNTs gave promising results and indicated the scope for developing nanotube-filled polymer films for dielectric applications. It was also observed that the B-MWCNT fillers performed better than the conventional MWCNTs for improving the dielectric properties.

The methods reported in this work help in overcoming the current processing issues associated with doped MWCNTs and help in their successful incorporation as fillers in composite films. Moreover, these techniques help to fully exploit the potential of conventional and doped MWCNTs in their pristine form, which till date could not be achieved successfully.

6.1.1. MWCNTs

The AACCVD produced MWCNTs were of a fairly good quality with moderately uniform nanotubes and were free of carbonaceous by-products. They presented characteristics of standard CVD produced nanotubes, such as agglomeration into bundles and entrapped catalyst particles. It was observed that nitrogen and boron doping resulted in significant structural changes in the nanotubes. N-MWCNTs exhibited relatively decreased lengths and diameters along with a bamboo-like internal structure due to the edge saturation effect by nitrogen atoms. On the other hand, boron acted as a surfactant during the nanotube growth, which resulted in relatively long and large diameter B-MWCNTs. Additionally, both nitrogen and boron doping induced additional defects in the nanotubes relative to their conventional counterpart. However, a relatively higher amount of disorder was observed in N-MWCNTs. It was also observed that the oxidation resistance of the nanotubes decreased with nitrogen doping and increased with boron doping. Furthermore, considering the implications of the inherent conducting nature of MWCNTs on the dielectric applications, a small amount of the produced MWCNTs was processed for an insulating silica coating through sol-gel technique. A fibrous, non-uniform SiO_2 coating (*ca*. 5 nm thick) was successfully formed on the surface of the MWCNTs.

6.1.2. MWCNT dispersions

Studies to understand the effects of sonication on the structure of MWCNTs were conducted, which aided in developing a 'destruction reduced' sonication protocol for forming MWCNT dispersions. Firstly, the effect of different US probes (UP 100H, UP 200S, Branson 450D) on conventional, and N-, B- MWCNTs was studied. It was observed that the US probe treatment of 1, 2, and 5 minutes resulted in a decrease of 1–4% and 5–15% of original lengths in conventional and N-MWCNTs respectively. Due to the agglomeration in B-MWCNTs, it was difficult to calculate the decrease in lengths in their case. The US probe treatments resulted in effective debundling of the nanotubes, but no particular effect on the diameters could be observed. Moreover, no new defects or major structural damage was observed in the nanotubes even after 5 minutes of the US probe treatment. Using these results a 'destruction reduced' sonication protocol was developed by combining US probe, US bath, and centrifugation. This protocol involved a mild sonication regime that aided in retaining the structural characteristics of the original nanotubes during processing. The sonication protocol was further used to understand the dispersing behaviour of conventional and doped MWCNTs in 22 different organic solvents with a range of surface energies (45.8–10.3 mJ/m^2). It was observed that the structural alterations in the nanotubes arising from doping significantly affected their dispersibility behaviour. N-MWCNTs could be dispersed in solvents of lower surface energies (65–70 mJ/m^2), while B-MWCNTs could be dispersed only in higher surface energy solvents (75–76 mJ/m^2). The study revealed that the suitable dispersing solvent varied with the surface energy of the nanotube. In this case the suitable dispersing solvents were: NMP for conventional MWCNTs, DMA and Benzylalcohol for N-MWCNTs, and GBL for B-MWCNTs. Furthermore, 82% of the initial N-MWCNT concentration could be retained in DMA; this is the highest concentration ever attained for pristine

MWCNTs in common organic solvents. Results of the first and second dispersion studies were further combined to develop labscale (*ca*. 10 ml) and upscale (*ca*. 150 ml) nanotube dispersions in their suitable solvents. These dispersions were visually monitored for stability and appeared to be stable with a minor sedimentation over a period of 3 years, except for the N-MWCNTs dispersion in Benzylalcohol that sedimented after 3 months.

6.1.3. MWCNT/polymer dielectric films

Drop casting, spin coating, electrospraying, and aerosol spraying were studied for forming MWCNT/polymer films. Drop casting and spin coating were found to be unsuitable for this work as the produced films presented inhomogeneity and poor quality due to issues associated with wetting of the glass substrates by the dispersions and the evaporation of the high boiling point solvents from the final film. However, electrospraying produced films that appeared homogeneous and were *ca*. 10 ± 4 μm thick. But the complexity in modifying the electrospray setup for large area film forming and the high boiling points of the dispersing solvents made it unsuitable for this work. On the other hand, aerosol spraying produced homogeneous and uniform films on a relatively larger area in safer conditions and proved to be a suitable choice for the nature of the materials used in this work. Preliminary aerosol spraying tests were conducted using aqueous nanotube dispersions containing SDBS surfactant. MWCNT/PFA and B-MWCNT/PFA films of thickness *ca*. 20–30 μm with 0–0.5 wt.% nanotube concentrations were formed. Impedance spectroscopy studies revealed that the dielectric properties from various locations on individual samples showed a very small deviation, which confirmed the homogeneity in the aerosol sprayed films. It was observed that for the same nanotube concentration, B-MWCNTs presented better dielectric properties than the conventional ones. The real and imaginary permittivities of the films seemed to be mostly independent on the frequency at room

temperature. Low dissipation factors of < 0.025 were recorded for all the samples for frequencies up to 100 kHz, after which an increase in the dissipation factors with the frequency was observed. However, the percolation threshold of either the conventional MWCNTs or the B-MWCNTs could not be determined.

6.2. Future work

It was observed in the current work that B-MWCNTs are instrumental as fillers for dielectric films. Hence, the dielectric properties of B-MWCNT/PFA films at the percolation threshold can be of significant value. Moreover, N-MWCNT and silica-covered MWCNT fillers can have a major impact on the dielectric properties; especially the silica covered B-MWCNTs can help in significantly improving the dielectric properties. This is an area that needs further investigation. Additionally, the effect of temperature on the dielectric properties of the films could not be studied in this work and is an important aspect that requires further studies.

The preliminary film forming experiments using aqueous MWCNT/PFA dispersions resulted in good quality composite films in this work. Therefore it is only logical to extend these results for forming films using the dispersions of pristine MWCNTs and polymers in organic solvents. This is an area that needs to be studied in the future. Moreover, the flexibility of the aerosol spray technique allows large-area film forming and offers the opportunity of upscaling. Additionally, variation of the nanomaterial filler and the polymer matrix can allow fabrication of composite films for a variety of applications such as flexible electronics and light weight protection coatings.